HYDROLYSIS OR CYCLIZATION OF ATP: REGULATING CHOLESTEROL

UTILIZATION IN *MYCOBACTERIUM TUBERCULOSIS*

A Dissertation

Presented to the Faculty of the Graduate School

of Cornell University

In Partial Fulfillment of the Requirements for the Degree of

Doctor of Philosophy

by

Kaley Milania Wilburn

December 2021

© 2021 Kaley Milania Wilburn

HYDROLYSIS OR CYCLIZATION OF ATP: REGULATING CHOLESTEROL UTILIZATION IN MYCOBACTERIUM TUBERCULOSIS

Kaley Milania Wilburn, Ph. D.

Cornell University 2021

Tuberculosis remains a major cause of human morbidity and mortality, and is caused by infection with the bacterium *Mycobacterium tuberculosis*. For thousands of years, *M. tuberculosis* has adapted virulence strategies that allow it to survive in humans, its sole natural host. After transmission by aerosol infection, *M. tuberculosis* provokes a complex series of interactions with the host immune system, allowing the bacterium to establish a persistent niche inside immune cells located within granuloma lesions at infection sites. The bacterium routinely survives for months or years within an individual host, eventually provoking pathology that leads to transmission and compromises lung function. The worldwide burden of *M. tuberculosis* infection is enormous, despite the existence of antibiotic regimens to treat this disease. Current antibiotic regimens for eliminating drug-sensitive *M. tuberculosis* are hampered by their length, and regimens for drug-resistant *M. tuberculosis* are relatively ineffective and riddled with side effects. One approach to develop improved antibiotic targets is to better understand the metabolic pathways that support *M. tuberculosis* survival and persistence during chronic infection and in the face of antibiotic pressures. Over the last decade, lipid utilization has been identified as a central pathway that contributes to *M. tuberculosis* survival and persistence under these conditions. However, mechanisms that can be leveraged to generate chemical inhibitors of lipid utilization in *M. tuberculosis* are poorly understood, and there are no antibiotics of this class represented yet in a

clinical setting. Here we have explored two mechanisms through which ATP lies at the center of lipid utilization in *M. tuberculosis*. We demonstrate the necessity of ATP hydrolysis to drive fatty acid and cholesterol import into *M. tuberculosis*, and identify differences in regulation of these two transport pathways. Examining promising chemical inhibitors of *M. tuberculosis* growth that were previously identified by a novel high-throughput screening technique, we characterize new compounds that inhibit cholesterol utilization in *M. tuberculosis* by upregulating the cyclization of ATP to form cyclic-AMP (cAMP). These represent a significant advance because the compounds show promising safety and pharmacokinetic profiles, and are the first *M. tuberculosis*-directed cholesterol utilization inhibitors suitable for testing in animal models. These compounds represent an unusual mechanism of action for an antimicrobial, in which activating excessive synthesis of a second-messenger disrupts pathogen fitness during infection. The compounds also initiated our efforts to characterize the unexpected link between cAMP signaling and cholesterol utilization in *M. tuberculosis*, in which the function of cAMP signaling in pathogenesis is generally not well characterized. Lastly, we have begun to examine whether these compounds have secondary effects on the host cell immune response, as cAMP is well-known for modulating immune cell phenotypes and Mtb is poised to secrete excess cAMP into the host cell when this pathway is chemically activated.

BIOGRAPHICAL SKETCH

Kaley Wilburn was awarded her Bachelor of Science degree in Biomedical Sciences from University of Central Florida's Burnett Honors College in 2015. Under the mentorship of Dr. Kyle Rohde, she was introduced to research in the mycobacterial system in 2014, working on development of drug discovery tools using the BSL-2 model organism *Mycobacterium smegmatis*. She subsequently joined the Biomedical and Biological Sciences Ph. D. program at Cornell University in 2015 with the goal of working on *Mycobacterium tuberculosis* during her Ph. D. studies. She joined Dr. Brian VanderVen's lab in 2016, and completed her dissertation research at Cornell University under his supervision.

To my husband, Ben Cook

my parents, Shelly and David Wilburn

and my favorite study buddy, Whitman

ACKNOWLEDGEMENTS

First, I would like to extend deepest thanks to my Ph. D. advisor Dr. Brian VanderVen. The phrase "taught me everything I know" has never felt more appropriate. Thank you for taking a chance on me as your first Ph. D. student, and for making my dream of working with the toughest, coolest bacterial pathogen come true. It's been real, *and* real fun. I would also like thank my committee members, past and present, for dedicating their time and energy to this project: Dr. Cindy Leifer for insightful questions and for teaching the singular class that convinced me to stop disliking immunology. Dr. Gunther Hollopeter for setting an exceptional example of genuine scientific enthusiasm and inquisitiveness during my rotation, and for agreeing to join us at the end. And Dr. Jeongmin Song and Dr. Holger Sondermann for sharing their expertise in bacterial pathogenesis and biochemistry, which significantly improved this work at many turns. Thank you to Dr. David Russell and his lab members, past and present, for their continuous scientific help and personal support. I would like to thank all of my lab mates, with special thanks to Dr. Christine Montague whose mentorship, outstanding hard work, and steady spirit were essential. Thank you to Dr. Kyle Rohde and the Rohde Lab family for sparking my love for research. Thanks also to Arla Hourigan and Dr. Dave Lin for working tirelessly on the BBS program.

Finally, I would like to thank the many people in my personal life whose care, humor, and encouragement made this possible: My parents, Shelly and Dave. My husband, Ben, and the extended Cook family. All of my BBS/Microbiology friends, especially Pragya, Duc, Divya, Shing, and Monique. The Bread of Life family, especially Fr. Ryan and Amy O'Dowd. And last but not least, Dr. Jennie Bernstein and Dr. Margaret Hurley.

TABLE OF CONTENTS

Chapter Three

Hydrolysis of ATP by MceG is required for cholesterol utilization in

M. tuberculosis

Chapter Four

Pharmacological and genetic activation of cAMP synthesis disrupts cholesterol

utilization in _M. tuberculosis_

Chapter Five

Chemically activating cAMP synthesis in *M. tuberculosis* during infection

decreases bacterial fitness and alters host inflammatory signatures

Chapter Six

Final discussion and future directions

LIST OF FIGURES

LIST OF TABLES

LIST OF ABBREVIATIONS

3OCh-CoA	3-oxocholest-4-en-26-oyl-CoA
ABC	ATP-binding cassette
AC	Adenylyl cyclase
AKAP	A-kinase anchoring protein
AM	Alveolar macrophage
AMP	Adenosine monophosphate
ATP	Adenosine triphosphate
BMDM	Bone marrow-derived macrophage
cAMP	3',5'-cyclic adenosine monophosphate
CCL, CXCL	Chemokine ligand
CREB	cAMP response element-binding protein
CRP	cAMP receptor protein
DC	Dendritic cell
DMSO	Dimethyl sulfoxide
EC_{50}	Half maximal effective concentration
ELISA	Enzyme-linked immunosorbent assay
EMB	Ethambutol
Epac	Guanine nucleotide exchange factor proteins directly activated by cAMP
EtOH	Ethanol
GFP	Green fluorescent protein
GPCR	G protein-coupled receptor

IFN	Interferon
IGRA	IFNγ release assay
IL	Interleukin
INH	Isoniazid
LDL	Low-density lipoprotein
LTBI	Latent TB Infection
M-PFC	Mycobacterial protein fragment complementation
MCC	Methylcitrate cycle
MDR-TB	Multi-drug resistant TB
MIC	Minimum inhibitory concentration
MOI	Multiplicity of infection
MOODA-CoA	4-methyl-5-oxo-octanedioic acid
Mtb	Mycobacterium tuberculosis
NADH	Nicotinamide adenine dinucleotide hydride
NET	Neutrophil extracellular trap
PAT	Poly-acylated trehalose
PDE	Phosphodiesterase
PDIM	Phiocerol-dimycoseroic acid
PEP	Phosphoenolpyruvate
PGE2	Prostoglandin E2
PKA	Protein kinase A
PZA	Pyrazinamide
RIF	Rifampicin

RNA-seq	RNA sequencing
SL	Sulfolipid
STING	Stimulator of interferon genes
TAG	Triacylglycerol
TB	Tuberculosis
TCA	Tricarboxylic acid
TLC	Thin-layer chromatography
TNFα	Tumor necrosis factor alpha
TST	Tuberculin skin test
UDP-GlcNAc	Uridine diphosphate N-acetylglucosamine
WT	Wild type
XDR-TB	Extensively drug resistant TB

<center>**CHAPTER ONE**</center>

<center>**Tuberculosis Pathogenesis and Control Measures**</center>

1.1 *M. tuberculosis* pathogenesis

1.1.1 Introduction

The pathogenesis of *M. tuberculosis* (Mtb) is complex and unfolds over the course of months or years within a single host. Infection with Mtb is initiated when the bacterium is transmitted through aerosolized droplets and reaches the alveolar space of the lung. This event initiates a cascade of interactions between Mtb and the host immune system, which canonically leads to the formation of the hallmark tissue lesion in tuberculosis (TB) disease, the granuloma. Granulomas are diverse but are broadly defined as aggregates of macrophages, and often other immune cells including dendritic cells (DCs), granulocytes, T cells, and B cells, that coalesce into a focally-organized structure around a site of persistent infection or inflammation (*1*). A granuloma is distinguished among chronic inflammatory infiltrates based on the presence of mature macrophages that are organized into a characteristic, compact structure around the foci of inflammation and may undergo additional phenotypic changes, including transformation into epithelioid cells, lipid-loaded foam cells, or multinucleated giant cells (*1*). Advances in TB immunology have contributed novel perspectives concerning the role of the granuloma in Mtb pathogenesis and disease outcome. For example, it is now clear that individuals who are exposed to Mtb exist on a spectrum of disease outcomes, and for those infected with Mtb, disease outcome is significantly influenced by the immune response found at the level of each granuloma (*2*). Although standard mouse models of TB are limited by their inability to develop the well-organized granulomatous structures observed in humans, information from alternative experimental animal models and human cohorts continues to supplement observations made in mice and to expand our

<center>1</center>

knowledge of TB pathogenesis. The responses of the immune cells that comprise the granuloma play important host protective roles during Mtb infection, but this perspective is complicated by studies that have identified host-detrimental and/or pro-bacterial features of the immune response. Studies examining correlates of host protection and host susceptibility to TB have contributed to emerging themes in Mtb pathogenesis, including the importance of a "balanced" immune response in controlling Mtb replication and dissemination, and the heterogeneous characteristics of the granulomas present within a single host and between individual hosts. For the purposes of this study, it is important to consider the host response to Mtb because it dictates the microenvironment the bacterium survives within during infection, and thereby directly affects which bacterial pathways are required for persistence and should be targeted by novel TB antibiotics.

Studying the chronology of Mtb pathogenesis and its underlying mechanisms presents significant challenges. From a translational perspective, it is ideal to understand Mtb pathogenesis in humans, given that humans are the sole reservoir of Mtb and TB treatments must ultimately address Mtb clearance in this context. Because the lung is the primary tissue of interest, a variety of minimally-invasive methods have been used to study Mtb pathogenesis and disease progression in TB patients (e.g. tracking granuloma inflammation using [18]Fluorodeoxyglucose PET-CT imaging, and analysis of peripheral blood or bronchoalveolar lavage samples). Studies utilizing lung tissue samples, acquired from surgical resection or from deceased patients, have also contributed valuable information. However, these samples are more challenging to acquire, provide limited snapshots of disease progression, and must be combined with other approaches to draw conclusions about events that occur during Mtb infection. During the 1940s, Georges Canetti published a classic study based on autopsies of 1,500 TB patients in which he documented the histopathologic features of human TB lesions and quantified the associated number of Mtb bacilli

(*3*). Based on the work of Canetti and others, human pulmonary TB lesions can be categorized by several key features. These include i) whether the center of the granuloma is cellular (dominated by mononuclear infiltrate) or acellular (dominated by necrosis, or calcification), ii) whether a fibrotic rim is present ("walling off" the granuloma from the surrounding lung alveoli) or absent (the aggregate of macrophages and lymphocytes spreads to fill surrounding alveolar space in a "tuberculous pneumonia"), and iii) whether erosion of the granuloma into an airway is present, creating an open cavity that exposes remnants of the necrotic core and Mtb to the airway (*4*). The organization of a classic mature TB granuloma is illustrated in Figure 1.1, featuring an acellular core composed of necrotic cell debris and Mtb bacilli, an inner rim of infected and uninfected mature macrophages, and a peripheral layer of T cells and B cells (*2*). Individuals with TB typically have multiple foci of infection in their lungs. Recent studies using [18]Fluorodeoxyglucose PET-CT imaging to track sites of inflammation have illustrated the dynamic nature and heterogeneity of human TB granulomas (*5, 6*). Correlations between various host immune responses and the control of Mtb pathogenesis is an area of interest in the field and its relevance is briefly discussed below.

Given the limitations of working with human TB samples, a variety of animal models (e.g. mice, zebrafish, rabbits, guinea pigs, and non-human primates) have been developed to augment our understanding of Mtb pathogenesis (*4*). Each of these recapitulates some aspects of human TB, but has its own drawbacks. The most accessible of these include standard inbred mouse strains, and the C3HeB/FeJ mouse. Mice can be infected with various Mtb strains, and have contributed significantly to our mechanistic understanding of Mtb pathogenesis. Mice infected with Mtb display a robust immune response and form cellular lesions characterized by admixed macrophages, lymphocytes, and neutrophils. These lesions contain many of the same cell types as human granulomas and the Mtb bacilli are mainly found intracellularly within macrophages during

chronic infection (*7*). However, relatively resistant mice do not form highly organized granuloma structures, and they lack features like necrosis, fibrosis, calcification, and sustained hypoxia found in human lesions (*4*). One alternative approach is to infect the genetically susceptible C3HeB/FeJ mouse (*8*). C3HeB/FeJ mice develop heterogeneous type I IFN- and neutrophil-driven pathology that includes development of well-organized necrotic granulomas during chronic infection and is characterized by high extracellular bacterial numbers (*7, 9-11*). Recently-introduced strategies for improving mouse models of TB include establishment of an ultra-low dose aerosol infection model and use of outbred, genetically-diverse groups of mouse strains (*12-14*). These replicate features such as heterogeneous Mtb burdens and diverse granuloma features. By contrast, non-human primates, specifically cynomolgus macaques, are the animal model that most closely replicates the full spectrum of human TB disease and pathology (*15*). Studies using the macaque model have contributed novel insights into the complexities of Mtb pathogenesis. However, logistical challenges of this model prohibit widespread use, and the heterogeneity and paucibacillary nature of the resulting infection can actually be disadvantageous for some studies. Another useful model for Mtb infection is the zebrafish, in which *Danio rerio* is infected with *Mycobacterium marinum*. This model has been leveraged most notably for live imaging studies, due to the optically clear nature of the zebrafish larvae (*16*). Combining data from across these models and comparing it to observations from humans has created a general framework for understanding the initiation and progression of Mtb infection. However, many of the specific roles of host responses to Mtb remain debatable, and are outside the scope of what is relevant to this study.

1.1.2 Key features of *M. tuberculosis* pathogenesis

Early events during infection

An infection begins when Mtb transmitted in aerosolized respiratory droplets is inhaled, reaches the alveolar space, and is phagocytosed by resident alveolar macrophages (AMs). To infect the deep gas-exchanging regions of the lung where AMs reside, Mtb presumably surpasses several first-line airway defenses, including the mucociliary clearance system and antimicrobial peptides (*17*). Mtb that reaches the lower airway accesses the alveoli, which contain AMs and alveolar epithelial cells coated by alveolar lining fluid (*17*). Direct knowledge of the earliest interactions between Mtb and lung immune cells (<14 days post-infection) has only emerged recently due to technical challenges, but it is generally thought that AMs are the first professional phagocytes Mtb encounters during initial infection. Cohen et al. demonstrated that AMs are the initial reservoir for Mtb infection and replication during the first 2-7 days post-infection, using a standard mouse model (*18*). As the infection progressed (>14 days post-infection) Mtb was increasingly distributed in recruited phagocytes (neutrophils and monocyte-derived cells) rather than AMs. Infected AMs mediate this transition by traversing from the alveolar space through the airway epithelium into the lung interstitium and proliferating, forming aggregates of infected cells that are predecessors of granuloma formation (*18*). This interstitial transition eventually corresponds with the spread of Mtb to other myeloid cells in the interstitium, including DCs, interstitial macrophages, recruited neutrophils, and monocytes or monocyte-derived cells (*18-20*).

After infection, but prior to the initiation of T cell immunity, the number of bacteria in the lungs increases, illustrating that the immune cells Mtb spreads within during this stage are not able to halt its proliferation (*21*). In mice, AMs infected with Mtb are relatively permissive to bacterial replication, and infected AMs as well as bystander cells mount a delayed pro-inflammatory response that isn't detected until ~10 days post-infection (*19, 22, 23*). Briefly, the pro-inflammatory response of resident and recruited myeloid cells during Mtb infection includes direct

or indirect stimulation of cytokine (e.g. TNFα, IL-6, IL-12, Type I IFNs, IL-1α/β, IL-10) and chemokine (e.g. CCL-2, -3,-4,-5,-17, CXCL-2,-3,-10) production (*24*). These factors ultimately contribute to mature granuloma formation by coordinating phagocyte activation, activation of T cell and B cell responses, and innate and adaptive cell recruitment, accumulation, and organization in the granuloma structure (*24*). There is no consensus on the exact mechanisms by which Mtb spreads from infected to uninfected cells during nascent granuloma formation, but macrophages and neutrophils that die by necrosis are thought to release Mtb into the tissue during lysis and facilitate spread of the bacteria to recruited phagocytes (*25*). In contrast, infected macrophages that die by apoptosis are hypothesized to be more protective for the host by containing the bacteria within the apoptotic cell after death and facilitating efferocytosis (*25*).

Events during the chronic stage of infection

When considering development of novel TB antibiotics, the features of granulomas present during chronic infection are more relevant to consider because they dictate the microenvironmental conditions the bacterium survives within at the anticipated time of treatment. This influences which bacterial adaptations are required for survival and drug tolerance, and therefore represent targets of interest for new antibiotics. The transition from nascent to mature granuloma formation during Mtb infection is typically marked by the development of an adaptive immune response in lung-draining lymph nodes. It is generally accepted that initiation of the adaptive response to Mtb is relatively delayed (~7-11 days post-infection in mice), which has been attributed to dysregulated migration and sub-optimal T cell stimulation by infected DCs and interstitial macrophages (*26, 27*). The migration of infected DCs and macrophages disseminates Mtb to extrapulmonary sites, including draining lymph nodes and eventually the spleen. As illustrated in Figure 1.1, antigen-

specific T and B cells are activated, recruited to the mature granuloma, and organized around the periphery of the focus of infected macrophages and neutrophils. Effector CD4^{+} T cells are an essential component of a protective immune response to Mtb, and a variety of T cell phenotypes can be identified in each granuloma and correlated with differential lesion sterilizing capacity (*28-31*). CD8^{+} T cells and B cells are also associated with granulomas, and whether these play a more significant role in protection against Mtb than initially predicted is and ongoing area of investigation (*30, 32, 33*).

Accumulation of lipids during Mtb infection

Importantly, macrophages undergo phenotypic changes within mature granulomas. They can fuse with one another to form multinucleated giant cells, develop into tightly interdigitated networks of epithelioid histiocytes, or accumulate lipid droplets to transform into foam cells (*34*). Foamy macrophages are associated with a number of maladaptive responses during Mtb infection including granuloma necrosis and tissue damage, increased lipid nutrient availability to Mtb and expansion of lipid-rich caseum, promotion of drug-tolerant non-replicative bacteria, dampened expression of pro-inflammatory cytokines, and impaired cell-autonomous antimicrobial functions such as phagocytosis (*35-38*). Recent work on foam cells has emphasized the context-specific nature of their biogenesis during different infectious, autoimmune, or metabolic diseases, and proposed that the composition of the lipid droplets stored in foam cells during Mtb infection is distinct from those generated during atherosclerosis (*35, 39*). Macrophage regions sampled from necrotic TB granulomas in animal models were more enriched in triglyceride species than free cholesterol or cholesteryl esters, while atherosclerotic lesions contain foam cells enriched primarily in cholesterol species (*39*). This finding was not verifiable in the limited number of

7

human lesions that were examined, but was reproduced in lipid droplets formed by human monocyte-derived macrophages infected with Mtb *in vitro*. This study also found that the lipid species signature of the granuloma caseum matches the signature of the macrophages surrounding it, which supports the hypothesis that dead macrophages release stored lipids that contribute to caseum formation over time. This is consistent with earlier findings published by Kim et al. who characterized the host cell expression signature and lipid composition of caseous lung granulomas resected from patients with severe TB disease (*40*). Caseous granulomas were characterized by transcriptional upregulation of a network of interconnected lipid synthesis genes, increased expression of two proteins involved in lipid synthesis/sequestration in the central caseum and surrounding cells relative to nascent or resolved lesions, and the presence of foam cells identified by neutral lipid staining (*40*). Caseous granulomas were enriched in triacylglycerol, cholesterol, and cholesterol esters relative to uninvolved, normal lung tissue (*40*). Interestingly, earlier studies using a mouse model intravenously infected with *Mycobacterium bovis* found that the progression of severe disease was associated with an increase in the proportion of cholesterol esterified with fatty acids in the lungs (*41*). Intracellular lipid body inclusions were also present in 3-86% of Mtb cells in the sputum of smear-positive TB patients, which is associated with a slow growing or persistent bacterial phenotype (*42*). Taken together, the data indicates that lipid accumulation is a defining characteristic of Mtb infection *in vivo*, and that triglycerides, cholesterol, and cholesterol esters are major lipid species enriched in mature granulomas.

A number of pro-lipogenic signals present during Mtb infection have been proposed to promote foam cell biogenesis, including components of the mycobacterial cell wall (oxygenated keto- and hydroxyl-mycolic acids), the secreted bacterial protein ESAT-6 and G_i protein-coupled receptor GPR109A signaling, TNFα signaling, IFNγ/HIF1α signaling, and hypoxia (*36, 37, 39,*

40, 43, 44). Current hypotheses addressing how Mtb utilizes host-derived fatty acids and cholesterol during infection are discussed in Chapter 2.1.

The continuum of tuberculosis disease states

It has become increasingly clear that individuals infected with Mtb experience a spectrum of disease presentations that develop over the course of months or years after the initial exposure. However, pulmonary TB has traditionally been divided more simply into latent or active disease in clinical and public health settings based on available testing criteria (Table 1.1). Both latent TB infection (LTBI) and active TB are characterized by a positive tuberculin skin test (TST) and/or IFN-γ release assay (IGRA) result (*45*). Because the TST and IGRA tests are not able to differentiate the presence of viable Mtb from a previously-resolved infection or poorly-primed immune response to Mtb, additional criteria are used to distinguish active TB from LTBI. Active pulmonary TB is characterized by the presentation of one or more disease symptoms, chest X-ray abnormalities, and positive sputum smear, nucleic acid amplification, and/or culture tests to confirm the presence of Mtb bacilli (*45, 46*). In contrast, LTBI is traditionally defined based on the absence of clinical symptoms, negative sputum smear, and normal chest radiograph (*45-47*). An estimated 5-15% of infected individuals progress to active TB within 2-5 years after the initial exposure, referred to as primary TB (*47, 48*). This means that the majority of immunocompetent individuals infected with Mtb develop LTBI after the primary infection. However, LTBI confers an estimated 5-10% lifetime risk of later progression to active TB disease (*49*). The delayed development of active disease after a latent period following the initial infection is referred to as post-primary or reactivation TB. Each individual's actual risk of developing post-primary TB is influenced by numerous factors including frequency of reinfection, age, co-morbidities, and access

9

to pre-emptive antibiotic treatment (*45, 49-51*). Both primary and post-primary TB permit the transmission of Mtb, as viable bacteria released from poorly-controlling granulomas access the airways and are expelled in aerosolized droplets during coughing or talking. The contagious spread of Mtb between human hosts is essential to the continued survival of this pathogen, as humans are the only natural reservoir of Mtb (*50*).

*** The local immune response at the level of each granuloma influences disease outcome***

Importantly, the binary distinction between active TB and LTBI has been challenged recently, in favor of models that better encompass the spectrum of disease states generated by the complex, heterogeneous pathogenesis underlying Mtb infection. These disease states include i) elimination of infection, with varying degrees of adaptive immune cell priming, ii) unresolved but well-controlled infection, with quiescent disease symptoms, iii) marginally-controlled infection, with subclinical disease symptoms and intermittent positive culture test results, and iv) poorly-controlled infection, with clinical disease symptoms (*46, 52*). These disease states have been proposed to align with a spectrum of underlying granuloma responses to the bacterium, categorized by the ability of each granuloma to restrict or resolve Mtb infection and the presence of different immune cell subtypes (*2*).

As mentioned above, it has long been appreciated that the granulomas that develop during Mtb infection are varied in their structures and cellular composition, but recent advances have begun to unravel how different lesion features influence TB disease progression (*3, 4*). In a key study, Lin et al. assessed the degree of bacterial killing within individual lesions using a macaque model of Mtb infection that generates animals with active disease or LTBI, and heterogeneous lesion histopathology in individual animals (*53*). While lesions from the active disease group had

higher bacterial numbers on average than lesions from LTBI animals, individual lesions from both the active and latent groups had a wide distribution of bacterial burdens that largely overlapped, and a variable number of sterilized lesions were present in both groups (*53*). The bacterial killing capacity of lesions from both the active disease and LTBI groups were also widely variable from lesion-to-lesion, even within individual animals (*53*). Overall, the average lesion bacterial killing capacity was similar in the active disease and LTBI groups, but sites of severe pathology (e.g. TB pneumonia) in animals with active disease had diminished bacterial killing capacity (*53*). Subsequent studies of lesion-to-lesion heterogeneity correlated inflammation or immune cell signatures at the local granuloma level with disease status, bacterial abundance or sterilization, restriction of dissemination to new lesions, and/or protection of surrounding lung tissue (*29, 54-56*). For example, isolated granulomas within individual macaques display heterogeneous T cell cytokine profiles, and the cytokine profiles overlap substantially between hosts with active disease and LTBI (*29*). However, when examined independently of disease status, sterile granulomas had modest increases in T cells producing certain cytokines (TNFα, IL-17, IFN-γ, and/or IL-2), and lesions with cells producing a combination of anti-inflammatory IL-10 with pro-inflammatory IL-2, IL-17, or TNFα were the most likely to be sterile (*29*). Substantial overlap in the characteristics of individual lesions were present for both active and latent disease groups in these studies. Importantly, where longitudinal measurements of these characteristics for individual lesions are not available, it is unclear whether the identified signatures precede and drive a particular lesion trajectory, or are simply associated with the lesion state at the time of sample collection. Collectively, the data on lesion-to-lesion heterogeneity supports a model in which each granuloma in a given host represents an individual microenvironment featuring an individual capacity for bacterial control and disease resolution that is significantly defined by the interplay between

immune cells and Mtb at the local level. This model also proposes that a small and variable number of unresolved and poorly controlled lesions in each individual host underlies the spectrum of LTBI, sub-clinical, and active TB disease outcomes.

Why all granulomas in an individual host do not follow parallel fates, despite existing in the context of one overarching systemic immune response, is not clear mechanistically. Systemic correlates of active TB versus LTBI have also been identified from blood signatures and are included below, but the dynamic between these peripheral signatures and immune responses at the local level of individual lesions is not completely defined. This is partly because collecting matched blood and granuloma tissue from humans with active TB versus LTBI is prohibitive. Recent studies using animal models have begun to address this. Both blood transcriptional signatures and trajectories of lesion inflammation early after infection can predict disease progression, suggesting that early innate immune responses likely skew the outcome of individual lesions significantly (*55, 57, 58*). Whole blood signatures do not necessarily indicate peripheral immune responses that themselves proceed to influence disease progression at the level of individual lesions, and may alternatively be understood as a limited downstream reporter of select (type I IFN- and neutrophil-related) interactions occurring between Mtb and immune cells at local sites of infection (*54, 57-60*). As host correlates of protection or progression have been identified, a model in which the local balance of anti-inflammatory and pro-inflammatory mediators is critical for control and resolution of Mtb infection is emerging (*2, 12*). This model is partly based on examples where both insufficient *and* excessive immune responses via certain cytokines or cell types have been found to drive TB disease progression, as described below.
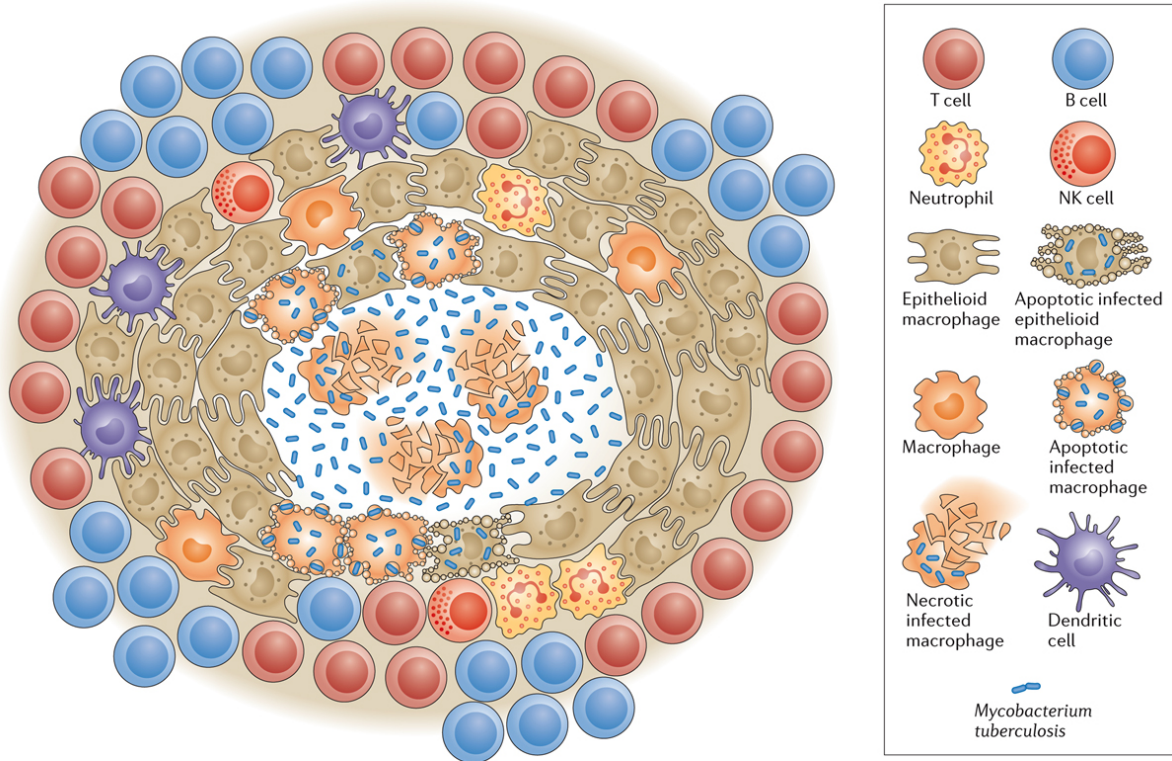
Figure 1.1 The organization of a classic mature TB granuloma. The acellular core is composed of necrotic cell debris and Mtb bacilli. An inner rim of infected and uninfected macrophages of different phenotypes surrounds the necrotic core. A peripheral layer contains T cells and B cells, which can be surrounded by fibrosis. Reproduced with permission from (*2*).

Parameter	Description
Tuberculin Skin Test (TST)	Tests T cell-mediated delayed type hypersensitivity reaction to mycobacterial antigens present in purified protein derivative (tuberculin) solution administered intradermally
IFN-γ Release Assay (IGRA)	Whole-blood test measuring T cell-mediated IFN-γ secretion in response to synthetic Mtb antigens (ESAT-6 and CFP-10); not confounded by BCG vaccination
Sputum Smear	Microscopy-based test for quantifying Mtb bacilli in sputum sample using acid-fast staining
Chest X-ray	Used to detect abnormalities in lungs consistent with pulmonary TB disease including signs of consolidation, nodules, cavities, or enlarged lymph nodes
Nucleic Acid Amplification	PCR-based test for detecting Mtb RNA or DNA from clinical specimens like sputum, recently with simultaneous detection of antibiotic resistance
Culture	Growth-based test, in which clinical specimen is inoculated onto a solid or liquid rich medium and examined for outgrowth over the course of 4 days-12 weeks
Disease Symptoms	Pulmonary TB symptoms include chronic cough, hemoptysis, chest pain, loss of appetite, unexplained weight loss, fatigue, night sweats, fever

Table 1.1 Testing methods used to distinguish TB disease status.

1.1.3   Host Correlates of Protection and Disease

Hallmarks of failed pulmonary granulomas in TB include erosion into the surrounding lung parenchyma, liquefaction of the central necrotic caseum leading this material to "discharge through an eroded airway or pleural space" which creates an open cavity, accompanied by a high bacterial burden (*4, 38*). When the cavity and its inverted material coincides with an airway it permits extracellular Mtb to access this space, allowing the bacteria to be expelled and transmitted. Three examples of components of the host immune response that significantly influence the progression of granulomas toward host protection versus disease are discussed here. How each of these are interconnected with networks of other immune mediators relevant during Mtb infection *in vivo* is a complex and poorly-understood point of ongoing investigation (*61*). These three host factors are highlighted because they overlap with immune factors that may be influenced by treatment with Rv1625c agonist compounds during Mtb infection, discussed in Chapter 5.

TNFα

TNFα is a major pro-inflammatory mediator that can be produced by macrophages, natural killer (NK) cells, and T cells. It triggers a range of downstream signaling events through the receptors TNFR1 and TNFR2, which are expressed by cells in all tissues or by specialized subsets of cells, respectively (*24, 62*). TNFα signaling can activate inflammatory signaling and cell survival, proliferation, and differentiation via the transcription factors AP-1 and NF-κB, or it can promote cell death through activation of necrosis or caspase-dependent apoptosis (*62*). During Mtb infection, a threshold of TNFα is required for host protection, but excess TNFα is a mediator of tissue damage and disease progression (*24, 63*). Treatment with anti-TNFα biologics for unrelated inflammatory diseases increased the incidence of LTBI reactivation, suggesting a requirement for

a certain threshold of TNFα to prevent disease progression in humans (*63, 64*). This was also observed in mouse and macaque models, where systemic neutralization of TNFα or deletion of its receptor resulted in hypersusceptibility to Mtb, including increased bacterial burden, disruption of the focal granuloma structure, increased dissemination of bacteria to extrapulmonary tissues, and increased necrosis (*63, 65*). The mechanisms through which TNFα coordinates protection against Mtb during *in vivo* infection are not well defined, but one possible mechanism is enhanced activation of cell-autonomous macrophage functions that are proposed to help control Mtb growth (e.g. nitric oxide synthase, guanylate binding proteins, antimicrobial peptides) (*12, 63, 66*). Additionally, TNFα may contribute to host protection by coordinating recruitment of immune cells to the lung critical for granuloma formation and maintenance (e.g. enhancing secretion of CXCL9, CXCL10, and CCL5 from macrophages to recruit T cells and B cells) (*67*).

On the other hand, excess TNFα has also been proposed to promote disease susceptibility and immunopathology, possibly by driving programmed necrosis of infected macrophages. While the role of apoptosis in host protection against Mtb is controversial, necrosis of infected macrophages is generally considered detrimental to the host (*63*). Current ideas about the consequences of excess TNFα during Mtb infection are intertwined in a complex manner with eicosanoid signaling and induction of necrosis. Genetic polymorphisms that generate increased production of the pro-inflammatory eicosanoid leukotriene B_4, which induces neutrophil, macrophage, and T cell recruitment, were associated with upregulation of *Tnfa* in the zebrafish model (*68*). In this model, the high-LTB_4 genotype drove disease susceptibility primarily through enhanced TNFα and macrophage necrosis, and susceptibility was rescued with genotype-matched immunotherapy to counter the excess LTB_4/TNFα signaling (*68*). Consistent with this idea, a cohort of human patients with a homologous high-LTB_4 genetic polymorphism benefitted

16

disproportionately from dexamethasone therapy during treatment for TB meningitis compared to patients with alleles that generate intermediate- or low-LTB$_4$ phenotypes (*68*). However, data from treatment with a more specific anti-TNFα immunotherapy in this population to link this outcome directly to TNFα, was not included. Importantly, many details of this model have yet to be elucidated in more relevant murine or macaque models, and during pulmonary Mtb infection. Notably, in a screen for correlates of disease using a genetically diverse, outbred panel of mice infected with Mtb, Niazi et al. found that levels of TNFα in the lung were strongly correlated with disease susceptibility and bacterial burden, but it is unclear if excess TNFα signaling is driving this phenotype or is better understood as a consequence of higher Mtb burden (*60, 69*). Overall, TNFα deficiency may lead to necrotic death of phagocytes through unrestricted Mtb growth and higher bacterial burden in each cell; in the case of excess TNFα, it may drive pro-necroptosis signals in phagocytes despite maintaining better short-term cell-autonomous control of Mtb (*63, 69*). In both cases, increased necrosis of infected cells would be detrimental to the host as Mtb escape into the extracellular environment to replicate and disseminate, and immunogenic cellular contents are released from the ruptured cell (*69*). Detailed mechanistic explanations of how the balance of TNFα impacts TB disease outcome, including how TNFα and other cytokines interact with one another during Mtb infection, await further investigation (*61*).

Neutrophils

Many details of the host-protective and host-detrimental roles of neutrophils during different stages of Mtb pathogenesis remain controversial. Neutrophils play essential host-protective roles in combatting pulmonary bacterial infections by releasing bactericidal products through degranulation, engulfing bacteria through phagocytosis and delivering bactericidal agents

via fusion with the lysosome, or trapping bacteria in neutrophil extracellular traps (NETs) (*70*). In TB, neutrophils have occasionally been attributed a positive role in early protection after infection and additional antimycobacterial effector functions like efferocytosis of infected macrophages and enhancement of CD4$^+$ T cell priming have been explored (*71*). However, mounting evidence correlates excessive neutrophil responses during Mtb infection with pathology and poor disease outcome. This may be attributable to specific subset(s) of neutrophils, but this is currently unknown. Active TB disease is associated with a higher proportion of neutrophils containing intracellular Mtb than macrophages in samples from resected human lung tissue, sputum, and bronchoalveolar lavage fluid (*72*). Similarly, granulomas from macaques with active TB accumulated more neutrophils producing inflammatory S100 proteins than those with LTBI (*73*). S100-producing neutrophils were also identified in lesions from humans with active TB, and S100 protein levels in the serum correlated with increased levels of the neutrophil-attracting chemokine CXCL1 in the serum (relative to healthy control, LTBI, or rheumatoid arthritis patients), increased neutrophils in the blood, and more severe lung damage (*73*). In genetic screens using outbred, genetically diverse populations of mice, higher levels of neutrophils and neutrophil-attracting chemokines (especially CXCL1, CXCL2, and CXCL5) in lung samples correlated with disease severity after Mtb infection, a feature that was conserved in human blood and macaque lung samples (*12, 60, 73*). Susceptibility in these mice was also positively correlated with CXCL1 levels in plasma and the degree of lung pathology including granuloma size, necrosis, and disruption of surrounding lung tissue (*60*). Independently, peripheral signatures of neutrophil recruitment and activation were correlated with disease severity in a model comparing susceptible C3HeB/FeJ mice to relatively resistant C57BL/6J mice (*10*).

Multiple knockout mice in a C57BL/6J background have also been described in which disrupting a single gene (*Irg1, Bhlhe40, Atg5, Ifng,* or *Nos2*) was sufficient to generate neutrophil-mediated immunopathology associated with higher bacterial burden and/or early death within 40 days post-infection with Mtb (*74-78*). Depleting neutrophils with an anti-Ly6G antibody was sufficient to prolong survival and reduce Mtb burden in both *Irg1*^{-/-} and *Atg5*^{-/-} mice, suggesting that neutrophils have a direct role in driving disease progression (*75, 76*). T cell-derived IFN-γ and its ability to induce nitric oxide production in macrophages have been assumed to promote host protection by enhancing the capacity of macrophages to restrict Mtb growth; however, nitric oxide has been proposed to play an alternative role in limiting pathways that lead to neutrophil-associated immunopathology and unrestricted bacterial growth during Mtb infection (*77, 78*). IFN-γ was proposed to limit neutrophil-driven pathology by inducing nitric oxide production in macrophages, which suppresses an IL-1- and 12/15-lipoxygenase-dependent neutrophil recruitment pathway during Mtb infection (*77, 78*). Inhibiting IL-1 receptor signaling, depleting granulocytic precursors, depleting neutrophils with an anti-Ly6G antibody, and/or inhibiting CXCR2 signaling reduced neutrophil accumulation in the lungs and restored control of Mtb growth in *Nos2*^{-/-} mice (*77-79*). Elevated type I IFN signaling, which is another consistent correlate of progressive TB disease, may also promote poor disease outcomes in part by enhancing neutrophil recruitment and activation in an IFN receptor-dependent manner, and indirectly driving excessive NET formation (*11, 80*). This is consistent with an emerging role for excessive neutrophil recruitment and NET formation as a correlate of disease in bacterial pneumonia and other lung-related diseases besides TB (*81*). Therefore, rather than contributing a primarily antimicrobial function, enhanced neutrophil accumulation contributes to poor disease outcomes in TB, including a growth-permissive granuloma environment for Mtb that is replete with iron and lipid nutrients (*77, 79*).

While direct causation has not been established, high numbers of neutrophils, increased bacterial burden, and the liquefaction of caseous necrotic granulomas have been repeatedly associated with one another (*3, 11, 38*). Collectively, these studies support the conclusion that neutrophils play a prominent role in the progression of active TB disease, and that exploring therapeutics to counterbalance excessive neutrophil accumulation may improve bacterial control and reduce tissue damage in hosts with progressive TB disease.

IL-1

IL-1 (IL-1α and IL-1β) is generally considered to play an essential, host-protective role during Mtb infection. Most innate immune cells can produce IL-1α/β in a tightly-regulated manner, and many tissue cells constitutively express pro-IL-1α that can be released in a cleaved, active form during necrosis (*82*). Given that both are ligands for the same receptor, IL-1α and IL-1β primarily differ in their activation pathways, which require proteolytic processing to activate signaling activity (*82*). IL-1α and IL-1β are agonists of the receptor IL-1R1, which is expressed by a variety of cells including endothelial cells, epithelial cells, macrophages, and sometimes T cells (*82*). The downstream effects of IL-1 are wide-ranging and cell type dependent. For example, IL-1 has indirect roles in stimulating emergency differentiation of myeloid cells in bone marrow, enhancing immune cell recruitment by facilitating diapedesis and inducing chemokine expression, promoting neutrophil degranulation and NET formation, and activating platelet aggregation (*82*). IL-1 can also promote proliferation and polarization of Th17 cells, prime dendritic cell maturation, and has a direct role in stimulating expression of NFκB-dependent cytokines (*82*).

Evidence for the host-protective role of IL-1 in TB comes from the murine model, in which knocking out IL-1R1, IL-1α, or IL-1β on a C57BL/6J background is sufficient to generate

susceptibility to Mtb, including increased pulmonary bacterial burden, death by 40 days post-infection, and lung necrosis (*83, 84*). Receptor deficient (*Il1r1$^{-/-}$*) or double-deficient (*Il1a$^{-/-}$*, *Il1b$^{-/-}$*) mice exhibit higher bacterial burden than mice that lack either IL-1α or IL-1β alone, and compensatory production of these cytokines was not observed in single-deficient mice (*83*). These observations suggest that the functions of IL-1α and IL-1β in host resistance to Mtb are either non-redundant or at least complementary to one another (*83*). Intracellular cytokine staining identified pulmonary inflammatory monocyte-macrophage and DC populations that are sources of IL-1 at 3-4 weeks post-infection, while pulmonary neutrophils were negative for IL-1 (*83*). Surprisingly, IL-1 dependent control of Mtb replication occurs through a mechanism that is not cell-autonomous; IL-1R signaling in either non-hematopoietic or hematopoietic cells *in vivo* is necessary and sufficient to maintain host protection in a paracrine fashion (*85*).

There is currently limited understanding of the mechanisms through which IL-1α and IL-1β protect the host during Mtb infection. One beneficial role of IL-1 signaling identified in the murine model is preferential induction of the eicosanoid prostaglandin E$_2$ (PGE2) in the lung. In this regulatory network, the IL-1/PGE2 pathway suppresses type I IFN production (*86*). Downstream, suppressing type I IFN signaling is proposed to be host-protective by limiting induction of the immunosuppressive cytokine IL-10 and preventing excessive recruitment of susceptible macrophages and neutrophils to the lung (*86*). In plasma samples from TB patients, severe disease could be distinguished from mild disease based on reduced IL-1 and/or increased type I IFN signaling which was associated with a decreased balance of PGE2 relative to other eicosanoids (*86*). Indeed, IL-1R1 deficient mice are partially rescued during Mtb infection when type I IFN receptor signaling is disabled, confirming that enhanced type I IFN signaling is a driver of disease susceptibility when IL-1 signaling is defective (*86*). Susceptibility to Mtb in IL-1-

deficient mice was also partially rescued by therapeutic administration of PGE2, but it is not yet known what additional functions of IL-1 are necessary to achieve full rescue of host protection (*86*).

Briefly, there are multiple native mechanisms that counter-regulate IL-1 production and signaling. For example, type I IFNs and IFNγ have both been implicated in suppressing IL-1 in macrophages and/or DCs during Mtb infection (*78, 83, 86*). Type I IFNs can mediate this directly by suppressing IL-1 production by pulmonary myeloid cells, or indirectly by inducing IL-10 or upregulating the competitive IL-1R1 antagonist, IL-1Ra (*9, 83*). Importantly, the balance between IL-1Ra and IL-1 influences the overall impact this has on IL-1 signaling, and can be influenced by bacterial load or the time post-infection (*9*). The decoy receptor IL-1R2 can also help balance the potent pro-inflammatory response of IL-1 (*82*). In some contexts, unbalanced IL-1 has been found to promote immunopathology. As discussed above, in the context of nitric oxide deficiency, increased IL-1 drives detrimental inflammation independent of bacterial burden, and unregulated IL-1 is associated with neutrophil recruitment and neutrophil-driven pathology (*77, 78*). Although plasma and bronchoalveolar lavage samples have different relationships to TB disease status, IL-1β levels were increased in lung samples from active TB patients compared to healthy controls (*86, 87*). Overall, IL-1, PGE2, type I IFN, and IL-10 have been assigned a complex role within a "counter-regulatory loop" at the center of host resistance to Mtb (Figure 1.2). Many details of how the balance of IL-1 signaling functions in this complex network, especially during chronic infection and in humans, have not yet been characterized.
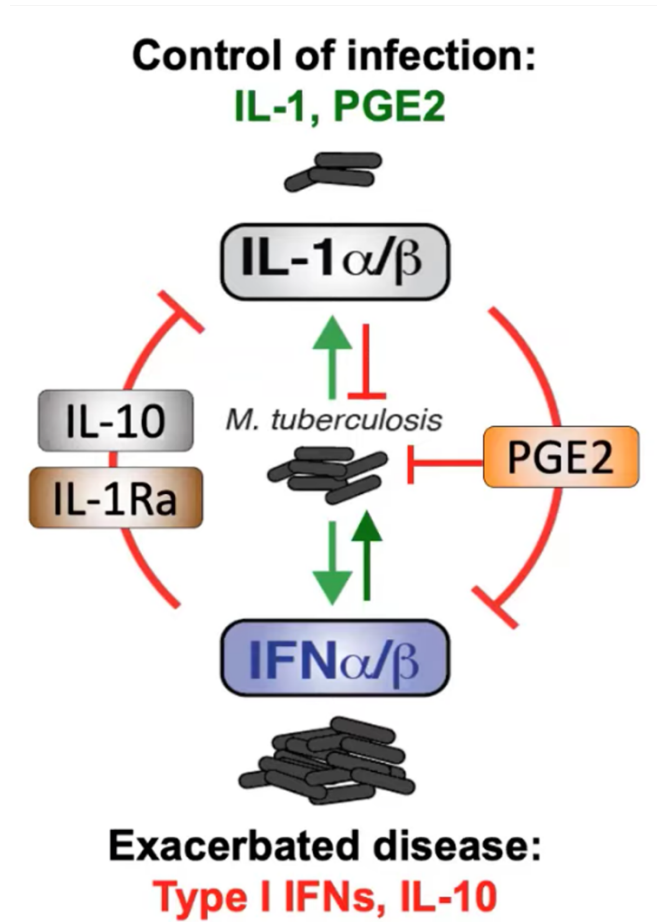
Figure 1.2 Counter-regulation of mediators at the center of infection control in TB. Adapted from (*88*).

1.2 Tuberculosis treatment and challenges to control measures

1.2.1 Introduction

Annually ~10 million people are afflicted with TB and ~1.4 million people die from TB disease (*89*). The onset of the COVID-19 pandemic has complicated TB diagnosis and reporting since 2020 and created setbacks in TB control measures, evidenced by a rise in TB deaths for the first time in over a decade (*90*). Given the current absence of a highly effective vaccine against TB, antibiotics remain an essential tool to reduce TB transmission and mortality (*91*). Over the last 20 years, approximately 50 million people worldwide were successfully treated with front-line TB antibiotic regimens (*89*). Despite this success, TB antibiotic regimens still have substantial drawbacks, and ongoing efforts to identify new antibiotics that more effectively target Mtb during infection remain important.

1.2.2 Current antibiotic regimens and their drawbacks

It is useful to divide drug treatment regimens for TB into two categories: treatment for drug-sensitive TB and treatment for drug-resistant TB. The standard treatment regimen for drug-susceptible TB requires a 2 month intensive phase with the front-line drugs isoniazid (INH), rifampicin (RIF), pyrazinamide (PZA), and ethambutol (EMB), followed by a 4 month continuation phase with INH and RIF alone (*92*). Drug-susceptible TB treatment has an ~85% success rate (*89*). For drug-susceptible LTBI, shorter 3 to 4 month courses including only INH and RIF/rifapentine are acceptable. Drug-resistant TB treatment is successful much less often (~56% success rate) (*89*). Treatment for drug-resistant TB is universally more complicated, lengthy, and side-effect prone than treatment for drug-susceptible TB (*92*). Multi-drug resistant TB (MDR-TB) is defined by resistance to both RIF and INH, while extensively drug-resistant TB (XDR-TB) is

additionally resistant to any fluoroquinolone and at least one injectable second-line drug (*92*). Globally, an average of 3.4% of new cases and 18% of previously treated TB cases are classified as MDR-TB or RIF-resistant TB, and approximately 6.2% of MDR-TB cases are also extensively drug resistant (*89*). Because the most safe and effective front-line TB antibiotics are rendered ineffective in these cases, treatment for MDR-TB requires healthcare providers to follow a stepwise approach to generate complex regimens composed of lower-tier drugs. When possible, this is guided by drug-susceptibility testing. A regimen composed of at least four likely-active drugs pulled from the highest-efficacy tier possible in each case is given for a minimum of 8 months, followed by a continuation phase of 12-18 months (*92*). MDR-TB regimens are impractical and more prone to generate toxic side-effects, such that ~15% of patients default on their treatment; this perpetuates opportunities for further drug-resistant strains of Mtb to develop and spread (*89*). Bacterial targets of various clinically relevant TB antibiotics are summarized in Figure 1.3. Although the newly-developed Nix-TB regimen (bedaquiline, pretomanid, and linezolid for 6 months) conferred a positive outcome in 90% of MDR-TB patients studied, more than half also experienced severe adverse events, usually derived from linezolid (*93*). While a regimen successfully combining three oral drugs like this one is a huge improvement over past options for MDR-TB, this illustrates why identifying new antibiotics that have better safety profiles and/or that can shorten this regimen further to preclude development of side effects continues to be a priority.

Current TB treatment regimens have downsides that are driving the search for new TB antibiotics. As indicated above, TB treatment is long and prone to causing side-effects. Even when treatment is completed, insufficient bacterial clearance is thought to be partly responsible for recurrent TB disease in a small proportion (~1-9%) of people within 1-2 years (*6, 94, 95*). Recent

efforts to shorten treatment have been associated with an increase in the relapse rate, and there is no clinical protocol in place to predict which patients could achieve durable cure with a shorter regimen (*94*). As discussed below, these issues are both related to adaptations of Mtb that are thought to generate populations of the bacteria that are killed more slowly or require higher concentrations of antibiotic exposure before they are eliminated. Different antibiotics also have different abilities to penetrate mature granulomas, potentially creating local regions of subinhibitory concentrations or monotherapy despite administration of multiple drugs (*96*). This has led some groups to postulate that host-directed therapies intended to "loosen" the peripheral granuloma structure will enhance access of antibiotics or immune cells to the bacterium and facilitate cure (*63, 97, 98*). Individual granulomas exhibit dynamic and heterogeneous responses early during antibiotic treatment; within a single host, some granulomas improve but unresponsive, worsened, or new lesions are observed simultaneously via ^{18}F-FDG PET-CT imaging (*5*). Even after treatment is completed and Mtb is no longer culturable from sputum samples, it is common for lung lesions to persist and patients to present post-TB pulmonary impairment (*6, 99, 100*). Both actively inflamed lesions and Mtb mRNA in bronchoalveolar lavage samples were commonly detectable at the end of successful treatment and 1 year afterwards, and this was not exclusive to patients who developed relapsed TB (*6*). This demonstrates the dual challenge of durably eliminating Mtb from the body and identifying therapies that promote lesion healing during or after treatment. Therefore, major goals of TB antibiotic research include generation of new regimens composed of drugs with novel targets that are active against drug-resistant TB, and/or introduction of new drugs that can shorten the duration of treatment by facilitating durable bacterial clearance faster.

1.2.3   *M. tuberculosis* adaptations that challenge antibiotic treatment

Features of Mtb that challenge antibiotic treatment can be broadly divided into three categories: drug resistance, drug persistence, and drug tolerance. TB treatment requires combination therapy composed of antibiotics with multiple mechanisms of action to limit the evolution of drug resistance and to target multiple differentially-susceptible subpopulations of bacteria. Drug resistance is defined by the heritable ability of a bacterial strain to grow under exposure to concentrations of an antibiotic above the minimum inhibitory concentration (MIC) (*101*). This is retained despite long periods of exposure at the MIC, or re-exposure to the drug. In Mtb, drug resistance is perpetuated by vertically transmitted chromosomal mutations, rather than horizontal acquisition of resistance plasmids (*102*). Mechanisms of acquired resistance in Mtb include those that confer modifications to the drug target, overexpression of the drug target, reduced pro-drug activation, cleavage/chemical modifications of the antibiotic in the cell, or stable induction of efflux pumps (*102*). Intrinsic features of mycobacteria like their relatively impenetrable cell wall and slow growth rate also contribute to underlying drug resistance.

Distinctions between tolerance and persistence are often blurred. Both are distinguished from drug resistance by the acquisition of phenotypic changes during antibiotic exposure, in the absence of stable genetic changes or a change in the MIC (*101*). Persistence is used to describe a small subpopulation of bacteria within a given genotype that survive exposure to a bactericidal antibiotic at or above the MIC, despite the majority of the population being killed (*101, 103*). When surviving cells are expanded in the absence of antibiotic and then re-exposed, they exhibit the same phenotype. By definition, persistence implies that the underlying mechanisms are pre-existing or inducible differences in a subpopulation of the bacteria that confer survival compared to the majority of the population that is susceptible. Thus, examples of persistence driving mechanisms

in Mtb are typically linked with phenotypic heterogeneity in cellular processes within the population. Suggested mechanisms in Mtb include asymmetrical cell division, stochastic expression of an enzyme required to convert a pro-drug into its active form, or stochastic overexpression of the drug target (*103*).

By contrast, tolerance describes a phenotypic trait present in many or most of the cells in a population that confers survival during transient exposure to an antibiotic at or above the MIC. This is typically associated with exposure to alternative environmental conditions that realign metabolism and halt the net growth rate of the bacterial population, rendering the target of an antibiotic less vital for bacterial survival (*101, 103*). Numerous conditions that promote growth arrest and antibiotic tolerance in Mtb have been described, including acidic pH, nutrient deprivation, oxygen limitation, and exposure to nitrosative stress (*103*). Importantly, Mtb tolerance to multiple TB antibiotics was enhanced within activated macrophages relative to resting cells isolated from infected mice, and was most strongly associated with nitrosative stress (*104*). Evidence of drug tolerance has been observed in other TB animal models and in human samples, and is thought to be associated with the lipid-rich caseum (*38, 94, 103*). Mtb adopts realignments in intersecting physiological pathways in response to host or antibiotic stress signals, conferring cross-tolerance to both environmental and antibiotic pressures. Generally, these include reduced growth rate, decreased protein biosynthesis, a shift away from aerobic respiration, maintenance of redox and ATP homeostasis, upregulation of lipid anabolism and storage, promotion of cell wall thickening, and transient upregulation of efflux pumps (*105*). Drug-specific tolerance mechanisms also exist, and the diverse mechanisms underlying tolerance are tightly linked to the conditions under which tolerance is induced (*103, 105*).
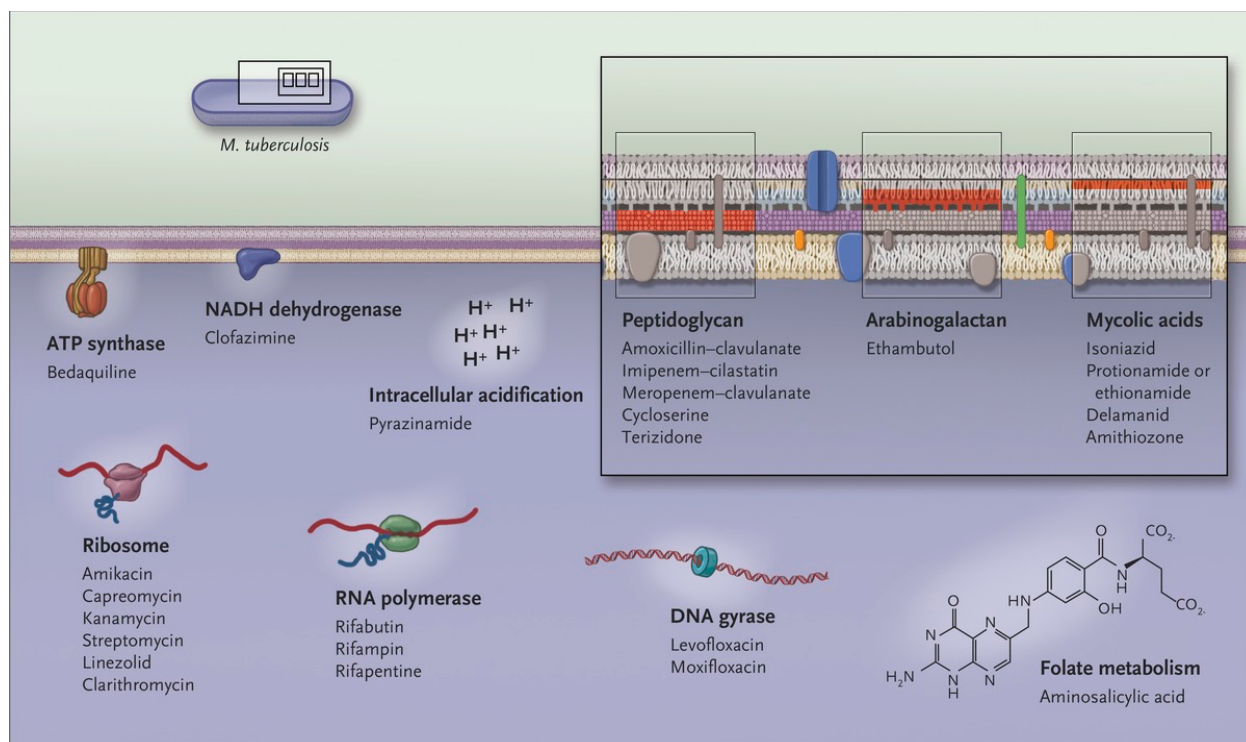
Figure 1.3 Bacterial targets of clinically relevant TB antibiotics. Isoniazid (INH) is a pro-drug that is converted to isonicotinoyl-NAD, which inhibits mycolic acid biosynthesis. Rifampicin (RIF) binds the RNA polymerase and inhibits RNA transcription. Pyrazinamide (PZA) is a pro-drug that is converted to pyrazinoic acid, which has multiple downstream effects in the presence of low pH conditions via acidification of the cytoplasm and disruption of the proton motive force. Ethambutol (EMB) targets the arabinosyl transferase enzyme to inhibit arabinogalactan and lipoarabinomannan synthesis. Bedaquiline (BDQ) inhibits the ATP synthase enzyme, reducing ATP synthesis. Pretomanid is a pro-drug that has complex effects on replicating and hypoxic Mtb, including halting mycolic acid biosynthesis and donating nitric oxide which disrupts electron shuttling in the electron transport chain. Linezolid binds to 23S rRNA in the catalytic site of the 50S ribosome, inhibiting protein translation. Reproduced with permission from (*94*), Copyright Massachusetts Medical Society.

1.3 References

1.   A. J. Pagan, L. Ramakrishnan, The Formation and Function of Granulomas. *Annu Rev Immunol* **36**, 639-665 (2018).

2.   A. M. Cadena, S. M. Fortune, J. L. Flynn, Heterogeneity in tuberculosis. *Nat Rev Immunol* **17**, 691-702 (2017).

3.   G. Canetti, *The Tubercle Bacillus*. (Springer Publishing Company, New York, 1955).

4.   A. Lenaerts, C. E. Barry, 3rd, V. Dartois, Heterogeneity in tuberculosis pathology, microenvironments and therapeutic responses. *Immunological Reviews* **264**, 288-307 (2015).

5.   Y. L. Xie, V. R. de Jager, R. Y. Chen, L. E. Dodd, P. Paripati, L. E. Via, D. Follmann, J. Wang, K. Lumbard, S. Lahouar, S. T. Malherbe, J. Andrews, X. Yu, L. C. Goldfeder, Y. Cai, K. Arora, A. G. Loxton, N. Vanker, M. Duvenhage, J. Winter, T. Song, G. Walzl, A. H. Diacon, C. E. Barry, 3rd, Fourteen-day PET/CT imaging to monitor drug combination activity in treated individuals with tuberculosis. *Science translational medicine* **13**, (2021).

6.   S. T. Malherbe, S. Shenai, K. Ronacher, A. G. Loxton, G. Dolganov, M. Kriel, T. Van, R. Y. Chen, J. Warwick, L. E. Via, T. Song, M. Lee, G. Schoolnik, G. Tromp, D. Alland, C. E. Barry, 3rd, J. Winter, G. Walzl, T. B. B. C. Catalysis, L. Lucas, G. V. Spuy, K. Stanley, L. Thiart, B. Smith, N. Du Plessis, C. G. Beltran, E. Maasdorp, A. Ellmann, H. Choi, J. Joh, L. E. Dodd, B. Allwood, C. Koegelenberg, M. Vorster, S. Griffith-Richards, Persisting positron emission tomography lesion activity and Mycobacterium tuberculosis mRNA after tuberculosis cure. *Nat Med* **22**, 1094-1100 (2016).

7.   E. R. Driver, G. J. Ryan, D. R. Hoff, S. M. Irwin, R. J. Basaraba, I. Kramnik, A. J. Lenaerts, Evaluation of a mouse model of necrotic granuloma formation using C3HeB/FeJ mice for

testing of drugs against Mycobacterium tuberculosis. *Antimicrobial agents and chemotherapy* **56**, 3181-3195 (2012).

8.   I. Kramnik, W. F. Dietrich, P. Demant, B. R. Bloom, Genetic control of resistance to experimental infection with virulent Mycobacterium tuberculosis. *Proceedings of the National Academy of Sciences of the United States of America* **97**, 8560-8565 (2000).

9.   D. X. Ji, L. H. Yamashiro, K. J. Chen, N. Mukaida, I. Kramnik, K. H. Darwin, R. E. Vance, Type I interferon-driven susceptibility to Mycobacterium tuberculosis is mediated by IL-1Ra. *Nature microbiology* **4**, 2128-2135 (2019).

10.   L. Moreira-Teixeira, O. Tabone, C. M. Graham, A. Singhania, E. Stavropoulos, P. S. Redford, P. Chakravarty, S. L. Priestnall, A. Suarez-Bonnet, E. Herbert, K. D. Mayer-Barber, A. Sher, K. L. Fonseca, J. Sousa, B. Ca, R. Verma, P. Haldar, M. Saraiva, A. O'Garra, Mouse transcriptome reveals potential signatures of protection and pathogenesis in human tuberculosis. *Nature immunology* **21**, 464-476 (2020).

11.   L. Moreira-Teixeira, P. J. Stimpson, E. Stavropoulos, S. Hadebe, P. Chakravarty, M. Ioannou, I. V. Aramburu, E. Herbert, S. L. Priestnall, A. Suarez-Bonnet, J. Sousa, K. L. Fonseca, Q. Wang, S. Vashakidze, P. Rodriguez-Martinez, C. Vilaplana, M. Saraiva, V. Papayannopoulos, A. O'Garra, Type I IFN exacerbates disease in tuberculosis-susceptible mice by inducing neutrophil-mediated lung inflammation and NETosis. *Nat Commun* **11**, 5566 (2020).

12.   M. Ahmed, S. Thirunavukkarasu, B. A. Rosa, K. A. Thomas, S. Das, J. Rangel-Moreno, L. Lu, S. Mehra, S. K. Mbandi, L. B. Thackray, M. S. Diamond, K. M. Murphy, T. Means, J. Martin, D. Kaushal, T. J. Scriba, M. Mitreva, S. A. Khader, Immune correlates of

tuberculosis disease and risk translate across species. *Science translational medicine* **12**, (2020).

13.   C. M. Smith, M. K. Proulx, R. Lai, M. C. Kiritsy, T. A. Bell, P. Hock, F. Pardo-Manuel de Villena, M. T. Ferris, R. E. Baker, S. M. Behar, C. M. Sassetti, Functionally Overlapping Variants Control Tuberculosis Susceptibility in Collaborative Cross Mice. *mBio* **10**, (2019).

14.   C. R. Plumlee, F. J. Duffy, B. H. Gern, J. L. Delahaye, S. B. Cohen, C. R. Stoltzfus, T. R. Rustad, S. G. Hansen, M. K. Axthelm, L. J. Picker, J. D. Aitchison, D. R. Sherman, V. V. Ganusov, M. Y. Gerner, D. E. Zak, K. B. Urdahl, Ultra-low Dose Aerosol Infection of Mice with Mycobacterium tuberculosis More Closely Models Human Tuberculosis. *Cell Host Microbe* **29**, 68-82 e65 (2021).

15.   J. L. Flynn, H. P. Gideon, J. T. Mattila, P. L. Lin, Immunology studies in non-human primate models of tuberculosis. *Immunol Rev* **264**, 60-73 (2015).

16.   M. R. Cronan, D. M. Tobin, Fit for consumption: zebrafish as a model for tuberculosis. *Dis Model Mech* **7**, 777-784 (2014).

17.   J. B. Torrelles, L. S. Schlesinger, Integrating Lung Physiology, Immunology, and Tuberculosis. *Trends Microbiol* **25**, 688-697 (2017).

18.   S. B. Cohen, B. H. Gern, J. L. Delahaye, K. N. Adams, C. R. Plumlee, J. K. Winkler, D. R. Sherman, M. Y. Gerner, K. B. Urdahl, Alveolar Macrophages Provide an Early Mycobacterium tuberculosis Niche and Initiate Dissemination. *Cell Host Microbe* **24**, 439-446.e434 (2018).

19.   L. Huang, E. V. Nazarova, S. Tan, Y. Liu, D. G. Russell, Growth of Mycobacterium tuberculosis in vivo segregates with host macrophage metabolism and ontogeny. *J Exp Med* **215**, 1135-1152 (2018).

20.   I. M. Orme, R. J. Basaraba, The formation of the granuloma in tuberculosis infection. *Seminars in immunology* **26**, 601-609 (2014).

21.   W. P. Gill, N. S. Harik, M. R. Whiddon, R. P. Liao, J. E. Mittler, D. R. Sherman, A replication clock for Mycobacterium tuberculosis. *Nat Med* **15**, 211-214 (2009).

22.   A. C. Rothchild, G. S. Olson, J. Nemeth, L. M. Amon, D. Mai, E. S. Gold, A. H. Diercks, A. Aderem, Alveolar macrophages generate a noncanonical NRF2-driven transcriptional response to Mycobacterium tuberculosis in vivo. *Sci Immunol* **4**, (2019).

23.   J. Lee, S. Boyce, J. Powers, C. Baer, C. M. Sassetti, S. M. Behar, CD11cHi monocyte-derived macrophages are a major cellular compartment infected by Mycobacterium tuberculosis. *PLoS Pathog* **16**, e1008621 (2020).

24.   R. Domingo-Gonzalez, O. Prince, A. Cooper, S. A. Khader, Cytokines and Chemokines in Mycobacterium tuberculosis Infection. *Microbiol Spectr* **4**, (2016).

25.   A. O'Garra, P. S. Redford, F. W. McNab, C. I. Bloom, R. J. Wilkinson, M. P. Berry, The immune response in tuberculosis. *Annu Rev Immunol* **31**, 475-527 (2013).

26.   A. J. Wolf, B. Linas, G. J. Trevejo-Nunez, E. Kincaid, T. Tamura, K. Takatsu, J. D. Ernst, Mycobacterium tuberculosis infects dendritic cells with high frequency and impairs their function in vivo. *J Immunol* **179**, 2509-2519 (2007).

27.   A. J. Wolf, L. Desvignes, B. Linas, N. Banaiee, T. Tamura, K. Takatsu, J. D. Ernst, Initiation of the adaptive immune response to Mycobacterium tuberculosis depends on antigen production in the local lymph node, not the lungs. *J Exp Med* **205**, 105-115 (2008).

28. B. M. Saunders, A. A. Frank, I. M. Orme, A. M. Cooper, CD4 is required for the development of a protective granulomatous response to pulmonary tuberculosis. *Cellular immunology* **216**, 65-72 (2002).

29. H. P. Gideon, J. Phuah, A. J. Myers, B. D. Bryson, M. A. Rodgers, M. T. Coleman, P. Maiello, T. Rutledge, S. Marino, S. M. Fortune, D. E. Kirschner, P. L. Lin, J. L. Flynn, Variability in tuberculosis granuloma T cell responses exists, but a balance of pro- and anti-inflammatory cytokines is associated with sterilization. *PLoS Pathog* **11**, e1004603 (2015).

30. H. P. Gideon, T. K. Hughes, M. H. Wadsworth, A. A. Tu, T. M. Gierahn, J. M. Peters, F. F. Hopkins, J.-R. Wei, C. Kummerlowe, N. L. Grant, K. Nargan, J. Phuah, H. J. Borish, P. Maiello, A. G. White, C. G. Winchell, S. K. Nyquist, S. K. C. Ganchua, A. Myers, K. V. Patel, C. L. Ameel, C. T. Cochran, S. Ibrahim, J. A. Tomko, L. J. Frye, J. M. Rosenberg, A. Shih, M. Chao, C. A. Scanga, J. Ordovas-Montanes, B. Berger, J. T. Mattila, R. Madansein, J. C. Love, P. L. Lin, A. Leslie, S. M. Behar, B. Bryson, J. L. Flynn, S. M. Fortune, A. K. Shalek, Multimodal profiling of lung granulomas reveals cellular correlates of tuberculosis control. *bioRxiv* **10.24.352492**, (2021).

31. P. L. Lin, T. Rutledge, A. M. Green, M. Bigbee, C. Fuhrman, E. Klein, J. L. Flynn, CD4 T cell depletion exacerbates acute Mycobacterium tuberculosis while reactivation of latent infection is dependent on severity of tissue depletion in cynomolgus macaques. *AIDS Res Hum Retroviruses* **28**, 1693-1702 (2012).

32. P. L. Lin, J. L. Flynn, CD8 T cells and Mycobacterium tuberculosis infection. *Seminars in immunopathology* **37**, 239-249 (2015).

33. P. J. Maglione, J. Chan, How B cells shape the immune response against Mycobacterium tuberculosis. *Eur J Immunol* **39**, 676-686 (2009).

34. C. M. McClean, D. M. Tobin, Macrophage form, function, and phenotype in mycobacterial infection: lessons from tuberculosis and other diseases. *Pathogens and disease* **74**, (2016).

35. V. Guerrini, M. L. Gennaro, Foam Cells: One Size Doesn't Fit All. *Trends Immunol* **40**, 1163-1179 (2019).

36. P. Peyron, J. Vaubourgeix, Y. Poquet, F. Levillain, C. Botanch, F. Bardou, M. Daffe, J. F. Emile, B. Marchou, P. J. Cardona, C. de Chastellier, F. Altare, Foamy macrophages from tuberculous patients' granulomas constitute a nutrient-rich reservoir for M. tuberculosis persistence. *PLoS pathogens* **4**, e1000204 (2008).

37. J. Daniel, H. Maamar, C. Deb, T. D. Sirakova, P. E. Kolattukudy, Mycobacterium tuberculosis uses host triacylglycerol to accumulate lipid droplets and acquires a dormancy-like phenotype in lipid-loaded macrophages. *PLoS pathogens* **7**, e1002093 (2011).

38. J. P. Sarathy, V. Dartois, Caseum: a Niche for Mycobacterium tuberculosis Drug-Tolerant Persisters. *Clinical microbiology reviews* **33**, (2020).

39. V. Guerrini, B. Prideaux, L. Blanc, N. Bruiners, R. Arrigucci, S. Singh, H. P. Ho-Liang, H. Salamon, P. Y. Chen, K. Lakehal, S. Subbian, P. O'Brien, L. E. Via, C. E. Barry, 3rd, V. Dartois, M. L. Gennaro, Storage lipid studies in tuberculosis reveal that foam cell biogenesis is disease-specific. *PLoS Pathog* **14**, e1007223 (2018).

40. M. J. Kim, H. C. Wainwright, M. Locketz, L. G. Bekker, G. B. Walther, C. Dittrich, A. Visser, W. Wang, F. F. Hsu, U. Wiehart, L. Tsenova, G. Kaplan, D. G. Russell, Caseation

of human tuberculosis granulomas correlates with elevated host lipid metabolism. *EMBO Molecular Medicine* **2**, 258-274 (2010).

41. E. Kondo, T. Murohashi, Esterification of tissue cholesterol with fatty acids in the lungs of tuberculous mice. *Japanese journal of medical science & biology* **24**, 345-356 (1971).

42. N. J. Garton, S. J. Waddell, A. L. Sherratt, S. M. Lee, R. J. Smith, C. Senner, J. Hinds, K. Rajakumar, R. A. Adegbola, G. S. Besra, P. D. Butcher, M. R. Barer, Cytological and transcript analyses reveal fat and lazy persister-like bacilli in tuberculous sputum. *PLoS Medicine* **5**, e75 (2008).

43. V. Singh, S. Jamwal, R. Jain, P. Verma, R. Gokhale, K. V. Rao, Mycobacterium tuberculosis-driven targeted recalibration of macrophage lipid homeostasis promotes the foamy phenotype. *Cell Host Microbe* **12**, 669-681 (2012).

44. M. Knight, J. Braverman, K. Asfaha, K. Gronert, S. Stanley, Lipid droplet formation in Mycobacterium tuberculosis infected macrophages requires IFN-gamma/HIF-1alpha signaling and supports host defense. *PLoS Pathog* **14**, e1006874 (2018).

45. D. M. Lewinsohn, M. K. Leonard, P. A. LoBue, D. L. Cohn, C. L. Daley, E. Desmond, J. Keane, D. A. Lewinsohn, A. M. Loeffler, G. H. Mazurek, R. J. O'Brien, M. Pai, L. Richeldi, M. Salfinger, T. M. Shinnick, T. R. Sterling, D. M. Warshauer, G. L. Woods, Official American Thoracic Society/Infectious Diseases Society of America/Centers for Disease Control and Prevention Clinical Practice Guidelines: Diagnosis of Tuberculosis in Adults and Children. *Clin Infect Dis* **64**, 111-115 (2017).

46. P. K. Drain, K. L. Bajema, D. Dowdy, K. Dheda, K. Naidoo, S. G. Schumacher, S. Ma, E. Meermeier, D. M. Lewinsohn, D. R. Sherman, Incipient and Subclinical Tuberculosis: a

Clinical Review of Early Stages and Progression of Infection. *Clinical microbiology reviews* **31**, (2018).

47. P. L. Lin, J. L. Flynn, Understanding latent tuberculosis: a moving target. *J Immunol* **185**, 15-22 (2010).

48. E. Vynnycky, P. E. Fine, The natural history of tuberculosis: the implications of age-dependent risks of disease and the role of reinfection. *Epidemiol Infect* **119**, 183-201 (1997).

49. J. R. Andrews, F. Noubary, R. P. Walensky, R. Cerda, E. Losina, C. R. Horsburgh, Risk of progression to active tuberculosis following reinfection with Mycobacterium tuberculosis. *Clin Infect Dis* **54**, 784-791 (2012).

50. M. Pai, M. A. Behr, D. Dowdy, K. Dheda, M. Divangahi, C. C. Boehme, A. Ginsberg, S. Swaminathan, M. Spigelman, H. Getahun, D. Menzies, M. Raviglione, Tuberculosis. *Nature reviews Disease primers* **2**, 16076 (2016).

51. M. A. Behr, P. H. Edelstein, L. Ramakrishnan, Revisiting the timetable of tuberculosis. *BMJ* **362**, k2738 (2018).

52. C. E. Barry, 3rd, H. I. Boshoff, V. Dartois, T. Dick, S. Ehrt, J. Flynn, D. Schnappinger, R. J. Wilkinson, D. Young, The spectrum of latent tuberculosis: rethinking the biology and intervention strategies. *Nat Rev Microbiol* **7**, 845-855 (2009).

53. P. L. Lin, C. B. Ford, M. T. Coleman, A. J. Myers, R. Gawande, T. Ioerger, J. Sacchettini, S. M. Fortune, J. L. Flynn, Sterilization of granulomas is common in active and latent tuberculosis despite within-host variability in bacterial killing. *Nat Med* **20**, 75-79 (2014).

54. S. Subbian, L. Tsenova, M. J. Kim, H. C. Wainwright, A. Visser, N. Bandyopadhyay, J. S. Bader, P. C. Karakousis, G. B. Murrmann, L. G. Bekker, D. G. Russell, G. Kaplan, Lesion-

Specific Immune Response in Granulomas of Patients with Pulmonary Tuberculosis: A Pilot Study. *PloS one* **10**, e0132249 (2015).

55.   M. T. Coleman, P. Maiello, J. Tomko, L. J. Frye, D. Fillmore, C. Janssen, E. Klein, P. L. Lin, Early Changes by (18)Fluorodeoxyglucose positron emission tomography coregistered with computed tomography predict outcome after Mycobacterium tuberculosis infection in cynomolgus macaques. *Infect Immun* **82**, 2400-2404 (2014).

56.   C. J. Martin, A. M. Cadena, V. W. Leung, P. L. Lin, P. Maiello, N. Hicks, M. R. Chase, J. L. Flynn, S. M. Fortune, Digitally Barcoding Mycobacterium tuberculosis Reveals In Vivo Infection Dynamics in the Macaque Model of Tuberculosis. *mBio* **8**, (2017).

57.   H. P. Gideon, J. A. Skinner, N. Baldwin, J. L. Flynn, P. L. Lin, Early Whole Blood Transcriptional Signatures Are Associated with Severity of Lung Inflammation in Cynomolgus Macaques with Mycobacterium tuberculosis Infection. *J Immunol* **197**, 4817-4828 (2016).

58.   D. E. Zak, A. Penn-Nicholson, T. J. Scriba, E. Thompson, S. Suliman, L. M. Amon, H. Mahomed, M. Erasmus, W. Whatney, G. D. Hussey, D. Abrahams, F. Kafaar, T. Hawkridge, S. Verver, E. J. Hughes, M. Ota, J. Sutherland, R. Howe, H. M. Dockrell, W. H. Boom, B. Thiel, T. H. M. Ottenhoff, H. Mayanja-Kizza, A. C. Crampin, K. Downing, M. Hatherill, J. Valvo, S. Shankar, S. K. Parida, S. H. E. Kaufmann, G. Walzl, A. Aderem, W. A. Hanekom, Acs, G. C. c. s. groups, A blood RNA signature for tuberculosis disease risk: a prospective cohort study. *Lancet* **387**, 2312-2322 (2016).

59.   M. P. Berry, C. M. Graham, F. W. McNab, Z. Xu, S. A. Bloch, T. Oni, K. A. Wilkinson, R. Banchereau, J. Skinner, R. J. Wilkinson, C. Quinn, D. Blankenship, R. Dhawan, J. J. Cush, A. Mejias, O. Ramilo, O. M. Kon, V. Pascual, J. Banchereau, D. Chaussabel, A.

O'Garra, An interferon-inducible neutrophil-driven blood transcriptional signature in human tuberculosis. *Nature* **466**, 973-977 (2010).

60.   M. K. Niazi, N. Dhulekar, D. Schmidt, S. Major, R. Cooper, C. Abeijon, D. M. Gatti, I. Kramnik, B. Yener, M. Gurcan, G. Beamer, Lung necrosis and neutrophils reflect common pathways of susceptibility to Mycobacterium tuberculosis in genetically diverse, immune-competent mice. *Dis Model Mech* **8**, 1141-1153 (2015).

61.   K. D. Mayer-Barber, A. Sher, Cytokine and lipid mediator networks in tuberculosis. *Immunol Rev* **264**, 264-275 (2015).

62.   J. Holbrook, S. Lara-Reyna, H. Jarosz-Griffiths, M. McDermott, Tumour necrosis factor signalling in health and disease. *F1000Res* **8**, (2019).

63.   M. A. Matty, F. J. Roca, M. R. Cronan, D. M. Tobin, Adventures within the speckled band: heterogeneity, angiogenesis, and balanced inflammation in the tuberculous granuloma. *Immunol Rev* **264**, 276-287 (2015).

64.   J. Keane, S. Gershon, R. P. Wise, E. Mirabile-Levens, J. Kasznica, W. D. Schwieterman, J. N. Siegel, M. M. Braun, Tuberculosis associated with infliximab, a tumor necrosis factor alpha-neutralizing agent. *N Engl J Med* **345**, 1098-1104 (2001).

65.   P. L. Lin, A. Myers, L. Smith, C. Bigbee, M. Bigbee, C. Fuhrman, H. Grieser, I. Chiosea, N. N. Voitenek, S. V. Capuano, E. Klein, J. L. Flynn, Tumor necrosis factor neutralization results in disseminated disease in acute and latent Mycobacterium tuberculosis infection with normal granuloma structure in a cynomolgus macaque model. *Arthritis and rheumatism* **62**, 340-350 (2010).

66.   J. D. MacMicking, Cell-autonomous effector mechanisms against mycobacterium tuberculosis. *Cold Spring Harb Perspect Med* **4**, (2014).

67.   H. M. Algood, P. L. Lin, J. L. Flynn, Tumor necrosis factor and chemokine interactions in the formation and maintenance of granulomas in tuberculosis. *Clin Infect Dis* **41 Suppl 3**, S189-193 (2005).

68.   D. M. Tobin, F. J. Roca, S. F. Oh, R. McFarland, T. W. Vickery, J. P. Ray, D. C. Ko, Y. Zou, N. D. Bang, T. T. Chau, J. C. Vary, T. R. Hawn, S. J. Dunstan, J. J. Farrar, G. E. Thwaites, M. C. King, C. N. Serhan, L. Ramakrishnan, Host genotype-specific therapies can optimize the inflammatory response to mycobacterial infections. *Cell* **148**, 434-446 (2012).

69.   K. Mohareer, S. Asalla, S. Banerjee, Cell death at the cross roads of host-pathogen interaction in Mycobacterium tuberculosis infection. *Tuberculosis (Edinb)* **113**, 99-121 (2018).

70.   A. Craig, J. Mai, S. Cai, S. Jeyaseelan, Neutrophil recruitment to the lungs during bacterial pneumonia. *Infect Immun* **77**, 568-575 (2009).

71.   K. D. Mayer-Barber, D. L. Barber, Innate and Adaptive Cellular Immune Responses to Mycobacterium tuberculosis Infection. *Cold Spring Harb Perspect Med* **5**, (2015).

72.   S. Y. Eum, J. H. Kong, M. S. Hong, Y. J. Lee, J. H. Kim, S. H. Hwang, S. N. Cho, L. E. Via, C. E. Barry, 3rd, Neutrophils are the predominant infected phagocytic cells in the airways of patients with active pulmonary TB. *Chest* **137**, 122-128 (2010).

73.   R. Gopal, L. Monin, D. Torres, S. Slight, S. Mehra, K. C. McKenna, B. A. Fallert Junecko, T. A. Reinhart, J. Kolls, R. Baez-Saldana, A. Cruz-Lagunas, T. S. Rodriguez-Reyna, N. P. Kumar, P. Tessier, J. Roth, M. Selman, E. Becerril-Villanueva, J. Baquera-Heredia, B. Cumming, V. O. Kasprowicz, A. J. Steyn, S. Babu, D. Kaushal, J. Zuniga, T. Vogl, J. Rangel-Moreno, S. A. Khader, S100A8/A9 proteins mediate neutrophilic inflammation

and lung pathology during tuberculosis. *Am J Respir Crit Care Med* **188**, 1137-1146 (2013).

74. J. P. Huynh, C. C. Lin, J. M. Kimmey, N. N. Jarjour, E. A. Schwarzkopf, T. R. Bradstreet, I. Shchukina, O. Shpynov, C. T. Weaver, R. Taneja, M. N. Artyomov, B. T. Edelson, C. L. Stallings, Bhlhe40 is an essential repressor of IL-10 during Mycobacterium tuberculosis infection. *J Exp Med* **215**, 1823-1838 (2018).

75. J. M. Kimmey, J. P. Huynh, L. A. Weiss, S. Park, A. Kambal, J. Debnath, H. W. Virgin, C. L. Stallings, Unique role for ATG5 in neutrophil-mediated immunopathology during M. tuberculosis infection. *Nature* **528**, 565-569 (2015).

76. S. Nair, J. P. Huynh, V. Lampropoulou, E. Loginicheva, E. Esaulova, A. P. Gounder, A. C. M. Boon, E. A. Schwarzkopf, T. R. Bradstreet, B. T. Edelson, M. N. Artyomov, C. L. Stallings, M. S. Diamond, Irg1 expression in myeloid cells prevents immunopathology during M. tuberculosis infection. *J Exp Med* **215**, 1035-1045 (2018).

77. B. B. Mishra, R. R. Lovewell, A. J. Olive, G. Zhang, W. Wang, E. Eugenin, C. M. Smith, J. Y. Phuah, J. E. Long, M. L. Dubuke, S. G. Palace, J. D. Goguen, R. E. Baker, S. Nambi, R. Mishra, M. G. Booty, C. E. Baer, S. A. Shaffer, V. Dartois, B. A. McCormick, X. Chen, C. M. Sassetti, Nitric oxide prevents a pathogen-permissive granulocytic inflammation during tuberculosis. *Nature microbiology* **2**, 17072 (2017).

78. B. B. Mishra, V. A. Rathinam, G. W. Martens, A. J. Martinot, H. Kornfeld, K. A. Fitzgerald, C. M. Sassetti, Nitric oxide controls the immunopathology of tuberculosis by inhibiting NLRP3 inflammasome-dependent processing of IL-1beta. *Nature immunology* **14**, 52-60 (2013).

79. R. R. Lovewell, C. E. Baer, B. B. Mishra, C. M. Smith, C. M. Sassetti, Granulocytes act as a niche for Mycobacterium tuberculosis growth. *Mucosal immunology* **14**, 229-241 (2021).

80. L. Moreira-Teixeira, K. Mayer-Barber, A. Sher, A. O'Garra, Type I interferons in tuberculosis: Foe and occasionally friend. *J Exp Med* **215**, 1273-1285 (2018).

81. H. Block, A. Zarbock, A Fragile Balance: Does Neutrophil Extracellular Trap Formation Drive Pulmonary Disease Progression? *Cells* **10**, (2021).

82. K. Pyrillou, L. C. Burzynski, M. C. H. Clarke, Alternative Pathways of IL-1 Activation, and Its Role in Health and Disease. *Frontiers in immunology* **11**, 613170 (2020).

83. K. D. Mayer-Barber, B. B. Andrade, D. L. Barber, S. Hieny, C. G. Feng, P. Caspar, S. Oland, S. Gordon, A. Sher, Innate and adaptive interferons suppress IL-1alpha and IL-1beta production by distinct pulmonary myeloid subsets during Mycobacterium tuberculosis infection. *Immunity* **35**, 1023-1034 (2011).

84. K. D. Mayer-Barber, D. L. Barber, K. Shenderov, S. D. White, M. S. Wilson, A. Cheever, D. Kugler, S. Hieny, P. Caspar, G. Nunez, D. Schlueter, R. A. Flavell, F. S. Sutterwala, A. Sher, Caspase-1 independent IL-1beta production is critical for host resistance to mycobacterium tuberculosis and does not require TLR signaling in vivo. *J Immunol* **184**, 3326-3330 (2010).

85. A. C. Bohrer, C. Tocheny, M. Assmann, V. V. Ganusov, K. D. Mayer-Barber, Cutting Edge: IL-1R1 Mediates Host Resistance to Mycobacterium tuberculosis by Trans-Protection of Infected Cells. *J Immunol* **201**, 1645-1650 (2018).

86. K. D. Mayer-Barber, B. B. Andrade, S. D. Oland, E. P. Amaral, D. L. Barber, J. Gonzales, S. C. Derrick, R. Shi, N. P. Kumar, W. Wei, X. Yuan, G. Zhang, Y. Cai, S. Babu, M. Catalfamo, A. M. Salazar, L. E. Via, C. E. Barry, 3rd, A. Sher, Host-directed therapy of

tuberculosis based on interleukin-1 and type I interferon crosstalk. *Nature* **511**, 99-103 (2014).

87.   T. C. Tsao, J. Hong, C. Huang, P. Yang, S. K. Liao, K. S. Chang, Increased TNF-alpha, IL-1 beta and IL-6 levels in the bronchoalveolar lavage fluid with the upregulation of their mRNA in macrophages lavaged from patients with active pulmonary tuberculosis. *Tuber Lung Dis* **79**, 279-285 (1999).

88.   K. Mayer-Barber, in *Global Immunotalks*. (2020).

89.   WHO, Global Tuberculosis Report 2019. WHO/HTM/TB Geneva, World Health Organization. (2019).

90.   WHO, Global Tuberculosis Report 2021. WHO/HTM/TB Geneva, World Health Organization. (2021).

91.   P. Andersen, T. J. Scriba, Moving tuberculosis vaccines from theory to practice. *Nat Rev Immunol* **19**, 550-562 (2019).

92.   A. Zumla, J. Chakaya, R. Centis, L. D'Ambrosio, P. Mwaba, M. Bates, N. Kapata, T. Nyirenda, D. Chanda, S. Mfinanga, M. Hoelscher, M. Maeurer, G. B. Migliori, Tuberculosis treatment and management--an update on treatment regimens, trials, new drugs, and adjunct therapies. *The Lancet Respiratory Medicine* **3**, 220-234 (2015).

93.   F. Conradie, A. H. Diacon, N. Ngubane, P. Howell, D. Everitt, A. M. Crook, C. M. Mendel, E. Egizi, J. Moreira, J. Timm, T. D. McHugh, G. H. Wills, A. Bateson, R. Hunt, C. Van Niekerk, M. Li, M. Olugbosi, M. Spigelman, T. B. T. T. Nix, Treatment of Highly Drug-Resistant Pulmonary Tuberculosis. *N Engl J Med* **382**, 893-902 (2020).

94.   C. R. Horsburgh, Jr., C. E. Barry, 3rd, C. Lange, Treatment of Tuberculosis. *N Engl J Med* **373**, 2149-2160 (2015).

95.   Y. Shao, H. Song, G. Li, Y. Li, Y. Li, L. Zhu, W. Lu, C. Chen, Relapse or Re-Infection, the Situation of Recurrent Tuberculosis in Eastern China. *Front Cell Infect Microbiol* **11**, 638990 (2021).

96.   V. Dartois, The path of anti-tuberculosis drugs: from blood to lesions to mycobacterial cells. *Nat Rev Microbiol* **12**, 159-167 (2014).

97.   M. Maiga, N. Agarwal, N. C. Ammerman, R. Gupta, H. Guo, M. C. Maiga, S. Lun, W. R. Bishai, Successful shortening of tuberculosis treatment using adjuvant host-directed therapy with FDA-approved phosphodiesterase inhibitors in the mouse model. *PloS one* **7**, e30749 (2012).

98.   S. Subbian, L. Tsenova, P. O'Brien, G. Yang, M. S. Koo, B. Peixoto, D. Fallows, V. Dartois, G. Muller, G. Kaplan, Phosphodiesterase-4 inhibition alters gene expression and improves isoniazid-mediated clearance of Mycobacterium tuberculosis in rabbit lungs. *PLoS Pathog* **7**, e1002262 (2011).

99.   H. J. Seon, Y. I. Kim, S. C. Lim, Y. H. Kim, Y. S. Kwon, Clinical significance of residual lesions in chest computed tomography after anti-tuberculosis treatment. *The international journal of tuberculosis and lung disease : the official journal of the International Union against Tuberculosis and Lung Disease* **18**, 341-346 (2014).

100.   M. Vecino, J. G. Pasipanodya, P. Slocum, S. Bae, G. Munguia, T. Miller, M. Fernandez, G. Drewyer, S. E. Weis, Evidence for chronic lung impairment in patients treated for pulmonary tuberculosis. *J Infect Public Health* **4**, 244-252 (2011).

101.   A. Brauner, O. Fridman, O. Gefen, N. Q. Balaban, Distinguishing between resistance, tolerance and persistence to antibiotic treatment. *Nat Rev Microbiol* **14**, 320-330 (2016).

102. S. M. Gygli, S. Borrell, A. Trauner, S. Gagneux, Antimicrobial resistance in Mycobacterium tuberculosis: mechanistic and evolutionary perspectives. *FEMS Microbiol Rev* **41**, 354-373 (2017).

103. B. Gold, C. Nathan, Targeting Phenotypically Tolerant Mycobacterium tuberculosis. *Microbiol Spectr* **5**, (2017).

104. Y. Liu, S. Tan, L. Huang, R. B. Abramovitch, K. H. Rohde, M. D. Zimmerman, C. Chen, V. Dartois, B. C. VanderVen, D. G. Russell, Immune activation of the host cell induces drug tolerance in Mycobacterium tuberculosis both in vitro and in vivo. *J Exp Med* **213**, 809-825 (2016).

105. S. N. Goossens, S. L. Sampson, A. Van Rie, Mechanisms of Drug-Induced Tolerance in Mycobacterium tuberculosis. *Clinical microbiology reviews* **34**, (2020).

CHAPTER TWO

Physiology of *M. tuberculosis*

2.1 The role of lipid utilization in *M. tuberculosis* pathogenesis

Partially adapted from

Cholesterol and fatty acids grease the wheels of Mycobacterium tuberculosis pathogenesis. Kaley M. Wilburn, Rachael A. Fieweger and Brian C. VanderVen. *Pathogens and Disease*. 76, (2018).

2.1.1 Introduction

Since at least the 1940s, scientists studying TB have questioned how the physiology of *Mycobacterium tuberculosis* (Mtb) differs during infection compared to cultivation on artificial media *in vitro* (*1*). An early study that provided evidence that Mtb utilizes lipids during infection dates to the 1950s, when Segal and Bloch demonstrated that Mtb isolated from the lungs of infected mice preferentially increased respiration when cultured *ex vivo* with fatty acids, but not carbohydrates (*2*). In the decades since, abundant evidence has confirmed that lipids are prominent in the granuloma environment (Chapter 1.1) and that Mtb has an extensive network of genes dedicated to cholesterol and fatty acid utilization. Genetic screening has repeatedly indicated that lipid utilization is functionally important for the survival or persistence of Mtb during infection. Many of the details explaining how lipid utilization supports Mtb survival during infection are still being identified, but it is clear that cholesterol and fatty acids contribute to the physiology of Mtb in complex ways. This includes fueling central metabolism and synthesis of cell wall components or lipid storage molecules, which influence interactions of the bacterium with host immune cells via virulence lipids and/or promote changes in bacterial physiology that are associated with

antibiotic or stress persistence (*3, 4*). Mtb resides in an early endosome-like phagosome during macrophage infection, and it is unclear whether the bacterium can acquire lipids derived from genuine host lipid droplets or instead accesses lipids by intersecting with other lipid trafficking pathways, like the uptake of LDL (*5-9*). The lipids accessed by Mtb during macrophage infection likely contain a mixture of cholesterol and fatty acids. As such, interest in how Mtb coordinates utilization of both fatty acids and cholesterol to support pathogenesis during infection is a growing area of interest.

2.1.2 Cholesterol utilization in *M. tuberculosis*

The cholesterol utilization pathway in Mtb begins with import of the cholesterol molecule across the characteristic lipid-rich outer layer of the mycobacterial cell wall, through the periplasmic space, and across the cytoplasmic membrane into the cytoplasm. This process requires coordination by a multiprotein ATP-binding cassette (ABC) -like complex called Mce4. ABC importers are composed of three main domains: 1) a substrate-binding domain for binding the ligand and shuttling it across the outer layers of the cell wall and periplasmic space, 2) a dimeric transmembrane permease that accepts the ligand from the substrate-binding domain and allows the ligand to translocate across the cytoplasmic membrane, and 3) a dimeric nucleotide binding domain that couples the binding and hydrolysis of ATP to energize transport through the complex (*10*). The Mce4 complex is encoded by a ten-gene operon (*rv3492c-rv3501c*) (Figure 2.1). This operon encodes two integral membrane proteins (Rv3501/YrbE4A and Rv3502/YrbE4B) thought to function as the transmembrane permease, and six cell wall proteins (Mce4A-F) that likely form the substrate-binding portion of the transporter (*11*). Deleting the YrbE4A permease subunit reduces cholesterol uptake, severely inhibits cholesterol metabolism, and reduces growth of this

strain in minimal media supplemented with cholesterol (*12, 13*). Genetic screening of a transposon mutant library verified that each of the genes in the Mce4 operon is required for optimal growth of Mtb in cholesterol media (*14*). Two accessory proteins (Mam4A and Mam4B) are also encoded in the Mce4 operon. Mam4B is required for cholesterol metabolism and interacts via its transmembrane domain with an additional regulatory protein that is encoded outside of this operon (Rv3723/LucA) (*12*). Transport by this complex is believed to be energized through ATP hydrolysis by the Rv0655/MceG protein (*14, 15*). Details of how each of the components of the Mce4 operon contribute to the structure and function of this complex are lacking, necessitating speculation based on homologous proteins from *E. coli* (*16*). Moreover, how regulation of this complex is coordinated, particularly in the presence of other lipids or carbon sources, is not established.

The cholesterol molecule is composed of four rings (A-D, C1-C19) and a side chain (C20-C27, and the cholesterol catabolism pathway can be divided into two stages accordingly (Figure 2.2). The side chain is degraded via three cycles of β-oxidation, which results in the release of two propionyl-CoA units and one acetyl-CoA unit from the cholesterol molecule. After the terminal carbon is hydroxylated by Cyp125, the acyl-CoA synthetase FadD19 performs an ATP-dependent reaction to attach a coenzyme-A (CoA) to the side chain, forming a fatty acyl-CoA (*17, 18*). These steps activate the side chain for subsequent β-oxidation. Most of the enzymes that perform each round of β-oxidation in this process have been characterized, with different proteins implicated in each dehydrogenation, hydration, and thiolysis reaction (Figure 2.2) (*19*). Degradation of the A and B rings results in the release of one propionyl-CoA unit and one pyruvate unit, via a series of previously characterized reactions (*20-27*). Degradation of the C and D rings releases at least one acetyl-CoA unit, and likely one unit of propionyl-CoA, pyruvate, or succinyl-CoA via a process

that involves opening of the D ring before the C ring (*28, 29*). The end products of 4-methyl-5-oxo-octanedioic acid (MOODA-CoA) are uncertain, but it is possible that acetyl-CoA, propionyl-CoA, and/or succinyl-CoA are derived from this intermediate (Figure 2.2). Metabolomic analyses indicate that propionyl-CoA pools increase when Mtb is grown in the presence of cholesterol, which is consistent with the products of the cholesterol breakdown pathway as illustrated here (*30*). The fate of these two- and three-carbon products is discussed below.

Importantly, cholesterol side-chain and ring degradation likely occurs in tandem to some degree. For example, a mutant that is defective in the last three steps of side chain degradation cannot complete the last round of β-oxidation of the side chain; nevertheless, the major accumulated metabolite in this mutant has its A and B rings degraded with the C and D rings intact (*31*) Also, the KshA/KshB hydroxylase complex that participates in A and B ring degradation shows preferential activity for a substrates that have a partially intact side chain, as compared to the ADD molecule that has its side chain entirely degraded, as shown in Figure 2.2 (*32*). Overall this suggests that cholesterol breakdown does not proceed in a strictly linear fashion, through the side chain and then into the rings. Rather, it is likely that the degradation process occurs somewhat simultaneously, and that there is a degree of flexibility in how it proceeds, such that blocking a single step in the pathway does not necessarily prevent other portions of the molecule from being degraded. Blocking certain steps in the cholesterol breakdown pathway (HsaC or IpdAB) is also proposed to generate toxic degradation intermediates, such that Mtb viability is lost when grown on cholesterol and/or its growth in the presence of cholesterol is not rescued in the presence of an alternative carbon source (*25, 29*) Both of these features of the cholesterol degradation pathway have important implications when developing cholesterol utilization inhibitors as Mtb antibiotics.

Lastly, transcriptional regulation of a large operon of cholesterol utilization genes, originally referred to as the Cho-region, plays an important role in regulating cholesterol breakdown in Mtb (*14, 33*). Transcription of these genes is regulated via two TetR-like transcriptional repressors named KstR1 and KstR2 (*34, 35*). Enzymes encoded in the 74-gene KstR1 regulon include those responsible for side chain and A-B ring degradation in Mtb, while the enzymes involved in C-D ring degradation are encoded in the 15-gene KstR2 regulon (*35-37*). These repressors bind to specific intermediates of cholesterol degradation and de-repress their respective genes, as well as exhibiting autoregulation, promoting rapid gene expression (*35*). The early catabolic intermediate 3-oxocholest-4-en-26-oyl-CoA (3OCh-CoA) de-represses KstR1, and KstR2 is de-repressed by 3aα-H-4α(3'-propanoyl-CoA)-7aβ-methylhexa-hydro-1,5-indanedione-CoA (HIP-CoA) which is produced later in the pathway, during ring degradation (Fig. 2.2) (*38, 39*). These intermediates inhibit DNA binding by KstR1 and KstR2, allowing RNA polymerase to access these genes. Not only are these transcriptional responses necessary to permit cholesterol degradation to occur efficiently, but measuring the expression levels of genes in the KstR1 and KstR2 regulons can be used as a reporter to indicate whether cholesterol catabolism is proceeding normally and producing these breakdown intermediates

2.1.3 Fatty acid utilization in *M. tuberculosis*

Similar to cholesterol utilization, fatty acid utilization in Mtb begins with import into the cell. Fatty acid uptake requires at least one other ABC-like complex called Mce1, which has a similar operon structure to the Mce4 locus. The Mce1 complex is composed of two permease subunits (YrbE1A and YrbE1B), six Mce proteins (Mce1A-F), and four accessory subunits (Mam1A-D) (Figure 2.2) (*11*). Transport through this complex is proposed to be powered by the

same nucleotide-binding ATPase (MceG) as Mce4 (*15, 40*). Two additional Mce loci (Mce2 and Mce3) with similar structures were identified in Mtb, but have not yet been assigned functions (*11*). Mtb strains lacking YrbE1A, or the entire Mce1 locus, are deficient in uptake and metabolism of the fatty acids oleate and palmitate, but not cholesterol (*12, 40*). Strains of Mtb that are deficient in Mce1 proteins, or deficient in proteins that participate in the function of both Mce4 and Mce1 transport complexes, also fail to accumulate internal lipid inclusions from externally supplied Bodipy-palmitate during macrophage infection (*40*).

Fatty acid breakdown occurs via β-oxidation, which liberates acetyl-CoA from even-chain fatty acids like oleate and palmitate. Odd-chain fatty acids can also release one unit of propionyl-CoA during β-oxidation. Even-chain fatty acids (carbon chain length of 2–26) account for >99% of the circulating fatty acids in humans (*41*). The abundance and origin of the detectable odd-chain fatty acids (C15, C17, C17:1, and C23) in mammalian tissues is debatable, but relatively low compared to even-chain fatty acids (*41*). Deconvoluting the specific genes that perform β-oxidation of diverse fatty acid substrates in Mtb has proven challenging, given that ~100 genes were originally annotated with functions in one of the five steps of β-oxidation (*42*). The potential redundancy in this part of the fatty acid utilization pathway makes genetic screening for essential fatty acid catabolism genes difficult (*43*).

Importantly, fatty acids can have a range of fates and do not necessarily undergo β-oxidation upon import into Mtb. Instead, they can be used to provide acyl-primers for cell wall lipid synthesis, become incorporated into phospholipids that are essential for cytoplasmic membrane maintenance, or stored as a future source of carbon in the form of triacylglycerol (TAG) (*4*). Specifically, fatty acids can enter the synthesis pathway for the virulence-associated cell wall lipids phiocerol-dimycoseroic acid (PDIM), poly-acylated trehaloses (PATs), or sulfolipid (SL) in

the form of acyl-AMP primers (*44*). Fatty acids with carbon lengths C16-C26 can also be modified by the FAS-I and FAS-II complexes to synthesize elongated acyl chains that are used to form mycolic acids which are incorporated as an essential component of the mycobacterial cell wall (*45*). Fatty acid catabolism requires NAD^+ as a co-factor and produces NADH, while fatty acid synthesis consumes NADH and regenerates NAD^+. NADH can be used to fuel oxidative phosphorylation via the NADH dehydrogenase complex (*46*). Because fatty acid breakdown and synthesis each have the potential to shift the NAD^+/NADH redox balance in Mtb, it has been proposed these processes are intricately regulated especially during growth in hypoxic environments, when oxygen is not readily available to serve as the terminal electron acceptor of the electron transport chain (*47-49*). Fatty acid utilization is at least partially regulated via transcriptional responses, as whole transcriptome analyses of Mtb isolated from murine-derived macrophages or the lungs of human TB patients noted upregulation of genes proposed to be involved in fatty acid utilization pathways (*50-52*).

2.1.4 Contributions of lipids to *M. tuberculosis* pathogenesis

Incorporation of cholesterol and fatty acid breakdown products into central metabolism

The two- and three-carbon intermediates generated by fatty acid and cholesterol breakdown can be incorporated into central carbon metabolism by entering the TCA cycle. Here their oxidation can fuel energy production via intermediates that enter the electron transport chain, or they can be used as precursors for biosynthetic pathways. To enter the TCA cycle, acetyl-CoA can be condensed with oxaloacetate to form citrate, and the chemical energy of acetyl-CoA can be converted into the reducing power of NADH (Fig. 2.3) (*53*). During growth on fatty acids, the

glyoxylate shunt can be used as an alternative to the canonical suite of oxidative TCA cycle reactions and the complete decarboxylation of every acetyl-CoA unit. Instead, the glyoxylate shunt is utilized to bypass two decarboxylation steps of the TCA cycle, allowing TCA cycle intermediates to be replenished and supporting carbohydrate synthesis via gluconeogenesis, which is required in the absence of glycolysis during growth on lipid substrates (*53-55*). In Mtb, the enzyme isocitrate lyase (Icl) facilitates the entry of isocitrate into the glyoxylate shunt. Mtb has two Icl enzymes, Icl1 and Icl2, with redundant functions (*55*). Importantly, Δ*icl1* Mtb has a growth defect during the chronic stage of infection in mice, and double-deficient Δ*icl1/2* Mtb are eliminated from the lungs by 2 weeks post-infection (*54, 55*). This was originally interpreted to mean that Mtb primarily uses fatty acids instead of carbohydrates during growth *in vivo*. However, Icl is a bifunctional enzyme that is required for detoxifying propionyl-CoA by integrating it into the TCA cycle, as discussed below. As such, the growth defect of Icl-deficient Mtb during infection is potentially related to a defect in the glyoxylate shunt, a defect in the detoxification of the propionyl-CoA that is primarily derived from cholesterol, or both. If lipids are a dominant carbon source during Mtb infection in the absence of glycolytic carbon sources, it would also be expected that gluconeogenesis would play an essential role in regenerating precursors for nucleic acid, amino acid, and cell wall synthesis (*56*). The phosphoenolpyruvate carboxykinase enzyme is required to generate phosphoenolpyruvate (PEP) from oxaloacetate, and PEP is an essential precursor for gluconeogenesis (Fig. 2.3). Indeed, Mtb or *Mycobacterium bovis* deficient in the gene that encodes phosphoenolpyruvate carboxykinase (Δ*pckA*) have survival defects during macrophage and murine infection, indicating that gluconeogenesis is likely important to maintain bacterial survival during infection (*57, 58*). Δ*pckA* Mtb is also unable to grow on fatty acids as a sole carbon source *in vitro*. Altogether, this confirms that central metabolic pathways that

incorporate the products of lipid breakdown are also necessary to maintain Mtb fitness during infection.

Propionyl-CoA has three downstream fates while it is incorporated into Mtb metabolism. First, propionyl-CoA can be condensed with oxaloacetate via the methylcitrate cycle (MCC), allowing it to be incorporated into the TCA cycle or the electron transport chain via the products pyruvate and succinate (Fig. 2.3) (*59, 60*). Inactivating the final step in the MCC, Icl1, causes a dead end pathway that drives the accumulation of propionyl-CoA derived intermediates, intoxicating Mtb and inhibiting bacterial growth in the presence of cholesterol or propionate even when alternative carbon sources (glucose, glycerol, and fatty acids) are available (*59, 61, 62*). This phenotype can be rescued by inhibiting the entry steps into the MCC (PrpC or PrpD) or some steps of cholesterol breakdown (Cyp125, HsaC, HsaA) (*12*). Second, propionyl-CoA can be converted into methylmalonyl-CoA via the methylmalonyl pathway (Fig. 2.3). From this point, the vitamin B12-dependent methylmalonyl-CoA mutase complex can incorporate methylmalonyl-CoA into the TCA cycle by converting it to succinate (*63*). Whether Mtb can synthesize vitamin B12 or access it *in vivo* to fuel this pathway is not known, as this was discovered *in vitro* where exogenous vitamin B12 was supplied to the bacteria. Third, the methylmalonyl-CoA can instead be incorporated directly by polyketide synthases to form methyl-branched lipids that are incorporated into the cell wall lipids PDIM and SL-1 (*30, 64-66*). When Mtb is supplied with propionate or cholesterol, the absolute amount of PDIM and SL-1 is increased, and the bacteria generates high-mass forms of PDIM and SL-1 in which the methyl-branched acyl chains of PDIM and SL-1 are lengthened by the addition of extra methylmalonyl-CoA units (*64*). Importantly, similar high mass forms of PDIM are present in Mtb isolated from murine lungs 19 days post-infection which

suggests this pathway is relevant during infection and Mtb access a source of propionyl-CoA, likely cholesterol, *in vivo* (*64*).

When propionyl-CoA pools increase in Mtb as a result of cholesterol or odd-chain fatty acid utilization, the bacteria can sink excess propionyl-CoA into excess methylmalonyl-CoA precursors for polyketide lipid synthesis (*61*). This becomes especially important if flux through the alternative pathways for incorporating propionyl-CoA into the TCA cycle are blocked. However, Mtb requires sufficient levels of free fatty acids to serve as fatty acid-AMP primers for polyketide synthase enzymes (*44*). Thus, this drives a requirement for fatty acid utilization if this pathway is to be used as a sink to prevent accumulation of potentially toxic propionyl-CoA intermediates (*61*). Simultaneously, directing fatty acids to form intermediates that fuel lipid synthesis may also help maintain redox homeostasis, by averting the NAD^+/NADH redox imbalance that can be generated during β-oxidation of long-chain fatty acids (*47, 49*). This illustrates an example of the complex, inter-dependent fates of fatty acid and cholesterol-derived intermediates and redox homeostasis in Mtb. *In vitro* studies have suggested that the central metabolism of Mtb may be characterized by non-canonical pathways, including compartmentalized co-catabolism of distinct carbon sources, a bifurcated TCA cycle and/or the ability to adopt a reductive TCA cycle (*47, 67, 68*). However, it is not clear how these observations translate to the presence of combinations of complex carbon substrates *in vitro* or during infection.

The significance of cholesterol utilization during infection

Over the last decade, evidence from a variety of experimental approaches has indicated that cholesterol utilization is important to Mtb pathogenesis in macrophages and during infection *in vivo*. Studies of the transcriptional response in Mtb have consistently indicated that the

bacterium upregulates genes within the cholesterol utilization pathway and/or genes required to assimilate propionyl-CoA during macrophage infection *in vitro*, during infection in mice, and in the lungs of some TB patients (*50-52, 69-71*). Functionally, cholesterol was confirmed to be a major source of propionyl-CoA during Mtb growth in macrophages because both chemical and genetic approaches that inhibit the MCC generate propionyl-CoA-related toxicity in Mtb during macrophage infection. This toxicity can be rescued by simultaneously disabling Mce4-dependent cholesterol import, indicating that cholesterol is a major source of the propionyl-CoA driving the experimentally-induced toxicity phenotype (*30*). Unbiased genetic screens have also repeatedly indicated that cholesterol utilization genes are necessary for Mtb growth and/or persistence during murine infection, with the most consistent phenotypes being noted during the chronic stage of disease (*15, 72, 73*). Subsequent experiments with transposon mutants and targeted mutants in the cholesterol pathway have verified this. For example, disrupting cholesterol uptake by mutating the first gene in the *mce4* locus, *yrbE4a*, is associated with a decrease in Mtb CFUs at 35-100 days post-infection relative to wild type bacteria, during a competitive infection in mice (*13, 15*). Mtb mutants deficient in cholesterol side chain (*fadA5*) and ring (*kshA/kshB* and *hsaC)* catabolism steps generate a similar loss in bacterial fitness during chronic infection in mice or guinea pigs (*25, 33, 74*).

As mentioned above, it is likely that some flexibility or non-linearity exists in the cholesterol degradation pathway. In keeping with this, it is interesting that a genetic screen using a panel of genetically-diverse mice that feature variable susceptibility to Mtb predicts that disrupting different genes in the cholesterol breakdown pathway is associated with varying degrees of growth deficiency in Mtb *in vivo*. For example, while the *mce4* locus belonged to a core set of required genes during infection, only some genes of the side chain (*cyp125, chsE1/chsE2, chsH2,*

ltp2) and ring (*hsaD, ipdF, fade30, ipdA/ipdB, fadA6, fadE32*) degradation pathways were also predicted to be required for Mtb fitness across 30 different mouse strains (*73*). Other steps in the pathway were required for full bacterial fitness in fewer (2 or more) mouse backgrounds. In the future, expanding our understanding of which step(s) in cholesterol utilization should be inhibited to maximally disrupt Mtb growth *in vivo* will provide important guidance for the development of potential new therapeutics targeting this pathway. Genetic screens have also predicted that the *mce1* locus is necessary for optimal growth of Mtb during infection, particularly during the acute stage (*15, 72, 73*). However, studies using targeted *mce1* mutants with differing routes of infection and different mouse backgrounds have produced mixed conclusions about this (*12, 75, 76*). Therefore, currently more clear evidence supports the conclusion that cholesterol utilization is required during infection to support Mtb pathogenesis.
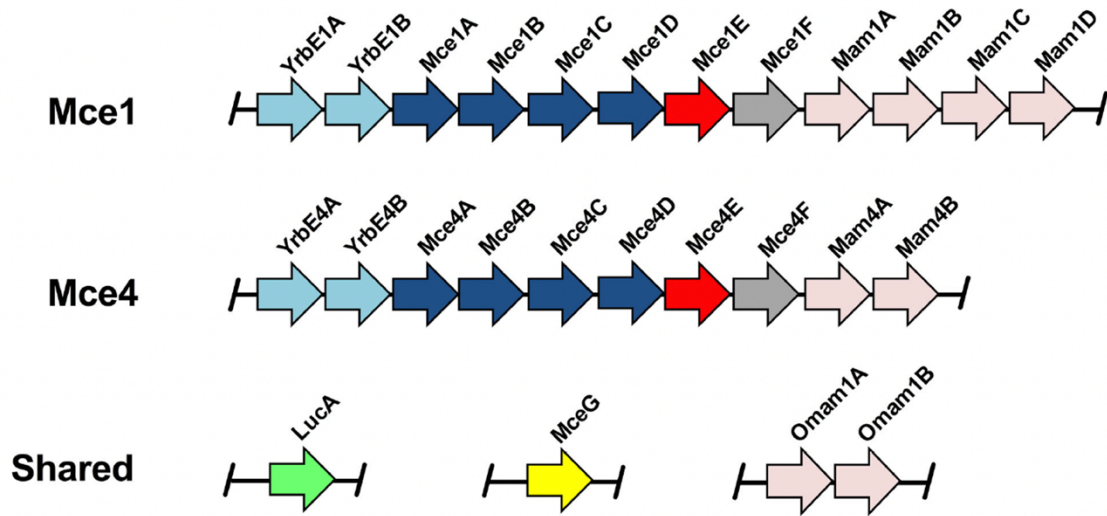
Figure 2.1 Genes of the fatty acid (Mce1) and cholesterol (Mce4) transporter complexes in Mtb. Reproduced with permission from (*19*).
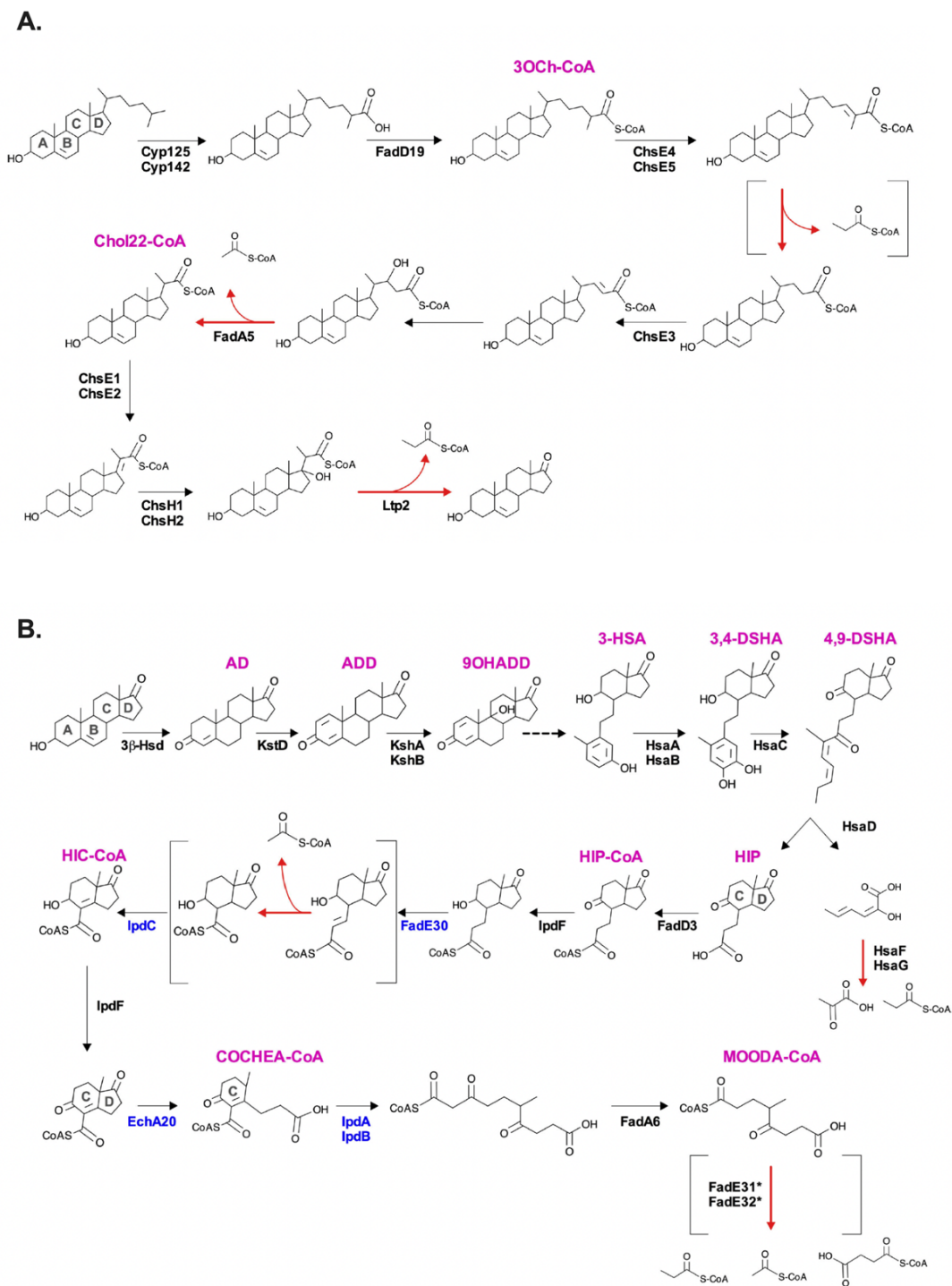
Figure 2.2. Proposed mechanism of cholesterol side chain (A) and ring (B) breakdown in Mtb. Confirmed enzymes are denoted with the enzyme names next to the reaction arrows. Brackets indicate stages in the pathway that require multiple enzymatic reactions. Pink text indicates chemical name abbreviations for the catabolic intermediates. Reproduced with permission from (*19*).

59
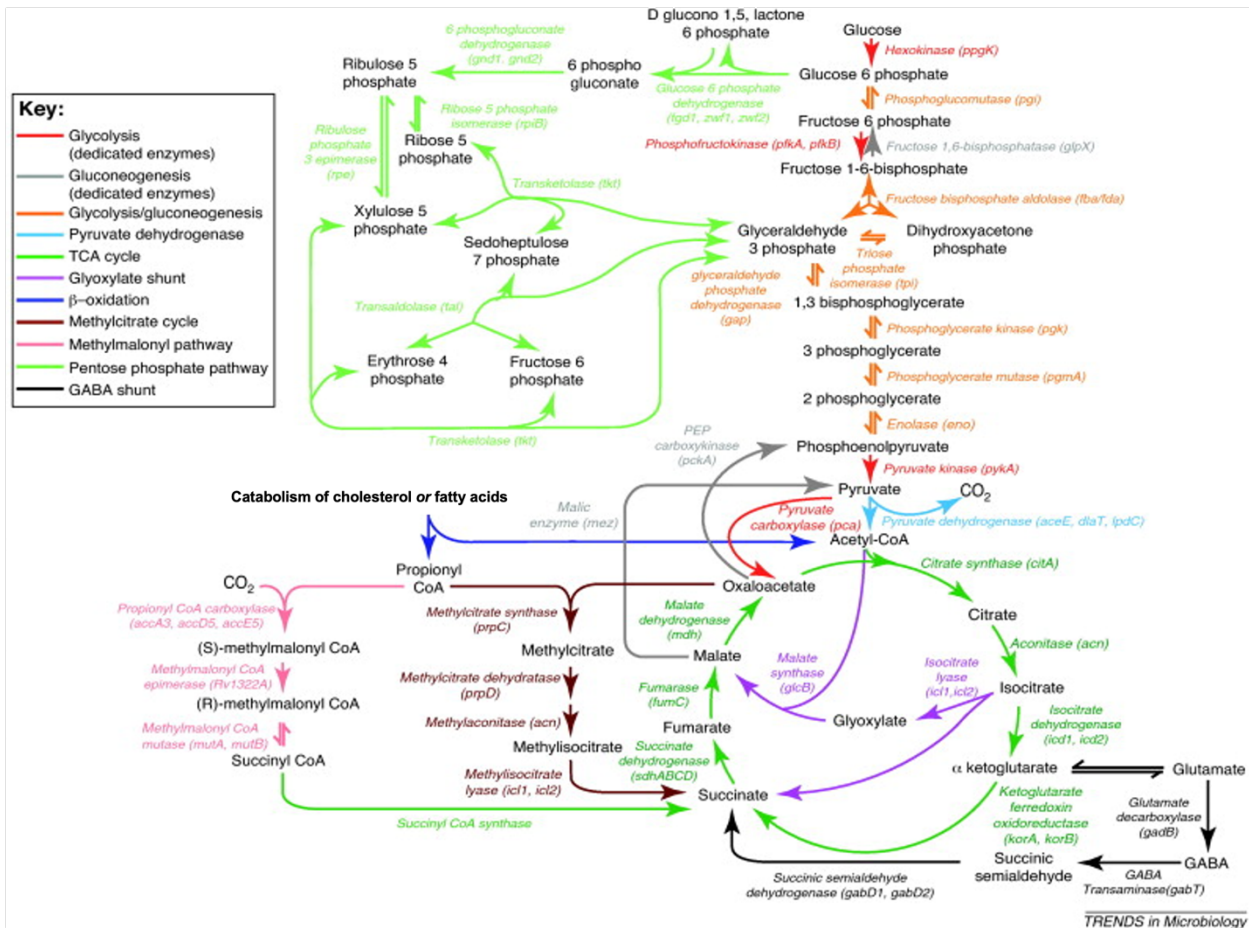
Figure 2.3 Central carbon metabolism pathways in Mtb. Depiction of the relationship between central carbon metabolism pathways in Mtb, including the TCA cycle, methylcitrate cycle, methylmalonyl pathway, and gluconeogenesis discussed in the text. Adapted and reproduced with permission from (*68*).

2.2 Adenylyl cyclase enzymes and cAMP signaling in *M. tuberculosis*

2.2.1 Basic components and functions of cAMP signaling in bacteria

3',5'-cyclic adenosine monophosphate (cAMP) is a universal second messenger that functions by relaying signals from transmembrane or intracellular receptors to downstream regulatory targets in the cell. In bacteria, cAMP signaling regulates an array of cellular processes, including pathways for coordinating homeostatic carbon metabolism and virulence-specific networks in pathogenic bacteria. The structure of cAMP signaling pathways in bacteria generally begins with activation of an adenylyl cyclase (AC) enzyme in response to an environmental signal, followed by the AC catalyzing the intramolecular cyclization of ATP to form cAMP (Fig. 2.4) (*77*). In bacteria, cAMP typically activates downstream cAMP-binding proteins via allosteric interactions that cause conformational changes to the proteins which confer changes to their function. To maintain cAMP homeostasis, bacteria also conserve phosphodiesterase (PDE) proteins that catalyze the hydrolytic degradation of cAMP to AMP.

Across many bacterial species, it is common for cAMP-binding proteins to act as transcription factors that regulate gene networks in a cAMP-responsive manner. These transcription factors of the cAMP-receptor protein family (Crp family) are directly activated by binding to cAMP, and are able to either promote or block transcription depending on the context. The cAMP-Crp complex in *E. coli* is considered a classic example of how cAMP is involved in regulating carbon metabolism in bacteria, via carbon catabolite repression. cAMP-Crp is integrated into the "glucose response" pathway in *E. coli*, and is necessary for the activation of genes (the *lac* operon) that allow lactose to be used as a secondary carbon source when the bacterium's preferred carbon source, glucose, is scarce (*77*). In this system, the activation state of the class I AC enzyme of *E. coli* is regulated by interactions with the EIIA domain of the glucose transporter; the ability

of the EIIA^{Glc} domain to activate the AC is dependent on its phosphorylation status, which is linked to the flux of glucose being transported into the cell via the phosphotransferase system and as well as the levels of the phosphate donor available in the cell (*78*). However, other operon-specific regulatory systems such as inducer exclusion and induction prevention cooperate with the global regulation of genes by cAMP-CRP and are essential to coordinate diauxic growth during primary and secondary carbon source utilization (*78*). In *E. coli*, cAMP-Crp can also regulate carbon flux through central metabolic pathways, modulating a glucose starvation-associated gluconeogenesis and glyoxylate shunt cycle (*79*). These examples illustrate how cAMP is integrated into complex, context-dependent signaling networks that cooperate with non-cAMP-responsive components. Notably, not all carbon catabolite repression mechanisms require gene regulation via cAMP-Crp, and not all bacteria utilize carbon catabolite repression systems or systems based on glucose as the preferred carbon source (*78, 80*).

Beyond carbon catabolite repression, cAMP regulates virulence functions within bacterial cells via diverse downstream signaling effects. cAMP-CRP can upregulate or suppress expression of global regulators including stress-associated RNA-polymerase σ-factors, or the expression of horizontally acquired pathogenicity islands (*77, 81, 82*). Crp or Crp-like transcription factors bound to cAMP regulate functions like expression of type III secretion systems, pili, and exotoxins, as well as quorum sensing and biofilm formation that facilitate colonization and persistence in the host (*83-86*). For example, *Vibrio cholerae* features a cAMP-dependent system that links the availability of glucose with regulation of biofilm formation, quorum sensing, virulence gene expression, and phage resistance through direct and indirect signaling mechanisms (*77*). There is at least one example of a Crp family transcription factor in *Pseudomonas aeruginosa* that alters expression of some virulence genes via a cAMP-dependent mechanism, but modulates expression

of a quorum sensing system via co-regulation by an unknown cAMP-independent cofactor (*85*). Thus, although there are common themes in the mechanisms through which cAMP regulates the physiology of pathogenic bacteria, the particular features of their cAMP-regulated networks are diverse even among those relying on Crp-family transcription factors.

In addition to cAMP-dependent signaling within bacterial cells, cAMP signaling is also used by bacteria to modulate responses of host cells during infection. The architecture of cAMP signaling in eukaryotic cells is different than in bacteria, and this is relevant to our understanding of how bacteria can manipulate host cell cAMP signaling. Briefly, the canonical cascade of cAMP signaling in eukaryotic cells is initiated when a ligand binds to a G protein-coupled receptor (GPCR) (*87*). Whether the GPCR is $G\alpha_s$-coupled or $G\alpha_i$-coupled determines the effect the ligand has on AC activity. Ligand binding to a $G\alpha_s$-coupled GPCR leads to activation of a transmembrane-associated AC via the dissociated $G\alpha_s$ subunit, while binding to a $G\alpha_i$-coupled GPCR leads to AC inhibition (*87*). Another group of soluble AC enzymes are directly regulated by bicarbonate and pH levels instead (*88*). Stimulation of AC activity increases cAMP, which can activate multiple intermediary targets downstream, including protein kinase A (PKA) and the guanine nucleotide exchange factor proteins directly activated by cAMP (Epac) (*87*). cAMP binding to the regulatory subunits of PKA frees its catalytic subunits to regulate numerous target proteins via phosphorylation of specific residues, and PKA is known to modulate transcription factors like Nf-κB and the cAMP response element-binding protein (CREB) (*87, 89*). The overall downstream effects of cAMP signaling are cell type dependent because there are numerous molecular species of many of the pathway components, in addition to mechanisms that create discrete subcellular pools of intracellular cAMP and its effectors (*87, 89-91*).

To modulate host cAMP signaling, pathogenic bacteria can secrete AC toxins that are activated in the host environment and synthesize cAMP directly (*77*). Alternatively, they can secrete toxins that modulate the AC enzymes of host cells via ADP-ribosylation modifications that lock Gα_s in an active state or lock Gα_i in an inactive state (*77*). Increased cAMP synthesis exerts pleiotropic effects on immune cells, and has been associated with regulating the production of inflammatory mediators, phagocytosis, and intracellular bacterial killing capacity in phagocytes (*87*). For example, *Bordetella pertussis* secretes two cAMP modulating toxins that can target phagocytes recruited to the site of infection: a CyaA toxin that functions as an AC enzyme, and the pertussis toxin which contains an enzymatically active subunit that ADP ribosylates the Gα_i subunit and prevents it from suppressing host AC activity (*92, 93*). Elevated cAMP synthesis due to these toxins within host phagocytes favors bacterial colonization and contributes to delayed neutrophil recruitment, reduced phagocytic functions, limited nitric oxide production, alterations in cytokines, and limited differentiation of infiltrating monocytes to macrophages (*92-94*). Chemical tools that induce cAMP synthesis in phagocytes have also associated increases in intracellular cAMP in macrophages with changes in cytokine and chemokine production, decreased phagocytosis, decreased H_2O_2 production, and/or reduced phagolysosome maturation (*89-91, 95-98*).

2.2.2 Adenylyl cyclase enzymes in *M. tuberculosis*

Mtb has an unusually large repertoire of AC enzymes, and its genome encodes at least 10 AC enzymes that have biochemically-confirmed enzymatic activity (*99*). Other bacteria like *E. coli*, *Bordetella pertussis*, *Pseudomonas aeruginosa*, or *Vibrio cholerae* have no more than three identified AC enzymes, including the secreted class II AC toxins discussed above (*77*). The ACs

of Mtb are class III cyclase enzymes, a ubiquitous and diverse class of nucleotidyl cyclases that includes all known eukaryotic ACs as well as many prokaryotic ACs (*88*). The ACs of Mtb are structurally diverse, including soluble, membrane-associated, and multidomain proteins, and they are variably conserved across multiple mycobacterial species (*100*). While all of these ACs feature a core catalytic domain, many of the ACs in Mtb also contain additional domains that can confer additional regulatory or biological functions (*101*). Each of these ACs encodes one cyclase domain per polypeptide. To generate an active catalytic core, the cyclase domains from two copies of the AC protein must homodimerize in a head-to-tail orientation. Dimerization generates two symmetrical active sites, in which each monomer contributes complementary residues that come together to form the conserved metal coordinating, substrate binding, and transition-state stabilizing sites within each active site (*88*).

One clear example of how the additional regulatory domains contribute to Mtb AC function is the soluble AC Rv1264, which is composed of an N-terminal domain that acts as a pH-responsive molecular switch and a C-terminal cyclase domain. At neutral pH, the N-terminal domain is autoinhibitory and a network of interactions between the N-terminal domain and the cyclase domain renders the protein inactive by disrupting homodimerization of the catalytic core (*102*). At low pH (6.0) the N-terminal domain undergoes conformational changes that facilitate dimerization of the catalytic core in the correct head-to-tail orientation, increasing cAMP synthesis 30-fold (*103*). Stimulatory environmental signals (low pH, high pH, fatty acids, CO_2, and the Mtb secreted protein Erp) have been proposed for five of the Mtb ACs, based on *in vitro* assays or biochemical assays using recombinantly expressed protein (*99, 100*). Thus, signals that can activate half of Mtb's AC enzymes have not been proposed, and it remains unclear whether the

activating signals that have been proposed for the other five ACs translate to Mtb pathogenesis *in vivo*.

2.2.3 Features of the Rv1625c adenylyl cyclase

Rv1625c is a membrane-bound AC in Mtb, with proposed orthologs in *M. bovis, M. marinum, M. avium,* and *M. leprae* but not in the non-pathogenic mycobacterium *M. smegmatis (100)*. Rv1625c is composed of at least four main structural elements: an N-terminal cytoplasmic domain and a six-helical transmembrane domain, followed by a cytoplasmic helical domain and a cyclase domain (Fig. 2.5). Rv1625c is often compared to one-half of a mammalian membrane-bound adenylyl cyclase, which form pseudo-heterodimers composed of two sequential sets of transmembrane and cyclase domains linked together in the same polypeptide. The cyclase domain of Rv1625c has residues that directly parallel those structurally confirmed to be essential in mammalian AC catalysis, and this facilitated functional confirmation of canonical catalytic core residues required for Rv1625c activity (*104*). In its active form, Rv1625c forms a homodimer that permits the formation of two active sites at the interface of the head-to-tail cyclase domains, where complementary residues from each monomer supply the residues necessary for binding and cyclization of ATP in the active sites (Fig. 2.5). Substrate-specifying residues located in the dimer interface of the catalytic sites contribute to productive dimer formation and Rv1625c activity (*105, 106*).

Outside of the catalytic core, other domains of Rv1625c contribute to enzyme activity. Two arginine residues within the N-terminal cytoplasmic tail are also required for enzymatic activity in Rv1625c, but the structural basis for this is unconfirmed (*107*). The transmembrane domain of Rv1625c also contributes to efficient dimerization of the protein, which enhances its activity

presumably by supporting stable associations between the cyclase domain residues (*108*). Similarly, the structure of a truncated, dimeric form of the Rv1625c homolog from *M. intracellulare* revealed that the cytoplasmic helical domain is formed by two tightly-associated helices in each monomer and contribute to dimer assembly and stability (*109*). Interestingly, it was recently demonstrated that six-helical transmembrane domains present in bacterial quorum-sensing receptors can be fused with the catalytic domain of Rv1625c to generate ligand-dependent AC activity (*110, 111*). Based on this, it was speculated that the transmembrane domain of Rv1625c may also serve the role of binding lipophilic ligands, similar to the autoinducers that activate quorum sensing receptors, to modulate AC signaling. However, a ligand capable of binding the transmembrane domain of Rv1625c and modulating AC activity has not been identified. On the basis of assays performed using an Rv1625c construct that only expressed the cyclase domain, it was previously proposed that CO_2 stimulates Rv1625c activity, similar to a mammalian G-protein regulated AC (*112*). However, this has not been confirmed using full-length Rv1625c protein, which clearly contains additional residues that are critical to the regulation of its function. Notably, full-length Rv1625c was not activated by exposure to other agonists of mammalian ACs (forskolin, calmodulin, or mammalian $G\alpha_s$) (*107*). As such, the native ligand(s) that activates Rv1625c in whole Mtb cells and during infection remains undetermined.

2.2.4 Characteristics of cAMP binding proteins in *M. tuberculosis*

Not only does Mtb feature diversity in its AC signaling pathways at the level of the AC proteins, but it also possesses a large repertoire of predicted downstream cAMP-binding effector proteins. Out of the ten predicted cAMP-binding proteins in Mtb, only four have begun to be functionally characterized (*99*).

Two of these proteins, CRP_{MT} and Cmr, contain conserved cAMP-binding and helix-tun-helix DNA-binding motifs, and they are proposed to act as cAMP-responsive transcription factors similar to the Crp proteins of other bacteria (*113-115*). Mtb deficient in CRP_{MT} has defects in persistence during infection in macrophages and in mice (*113*). A large regulon of ~100 genes are proposed to be targets for regulation by CRP_{MT} based on experiments examining transcriptional changes in ΔCRP_{MT} bacteria in standard liquid culture and consensus sequence predictions in Mtb, plus ChIP-seq in *M. bovis* (*113, 114, 116, 117*). These genes include components of the ESX-1 secretion system, a resuscitation promoting factor, a nitric oxide-sensitive transcription factor, a copper transporter, and two operons associated with central metabolism (the succinate dehydrogenase and fumarate reductase operons). Binding of CRP_{MT} to target DNA is somewhat enhanced in the presence of cAMP, but it features noncanonical cAMP-regulated DNA binding properties compared to the *E. coli* Crp (*114, 118*). Clearly more work is needed to determine how cAMP-responsive regulation of specific genes in the predicted CRP_{MT} regulon may contribute to Mtb pathogenesis. The second proposed cAMP-responsive transcription factor in Mtb, Cmr, has the potential to bind ~200 genomic regions, but only a handful of targets have been investigated further (*99*). Cmr is directly involved in regulating three targets in *M. bovis*, including during macrophage infection, but its regulation appears to be cAMP-independent for some targets (*99, 115, 119*). Later, Cmr was identified as a repressor of genes in the DosR regulon, but was found to be primarily redox-responsive rather than cAMP-responsive in this context (*119*). Better methods for interrogating Cmr-dependent gene regulation in response to increased cAMP levels in whole Mtb cells are needed before clear conclusions can be drawn about whether cAMP directly or indirectly influences the role of Cmr in Mtb pathogenesis.

The other two effectors, Mt-Pat and Rv1636, are novel cAMP-binding effector proteins. Mt-Pat possesses both cAMP-binding and lysine acetyltransferase activity. When Mt-Pat binds cAMP, it can acetylate lysine residues on various enzyme targets, which inactivates them. Confirmed targets of acetylation by Mt-Pat include the acetyl-CoA/propionyl-CoA synthetase and ten FadD acyl-CoA ligase enzymes in Mtb, which regulate the incorporation of 2- and 3-carbon precursors from fatty acids into central metabolism (*47, 120-123*). Under hypoxia, Mt-Pat plays an important role in maintaining the NAD^+/NADH balance when Mtb has access to fatty acids, and is hypothesized to direct fatty acids away from catabolism and promote reductive TCA cycle reactions to avoid accumulating NADH in the absence of oxygen as a terminal electron acceptor. This is broadly consistent with an accompanying role for the DosR regulon in supporting lipid anabolism during hypoxia via upregulation of the triacylglycerol synthase gene (*tgs1*), which supports synthesis of triacylglycerols and lipid body accumulation from excess fatty acid precursors (*49, 52*). Rv1636 is a universal stress protein that contains an ATP-binding motif, yet binds cAMP with higher affinity than ATP (*124*). Its biological function is unknown, but it was hypothesized that Rv1636 may participate in cAMP-dependent release of ATP into the cytosol during stress. Functions for the remaining six predicted cAMP-binding effector proteins in Mtb have yet to be suggested. Given the apparent complexity and noncanonical mechanisms exemplified by those that have been initially characterized, there is significant work left to be done before a complete picture of cAMP signaling pathways participating in Mtb pathogenesis can be proposed.

2.2.5 Identification of potential Rv1625c agonists in a high-throughput screen

Previously, we sought to identify small molecule compounds that inhibit growth of Mtb during macrophage infection *in vitro*. The chemical screening approach applied in this study was novel because screening assays historically tested compounds against Mtb grown in liquid media. In this study, J774 macrophages were infected with an mCherry-expressing strain of Mtb in a high-throughput 384-well format (*62*). The mCherry fluorescent protein is constitutively expressed in this strain of Mtb, and over the course of the macrophage infection, the mCherry fluorescent signal increases as the bacteria grow. A library of ~340,000 synthetic small molecules and natural products were screened for inhibition of mCherry signal during a six-day macrophage infection. Of these, ~4000 compounds inhibited Mtb growth (30–100% inhibition) relative to the positive control rifampin (100% inhibition) (*62*). When the most potent 1,359 hits against Mtb from macrophages were tested against Mtb in standard liquid media, a subset of 132 compounds that inhibit Mtb more potently in macrophages than in liquid media were identified (Fig. 2.6). These were categorized as "conditionally-active compounds" and >95% of these compounds were not related to other compounds reported previously in the literature, indicating that they included potentially novel mechanisms of action against Mtb (*62*). Because cholesterol is known to be a prominent carbon source during macrophage infection, the activities of these compounds against Mtb were also tested in liquid media containing cholesterol as the primary carbon source. More than half of the conditionally-active compounds inhibited Mtb replication in this condition, suggesting that their mechanisms of action were dependent on cholesterol utilization by Mtb. It was subsequently determined that several of these conditionally-active compounds targeted cholesterol utilization in Mtb directly, including apparent inhibitors of the methylcitrate cycle enzyme PrpC, and the HsaAB complex involved in ring catabolism (*62*). However, a set of potent inhibitors with an unknown mechanism of action were identified and designated as "orphan

cholesterol inhibitors." Initial characterization of three of these molecules (V-58, V-60, V-79) confirmed that they inhibit growth in cholesterol media, suppress expression of the KstR regulon, and cholesterol metabolism (*62*). Supplementing cholesterol media with the two-carbon fatty acid acetate rescued growth during treatment with these compounds, but supplementation with glucose did not. An initial screen seeking transposon mutations in Mtb that confer resistance to the V-58 compound identified multiple clones with mutations in *rv1625c*. All three orphan cholesterol inhibitors increased cAMP levels in Mtb relative to the vehicle control, consistent with the hypothesis that these compounds may activate the AC enzyme Rv1625c to increase cAMP synthesis (*62*).

A relationship between cAMP synthesis and cholesterol utilization had not been previously predicted prior to the discovery of the *rv1625c*-dependent orphan cholesterol inhibitors. Since cAMP is synthesized from ATP, we anticipated that resolving the importance of ATP hydrolysis-driven import of cholesterol and fatty acids by MceG would assist in interpretation of the cAMP induction studies. Previously, a role for cAMP secreted from Mtb in modulating macrophage functions had also been speculated but not carefully verified.
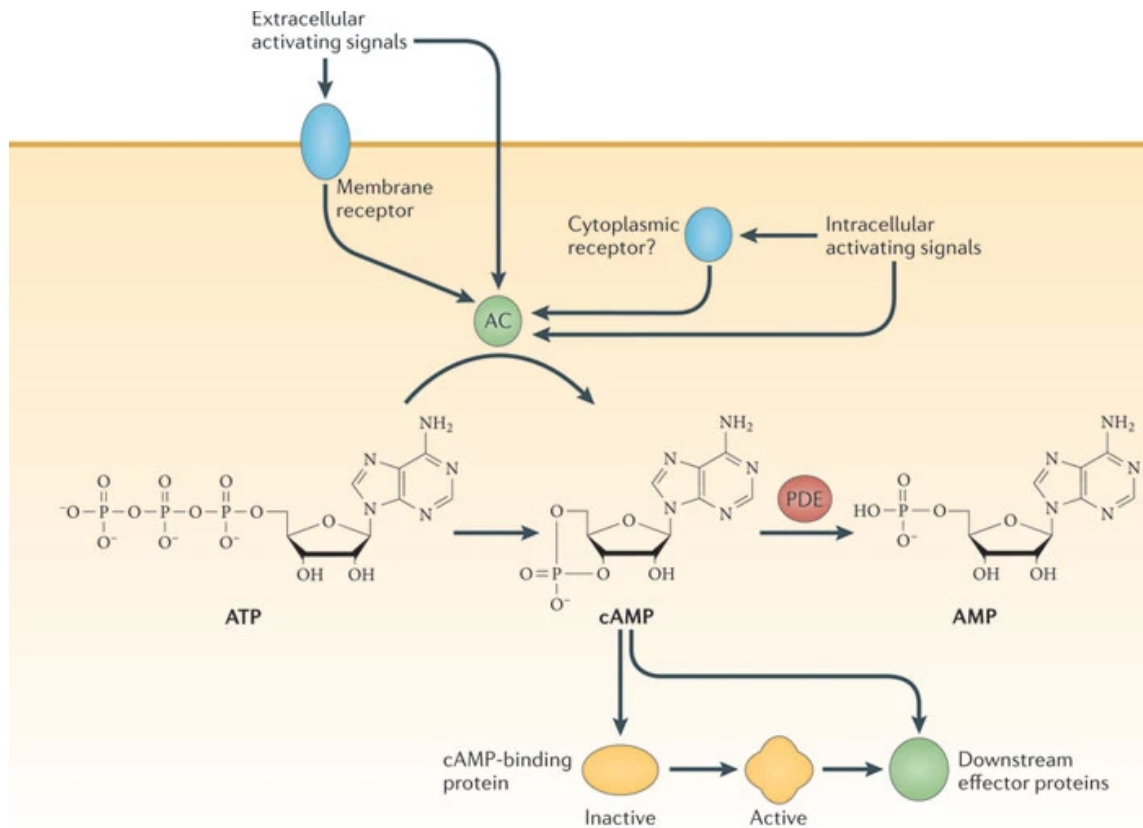
Figure 2.4 Common features of cAMP signaling networks. Reproduced with permission from (*77*).

A.

Transmembrane Domain

Helical Domain

Cytoplasmic Tail

D256
K296
D300
D365
R376

Cyclase Domain

B.

wildtype homodimer
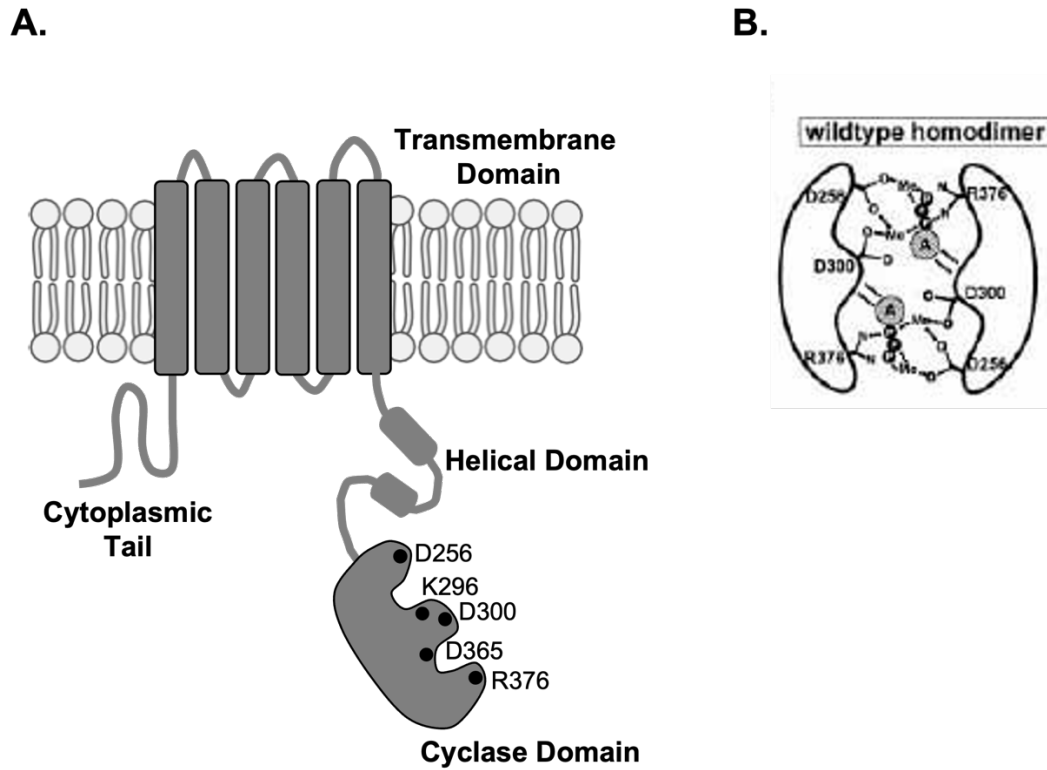
Figure 2.5 Topological diagram of the Rv1625c monomer and its domains. (A) Rv1625c is composed of an N-terminal cytoplasmic tail and six-helical transmembrane domain, followed by a cytoplasmic helical domain and the conserved cyclase domain. Dots illustrate conserved residues within the cyclase domain required for catalytic activity. **(B)** Illustration of the complementary residues in the catalytic sites of the homodimerized cyclase domains of Rv1625c. Figure in (B) reproduced with permission from (*104*).
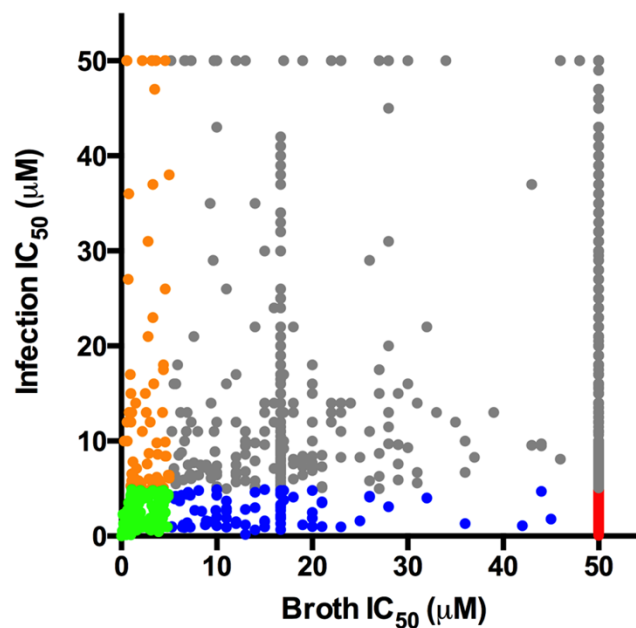
Figure 2.6 Distribution of screening hit compound IC$_{50}$ values in macrophages versus in standard liquid media. Dot plot depicting the half maximal inhibitory concentration (IC$_{50}$) values for the most potent 1,359 compounds in 7H9 OADC versus in the macrophage infection assays. Universally active compounds with IC$_{50}$ values < 5.0 μM in macrophages and < 5.0 μM in 7H9 OADC are indicated in green. The conditionally active compounds with IC$_{50}$ values < 5.0 μM in macrophages and > 50.0 μM 7H9 OADC are depicted in red. This group includes the set of chemical hits from which our Rv1625c agonist compounds were derived. Reproduced from (*62*) under the Creative Commons Attribution license.

2.3 Aims of this study

The purpose of this work is to examine the relationship between elevated cAMP synthesis, cholesterol utilization, and pathogenesis in Mtb.

I. Resolve the importance of ATP hydrolysis-dependent import of cholesterol by MceG.

II. Develop complementary chemical and genetic tools to investigate the relationship between Rv1625c, cAMP synthesis, ATP, and cholesterol utilization in Mtb.

III. Characterize the pharmacokinetic properties of orphan cholesterol utilization inhibitors, and identify a potent Rv1625c agonist suitable for use during infection studies in mice.

IV. Determine whether Rv1625c agonists disrupt Mtb pathogenesis in models of chronic TB.

V. Test the hypothesis that increasing cAMP synthesis in Mtb modulates macrophage inflammatory responses.

2.4 References

1.   R. J. Anderson, The Chemistry of the Lipids of the Tubercle Bacillus. *Yale J Biol Med* **15**, 311-345 (1943).

2.   H. Bloch, W. Segal, Biochemical differentiation of Mycobacterium tuberculosis grown in vivo and in vitro. *J Bacteriol* **72**, 132-141 (1956).

3.   C. L. Dulberger, E. J. Rubin, C. C. Boutte, The mycobacterial cell envelope - a moving target. *Nat Rev Microbiol* **18**, 47-59 (2020).

4.   R. R. Lovewell, C. M. Sassetti, B. C. VanderVen, Chewing the fat: lipid metabolism and homeostasis during M. tuberculosis infection. *Current Opinion in Microbiology* **29**, 30-36 (2016).

5.   M. Knight, J. Braverman, K. Asfaha, K. Gronert, S. Stanley, Lipid droplet formation in Mycobacterium tuberculosis infected macrophages requires IFN-gamma/HIF-1alpha signaling and supports host defense. *PLoS Pathog* **14**, e1006874 (2018).

6.   P. Peyron, J. Vaubourgeix, Y. Poquet, F. Levillain, C. Botanch, F. Bardou, M. Daffe, J. F. Emile, B. Marchou, P. J. Cardona, C. de Chastellier, F. Altare, Foamy macrophages from tuberculous patients' granulomas constitute a nutrient-rich reservoir for M. tuberculosis persistence. *PLoS pathogens* **4**, e1000204 (2008).

7.   J. Daniel, H. Maamar, C. Deb, T. D. Sirakova, P. E. Kolattukudy, Mycobacterium tuberculosis uses host triacylglycerol to accumulate lipid droplets and acquires a dormancy-like phenotype in lipid-loaded macrophages. *PLoS pathogens* **7**, e1002093 (2011).

8.   D. Menon, K. Singh, S. M. Pinto, A. Nandy, N. Jaisinghani, R. Kutum, D. Dash, T. S. K. Prasad, S. Gandotra, Quantitative Lipid Droplet Proteomics Reveals Mycobacterium

tuberculosis Induced Alterations in Macrophage Response to Infection. *ACS infectious diseases* **5**, 559-569 (2019).

9.   V. N. Sukhorukov, V. A. Khotina, Y. S. Chegodaev, E. Ivanova, I. A. Sobenin, A. N. Orekhov, Lipid Metabolism in Macrophages: Focus on Atherosclerosis. *Biomedicines* **8**, (2020).

10.   K. Beis, Structural basis for the mechanism of ABC transporters. *Biochem Soc Trans* **43**, 889-893 (2015).

11.   N. Casali, L. W. Riley, A phylogenomic analysis of the Actinomycetales mce operons. *BMC genomics* **8**, 60 (2007).

12.   E. V. Nazarova, C. R. Montague, T. La, K. M. Wilburn, N. Sukumar, W. Lee, S. Caldwell, D. G. Russell, B. C. VanderVen, Rv3723/LucA coordinates fatty acid and cholesterol uptake in Mycobacterium tuberculosis. *eLife* **6**, (2017).

13.   A. K. Pandey, C. M. Sassetti, Mycobacterial persistence requires the utilization of host cholesterol. *Proceedings of the National Academy of Sciences of the United States of America* **105**, 4376-4380 (2008).

14.   J. E. Griffin, J. D. Gawronski, M. A. DeJesus, T. R. Ioerger, B. J. Akerley, C. M. Sassetti, High-Resolution Phenotypic Profiling Defines Genes Essential for Mycobacterial Growth and Cholesterol Catabolism. *PLoS Pathog* **7**, (2011).

15.   S. M. Joshi, A. K. Pandey, N. Capite, S. M. Fortune, E. J. Rubin, C. M. Sassetti, Characterization of mycobacterial virulence genes through genetic interaction mapping. *Proceedings of the National Academy of Sciences of the United States of America* **103**, 11760-11765 (2006).

16. D. C. Ekiert, G. Bhabha, G. L. Isom, G. Greenan, S. Ovchinnikov, I. R. Henderson, J. S. Cox, R. D. Vale, Architectures of Lipid Transport Systems for the Bacterial Outer Membrane. *Cell* **169**, 273-285.e217 (2017).

17. H. Ouellet, S. Guan, J. B. Johnston, E. D. Chow, P. M. Kells, A. L. Burlingame, J. S. Cox, L. M. Podust, P. R. de Montellano, Mycobacterium tuberculosis CYP125A1, a steroid C27 monooxygenase that detoxifies intracellularly generated cholest-4-en-3-one. *Molecular microbiology* **77**, 730-742 (2010).

18. I. Casabon, K. Swain, A. M. Crowe, L. D. Eltis, W. W. Mohn, Actinobacterial acyl coenzyme A synthetases involved in steroid side-chain catabolism. *Journal of Bacteriology* **196**, 579-587 (2014).

19. K. M. Wilburn, R. A. Fieweger, B. C. VanderVen, Cholesterol and fatty acids grease the wheels of Mycobacterium tuberculosis pathogenesis. *Pathogens and Disease* **76**, (2018).

20. X. Yang, E. Dubnau, I. Smith, N. S. Sampson, Rv1106c from Mycobacterium tuberculosis is a 3beta-hydroxysteroid dehydrogenase. *Biochemistry* **46**, 9058-9067 (2007).

21. J. Knol, K. Bodewits, G. I. Hessels, L. Dijkhuizen, R. van der Geize, 3-Keto-5alpha-steroid Delta(1)-dehydrogenase from Rhodococcus erythropolis SQ1 and its orthologue in Mycobacterium tuberculosis H37Rv are highly specific enzymes that function in cholesterol catabolism. *The Biochemical journal* **410**, 339-346 (2008).

22. J. K. Capyk, I. Casabon, R. Gruninger, N. C. Strynadka, L. D. Eltis, Activity of 3-ketosteroid 9alpha-hydroxylase (KshAB) indicates cholesterol side chain and ring degradation occur simultaneously in Mycobacterium tuberculosis. *Journal of Biological Chemistry* **286**, 40717-40724 (2011).

23. J. K. Capyk, I. D'Angelo, N. C. Strynadka, L. D. Eltis, Characterization of 3-ketosteroid 9{alpha}-hydroxylase, a Rieske oxygenase in the cholesterol degradation pathway of Mycobacterium tuberculosis. *J Biol Chem* **284**, 9937-9946 (2009).

24. C. Dresen, L. Y. Lin, I. D'Angelo, E. I. Tocheva, N. Strynadka, L. D. Eltis, A flavin-dependent monooxygenase from Mycobacterium tuberculosis involved in cholesterol catabolism. *J Biol Chem* **285**, 22264-22275 (2010).

25. K. C. Yam, I. D'Angelo, R. Kalscheuer, H. Zhu, J.-X. Wang, V. Snieckus, L. H. Ly, P. J. Converse, W. R. Jacobs, Jr., N. Strynadka, L. D. Eltis, Studies of a Ring-Cleaving Dioxygenase Illuminate the Role of Cholesterol Metabolism in the Pathogenesis of Mycobacterium tuberculosis. *PLoS Pathogens* **5**, e1000344 (2009).

26. N. A. Lack, K. C. Yam, E. D. Lowe, G. P. Horsman, R. L. Owen, E. Sim, L. D. Eltis, Characterization of a carbon-carbon hydrolase from Mycobacterium tuberculosis involved in cholesterol metabolism. *J Biol Chem* **285**, 434-443 (2010).

27. J. Carere, S. E. McKenna, M. S. Kimber, S. Y. Seah, Characterization of an aldolase-dehydrogenase complex from the cholesterol degradation pathway of Mycobacterium tuberculosis. *Biochemistry* **52**, 3502-3511 (2013).

28. I. Casabon, A. M. Crowe, J. Liu, L. D. Eltis, FadD3 is an acyl-CoA synthetase that initiates catabolism of cholesterol rings C and D in actinobacteria. *Molecular microbiology* **87**, 269-283 (2013).

29. A. M. Crowe, I. Casabon, K. L. Brown, J. Liu, J. Lian, J. C. Rogalski, T. E. Hurst, V. Snieckus, L. J. Foster, L. D. Eltis, Catabolism of the Last Two Steroid Rings in Mycobacterium tuberculosis and Other Bacteria. *mBio* **8**, (2017).

30. J. E. Griffin, A. K. Pandey, S. A. Gilmore, V. Mizrahi, J. D. McKinney, C. R. Bertozzi, C. M. Sassetti, Cholesterol catabolism by Mycobacterium tuberculosis requires transcriptional and metabolic adaptations. *Chemistry & Biology* **19**, 218-227 (2012).

31. S. T. Thomas, B. C. VanderVen, D. R. Sherman, D. G. Russell, N. S. Sampson, Pathway Profiling in Mycobacterium tuberculosis: elucidation of a cholesterol-derived catabolite and the enzymes that catalyze its metabolism. *Journal of Biological Chemistry* **286**, 43668-43678 (2011).

32. J. K. Capyk, I. Casabon, R. Gruninger, N. C. Strynadka, L. D. Eltis, Activity of 3-ketosteroid 9alpha-hydroxylase (KshAB) indicates cholesterol side chain and ring degradation occur simultaneously in Mycobacterium tuberculosis. *J Biol Chem* **286**, 40717-40724 (2011).

33. N. M. Nesbitt, X. Yang, P. Fontan, I. Kolesnikova, I. Smith, N. S. Sampson, E. Dubnau, A thiolase of Mycobacterium tuberculosis is required for virulence and production of androstenedione and androstadienedione from cholesterol *Infection and Immunity* **78**, 275-282 (2010).

34. M. F. Wipperman, N. S. Sampson, S. T. Thomas, Pathogen roid rage: cholesterol utilization by Mycobacterium tuberculosis. *Critical Reviews in Biochemistry and Molecular Biology* **49**, 269-293 (2014).

35. S. L. Kendall, P. Burgess, R. Balhana, M. Withers, A. Ten Bokum, J. S. Lott, C. Gao, I. Uhia-Castro, N. G. Stoker, Cholesterol utilization in mycobacteria is controlled by two TetR-type transcriptional regulators: kstR and kstR2. *Microbiology* **156**, 1362-1371 (2010).

36.   S. L. Kendall, M. Withers, C. N. Soffair, N. J. Moreland, S. Gurcha, B. Sidders, R. Frita, A. Ten Bokum, G. S. Besra, J. S. Lott, N. G. Stoker, A highly conserved transcriptional repressor controls a large regulon involved in lipid degradation in Mycobacterium smegmatis and Mycobacterium tuberculosis. *Molecular Microbiology* **65**, 684-699 (2007).

37.   R. Van der Geize, K. Yam, T. Heuser, M. H. Wilbrink, H. Hara, M. C. Anderton, E. Sim, L. Dijkhuizen, J. E. Davies, W. W. Mohn, L. D. Eltis, A gene cluster encoding cholesterol catabolism in a soil actinomycete provides insight into Mycobacterium tuberculosis survival in macrophages. *Proceedings of the National Academy of Sciences* **104**, 1947-1952 (2007).

38.   N. A. Ho, S. S. Dawes, A. M. Crowe, I. Casabon, C. Gao, S. L. Kendall, E. N. Baker, L. D. Eltis, J. S. Lott, The Structure of the Transcriptional Repressor KstR in Complex with CoA Thioester Cholesterol Metabolites Sheds Light on the Regulation of Cholesterol Catabolism in Mycobacterium tuberculosis. *Journal of Biological Chemistry* **291**, 7256-7266 (2016).

39.   I. Casabon, S. H. Zhu, H. Otani, J. Liu, W. W. Mohn, L. D. Eltis, Regulation of the KstR2 regulon of Mycobacterium tuberculosis by a cholesterol catabolite. *Molecular microbiology* **89**, 1201-1212 (2013).

40.   E. V. Nazarova, C. R. Montague, L. Huang, T. La, D. Russell, B. C. VanderVen, The genetic requirements of fatty acid import by Mycobacterium tuberculosis within macrophages. *eLife* **8**, (2019).

41.   B. Jenkins, J. A. West, A. Koulman, A review of odd-chain fatty acid metabolism and the role of pentadecanoic Acid (c15:0) and heptadecanoic Acid (c17:0) in health and disease. *Molecules* **20**, 2425-2444 (2015).

42. S. T. Cole, R. Brosch, J. Parkhill, T. Garnier, C. Churcher, D. Harris, S. V. Gordon, K. Eiglmeier, S. Gas, C. E. Barry, 3rd, F. Tekaia, K. Badcock, D. Basham, D. Brown, T. Chillingworth, R. Connor, R. Davies, K. Devlin, T. Feltwell, S. Gentles, N. Hamlin, S. Holroyd, T. Hornsby, K. Jagels, A. Krogh, J. McLean, S. Moule, L. Murphy, K. Oliver, J. Osborne, M. A. Quail, M. A. Rajandream, J. Rogers, S. Rutter, K. Seeger, J. Skelton, R. Squares, S. Squares, J. E. Sulston, K. Taylor, S. Whitehead, B. G. Barrell, Deciphering the biology of Mycobacterium tuberculosis from the complete genome sequence. *Nature* **393**, 537-544 (1998).

43. K. J. Williams, H. I. Boshoff, N. Krishnan, J. Gonzales, D. Schnappinger, B. D. Robertson, The Mycobacterium tuberculosis beta-oxidation genes echA5 and fadB3 are dispensable for growth in vitro and in vivo. *Tuberculosis (Edinb)* **91**, 549-555 (2011).

44. L. E. Quadri, Biosynthesis of mycobacterial lipids by polyketide synthases and beyond. *Critical reviews in biochemistry and molecular biology* **49**, 179-211 (2014).

45. M. Jankute, J. A. Cox, J. Harrison, G. S. Besra, Assembly of the Mycobacterial Cell Wall. *Annu Rev Microbiol* **69**, 405-423 (2015).

46. G. M. Cook, K. Hards, C. Vilcheze, T. Hartman, M. Berney, Energetics of Respiration and Oxidative Phosphorylation in Mycobacteria. *Microbiol Spectr* **2**, (2014).

47. E. S. C. Rittershaus, S. H. Baek, I. V. Krieger, S. J. Nelson, Y. S. Cheng, S. Nambi, R. E. Baker, J. D. Leszyk, S. A. Shaffer, J. C. Sacchettini, C. M. Sassetti, A Lysine Acetyltransferase Contributes to the Metabolic Adaptation to Hypoxia in Mycobacterium tuberculosis. *Cell Chemical Biology* **25**, 1495-1505 e1493 (2018).

48. T. Beites, K. O'Brien, D. Tiwari, C. A. Engelhart, S. Walters, J. Andrews, H. J. Yang, M. L. Sutphen, D. M. Weiner, E. K. Dayao, M. Zimmerman, B. Prideaux, P. V. Desai, T.

Masquelin, L. E. Via, V. Dartois, H. I. Boshoff, C. E. Barry, 3rd, S. Ehrt, D. Schnappinger, Plasticity of the Mycobacterium tuberculosis respiratory chain and its impact on tuberculosis drug development. *Nature Communications* **10**, 4970 (2019).

49.   A. Singh, D. K. Crossman, D. Mai, L. Guidry, M. I. Voskuil, M. B. Renfrow, A. J. Steyn, Mycobacterium tuberculosis WhiB3 maintains redox homeostasis by regulating virulence lipid anabolism to modulate macrophage response. *PLoS Pathog* **5**, e1000545 (2009).

50.   K. H. Rohde, D. F. Veiga, S. Caldwell, G. Balazsi, D. G. Russell, Linking the transcriptional profiles and the physiological states of Mycobacterium tuberculosis during an extended intracellular infection. *PLoS Pathog* **8**, (2012).

51.   D. Schnappinger, S. Ehrt, M. I. Voskuil, Y. Liu, J. A. Mangan, I. M. Monahan, G. Dolganov, B. Efron, P. D. Butcher, C. Nathan, G. K. Schoolnik, Transcriptional Adaptation of Mycobacterium tuberculosis within Macrophages: Insights into the Phagosomal Environment. *The Journal of Experimental Medicine* **198**, 693-704 (2003).

52.   N. J. Garton, S. J. Waddell, A. L. Sherratt, S. M. Lee, R. J. Smith, C. Senner, J. Hinds, K. Rajakumar, R. A. Adegbola, G. S. Besra, P. D. Butcher, M. R. Barer, Cytological and transcript analyses reveal fat and lazy persister-like bacilli in tuberculous sputum. *PLoS Medicine* **5**, e75 (2008).

53.   A. D. Baughn, K. Y. Rhee, Metabolomics of Central Carbon Metabolism in Mycobacterium tuberculosis. *Microbiol Spectr* **2**, (2014).

54.   J. D. McKinney, K. H. zu Bentrup, E. J. Munoz-Elias, A. Miczak, B. Chen, W.-T. Chan, D. Swenson, J. C. Sacchettini, W. R. Jacobs, D. G. Russell, Persistence of Mycobacterium tuberculosis in macrophages and mice requires the glyoxylate shunt enzyme isocitrate lyase. *Nature* **406**, 735-738 (2000).

55.   E. J. Munoz-Elias, J. D. McKinney, Mycobacterium tuberculosis isocitrate lyases 1 and 2 are jointly required for in vivo growth and virulence. *Nat Med* **11**, 638-644 (2005).

56.   J. S. B. Paul R. Wheeler, in *Tuberculosis and the Tubercle Bacillus,* S. T. Cole, Ed. (ASM Press, Washington DC, 2005), vol. 1, chap. 20, pp. 321.

57.   K. Liu, J. Yu, D. G. Russell, pckA-deficient Mycobacterium bovis BCG shows attenuated virulence in mice and in macrophages. *Microbiology (Reading)* **149**, 1829-1835 (2003).

58.   J. Marrero, K. Y. Rhee, D. Schnappinger, K. Pethe, S. Ehrt, Gluconeogenic carbon flow of tricarboxylic acid cycle intermediates is critical for Mycobacterium tuberculosis to establish and maintain infection. *Proceedings of the National Academy of Sciences of the United States of America* **107**, 9819-9824 (2010).

59.   H. Eoh, K. Y. Rhee, Methylcitrate cycle defines the bactericidal essentiality of isocitrate lyase for survival of Mycobacterium tuberculosis on fatty acids. *Proceedings of the National Academy of Sciences of the United States of America* **111**, 4976-4981 (2014).

60.   E. J. Munoz-Elias, A. M. Upton, J. Cherian, J. D. McKinney, Role of the methylcitrate cycle in Mycobacterium tuberculosis metabolism, intracellular growth, and virulence. *Molecular microbiology* **60**, 1109-1122 (2006).

61.   W. Lee, B. C. VanderVen, R. J. Fahey, D. G. Russell, Intracellular Mycobacterium tuberculosis exploits host-derived fatty acids to limit metabolic stress. *Journal of Biological Chemistry* **288**, 6788-6800 (2013).

62.   B. C. VanderVen, R. J. Fahey, W. Lee, Y. Liu, R. B. Abramovitch, C. Memmott, A. M. Crowe, L. D. Eltis, E. Perola, D. D. Deininger, T. Wang, C. P. Locher, D. G. Russell, Novel inhibitors of cholesterol degradation in Mycobacterium tuberculosis reveal how the

bacterium's metabolism is constrained by the intracellular environment. *PLoS Pathogens* **11**, e1004679 (2015).

63.   S. Savvi, D. F. Warner, B. D. Kana, J. D. McKinney, V. Mizrahi, S. S. Dawes, Functional Characterization of a Vitamin B12-Dependent Methylmalonyl Pathway in Mycobacterium tuberculosis: Implications for Propionate Metabolism during Growth on Fatty Acids. *Journal of Bacteriology* **190**, 3886-3895 (2008).

64.   M. Jain, C. J. Petzold, M. W. Schelle, M. D. Leavell, J. D. Mougous, C. R. Bertozzi, J. A. Leary, J. S. Cox, Lipidomics reveals control of Mycobacterium tuberculosis virulence lipids via metabolic coupling. *Proceedings of the National Academy of Sciences of the United States of America* **104**, 5133-5138 (2007).

65.   X. Yang, N. M. Nesbitt, E. Dubnau, I. Smith, N. S. Sampson, Cholesterol Metabolism Increases the Metabolic Pool of Propionate in Mycobacterium tuberculosis. *Biochemistry* **48**, 3819-3821 (2009).

66.   D. E. Minnikin, L. Kremer, L. G. Dover, G. S. Besra, The methyl-branched fortifications of Mycobacterium tuberculosis. *Chemistry & biology* **9**, 545-553 (2002).

67.   S. Ehrt, D. Schnappinger, K. Y. Rhee, Metabolic principles of persistence and pathogenicity in Mycobacterium tuberculosis. *Nat Rev Microbiol* **16**, 496-507 (2018).

68.   K. Y. Rhee, L. P. de Carvalho, R. Bryk, S. Ehrt, J. Marrero, S. W. Park, D. Schnappinger, A. Venugopal, C. Nathan, Central carbon metabolism in Mycobacterium tuberculosis: an unexpected frontier. *Trends Microbiol* **19**, 307-314 (2011).

69.   D. Pisu, L. Huang, J. K. Grenier, D. G. Russell, Dual RNA-Seq of Mtb-Infected Macrophages In Vivo Reveals Ontologically Distinct Host-Pathogen Interactions. *Cell Rep* **30**, 335-350 e334 (2020).

70.   P. Aiewsakun, P. Prombutara, T. A. P. Siregar, T. Laopanupong, P. Kanjanasirirat, T. Khumpanied, S. Borwornpinyo, P. Tong-Ngam, A. Tubsuwan, P. Srilohasin, A. Chaiprasert, W. Ruangchai, P. Palittapongarnpim, T. Prammananan, B. C. VanderVen, M. Ponpuak, Transcriptional response to the host cell environment of a multidrug-resistant Mycobacterium tuberculosis clonal outbreak Beijing strain reveals its pathogenic features. *Scientific Reports* **11**, 3199 (2021).

71.   J. Timm, F. A. Post, L. G. Bekker, G. B. Walther, H. C. Wainwright, R. Manganelli, W. T. Chan, L. Tsenova, B. Gold, I. Smith, G. Kaplan, J. D. McKinney, Differential expression of iron-, carbon-, and oxygen-responsive mycobacterial genes in the lungs of chronically infected mice and tuberculosis patients. *Proceedings of the National Academy of Sciences of the United States of America* **100**, 14321-14326 (2003).

72.   C. M. Sassetti, E. J. Rubin, Genetic requirements for mycobacterial survival during infection. *Proceedings of the National Academy of Sciences of the United States of America* **100**, 12989-12994 (2003).

73.   C. M. Smith, R. E. Baker, M. K. Proulx, B. B. Mishra, J. E. Long, S. Park, H. Lee, M. C. Kiritsy, M. M. Bellerose, A. J. Olive, K. C. Murphy, K. Papavinasasundaram, F. J. Boehm, C. J. Reames, R. K. Meade, B. K. Hampton, C. L. Linnertz, G. D. Shaw, P. Hock, T. A. Bell, S. Ehrt, D. Schnappinger, F. Pardo-Manuel de Villena, M. T. Ferris, T. R. Ioerger, C. M. Sassetti, Host-pathogen genetic interactions underlie tuberculosis susceptibility. *bioRxiv* **2020.12.01.405514**, (2021).

74.   Y. Hu, R. van der Geize, G. S. Besra, S. S. Gurcha, A. Liu, M. Rohde, M. Singh, A. Coates, 3-Ketosteroid 9alpha-hydroxylase is an essential factor in the pathogenesis of Mycobacterium tuberculosis. *Molecular Microbiology* **75**, 107-121 (2010).

75. N. Shimono, L. Morici, N. Casali, S. Cantrell, B. Sidders, S. Ehrt, L. W. Riley, Hypervirulent mutant of Mycobacterium tuberculosis resulting from disruption of the mce1 operon. *Proceedings of the National Academy of Sciences of the United States of America* **100**, 15918-15923 (2003).

76. A. Gioffre, E. Infante, D. Aguilar, M. P. Santangelo, L. Klepp, A. Amadio, V. Meikle, I. Etchechoury, M. I. Romano, A. Cataldi, R. P. Hernandez, F. Bigi, Mutation in mce operons attenuates Mycobacterium tuberculosis virulence. *Microbes Infect* **7**, 325-334 (2005).

77. K. A. McDonough, A. Rodriguez, The myriad roles of cyclic AMP in microbial pathogens: from signal to sword. *Nature Reviews Microbiology* **10**, 27-38 (2011).

78. B. Gorke, J. Stulke, Carbon catabolite repression in bacteria: many ways to make the most out of nutrients. *Nature Reviews Microbiology* **6**, 613-624 (2008).

79. A. Nanchen, A. Schicker, O. Revelles, U. Sauer, Cyclic AMP-dependent catabolite repression is the dominant control mechanism of metabolic fluxes under glucose limitation in Escherichia coli. *J Bacteriol* **190**, 2323-2330 (2008).

80. A. Romero-Rodriguez, D. Rocha, B. Ruiz-Villafan, S. Guzman-Trampe, N. Maldonado-Carmona, M. Vazquez-Hernandez, A. Zelarayan, R. Rodriguez-Sanoja, S. Sanchez, Carbon catabolite regulation in Streptomyces: new insights and lessons learned. *World J Microbiol Biotechnol* **33**, 162 (2017).

81. H. J. Lee, S. J. Park, S. H. Choi, K. H. Lee, Vibrio vulnificus rpoS expression is repressed by direct binding of cAMP-cAMP receptor protein complex to its two promoter regions. *J Biol Chem* **283**, 30438-30450 (2008).

82.	A. T. Nielsen, N. A. Dolganov, T. Rasmussen, G. Otto, M. C. Miller, S. A. Felt, S. Torreilles, G. K. Schoolnik, A bistable switch and anatomical site control Vibrio cholerae virulence gene expression in the intestine. *PLoS Pathog* **6**, e1001102 (2010).

83.	L. Zhan, L. Yang, L. Zhou, Y. Li, H. Gao, Z. Guo, L. Zhang, C. Qin, D. Zhou, R. Yang, Direct and negative regulation of the sycO-ypkA-ypoJ operon by cyclic AMP receptor protein (CRP) in Yersinia pestis. *BMC microbiology* **9**, 178 (2009).

84.	M. C. Wolfgang, V. T. Lee, M. E. Gilmore, S. Lory, Coordinate regulation of bacterial virulence genes by a novel adenylate cyclase-dependent signaling pathway. *Developmental cell* **4**, 253-263 (2003).

85.	E. L. Fuchs, E. D. Brutinel, A. K. Jones, N. B. Fulcher, M. L. Urbanowski, T. L. Yahr, M. C. Wolfgang, The Pseudomonas aeruginosa Vfr regulator controls global virulence factor expression through cyclic AMP-dependent and -independent mechanisms. *J Bacteriol* **192**, 3553-3564 (2010).

86.	W. Liang, A. Pascual-Montano, A. J. Silva, J. A. Benitez, The cyclic AMP receptor protein modulates quorum sensing, motility and multiple genes that affect intestinal colonization in Vibrio cholerae. *Microbiology (Reading)* **153**, 2964-2975 (2007).

87.	C. H. Serezani, M. N. Ballinger, D. M. Aronoff, M. Peters-Golden, Cyclic AMP: master regulator of innate immune cell function. *Am J Respir Cell Mol Biol* **39**, 127-132 (2008).

88.	C. Steegborn, Structure, mechanism, and regulation of soluble adenylyl cyclases - similarities and differences to transmembrane adenylyl cyclases. *Biochimica et Biophysica Acta* **1842**, 2535-2547 (2014).

89.	S. Gerlo, R. Kooijman, I. M. Beck, K. Kolmus, A. Spooren, G. Haegeman, Cyclic AMP: a selective modulator of NF-kappaB action. *Cell Mol Life Sci* **68**, 3823-3841 (2011).

90. E. A. Wall, J. R. Zavzavadjian, M. S. Chang, B. Randhawa, X. Zhu, R. C. Hsueh, J. Liu, A. Driver, X. R. Bao, P. C. Sternweis, M. I. Simon, I. D. Fraser, Suppression of LPS-induced TNF-alpha production in macrophages by cAMP is mediated by PKA-AKAP95-p105. *Sci Signal* **2**, ra28 (2009).

91. S. H. Kim, C. H. Serezani, K. Okunishi, Z. Zaslona, D. M. Aronoff, M. Peters-Golden, Distinct protein kinase A anchoring proteins direct prostaglandin E2 modulation of Toll-like receptor signaling in alveolar macrophages. *J Biol Chem* **286**, 8875-8883 (2011).

92. J. Vojtova, J. Kamanova, P. Sebo, Bordetella adenylate cyclase toxin: a swift saboteur of host defense. *Current opinion in microbiology* **9**, 69-75 (2006).

93. N. H. Carbonetti, G. V. Artamonova, C. Andreasen, N. Bushar, Pertussis toxin and adenylate cyclase toxin provide a one-two punch for establishment of Bordetella pertussis infection of the respiratory tract. *Infect Immun* **73**, 2698-2703 (2005).

94. J. N. Ahmad, P. Sebo, Adenylate Cyclase Toxin Tinkering With Monocyte-Macrophage Differentiation. *Frontiers in immunology* **11**, 2181 (2020).

95. D. M. Aronoff, J. K. Carstens, G. H. Chen, G. B. Toews, M. Peters-Golden, Short communication: differences between macrophages and dendritic cells in the cyclic AMP-dependent regulation of lipopolysaccharide-induced cytokine and chemokine synthesis. *J Interferon Cytokine Res* **26**, 827-833 (2006).

96. D. M. Aronoff, C. Canetti, C. H. Serezani, M. Luo, M. Peters-Golden, Cutting edge: macrophage inhibition by cyclic AMP (cAMP): differential roles of protein kinase A and exchange protein directly activated by cAMP-1. *J Immunol* **174**, 595-599 (2005).

97.	D. M. Aronoff, C. Canetti, M. Peters-Golden, Prostaglandin E2 inhibits alveolar macrophage phagocytosis through an E-prostanoid 2 receptor-mediated increase in intracellular cyclic AMP. *J Immunol* **173**, 559-565 (2004).

98.	B. Luan, Y. S. Yoon, J. Le Lay, K. H. Kaestner, S. Hedrick, M. Montminy, CREB pathway links PGE2 signaling with macrophage polarization. *Proceedings of the National Academy of Sciences of the United States of America* **112**, 15642-15647 (2015).

99.	R. M. Johnson, K. A. McDonough, Cyclic nucleotide signaling in Mycobacterium tuberculosis: an expanding repertoire. *Pathogens and Disease* **76**, (2018).

100.	G. S. Knapp, K. A. McDonough, Cyclic AMP Signaling in Mycobacteria. *Microbiol Spectr* **2**, (2014).

101.	A. R. Shenoy, S. S. Visweswariah, New messages from old messengers: cAMP and mycobacteria. *Trends Microbiol* **14**, 543-550 (2006).

102.	A. R. Shenoy, S. S. Visweswariah, Mycobacterial adenylyl cyclases: biochemical diversity and structural plasticity. *FEBS Lett* **580**, 3344-3352 (2006).

103.	I. Tews, F. Findeisen, I. Sinning, A. Schultz, J. E. Schultz, J. U. Linder, The structure of a pH-sensing mycobacterial adenylyl cyclase holoenzyme. *Science* **308**, 1020-1023 (2005).

104.	Y. L. Guo, T. Seebacher, U. Kurz, J. U. Linder, J. E. Schultz, Adenylyl cyclase Rv1625c of Mycobacterium tuberculosis: a progenitor of mammalian adenylyl cyclases. *EMBO Journal* **20**, 3667-3675 (2001).

105.	A. R. Shenoy, N. Srinivasan, M. Subramaniam, S. S. Visweswariah, Mutational analysis of the Mycobacterium tuberculosis Rv1625c adenylyl cyclase: residues that confer nucleotide specificity contribute to dimerization. *FEBS Lett* **545**, 253-259 (2003).

106. A. D. Ketkar, A. R. Shenoy, U. A. Ramagopal, S. S. Visweswariah, K. Suguna, A structural basis for the role of nucleotide specifying residues in regulating the oligomerization of the Rv1625c adenylyl cyclase from M. tuberculosis. *Journal of molecular biology* **356**, 904-916 (2006).

107. S. K. Reddy, M. Kamireddi, K. Dhanireddy, L. Young, A. Davis, P. T. Reddy, Eukaryotic-like adenylyl cyclases in Mycobacterium tuberculosis H37Rv: cloning and characterization. *Journal of Biological Chemistry* **276**, 35141-35149 (2001).

108. Y. L. Guo, U. Kurz, A. Schultz, J. U. Linder, D. Dittrich, C. Keller, S. Ehlers, P. Sander, J. E. Schultz, Interaction of Rv1625c, a mycobacterial class IIIa adenylyl cyclase, with a mammalian congener. *Molecular microbiology* **57**, 667-677 (2005).

109. I. Vercellino, L. Rezabkova, V. Olieric, Y. Polyhach, T. Weinert, R. A. Kammerer, G. Jeschke, V. M. Korkhov, Role of the nucleotidyl cyclase helical domain in catalytically active dimer formation. *Proceedings of the National Academy of Sciences of the United States of America* **114**, E9821-E9828 (2017).

110. S. Beltz, J. Bassler, J. E. Schultz, Regulation by the quorum sensor from Vibrio indicates a receptor function for the membrane anchors of adenylate cyclases. *eLife* **5**, (2016).

111. M. Ziegler, J. Bassler, S. Beltz, A. Schultz, A. N. Lupas, J. E. Schultz, Characterization of a novel signal transducer element intrinsic to class IIIa/b adenylate cyclases and guanylate cyclases. *FEBS Journal* **284**, 1204-1217 (2017).

112. P. D. Townsend, P. M. Holliday, S. Fenyk, K. C. Hess, M. A. Gray, D. R. Hodgson, M. J. Cann, Stimulation of mammalian G-protein-responsive adenylyl cyclases by carbon dioxide. *J Biol Chem* **284**, 784-791 (2009).

113.   L. Rickman, C. Scott, D. M. Hunt, T. Hutchinson, M. C. Menendez, R. Whalan, J. Hinds, M. J. Colston, J. Green, R. S. Buxton, A member of the cAMP receptor protein family of transcription regulators in Mycobacterium tuberculosis is required for virulence in mice and controls transcription of the rpfA gene coding for a resuscitation promoting factor. *Molecular microbiology* **56**, 1274-1286 (2005).

114.   G. Bai, L. A. McCue, K. A. McDonough, Characterization of Mycobacterium tuberculosis Rv3676 (CRPMt), a cyclic AMP receptor protein-like DNA binding protein. *J Bacteriol* **187**, 7795-7804 (2005).

115.   M. A. Gazdik, G. Bai, Y. Wu, K. A. McDonough, Rv1675c (cmr) regulates intramacrophage and cyclic AMP-induced gene expression in Mycobacterium tuberculosis-complex mycobacteria. *Molecular microbiology* **71**, 434-448 (2009).

116.   G. S. Knapp, A. Lyubetskaya, M. W. Peterson, A. L. Gomes, Z. Ma, J. E. Galagan, K. A. McDonough, Role of intragenic binding of cAMP responsive protein (CRP) in regulation of the succinate dehydrogenase genes Rv0249c-Rv0247c in TB complex mycobacteria. *Nucleic acids research* **43**, 5377-5393 (2015).

117.   Y. Akhter, S. Yellaboina, A. Farhana, A. Ranjan, N. Ahmed, S. E. Hasnain, Genome scale portrait of cAMP-receptor protein (CRP) regulons in mycobacteria points to their role in pathogenesis. *Gene* **407**, 148-158 (2008).

118.   M. Stapleton, I. Haq, D. M. Hunt, K. B. Arnvig, P. J. Artymiuk, R. S. Buxton, J. Green, Mycobacterium tuberculosis cAMP receptor protein (Rv3676) differs from the Escherichia coli paradigm in its cAMP binding and DNA binding properties and transcription activation properties. *J Biol Chem* **285**, 7016-7027 (2010).

119. L. J. Smith, A. Bochkareva, M. D. Rolfe, D. M. Hunt, C. Kahramanoglou, Y. Braun, A. Rodgers, A. Blockley, S. Coade, K. E. A. Lougheed, N. A. Hafneh, S. M. Glenn, J. C. Crack, N. E. Le Brun, J. W. Saldanha, V. Makarov, I. Nobeli, K. Arnvig, G. V. Mukamolova, R. S. Buxton, J. Green, Cmr is a redox-responsive regulator of DosR that contributes to M. tuberculosis virulence. *Nucleic acids research* **45**, 6600-6612 (2017).

120. H. Xu, S. S. Hegde, J. S. Blanchard, Reversible acetylation and inactivation of Mycobacterium tuberculosis acetyl-CoA synthetase is dependent on cAMP. *Biochemistry* **50**, 5883-5892 (2011).

121. S. Nambi, K. Gupta, M. Bhattacharyya, P. Ramakrishnan, V. Ravikumar, N. Siddiqui, A. T. Thomas, S. S. Visweswariah, Cyclic AMP-dependent protein lysine acylation in mycobacteria regulates fatty acid and propionate metabolism. *Journal of Biological Chemistry* **288**, 14114-14124 (2013).

122. H. J. Lee, P. T. Lang, S. M. Fortune, C. M. Sassetti, T. Alber, Cyclic AMP regulation of protein lysine acetylation in Mycobacterium tuberculosis. *Nature Structural & Molecular Biology* **19**, 811-818 (2012).

123. J. D. Hayden, L. R. Brown, H. P. Gunawardena, E. F. Perkowski, X. Chen, M. Braunstein, Reversible acetylation regulates acetate and propionate metabolism in Mycobacterium smegmatis. *Microbiology (Reading)* **159**, 1986-1999 (2013).

124. A. Banerjee, R. S. Adolph, J. Gopalakrishnapai, S. Kleinboelting, C. Emmerich, C. Steegborn, S. S. Visweswariah, A universal stress protein (USP) in mycobacteria binds cAMP. *J Biol Chem* **290**, 12731-12743 (2015).

CHAPTER THREE

Hydrolysis of ATP by MceG is required for cholesterol and fatty acid utilization in *M. tuberculosis*

Adapted from

The ATPase activity of MceG is required to facilitate fatty acid and cholesterol import in *Mycobacterium tuberculosis*. Rachael A. Fieweger*, Kaley M. Wilburn*, Christine R. Montague, Carolyn M. Kelly, Teresa L. Southard, Holger Sondermann, Evgeniya V. Nazarova, and Brian C. VanderVen. Manuscript in preparation. *Authors contributed equally. Immunoblotting, MceG ATPase activity assay, and fatty acid utilization assays were performed by R.Fieweger.*

ABSTRACT

Over the last decade, it has been confirmed repeatedly that *Mycobacterium tuberculosis* (Mtb) requires intact lipid utilization pathways to maintain optimal fitness during infection. Specifically, pathways that carry out fatty acid and cholesterol breakdown within the bacterial cell have begun to be elucidated. However, the cell envelope of Mtb has several unique features that present a logistical challenge for importing lipid nutrients. Here, we characterize a shared subunit of the fatty acid and cholesterol import systems in Mtb, named MceG/Rv0655. MceG is a predicted ATPase, and its ATPase activity is hypothesized to energize both the fatty acid (Mce1) and cholesterol (Mce4) import complexes. Here, we demonstrate that the ATPase activity of MceG is required during both fatty acid and cholesterol import, via both shared and unique mechanisms. MceG is required for full bacterial fitness *in vivo*, and Mtb lacking MceG ATPase activity display colonization defects in mice. These findings expand our understanding of MceG-dependent lipid transport in Mtb.

3.1 Introduction

Mycobacterium tuberculosis (Mtb) is a highly successful pathogen that is adapted to persist long-term during infection of the human lung. To achieve transmission, Mtb routinely remains viable in an individual host's lungs for years (*1*). This requires the bacterium to adopt various metabolic adaptations that allow it to acquire and utilize nutrients within the constraints of conditions imposed by the host environment (*2*). Mtb spends the majority of its life cycle intracellularly in macrophages or neutrophils, or in the extracellular caseum of granulomas (*3*). Because of this, interest in how Mtb acquires and utilizes host-derived nutrients to fuel critical metabolic and biosynthetic pathways across these dynamic environments has grown. It would be ideal to identify essential components of nutrient utilization pathways that support Mtb viability across the diverse conditions it encounters in the host, as these may represent novel bacterial pathways that could be targeted for antibiotic development (*1, 4, 5*).

The cell envelope of Mtb is an intricate structure composed of many layers. From inside to outside, it includes the cytoplasmic membrane, periplasmic space, cross-linked peptidoglycan layer, arabinogalactan polymers covalently attached to the inner peptidoglycan layer and to glycolipid species, a layer of mycolic acids attached to the arabinogalactan layer, and a thick outer layer of mycolic acids and other surface lipids (*6*). This waxy envelope is a defining feature of the mycobacterial cell. Compared to Gram-negative bacteria, the overall composition of the Mtb cell envelope provides a significant barrier to permeability that excludes many macromolecules, including β-lactam antibiotics (*6, 7*). The import of some small, hydrophilic nutrients across the cell envelope is facilitated through porin-like channels and driven by diffusion (*7*). Import of some other large and/or scarce molecules that cannot be transported effectively through porins have been shown to be coordinated by ABC transporters (*7, 8*).

Mtb is exposed to a variety of potential nutrients during infection; however, there is expanding evidence that fatty acids and cholesterol are key host-derived nutrients required for the bacterium to maintain viability during infection (*3, 9-13*). Fatty acids and cholesterol play overlapping and complementary roles in Mtb metabolism (*14*). However, mechanisms utilized by the bacterium to coordinate the import of these substrates into the cell are not well understood. It is important to characterize these mechanisms because they may represent novel antibiotic targets that, when inhibited, could prevent utilization of two complementary carbon sources that support Mtb viability during infection (*9*). To import hydrophobic substrates like fatty acids and cholesterol, Mtb uses the Mce1 and Mce4 transporter complexes, respectively (*9*). These transporters are multi-protein complexes related to bacterial ABC transporters, which bind substrates and provide the energy required for membrane passage by hydrolyzing ATP (*8*). It is thought that the substrate-specific protein subunits of the Mce1 and Mce4 transporters are encoded in two separate mce operons in the Mtb genome (*15, 16*). Based on structures of Mce proteins from *E. coli*, it has been hypothesized that the Mce1 and Mce4 complexes transport substrates through the long-chain lipid layers and the periplasmic region of the Mtb cell envelope to deliver their substrates to permease proteins embedded in the cytoplasmic membrane (*8, 9, 17*).

Growing evidence indicates that the Mce1 and Mce4 transporters require shared proteins that are not encoded in any of the four mce operons to maintain their stability and function. Previously, we determined that although these transporters are specific for their respective substrates, Mce1 and Mce4 share a common protein (LucA/Rv3723) that facilitates transporter activity (*18*). LucA is not encoded in an mce operon, yet this protein stabilizes Mce1 and facilitates Mce1- and Mce4-mediated transport (*18, 19*). Specific members of the orphaned Mce-associated membrane protein (Omam) family also stabilize Mce1 and Mce4 transporters in *M. smegmatis (16,*

20). It was also previously proposed that the Mce1 and Mce4 transporters both require the shared ATPase MceG to provide energy to drive import of their substrates (*19, 21*). This was based on a genetic interaction mapping screen that predicted *mceG* functions in the same pathway as the *mce1* and *mce4* loci (*21*). MceG is also homologous to the nucleotide binding domain subunits of ABC transporters, and it was hypothesized that MceG associates with the YrbEAB proteins of the Mce complexes, which are homologous to the permease subunits of ABC transporters. MceG and its homologs have been characterized in the context of cholesterol utilization, and these proteins are necessary for cholesterol import in *Rhodococcus josti, Mycobacterium smegmatis,* and Mtb *(22-24).* A recent genetic screen also confirmed that MceG is necessary during fatty acid import, supporting the hypothesis that MceG is the universal ATPase of the Mce transporters in Mtb (*19*). Here, we demonstrate that the ATPase activity of MceG is required for transport of Mce1 and Mce4 lipid substrates. Surprisingly, MceG is essential for stabilization of substrate binding proteins in the Mce1 complex, but less important for stabilization of proteins in the Mce4 complex. Mtb mutants lacking MceG or expressing a catalytically inactive version of MceG display fitness defects in mice associated with an inability to import fatty acids and cholesterol. Together these results confirm that the ATPase activity of MceG is a weakness in Mtb nutrient utilization that is required for two distinct lipid transporters, and this may represent a novel target for tuberculosis drug discovery.

3.2   Materials and Methods

Strains and growth conditions

The *E coli* strains Top10 (Invitrogen) and T7 Express (New England Biolabs) were used for cloning. *E. coli* strains were grown in LB medium and transformants were selected on LB plates containing kanamycin (25 µg ml^{-1}), ampicillin (100 µg ml^{-1}) or hygromycin (100 µg ml^{-1}). For protein expression, the *E coli* strain BL21 (DE3) (Stratagene), was used and strains were grown in LB medium or Terrific Broth media containing antibiotics. Mtb Erdman strains were cultivated in 7H9 medium (BD Biosciences) containing OADC supplement (BD Biosciences) unless otherwise noted. 7H12 base medium was used as previously described (*13*) and supplemented with cholesterol (100 µM), fatty acids (100 µM), or sodium acetate (0.1%). Stock solutions (1000x) of lipid substrates were solubilized in a ($1{:}1$ v/v) solution of tyloxapol (Sigma) and ethanol and heated to $65°C$ prior to adding into media, with the final concentration of tyloxapol at 0.05%. The Δmce1 and ΔlucA mutant strains were generated as described (*18*). To create the ΔmceG mutant strain, the internal region of the *rv0655* open reading frame (111 bp -499 bp) was replaced with a hygromycin cassette via allelic exchange and confirmed with sequencing (*25*). For fatty acid toxicity studies Mtb strains were cultured to mid-log phase in 7H9 OADC + 0.05% tyloxapol, and then inoculated at an OD$_{600}$ of 0.005 into 10 ml of 7H12 media lacking casitone and supplemented with 25 µM palmitate. Cultures were incubated at $37°C$ for 21 days and an OD$_{600}$ measurement was taken every 3-4 days over the course of the incubation period.

Western blot analysis

To obtain lysates for western blot analysis, Mtb strains were cultured in 40 ml of 7H9 OADC + 0.05% tyloxapol to an OD_{600} of 0.6. Bacteria were harvested through centrifugation and fixed for 1 hour with 4% PFA. Cells were washed with PBS 0.05% tyloxapol and lysed in 1% SDS using sonication. After separation via SDS-PAGE, proteins were transferred to a nitrocellulose membrane. Antibodies for GroEL were obtained from BEI resources and anti-MceG antibodies were generated as previously described (*18*). Antibodies for Mce1A, Mce1D, and Mce1E were a gift from Dr. Christopher Sassetti (*26*).

Protein expression and purification

To express recombinant MceG, a plasmid containing a truncated version of wild type or mutant MceG fused at the N-terminus to a His_6-SUMO tag were transformed into *E. coli* BL21 (DE3) cells. To generate MceG point mutants, site-directed mutagenesis was performed using the QuickChange method (Agilent). For protein expression, these strains were cultured in 18.0 liters of Terrific Broth medium containing kanamycin (50 µg ml^{-1}) to an OD_{600} of 0.6 at 37˚C. The temperature was then lowered to 18˚C and 0.5 mM IPTG (Sigma) was added to induce gene expression. Cultures were incubated for 16 hours at 18˚C and shaking at 220 rpm. Cells were harvested by centrifugation and sonicated in Buffer A (25 mM Tris HCl, pH 8.5, 500 mM NaCl, 20 mM imidazole). Centrifugation was used to remove debris and the His-tagged proteins were affinity purified using Ni-NTA resin. Protein was eluted off the resin with Buffer B (25 mM Tris HCl, pH 8.5, 500 mM NaCl, 500 mM imidazole). A HiPrep 26/10 Desalting column (GE Life Sciences) was used to buffer exchange the protein into gel filtration buffer (25 mM Tris HCl, pH 7.5, 150 mM NaCl), and it was further purified using an S200 size exclusion chromatography

column (GE). Purified protein from peak fractions was concentrated to 10 mg ml^{-1} and stored at - 80 ˚C. Protein purity was assessed via SDS-PAGE and Coomassie staining.

ATPase assay

ATPase activity of recombinant wild type or mutant MceG was measured using the Enzcheck Phosphate Assay kit (Invitrogen). A reaction mixture was made following the kit instructions and scaled to reaction volume of 200 µL. The reaction mixture was added to a 96-well plate along with recombinant wild type or mutant MceG at concentrations of 2.5, 5, 12.5, and 25 µM. Following the addition of 0.5 mM ATP, inorganic phosphate accumulation was assessed over time through measurement of the absorbance at 360 nm using an Envision plate reader (Perkin Elmer).

Lipid uptake assays

Lipid uptake was quantified as described previously (*18*) with slight modifications. Briefly, Mtb was cultured in T25 tissue culture flasks with 7H9 AD supplemented with 0.01% glycerol and 0.05% tyloxapol for five days. Cultures were then concentrated to an OD$_{600}$ of 0.7 in 7.0 ml using spent medium and were incubated with 1 µCi of [^{14}C(U)]-palmitate (Perkin Elmer) or [4-^{14}C] cholesterol (Perkin Elmer) at 37˚C for 2 hours. As done previously, samples of 1.5 ml were removed at 5, 30, 60, and 120-minute time points. Cells were washed three times and then fixed in 4% PFA. Lipid assimilation was quantified by scintillation counting. For sodium azide experiments, flasks were inoculated with sodium azide at a final concentration of 60mM and incubated at room temperature for 10 minutes before radiolabel was added.

Radiorespirometry assays

Catabolism of radiolabeled lipids was quantified as previously described (*18*). For sodium azide experiments, flasks were inoculated with sodium azide at a final concentration of 60mM and incubated at room temperature for 10 minutes before radiolabel was added.

Isolation of RNA and qPCR analysis

RNA was purified from WT, MceG mutant, complement, D188N or E189Q complement Mtb growing in exponential phase. Bacteria were pelleted and lysed in Trizol LS (Invitrogen) with 0.1 mm silica beads in a FastPrep-24 bead beating grinder (MP Biomedicals). The RNA was purified using Trizol LS per manufacturer instructions with the addition of a second chloroform extraction and a second ethanol wash. The DNA was digested using TURBO DNA-free Kit (Invitrogen). For relative quantification of gene expression, cDNA was generated from 250 ng of RNA using iScript cDNA synthesis kit (Biorad) and real-time PCR was performed using the iTaq SYBR Green kit (Biorad) on the 7500 Fast Real-Time PCR System (Applied Biosystems). Gene-specific primers were designed using Primer3 software (http://bioinfo.ut.ee/primer3-0.4.0/primer3/) and synthesized (IDT). The sigma factor gene sigA (Rv2703) was used to normalize each sample and approximate fold induction compared to WT was calculated using the $2^{-\Delta\Delta CT}$ method (*27*). Average and range of fold induction were calculated using the average and standard deviation of $\Delta\Delta CT$ from 4 experimental replicates, and statistical changes in $\Delta\Delta CT$ were determined using two-way ANOVA and Dunnett's multiple comparisons (*28*).

Mouse infection studies

Six to eight-week-old female BALB/cJ wild type mice (Jackson Laboratories) were infected with 1000 CFU of Mtb strains via an intranasal delivery method as described (*29*). The mice were

anesthetized with isoflurane and 25 µl of bacteria were introduced into both nares. For aerosol infection studies, the mice were infected using an aerosol inhalation exposure system (Glass-Col) with a calibrated dose of 100 bacilli. At sacrifice, the lungs were removed and half of the lungs were fixed in 4% PFA overnight for histology studies, while another half was used for bacterial load quantification. For the latter, lungs were homogenized in PBS 0.05% Tween-80 and plated on 7H10 OADC agar. CFU were quantified after 3–4 weeks incubation at 37°C.

3.3   Results

3.3.1   MceG exhibits ATPase activity

MceG contains the conserved canonical Walker A and B motifs required for ATP binding and hydrolysis, as well as an ABC transporter family signature motif (*8*). MceG is necessary for Mce4 mediated transport of cholesterol in Mtb, and a conserved residue in the Waker A motif (K66) is required for MceG function and Mtb viability during infection (*21*). Additionally, import of cholesterol in the related Actinobacteria, *Rhodococcus jostii* RHA1, and in *M. smegmatis* can be abolished via treatment with the ATPase inhibitors DCCD or vanadate, suggesting that cholesterol import is dependent on ATP hydrolysis (*22, 23, 30*). Moreover, no other *mceG*-like gene has been identified in Mtb (*23*). While these observations strongly suggest that the ATPase activity of MceG is required for Mce-mediated transport, the activity of MceG has yet to be demonstrated directly. To test this, we selected a highly conserved aspartic acid residue within the Walker B motif predicted to be necessary for ATPase activity, and created an expression plasmid to mutate it to an asparagine residue (D188N). Then, recombinant forms of the wild type MceG and a catalytically inactive version of MceG (MceG$_{D188N}$) protein were fused to an N-terminal His$_6$-SUMO tag to enhance solubility and facilitate purification (Figure 3.1a). The recombinant proteins were purified to homogeneity and analyzed for ATPase activity (Figure 3.1b). The effective activity (background subtracted) for wild type MceG was 0.102 +/- 0.007 P$_i$ min^{-1} (Figure 3.1b and 3.1c). Background ATPase activity was detected when recombinant MceG$_{D188N}$ activity was assessed, which may be due to partial inactivation of the enzyme via this single mutation, or to contaminating ATPases carried over from the purification process. We predict that the low but detectable ATPase activity measured here reflects a requirement for additional components of the various Mce complexes to

activate or stabilize the MceG ATPase, similar to what has been observed with the related *E. coli* transporter complex, MlaFEBD (*31, 32*).

3.3.2 The ATPase activity of MceG is required for cholesterol and fatty acid utilization

We next quantified fatty acid import and metabolism of this substrate in Mtb lacking either MceG or Mtb expressing MceG lacking ATPase activity. For this, we generated an Mtb mutant with *mceG/rv0655* deleted by allelic exchange (ΔMceG), and we complemented this strain with an integrating vector that expresses wild type MceG (ΔMceG +MceG$_{WT}$) from the native *mceG* promoter. We also generated point mutations in conserved residues of the Walker B motif in *mceG* in the complementing plasmid to generate catalytically inactive versions of MceG (ΔMceG +MceG$_{D188N}$ or ΔMceG+MceG$_{E189Q}$). Relative to wild type or ΔMceG +MceG$_{WT}$, the ΔMceG mutant has a ~90% reduction in the rate of ^{14}C-palmitic acid import (Fig. 3.1d). Bacteria expressing the catalytically inactive versions of MceG displayed a similar reduction in the rate of fatty acid import (Fig. 3.1d). We also measured oxidation of ^{14}C-palmitic acid and found that there was an ~85% reduction in the amount of fatty acid oxidized by the ΔMceG mutant relative to wild type and the complemented control (Fig. 3.1e). Catalytically inactive versions of MceG failed to complement the ΔMceG mutant and displayed a similar reduction in levels of fatty acid oxidation (Fig. 3.1e).

We also measured requirement of the ATPase activity of MceG in cholesterol import and metabolism. Relative to wild type or the complemented control, the ΔMceG mutant has a ~50% reduction in the rate of ^{14}C-cholesterol import (Fig. 3.1f). The catalytically inactive versions of MceG failed to fully complement the mutation, and displayed a ~25% reduction in the rate of ^{14}C-cholesterol import (Fig. 3.1f). Metabolism of ^{14}C-cholesterol was also decreased in bacteria

lacking MceG or MceG ATPase activity. The ΔMceG mutant had defective (~90% decrease) ^{14}C-cholesterol metabolism relative to wild type and ΔMceG +MceG$_{WT}$ bacteria. The catalytically inactive versions of MceG also failed to complement the ΔMceG mutant and displayed a similar reduction in the levels of cholesterol metabolism by these bacteria (Fig. 3.1g).

Notably, quantifying the rate of ^{14}C-cholesterol uptake in Mtb is challenging due to the hydrophobic nature of both the bacterial cell wall and cholesterol. Surface bound ^{14}C-cholesterol may account for ~30-50% of the radioactive counts we observed in the uptake assay, which can still be detected even when the Mce4 cholesterol transporter is mutated (Fig. 3.1f) and (*18, 20, 24*). This residual cholesterol binding is detected despite the fact that deleting the permease subunit of the Mce4 cholesterol transporter (YrbE4A) leads to a ~90% decrease in ^{14}C-cholesterol metabolism via the CO^2 release assay (*18*). To determine how much of the bound ^{14}C-cholesterol quantified in the uptake assay is ATP-dependent, we assessed the ability of wild type and ΔMceG mutant bacteria to import cholesterol in the presence of sodium azide. Sodium azide can inhibit metalloenzymes in the respiratory chain by binding their metal groups, and has been shown to inhibit ATP hydrolysis by ATPases, effectively abolishing active transport into the cell that is ATP-dependent (*33*). In ΔMceG mutant bacteria, sodium azide treatment completely abolished the remaining levels of palmitate binding to the cells (Fig. 3.2a). This suggests that the residual radioactive counts associated with palmitate binding in the ΔMceG strain were dependent on active uptake, and this can be differentiated during our routine protocol for washing excess substrate off of the cells prior to scintillation counting. However, azide treatment did not decrease the levels of radioactive counts detected on either WT or ΔMceG Mtb when cholesterol binding was assessed (Fig. 3.2b). This suggests that in our uptake assay, radiolabeled cholesterol is binding to the bacterial cells in both WT and ΔMceG Mtb in a manner that is not dependent on ATP-driven

transport. In parallel, sodium azide was sufficient to abolish ^{14}C-cholesterol metabolism in WT Mtb and ΔMceG +MceG$_{WT}$ bacteria (Fig. 3.2c).
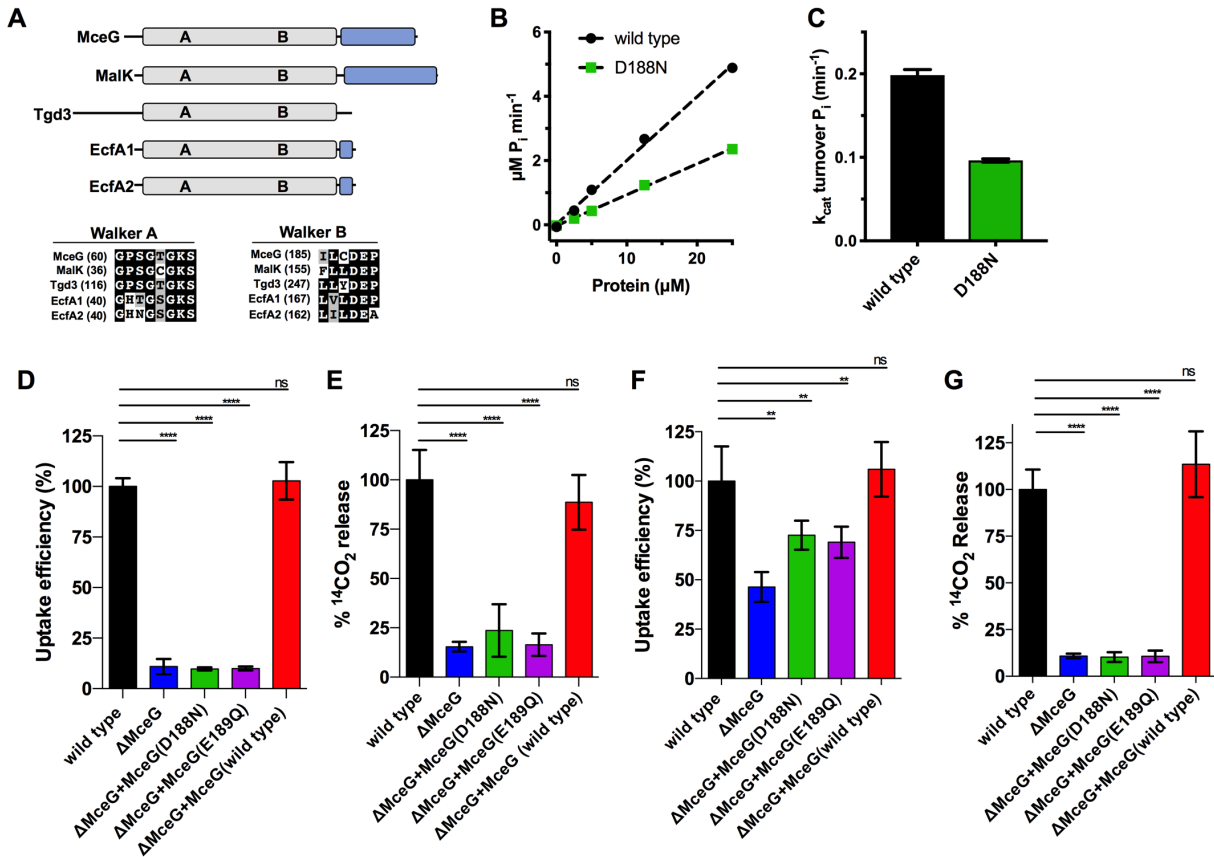
Figure 3.1. The ATPase activity of MceG is required for utilization of cholesterol and fatty acid. (A) The domain arrangement of relevant transporter ATPase subunits. The maltose transporter ATPase (MalK), The triglactosyl-diacylglycerol transporter ATPase subunit of plastids (Tgd3), ATPase subunits of the class II, energy-coupling factor or ECF transporters (EcfA1 and EcfA2). The (A&B) designation indicate the position of the Walker A and B motifs in the ATPase subunits. The C-terminal extensions depicted in blue indicate the ATPase regulatory regions. The conserved ATPase catalytic residues of MceG are present within the canonical Walker A and B motifs. **(B)** ATPase activity of recombinant wild type MceG and catalytically inactive MceG (D188N). Phosphate release kinetics were measured over five protein concentrations, with the average of six technical and one biological replicate plotted in μM P_i released min^{-1}. **(C)** k_{cat} values calculated from the rates displayed in panel B. Error bars show SEM of average turnover rate for WT and D188N mutant. **(D)** Whole cell quantification of the rate of palmitic acid import by Mtb cells. **(E)** Metabolic oxidation of palmitic acid to CO_2. **(F)** Whole cell quantification of the rate of cholesterol import by Mtb cells. **(G)** Catabolic release of CO_2 from cholesterol. Lipid utilization data (n ≥ 4) ± SEM. Significance was calculated using the Student's t-test (**** $P < 0.0001$, ** $P < 0.05$).
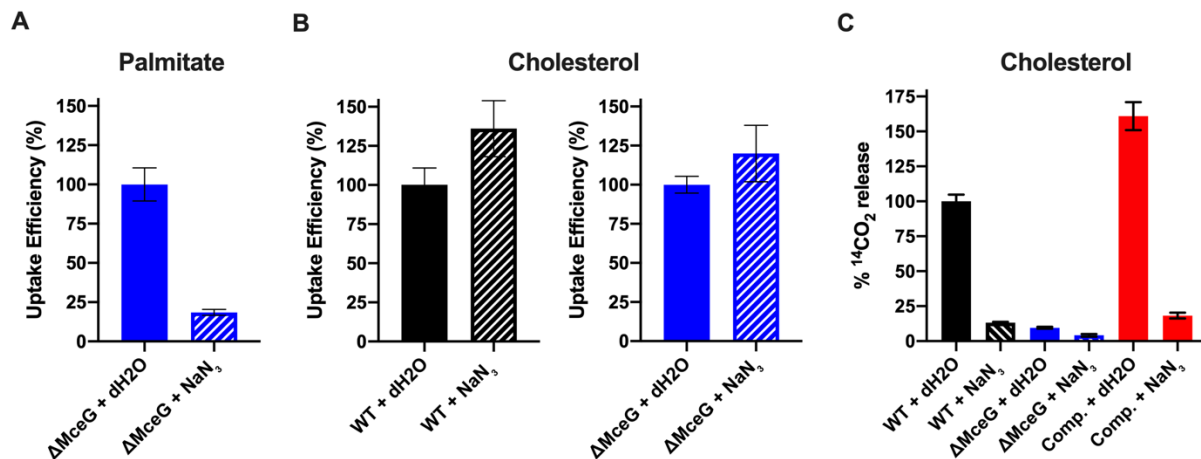
Figure 3.2. Residual binding of ^{14}C-palmitate in ΔMceG Mtb is ATP-dependent, while ^{14}C-cholesterol is not. (A) Whole cell quantification of the rate of palmitate import by ΔMceG mutant Mtb cells, treated with dH$_2$O control or sodium azide (NaN$_3$). **(B)** Whole cell quantification of the rate of cholesterol import by WT (left) or ΔMceG mutant (right) Mtb cells, treated with dH$_2$O control or sodium azide. **(C)** Catabolic release of CO$_2$ from cholesterol in Mtb strains treated with dH$_2$O control or sodium azide). Comp. = ΔMceG +MceG$_{WT}$ strain. Data are from one (A and C) or two experiments (B), with ≥2 technical replicates each.
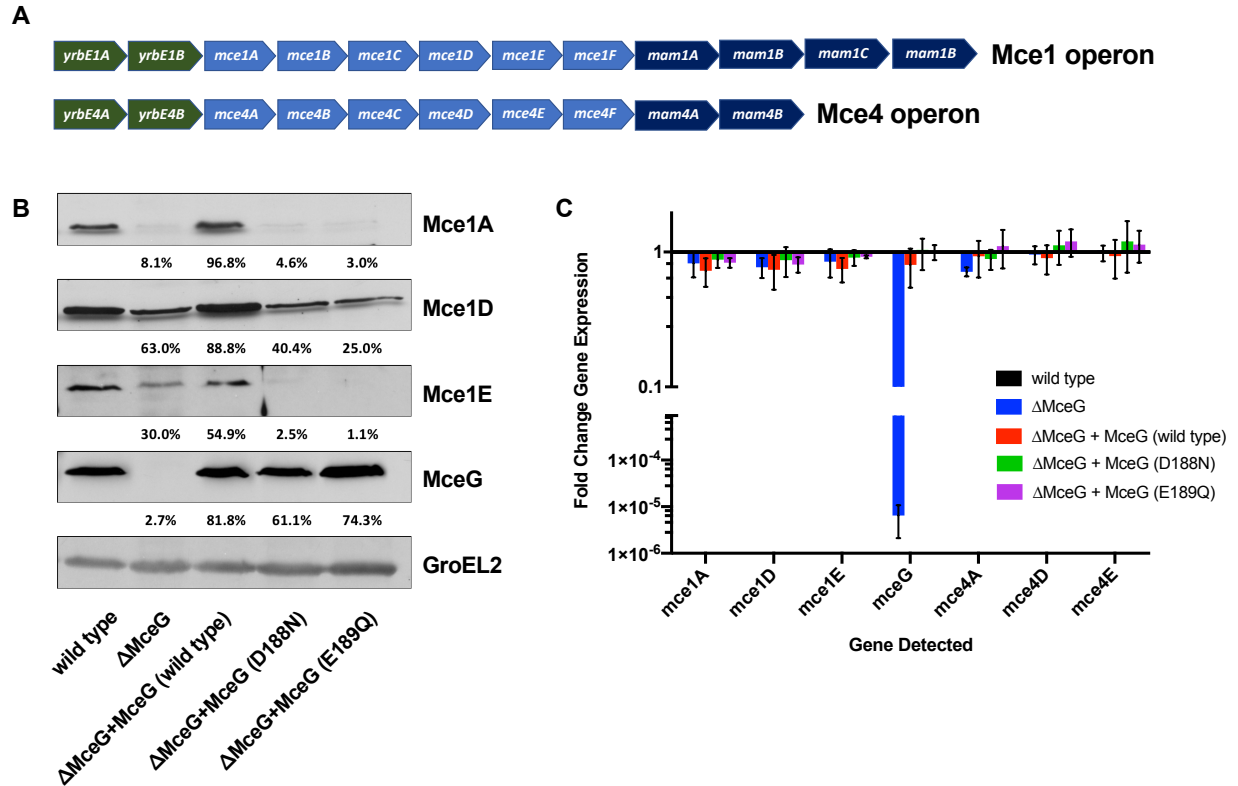
### 3.3.3 The ATPase activity of MceG is required to stabilize Mce proteins

Recent evidence indicates that the Mce1 transporter is destabilized or improperly assembled when key subunits of the transporter complex are deleted. For example, Mce1 proteins are degraded in the absence of LucA (*18*) and OmamA (*16, 20*). Until recently, antibodies were not available to assess degradation of Mce4 complex proteins in parallel, so their status in these mutant backgrounds is not yet known. To investigate the effect of inactivating MceG-dependent ATPase activity, we analyzed bacterial lysates by immunoblotting for Mce1 and Mce4 proteins in MceG deficient versus sufficient strains. We found that the putative substrate binding protein of the Mce1 transporter (Mce1A) is depleted in the MceG mutant (Fig. 3.3a,b). Additionally, putative substrate binding proteins of Mce1 (Mce1A and Mce1E) are depleted in bacterial strains expressing catalytically inactive variants of MceG ($MceG_{D188N}$ or $MceG_{E189Q}$) (Fig. 3.3b). Quantification of *mce1* transcript levels with qPCR confirmed that expression of the genes in this operon were not significantly different in the $\Delta MceG$, $\Delta MceG + MceG_{D188N}$, $\Delta MceG + MceG_{E189Q}$ strains relative to WT (Fig. 3.3c). Thus, the absence of Mce1 proteins in strains lacking functional MceG is not due to an absence in gene expression. This suggests that the MceG protein, and its ATPase activity in particular, are required for the stabilization of Mce1 complex proteins.

In parallel, we performed immunoblotting for select Mce4 complex proteins. In contrast to our findings with the Mce1 complex, we observed less significant reductions in substrate binding proteins of the Mce4 complex (Mce4A and Mce4E) in the MceG-deficient strains (Fig. 3.4). The *mce4* transcript levels were equivalent between all strains (Fig. 3.3c). Together, these data provide evidence that MceG, and more specifically the ATPase activity of MceG, plays a role in stabilizing components of the Mce1 transporter complex, but a lesser role in stabilizing components of the

Mce4 complex, which is consistent with our proposed interpretation of the cholesterol uptake and metabolism assays above.

Figure 3.3. MceG ATPase activity is required to stabilize the Mce1 transporter complex. (A) Organization of genes in the Mce1 and Mce4 operons. **(B)** Mtb whole cell lysates probed with anti-Mce1A (1:1,000), anti-Mce1D (1:1,000), anti-Mce1E (1:1,000) or anti-GroEL2 (1:10,000). GroEL2 as the loading control, Western blots depicted are representative images of two independent replicates. Densitometry was performed with each western blot and all values were normalized to those of the corresponding loading control. Ratios of the proteins levels of an individual lysate compared to the corresponding wild type lysate are expressed as percentages inset below each blot. **(C)** qPCR quantification of RNA transcripts from the Mce1 and Mce4 operons. Transcript levels were normalized to the housekeeping gene *sigA*.
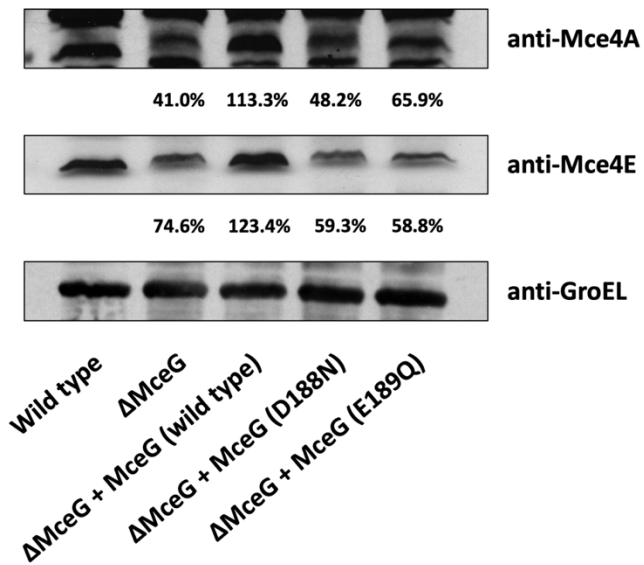
Figure 3.4. Abolishing MceG ATPase activity less severely impacts stabilization of Mce4 complex proteins. Mtb whole cell lysates probed with anti-Mce4A, anti-Mce4E, or anti-GroEL2. GroEL2 is the loading control. Western blots depicted are representative images of two independent replicates Densitometry was performed with each western blot and all values were normalized to those of the corresponding loading control. Ratios of the proteins levels of an individual lysate compared to the corresponding wild type lysate are expressed as percentages inset below each blot.

3.3.4 MceG ATPase activity is required for full fitness of Mtb during murine infection

The *in vivo* fitness of an MceG mutant has only been reported from mice using an intravenous, competitive infection assay (*21*). Previously, we determined that Mtb mutants that are unable to utilize both cholesterol and fatty acids have a colonization defect in the lungs of mice (*18*). Using the same intranasal infection model, we characterized the fitness of Mtb lacking MceG. We found that the ΔMceG mutant displayed a characteristic delay in bacterial numbers during the first 2-3 weeks post-infection, resulting in a ~0.5-1.0 $\log_{10}$ reduction in CFUs across the remainder of the infection (Fig. 3.5a). The decrease in bacterial CFUs correlates with reduced inflammation in the lungs (Fig. 3.5b). Additionally, the bacterial burden of the ΔMceG mutant was reduced by a greater magnitude (~2.0-3.0 $\log_{10}$ CFU) in the spleens of the animals, which is a measurement used to assess dissemination of bacteria from the lungs (Fig 3.5c). Lastly, we aerosol challenged mice with wild type Mtb, ΔMceG, or the catalytically inactive MceG$_{D188N}$ strain and quantified the bacterial burden at 4-weeks post infection. Relative to wild type, bacteria expressing inactive MceG had a ~0.5-1.0 $\log_{10}$ reduction in CFUs at this time point, similar to the ΔMceG mutant (Fig. 3.5d). Together these data confirm that MceG plays a critical role in facilitating nutrient import necessary for full virulence in Mtb and that blocking the ATPase activity of MceG impairs Mtb fitness during infection.
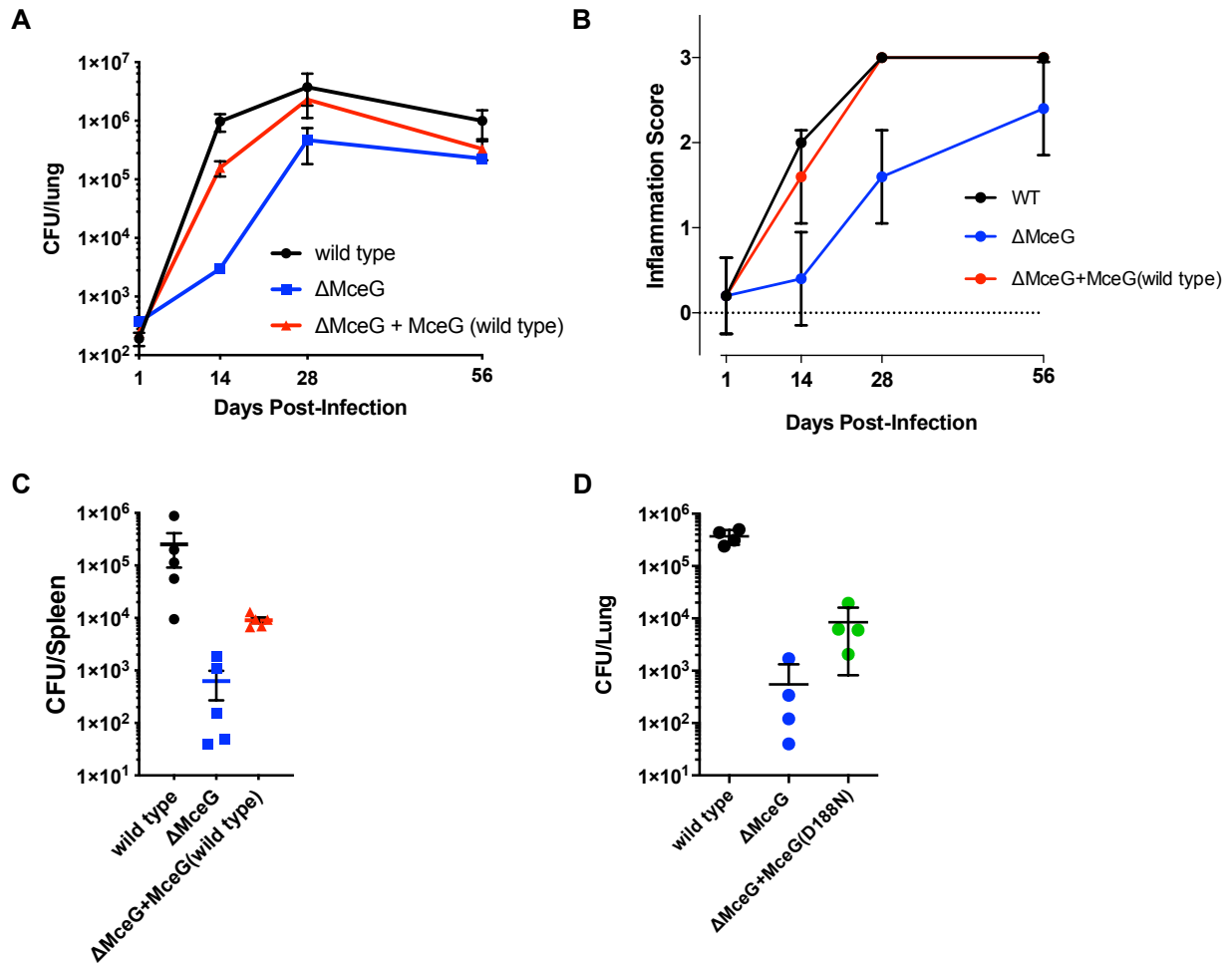
Figure 3.5. McceG is required for complete Mtb fitness *in vivo*. (A-D) BALB/c mice were infected by intranasal inoculation using similar numbers of bacteria. (**A**) Colony forming units of wild type, ΔMceG, and ΔMceG+MceG(wild type) bacteria from the lungs of mice individually plotted. (**B**) Histopathology as scored by a pathologist in a blinded manner. Score numbers represent the extent of inflammatory lesions: 0, no lesions; 1, mild inflammation; 2, moderate inflammation; 3, marked inflammation. Data represent two or more independent experiments. (**C**) Colony forming units of wild type, ΔMceG, and ΔMceG+MceG(wild type) bacteria isolated from the spleens of mice at day 56. All data in are for n = 5 mice per time point. Data are means ± SEM. Significance was calculated using Mann-Whitney test (* $P < 0.05$, ** $P < 0.005$). (**D**) Colony forming units on day 28 post infection from the lungs of mice that were aerosol infected with 100 CFU wild type, ΔMceG, and ΔMceG+MceG(D188N). Data in (**D**) are for n = 4 mice per time point. Data are means ± SEM. Significance was calculated using Mann-Whitney test (* $P < 0.05$).

3.4   Discussion

The Mtb genome contains four closely related *mce* operons (*mce1-4*) that likely encode four separate, substrate-specific transporters. It is established that Mce1 imports fatty acids and Mce4 imports cholesterol, but the substrates of Mce2 and Mce3 remain unknown (*18, 24*). Recently, we discovered that transport activity of Mce1 and Mce4 require the protein LucA. Although LucA is not encoded in any *mce* operon, it is necessary to stabilize the Mce1 transporter complex (*18*). This finding and others support a model in which each of the substrate-specific Mce transporters also require shared proteins to regulate and/or facilitate transport activity (*20*). Our recent genetic screen also revealed that transposon insertions in MceG disrupted fatty acid uptake in the bacteria during infection in macrophages (*19*). With the exception of one study that examined the fitness cost of mutating a residue (K66N) in the Walker A motif of MceG, previous conclusions drawn from whole cell and *in vivo* studies about the functions of MceG in Mtb were based on MceG deletion mutants. Thus, it had not been directly confirmed that i) MceG has ATPase activity and ii) this activity is required for the function of MceG in lipid translocation in to Mtb. Therefore, this work sought to confirm the ATPase activity of MceG and to examine the relationship between MceG ATPase activity and the binding and translocation of two different substrates (cholesterol and fatty acids) for metabolism. Additionally, we sought to examine whether loss of MceG activity confers a fitness cost to Mtb in a model of TB infection that did not rely on intravenous or competitive infection, but instead infected the lung as the primary site (*21*). Using the same infection model we used while studying the LucA mutant allowed us to draw comparisons between the roles of LucA and MceG during infection.

Here, we used purified recombinant MceG to confirm the ATPase activity of this protein. We also confirmed that a point mutation in a conserved residue of the Walker B motif decreases

ATPase activity of MceG. Complementing the ΔMceG strain with this catalytically inactive point mutant compared to wild type *mceG* allowed us to confirm that the ATPase activity of MceG is required for fatty acid and cholesterol metabolism, and that MceG plays a preferential role in stabilizing Mce1 complex proteins or preventing their degradation. The Mce4 complex proteins appear to be partially or fully in tact in the MceG mutant strains. Quantification of transcription confirmed that this was not due to differences in *mce* gene expression. In the future, pre-treating cultures with chloramphenicol to suppress synthesis of new protein in the bacteria prior to generating lysates for Western blots may help clarify the degree to which Mce proteins are degraded (*18*). In murine models of infection, MceG was required for colonization and dissemination or maintenance of bacterial CFUs in the spleen during chronic infection. This phenotype was similar to the ΔLucA strain. Interestingly, ΔLucA Mtb exhibited MceG protein degradation, and this effect on MceG was offered as one potential explanation for the dual defect the LucA mutant has in fatty acid and cholesterol utilization, and its fitness defect during infection (*18*). Together these data suggests that MceG is a universal ATPase that is required to power translocation of substrates via the Mce1 and Mce4 complexes, and may function as the nucleotide binding domain protein for all of the Mce transporters in Mtb.

Notably, we identified a discrepancy between the cholesterol uptake and metabolism assays in the ΔMceG strain. We observed a partial defect in cholesterol uptake in ΔMceG relative to WT, and a more significant defect in cholesterol metabolism. In both the WT and the ΔMceG strains, treatment with sodium azide to abolish active transport into the cytoplasm was not associated with a further decrease in radiolabeled cholesterol binding to the cells during the uptake assay. However, sodium azide did inhibit cholesterol metabolism. This is in contrast to our results using radiolabeled fatty acid, where we observed little residual binding of the fatty acid in ΔMceG

bacteria, and sodium azide treatment abolished the remaining binding of fatty acid to the cells. Combined with our observation that Mce4 but not the Mce1 substrate binding proteins remain intact in the ΔMceG strain, these results are consistent with a model in which cholesterol binds in proportion to the Mce4 complex proteins present on the cells in a mechanism that is not dependent on ATP, but ATP-dependent translocation of cholesterol across the inner membrane is required for cholesterol catabolism. In this model, sodium azide treatment would impair cholesterol metabolism but not cholesterol binding in WT Mtb because the cholesterol can bind to the cell but cannot be translocated into the cytoplasm. Similarly, if Mce4 proteins are partially or fully intact on ΔMceG bacteria, then cholesterol binding would be minimally changed relative to WT and sodium azide would not abolish cholesterol binding any further, but cholesterol metabolism would be reduced significantly relative to WT. It is possible that cholesterol binds to the cells in a manner than is non-specific for the presence or proportion of Mce4 substrate binding proteins present, and is instead proportional to the presence of another unidentified surface lipid or protein. However, the assay is unlikely to be measuring cholesterol binding that is entirely non-specific. If the binding were entirely non-specific, then we should not have been able to detect the significant differences we identified in the rate of cholesterol uptake with the LucA, Mce4, and MceG mutants (*18*). Previous uptake assays examined Mce4 mutants in which only the permease subunit (YrbE4A) was deleted (*18, 24*). Although this was predicted to have polar effects on the entire operon, it remains possible that some of the downstream Mce4 substrate binding proteins are still expressed in this strain, generating the partial defect in cholesterol binding (~40%) but a large (~85%) decrease in cholesterol metabolism that was reported in this mutant (*18*). Indeed, the decoupling of cholesterol binding and metabolism was also observed previously in a strain of Mtb in which the last gene in the *mce4* operon was deleted (ΔMam4B) which plausibly leaves the substrate

binding proteins of Mce4 intact. No significant difference in cholesterol uptake was observed in ΔMam4B Mtb, while cholesterol metabolism was reduced by ~85% (*18*). In the future, it would be helpful to examine this hypothesis directly by characterizing these other mutants via anti-Mce4 immunoblotting or proteomics to determine if Mce4 proteins are intact.

Precisely how MceG interacts with the different Mce transporters remains unknown. Each of the four *mce* operons encode two integral membrane permease subunits (YrbEAB). All eight of these putative Mce permease subunits have a similar predicted transmembrane topology with a highly conserved, 47 amino acid "EExDA motif" located in the penultimate cytosolic loop (*15*). This cytosolic motif was hypothesized to be a shared interaction site for MceG on each of the transporters (*15*). It is likely that MceG binds and stabilizes the individual Mce transporters in Mtb since co-expression of any Mce locus or the Mce1 permease subunits increases the stable expression of MceG in a heterologous expression system (*21*). Consistent with this, we found that deleting the *mceG* gene or expressing a catalytically inactive version of MceG was sufficient to destabilize or degrade proteins of the Mce1 transporter in Mtb. A recent report describes a stability-based mechanism to regulate ABC transporters that are related to the Mce transporters of Mtb. The *E. coli* Mla transporter facilitates movement of phospholipids across the periplasm and utilizes an ABC ATPase, MlaF, to energize this process (*17*). The permease protein in this system, MlaE, was modeled to interact with MlaF via co-evolved residue pairs on the cytoplasmic end of MlaE and the membrane-apposed surface of MlaF (*17*). Importantly, a soluble STAS-domain containing protein, MlaB, is proposed to regulate the Mla transporter by stabilizing the MlaF dimer, either by preventing its degradation or by increasing affinity of MlaF for the transporter (*31*). Therefore, it is possible that additional proteins such as LucA may be required to facilitate the binding of MceG

to the Mce transporters leading to stabilization of the Mce transporters (*18*). This is particularly relevant given that LucA was required to maintain MceG protein levels in Mtb.

Here, we have described the first account of ATPase activity for MceG, but details of the relationship between its ATPase activity and regulation of the Mce complexes remain to be investigated. Purification of MceG proved to be difficult, but low levels of specific ATPase activity were detectable using recombinant protein. Interestingly, Kolich et al. also described difficulty in purifying the MlaF ATPase alone and only achieved purification when MlaB was co-expressed, and the ATPase activity of MlaF was established when MlaF was purified in complex with the Mla transporter (*31, 32*). MceG conserves a canonical Walker A domain that likely coordinates ATP via hydrogen bonding with the β-phosphate and a Walker B domain which is expected to provide the carboxylate residue needed to coordinate Mg^{2+} for ATP hydrolysis (*34*). We focused on the catalytic residues found in the Walker B motif of MceG because enzymes (e.g. chaperone ATPases) lacking these residues typically still bind but do not hydrolyze ATP (*35*). ABC transporters harness energy from ATP binding and hydrolysis to do mechanical work by driving conformational changes in their associated transmembrane domain proteins (*36*). The conformational changes adopted by this family of related ATPase enzymes are often dramatic (*37*) and likely have a stabilizing role for the transporters they engage (*38-41*). If the transport cycle driven by MceG parallels other ATPases in the literature, we would predict that the point mutations we generated could allow MceG to bind ATP but not to hydrolyze it, precluding conformational changes from an outward-facing, pre-hydrolysis state to an inward-facing, post-hydrolysis or resting state and preventing translocation of Mce lipid substrates (*36*).

To conclude, these findings confirm the ATPase activity of MceG and demonstrate that this activity contributes significantly to Mtb virulence and pathogenesis. Inactivating ATPase activity

of MceG blocks the import and metabolism of multiple lipid substrates. Since inactivating MceG results in a loss of fitness in Mtb during infection, we view this as a potential strategy to block Mtb's ability to utilize multiple nutrients. In particular, by chemically inhibiting MceG it may be possible to negatively impact Mtb's fitness and enhance our current treatment options. Very little is known about how Mtb coordinates the utilization of multiple, complex carbon sources during infection, and in controlled *in vitro* conditions Mtb appears to lack traditional carbon catabolite repression systems and instead co-catabolizes multiple carbon sources simultaneously (*42*). Although ΔMceG Mtb exhibits a significant growth defect during infection in mice, this defect was not sufficient to preclude bacterial survival altogether. In the future it would be interesting to characterize the alternative carbon sources or stress adaptations that ΔMceG Mtb adopts to survive despite the severe defect in cholesterol and fatty acid metabolism it exhibits *in vitro*. This may provide additional insights into how to maximize the efficacy of chemically targeting the MceG pathway in combination with other bacterial adaptations in the future.

3.5   References

1.   C. E. Barry, 3rd, H. I. Boshoff, V. Dartois, T. Dick, S. Ehrt, J. Flynn, D. Schnappinger, R. J. Wilkinson, D. Young, The spectrum of latent tuberculosis: rethinking the biology and intervention strategies. *Nat Rev Microbiol* **7**, 845-855 (2009).

2.   S. Ehrt, D. Schnappinger, K. Y. Rhee, Metabolic principles of persistence and pathogenicity in Mycobacterium tuberculosis. *Nat Rev Microbiol* **16**, 496-507 (2018).

3.   J. P. Sarathy, V. Dartois, Caseum: a Niche for Mycobacterium tuberculosis Drug-Tolerant Persisters. *Clinical microbiology reviews* **33**, (2020).

4.   K. Y. Rhee, L. P. de Carvalho, R. Bryk, S. Ehrt, J. Marrero, S. W. Park, D. Schnappinger, A. Venugopal, C. Nathan, Central carbon metabolism in Mycobacterium tuberculosis: an unexpected frontier. *Trends Microbiol* **19**, 307-314 (2011).

5.   A. Abuhammad, Cholesterol metabolism: a potential therapeutic target in Mycobacteria. *Br J Pharmacol* **174**, 2194-2208 (2017).

6.   C. L. Dulberger, E. J. Rubin, C. C. Boutte, The mycobacterial cell envelope - a moving target. *Nat Rev Microbiol* **18**, 47-59 (2020).

7.   M. Jackson, C. M. Stevens, L. Zhang, H. I. Zgurskaya, M. Niederweis, Transporters Involved in the Biogenesis and Functionalization of the Mycobacterial Cell Envelope. *Chem Rev* **121**, 5124-5157 (2021).

8.   S. Wilkens, Structure and mechanism of ABC transporters. *F1000prime reports* **7**, 14 (2015).

9.   K. M. Wilburn, R. A. Fieweger, B. C. VanderVen, Cholesterol and fatty acids grease the wheels of Mycobacterium tuberculosis pathogenesis. *Pathogens and Disease* **76**, (2018).

10. G. T. Mashabela, T. J. de Wet, D. F. Warner, Mycobacterium tuberculosis Metabolism. *Microbiol Spectr* **7**, (2019).

11. V. Guerrini, B. Prideaux, L. Blanc, N. Bruiners, R. Arrigucci, S. Singh, H. P. Ho-Liang, H. Salamon, P. Y. Chen, K. Lakehal, S. Subbian, P. O'Brien, L. E. Via, C. E. Barry, 3rd, V. Dartois, M. L. Gennaro, Storage lipid studies in tuberculosis reveal that foam cell biogenesis is disease-specific. *PLoS Pathog* **14**, e1007223 (2018).

12. M. J. Kim, H. C. Wainwright, M. Locketz, L. G. Bekker, G. B. Walther, C. Dittrich, A. Visser, W. Wang, F. F. Hsu, U. Wiehart, L. Tsenova, G. Kaplan, D. G. Russell, Caseation of human tuberculosis granulomas correlates with elevated host lipid metabolism. *EMBO Molecular Medicine* **2**, 258-274 (2010).

13. B. C. VanderVen, R. J. Fahey, W. Lee, Y. Liu, R. B. Abramovitch, C. Memmott, A. M. Crowe, L. D. Eltis, E. Perola, D. D. Deininger, T. Wang, C. P. Locher, D. G. Russell, Novel inhibitors of cholesterol degradation in Mycobacterium tuberculosis reveal how the bacterium's metabolism is constrained by the intracellular environment. *PLoS Pathogens* **11**, e1004679 (2015).

14. W. Lee, B. C. VanderVen, R. J. Fahey, D. G. Russell, Intracellular Mycobacterium tuberculosis exploits host-derived fatty acids to limit metabolic stress. *Journal of Biological Chemistry* **288**, 6788-6800 (2013).

15. N. Casali, L. W. Riley, A phylogenomic analysis of the Actinomycetales mce operons. *BMC genomics* **8**, 60 (2007).

16. L. Rank, L. E. Herring, M. Braunstein, Evidence for the Mycobacterial Mce4 Transporter Being a Multiprotein Complex. *J Bacteriol* **203**, (2021).

17. D. C. Ekiert, G. Bhabha, G. L. Isom, G. Greenan, S. Ovchinnikov, I. R. Henderson, J. S. Cox, R. D. Vale, Architectures of Lipid Transport Systems for the Bacterial Outer Membrane. *Cell* **169**, 273-285.e217 (2017).

18. E. V. Nazarova, C. R. Montague, T. La, K. M. Wilburn, N. Sukumar, W. Lee, S. Caldwell, D. G. Russell, B. C. VanderVen, Rv3723/LucA coordinates fatty acid and cholesterol uptake in Mycobacterium tuberculosis. *eLife* **6**, (2017).

19. E. V. Nazarova, C. R. Montague, L. Huang, T. La, D. Russell, B. C. VanderVen, The genetic requirements of fatty acid import by Mycobacterium tuberculosis within macrophages. *eLife* **8**, (2019).

20. E. F. Perkowski, B. K. Miller, J. R. McCann, J. T. Sullivan, S. Malik, I. C. Allen, V. Godfrey, J. D. Hayden, M. Braunstein, An orphaned Mce-associated membrane protein of Mycobacterium tuberculosis is a virulence factor that stabilizes Mce transporters. *Molecular microbiology* **100**, 90-107 (2016).

21. S. M. Joshi, A. K. Pandey, N. Capite, S. M. Fortune, E. J. Rubin, C. M. Sassetti, Characterization of mycobacterial virulence genes through genetic interaction mapping. *Proceedings of the National Academy of Sciences of the United States of America* **103**, 11760-11765 (2006).

22. W. W. Mohn, R. van der Geize, G. R. Stewart, S. Okamoto, J. Liu, L. Dijkhuizen, L. D. Eltis, The actinobacterial mce4 locus encodes a steroid transporter. *J Biol Chem* **283**, 35368-35374 (2008).

23. J. Garcia-Fernandez, K. Papavinasasundaram, B. Galan, C. M. Sassetti, J. L. Garcia, Unraveling the pleiotropic role of the MceG ATPase in Mycobacterium smegmatis. *Environmental microbiology*, (2017).

24.   A. K. Pandey, C. M. Sassetti, Mycobacterial persistence requires the utilization of host cholesterol. *Proceedings of the National Academy of Sciences of the United States of America* **105**, 4376-4380 (2008).

25.   F. M. Mann, B. C. VanderVen, R. J. Peters, Magnesium depletion triggers production of an immune modulating diterpenoid in Mycobacterium tuberculosis. *Molecular microbiology* **79**, 1594-1601 (2011).

26.   M. E. Feltcher, H. P. Gunawardena, K. E. Zulauf, S. Malik, J. E. Griffin, C. M. Sassetti, X. Chen, M. Braunstein, Label-free Quantitative Proteomics Reveals a Role for the Mycobacterium tuberculosis SecA2 Pathway in Exporting Solute Binding Proteins and Mce Transporters to the Cell Wall. *Molecular & cellular proteomics : MCP* **14**, 1501-1516 (2015).

27.   K. J. Livak, T. D. Schmittgen, Analysis of relative gene expression data using real-time quantitative PCR and the 2(-Delta Delta C(T)) Method.

28.   J. S. Yuan, F. Reed A Fau - Chen, C. N. Chen F Fau - Stewart, Jr., C. N. Stewart, Jr., Statistical analysis of real-time PCR data.

29.   N. Sukumar, S. Tan, B. B. Aldridge, D. G. Russell, Exploitation of Mycobacterium tuberculosis reporter strains to probe the impact of vaccination at sites of infection. *PLoS Pathog* **10**, e1004394 (2014).

30.   N. Agarwal, V. K. Kalra, Purification and functional properties of the DCCD-reactive proteolipid subunit of the H+-translocating ATPase from Mycobacterium phlei. *Biochim Biophys Acta* **723**, 150-159 (1983).

31.   L. R. Kolich, Y. T. Chang, N. Coudray, S. I. Giacometti, M. R. MacRae, G. L. Isom, E. M. Teran, G. Bhabha, D. C. Ekiert, Structure of MlaFB uncovers novel mechanisms of ABC transporter regulation. *eLife* **9**, (2020).

32.   S. Thong, B. Ercan, F. Torta, Z. Y. Fong, H. Y. Wong, M. R. Wenk, S. S. Chng, Defining key roles for auxiliary proteins in an ABC transporter that maintains bacterial outer membrane lipid asymmetry. **5**, (2016).

33.   M. W. Bowler, M. G. Montgomery, A. G. Leslie, J. E. Walker, How azide inhibits ATP hydrolysis by the F-ATPases. *Proceedings of the National Academy of Sciences of the United States of America* **103**, 8646-8649 (2006).

34.   I. L. Urbatsch, M. Julien, I. Carrier, M. E. Rousseau, R. Cayrol, P. Gros, Mutational analysis of conserved carboxylate residues in the nucleotide binding sites of P-glycoprotein. *Biochemistry* **39**, 14138-14149 (2000).

35.   A. Schaupp, M. Marcinowski, V. Grimminger, B. Bosl, S. Walter, Processing of proteins by the molecular chaperone Hsp104. *Journal of molecular biology* **370**, 674-686 (2007).

36.   K. Beis, Structural basis for the mechanism of ABC transporters. *Biochem Soc Trans* **43**, 889-893 (2015).

37.   G. Lu, J. M. Westbrooks, A. L. Davidson, J. Chen, ATP hydrolysis is required to reset the ATP-binding cassette dimer into the resting-state conformation. *Proceedings of the National Academy of Sciences of the United States of America* **102**, 17969-17974 (2005).

38.   J. Chen, G. Lu, J. Lin, A. L. Davidson, F. A. Quiocho, A tweezers-like motion of the ATP-binding cassette dimer in an ABC transport cycle. *Molecular cell* **12**, 651-661 (2003).

39. K. P. Hopfner, A. Karcher, D. S. Shin, L. Craig, L. M. Arthur, J. P. Carney, J. A. Tainer, Structural biology of Rad50 ATPase: ATP-driven conformational control in DNA double-strand break repair and the ABC-ATPase superfamily. *Cell* **101**, 789-800 (2000).

40. P. C. Smith, N. Karpowich, L. Millen, J. E. Moody, J. Rosen, P. J. Thomas, J. F. Hunt, ATP binding to the motor domain from an ABC transporter drives formation of a nucleotide sandwich dimer. *Molecular cell* **10**, 139-149 (2002).

41. J. Zaitseva, S. Jenewein, T. Jumpertz, I. B. Holland, L. Schmitt, H662 is the linchpin of ATP hydrolysis in the nucleotide-binding domain of the ABC transporter HlyB. *The EMBO journal* **24**, 1901-1910 (2005).

42. L. P. de Carvalho, S. M. Fischer, J. Marrero, C. Nathan, S. Ehrt, K. Y. Rhee, Metabolomics of Mycobacterium tuberculosis reveals compartmentalized co-catabolism of carbon substrates. *Chemistry & biology* **17**, 1122-1131 (2010).

CHAPTER FOUR

Pharmacological and genetic activation of cAMP synthesis disrupts cholesterol utilization

in *M. tuberculosis*

ABSTRACT

There is a growing appreciation for the idea that bacterial utilization of host-derived lipids, including cholesterol, supports *Mycobacterium tuberculosis* (Mtb) pathogenesis. This has generated interest in identifying novel antibiotics that can disrupt cholesterol utilization by Mtb *in vivo*. Here we identify a novel small molecule agonist (V-59) of the Mtb adenylyl cyclase Rv1625c, which stimulates 3', 5'-cyclic adenosine monophosphate (cAMP) synthesis and inhibits cholesterol utilization by Mtb. Similarly, using a complementary genetic approach that induces bacterial cAMP synthesis independent of Rv1625c, we demonstrate that inducing cAMP synthesis is sufficient to inhibit cholesterol utilization in Mtb. Although the physiological roles of individual adenylyl cyclase enzymes in Mtb are largely unknown, here we demonstrate that the transmembrane region of Rv1625c is required for cholesterol metabolism. Finally, in this work the pharmacokinetic properties of Rv1625c agonists are optimized, producing an orally-available Rv1625c agonist that impairs Mtb pathogenesis in infected mice. Collectively, this work demonstrates a novel role for Rv1625c and cAMP signaling in controlling cholesterol metabolism in Mtb and establishes that cAMP signaling can be pharmacologically manipulated for the development of new antibiotic strategies.

4.1 Introduction

Tuberculosis (TB) remains a prevalent infectious disease worldwide that claims ~1.4 million lives and afflicts ~10 million new individuals annually (*1*). TB is caused by *Mycobacterium tuberculosis* (Mtb), and it is an ongoing challenge to identify antibiotics with novel bacterial targets that can shorten treatment, limit side-effects, and reduce disease relapse. An important aspect of Mtb pathogenesis is that the bacterium persists in the human lung within lipid-rich phagocytes and/or tissue lesions while promoting pathology that is required for dissemination and transmission (*2*). Mtb primarily lives within macrophages and stimulates the formation of lipid-loaded cells (*3, 4*), but the bacterium can also survive in the acellular core of necrotic granulomas that are rich in cholesterol, cholesterol ester, and triacylglycerol (*2, 5*). It is generally understood that Mtb utilizes host-derived lipids, including cholesterol, as key nutrients to survive during persistent infection (*6*). Mtb completely degrades cholesterol into two- and three-carbon intermediates that are metabolized for energy production or serve as biosynthetic precursors of cell wall or virulence lipids (*6*). In animal models, Mtb requires cholesterol metabolism to maintain optimal chronic lung infection (*7-11*) and cholesterol utilization was recently found to belong to a set of "core virulence functions" required for Mtb survival *in vivo* across a genetically diverse panel of mice (*12*). Furthermore, it was recently demonstrated that a multi-drug resistant strain of Mtb is more dependent on cholesterol for growth than an H37Rv reference strain (*13*). Thus, the cholesterol metabolic pathway in Mtb represents a novel, genetically validated target for drug discovery. However, tools to pharmacologically inhibit this pathway during infection *in vivo* have yet to be developed.

Signaling through the universal second-messenger 3',5'-cyclic adenosine monophosphate (cAMP) has long been studied in a variety of prokaryotic and eukaryotic systems. In pathogenic

bacteria, cAMP is essential in regulating functions such as carbon metabolism, virulence gene expression, biofilm formation, drug tolerance, and manipulation of host cell signaling (*14-16*). How cAMP signaling regulates Mtb physiology during infection is not well understood, partly due to the limited tools available for investigating this and the myriad of pathway components present in Mtb. The Mtb genome encodes an unusually large repertoire of at least ten biochemically active class III adenylyl cyclase (AC) enzymes, which catalyze the intramolecular cyclization of ATP to form cAMP when activated. These ACs are structurally diverse, and the majority of these proteins are composed of a catalytic domain along with other accessory domains, which are thought to participate in regulatory or effector functions (*17*). Studies using recombinant expression systems have proposed environmental stimuli (e.g. pH, fatty acids, or HCO_3^-/CO_2) for five Mtb ACs (*18-22*). Additionally, Mtb possesses twelve predicted downstream cAMP-binding effector proteins, only four of which have been functionally characterized (*23-28*). Thus, our understanding of how individual ACs and downstream cAMP-dependent effector proteins regulate specific aspects of Mtb physiology is extremely limited. To date, no individual AC enzyme has been directly linked to the regulation of a specific biological or metabolic process in Mtb.

We previously identified a series of compounds that inhibit Mtb growth in macrophages and in media containing cholesterol (*29*). The activity of a subset of these compounds was dependent on the AC Rv1625c, and compound treatment increased cAMP production in Mtb (*29*). The Rv1625c protein is composed of at least four structural elements: an N-terminal cytoplasmic tail, a six-helical transmembrane domain, a cytoplasmic helical domain, and a C-terminal cyclase domain. Based on its topology and sequence homology, Rv1625c is comparable to 'one-half' of a mammalian membrane-associated AC (*30*). Rv1625c forms a homodimer to generate two active sites composed of complementary residues, and conserved active site residues as well as the

cytoplasmic tail and helical domain have been linked to its catalytic activity (*31-33*). Although it has been proposed that Rv1625c may be activated by binding HCO_3^-/CO_2 or lipophilic ligands, it remains unclear what the native role of Rv1625c is in Mtb during infection (*19, 34, 35*). The possibility that we had identified chemical tools comparable to forskolin in the Mtb system led us to investigate the mechanism of these Rv1625c-dependent compounds and their impact on Mtb carbon metabolism and pathogenesis. We were especially motivated to test the hypothesis that activating cAMP synthesis in Mtb through an Rv1625c agonist could disable cholesterol utilization and undermine Mtb persistence during infection in mice.

To carry out these studies, we re-examined our previously identified screening hits for Rv1625c-dependent compounds with favorable pharmacokinetic properties. From these, we selected a potent compound (V-59) that permitted both *in vitro* and *in vivo* studies to examine the impact that chemically activating cAMP signaling has on Mtb metabolism. In this work, we determined that V-59 is an Rv1625c agonist, and its ability to inhibit Mtb growth in macrophages and cholesterol is dependent on Rv1625c and an associated increase in cAMP synthesis. Additionally, we found that the transmembrane domain of Rv1625c is necessary for the complete metabolism of cholesterol, linking the protein target of V-59 directly to the cholesterol utilization pathway. This finding connects a single AC to the regulation of a downstream metabolic pathway in Mtb for the first time. Using a complementary genetic approach, we developed an inducible system to activate cAMP synthesis independent of V-59 and Rv1625c, and determined that upregulating cAMP synthesis is sufficient to inhibit cholesterol utilization in Mtb. V-59 was optimized through medicinal chemistry, which produced a lead compound (mCLB073) with improved potency and *in vivo* activity against Mtb when delivered orally to infected mice. Collectively, our results reveal a novel cAMP signaling mechanism in Mtb that inhibits cholesterol

utilization and may represent an improvement over developing conventional single-step inhibitors against this complex pathway. Using a small molecule AC agonist as an antimicrobial compound is an unconventional approach, and this study is the first to explore this as a mechanism of action to inhibit growth of a bacterial pathogen during infection.

4.2   Materials and Methods

Bacterial culture

Unless noted, Mtb strains were grown in Middlebrook 7H9 medium supplemented with glycerol and OADC (oleic acid, albumin, dextrose, catalase) (Difco). 7H12 medium contained Middlebrook 7H9 powder (Becton Dickinson), 0.1% casitone, and 100 mmol MES free acid monohydrate, pH 6.6. Prior to culturing in media containing different carbon sources, bacteria were washed in 7H12 media without additional carbon sources. Cholesterol was added as tyloxapol:ethanol micelles to a final concentration of 100 µM (*29*). Where specified, 0.1% acetate was added. All liquid media contained 0.05% tyloxapol (Acros Organics). Mtb was cultured on Middlebrook 7H10 agar supplemented with glycerol and OADC (Difco). Strains were maintained with selective antibiotics as described in Table S2. Anhydrotetracyline was prepared in 100% EtOH and used at final concentrations of 500 ng/mL or 50 ng/mL.

Construction of mutants and TetOn-cAMP strains

The *rv1625c* gene was disrupted in CDC1551 Mtb using allelic exchange (*36*). ΔRv1625c was complemented by overexpressing full-length Rv1625c or the transmembrane domain (amino acids V1-D204), from an integrating vector under the control of the *hsp60* promoter. The TetOn-cAMP strain expresses the His-tagged catalytic domain of Rv1264, under control of the *p606* Atc-inducible promoter. A single amino acid change (D265A) was introduced in the *rv1264* sequence using site-directed mutagenesis. Base pairs 794-795 were mutated (GAC to GCG) and confirmed by sequencing. Details of strains and constructs are listed in Table S2.

Growth inhibition measurements

Growth assays were conducted by inoculating Mtb strains into liquid media at an OD_{600} of 0.05, and measuring the OD_{600} at three-day intervals. Compounds were added at the indicated concentrations initially and every three days throughout. For EC_{50} measurements, Mtb strains were pre-grown in 7H12+acetate media and assayed as described (*29*). For macrophage infections, bone marrow-derived macrophages (BMDMs) were isolated and differentiated from BALB/c mice (*36*). BMDMs were seeded in media without antibiotics in 24-well plates before infection. Cells were infected with Mtb. After 2 hours, extracellular bacteria were removed and replaced with fresh media containing indicated treatments. Media was replaced every 24 hours for the duration of the experiment. Fold changes in CFU's were determined by lysing macrophages in SDS (0.01%) and plating on agar plates.

$^{14}CO_2$ release experiments

Catabolism of [4-^{14}C]-cholesterol to $^{14}CO_2$ was quantified as described previously, with minor modifications (*36*). Briefly, Mtb cultures were pre-grown in 7H12+cholesterol+acetate media for one week and adjusted to an OD_{600} of 0.5. DMSO or V-59 were added 45 minutes prior to adding [4-^{14}C]-cholesterol. For TetOn-cAMP experiments, bacteria were inoculated at an OD_{600} of 0.1 into 7H12+cholesterol+acetate media and treated with EtOH, Atc, or V-59 at the indicated concentrations overnight, and again one hour prior to beginning the $^{14}CO_2$ release assay. Cultures were adjusted to an OD_{600} of 0.5 in their respective media and [4-^{14}C]-cholesterol was added. In both cases, $^{14}CO_2$ released from the vented Mtb culture flasks was collected as described (*36*).

Thin-layer chromatography

Mtb cultures were grown to an OD of 0.6, then inoculated at an OD_{600} of 0.4 into 7H12+cholesterol media for three days. Cultures were concentrated in their respective media, then [4-^{14}C]-cholesterol was added, the culture supernatant was collected after 24 hours, extracted in ethyl acetate, quantified by scintillation counting, and equal counts (10,000 CPM per lane) were spotted for each sample on a silica gel TLC plate (EMD Chemicals). Plates were run in toluene:acetone (75:25, v/v) and imaged by phosphorimaging.

Heterologous expression of Rv1625c in cya$^-$ E. coli

The cya-deficient *E. coli* strain HS26, derived from the TP610 strain, was transformed with the pMBC530 plasmid expressing the full Rv1625c ORF or the empty vector control plasmid pMBC529 and the strains were grown and induced as previously described (*37*). After 18 hours, sample OD_{600} values were recorded and supernatants were collected and used to quantify cAMP by ELISA.

Quantification of bacterial cAMP

Bacteria were pre-grown in 7H12+cholesterol+acetate before inoculation into fresh media at an OD_{600} of 0.1 containing either a cAMP-inducing compound (V-59 or Atc) or vehicle control. After 24-hour incubation, bacteria were collected by centrifugation, and the supernatant was reserved to measure secreted cAMP. The pellet was washed with fresh media, resuspended in lysis buffer (0.1M HCl, 1% Triton X-100 in H_2O), and disrupted by bead beating (MP Biomedical). Cell-free

lysates were reserved to measure internal cAMP by ELISA (Enzo Life Sciences). The sum of the internal and external values, or the external values alone, for each sample were used to estimate the total cAMP produced per 1×10^8 bacteria.

RNA-seq analysis

Bacteria were cultured in 7H9OADC before inoculation into fresh media containing a cAMP-inducing compound (10 µM V-59 or 500 ng/mL Atc) or vehicle control (DMSO or EtOH) at an OD_{600} of 0.1. The following day, bacteria were inoculated into 7H12+cholesterol media containing fresh compound or vehicle control. After four hours, cultures were pelleted by centrifugation, washed with guanidine thiocyanate-based buffer and stored at -80°C. Pellets were washed and suspended in Trizol LS (Ambion) and lysed by bead beating. Total RNA was isolated by chloroform extraction and precipitated in isopropanol with GlycoBlue reagent (Thermo Fisher). RNA was resuspended in nuclease-free water, genomic DNA contamination was removed using the Turbo-DNA free kit (Invitrogen), and rRNA was depleted using the Ribo-Zero Gold rRNA removal kit (Illumina). Sample quality was determined via Fragment Analyzer (Advanced Analytical) and TruSeq-barcoded RNAseq libraries were generated with the NEBNext Ultra II Directional RNA Library Prep Kit (New England Biolabs). Sequencing was performed at the Cornell University Transcriptional Regulation and Expression Facility on a NextSeq500 instrument (Illumina) at a depth of 15 M single-end 75 bp reads. Reads were trimmed for low quality and adaptor sequences with TrimGalore, and aligned to the *Mycobacterium tuberculosis* CDC1551 reference genome (GCA_000008585.1) with STAR. DESeq2 was used with default parameters and alpha = 0.05 to generate the differential gene expression results. Multiple test correction was performed using the Benjamini Hochberg method.

Propionyl-CoA reporter Assays

Fluorescent *prpD'*::GFP assays in liquid media were conducted in 7H12+cholesterol+acetate as described (*36*). BMDMs were infected at an MOI of 5. Extracellular Mtb was removed after 2 hours, and replaced with fresh media containing DMSO or V-59. For intracellular TetOn-cAMP experiments, the TetOn-cAMP *prpD'*::GFP strain was pre-induced in 7H9OADC media with EtOH, Atc (500 ng/mL), or V-59 (10 µM) for 24 hours prior to infection. After extracellular Mtb was removed, fresh media containing EtOH, Atc (3 µg/mL), or V-59 (10 µM) was added to the infected BMDMs. After 24 hours, infected BMDMs were scraped and fixed in paraformaldehyde. Fixed BMDMs were suspended in lysis buffer (0.1% SDS, 0.1 mg/mL Proteinase K in H_2O) and lysed by passage through a 25-gauge needle. Pellets were retained for analysis. The GFP MFI was quantified from 10,000 bacteria by flow cytometry and analyzed using FlowJo (Becton Dickinson). Details of reporter plasmid constructs are listed in Table S2.

Compound optimization

To identify mCLB073, the potency, safety, and pharmacokinetic properties of the oxadiazole series represented by V-59 was optimized. The cellular activity of V-59 analogs were assessed based on *in vitro* potency against Mtb in cholesterol-based media and intramacrophage assays, and cytotoxicity counterscreens against mammalian cells to ensure high selectivity.

Pharmacokinetic studies

Pharmacokinetic profiles were determined in male CD-1 mice after single dose oral administration (20 mg/kg). Stock solutions were prepared in 75% PEG 300, 25% D5W. An aliquot of the dose solutions was taken before and after dosing, and stored at –20°C for subsequent analysis. Blood samples were collected at standard time points through a retro-orbital bleed from 3 mice per time point. Heparinized blood was collected from each mouse and centrifuged to separate plasma for quantification of drug concentration by LC/MS analysis.

Analysis of spontaneous resistance to mCLB073

The frequency of spontaneous resistance to mCLB073 *in vitro* was estimated by plating Mtb on cholesterol agar plates containing mCLB073 (25 µM to 100 µM). Cholesterol was dissolved in 500 mM methyl-β-cyclodextrin and added to 7H10 agar at 100 µM. 7×10^5 CFU WT Erdman Mtb was spread per 150 mm plate and colonies were enumerated. Mutant clones were isolated, and subjected to EC_{50} assay. The *rv1625c* region was amplified by PCR and sequenced to determine the location of each mutation.

Western blot analysis

To confirm expression of His-tagged Rv1264 and Rv1264D265A in the Tet-On Mtb strains, bacteria were grown to an OD of 0.6 in 7H9OADC and then inoculated into 7H12+acetate containing EtOH or Atc (500 ng/mL) at an OD of 0.15. The following day, an equivalent number of bacteria were pelleted for each strain and treatment, and the pellets were fixed in paraformaldehyde (4%) for one hour and stored at -80°C. Fixed Mtb pellets were suspended in SDS (1%) and probe sonicated (3 x 1 minute cycles). Bacterial debris was removed by

centrifugation, and the supernatants were suspended in SDS PAGE loading buffer and boiled for 30 minutes with periodic vortexing. Equivalent volumes of each sample were resolved by SDS-PAGE gel and transferred to nitrocellulose membranes. Western blotting was performed using either mouse anti-5His (Qiagen), or mouse anti-Mycobacterium tuberculosis GroEL2 (BEI Resources, Clone IT-70) primary antibody, and HRP-conjugated goat anti-mouse IgG (Jackson ImmunoResearch) secondary antibody. Chemiluminescent substrate (Thermo Fisher Scientific) was added and Westerns were imaged by film for anti-His or by ChemiDoc (Bio-Rad) for anti-GroEL2.

Statistical Analysis

Averages were chosen as a measure of central tendency throughout. Analyses were performed using GraphPad Prism. When data were expected to fit an approximately normal distribution Ordinary one-way ANOVA was applied. For multiple comparisons between pre-selected pairs of control versus treatment groups, Sidak's multiple comparisons test was used. For comparisons between multiple treatment groups relative to a single control group, Dunnet's multiple comparisons test was selected. Ordinary two-way ANOVA with Tukey's multiple comparisons test was used when it was necessary to analyze the impact of both the strain background and compound versus control treatments. Data from mouse experiments were analyzed using non-parametric tests. For a single pre-planned comparison, a Mann-Whitney test was selected. For multiple comparisons, the Kruskal-Wallis test and Dunn's multiple comparisons test were used. Differences with P values < 0.05 were considered significant. For RNA-seq results, significance of the $\log_2$ fold-change between groups was assigned based on the adjusted p-value for differential expression analysis, where significance was assigned when the p-adj value was < 0.05.
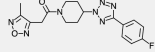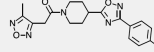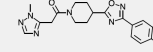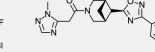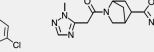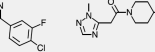
4.3 Results

4.3.1 V-59 inhibits Mtb growth and requires Rv1625c for activity

We previously identified compounds that inhibit Mtb replication in macrophages (*29*) and determined that one of these compounds (V-58) preferentially inhibits Mtb growth in cholesterol media in an Rv1625c dependent manner (*37*). Unfortunately, these previously identified compounds have poor potency and pharmacological properties. For example, a resynthesized analog of V-58 (sCEB942) displayed sub-optimal intramacrophage potency that could not be improved (Fig. 4.1). Similarly, the previously identified compound (mCCY224) displayed poor solubility, high plasma protein binding, and high levels of caseum binding (Fig. 4.1). These properties precluded the use of these Rv1625c-dependent compounds in mice. Since a primary goal of this work was to investigate the impact that activating cAMP synthesis has on Mtb physiology during infection in mice, we re-examined our screening hits to identify candidate Rv1625c-dependent compounds with more favorable pharmacological properties that are permissible for both *in vivo* and *in vitro* studies. This effort revealed a small molecule 1-(4-(5-(4-fluorophenyl)-2H-tetrazol-2-yl)piperidin-1-yl)-2-(4-methyl-1,2,5-oxadiazol-3-yl)ethan-1-one, named V-59, that inhibits Mtb replication in macrophages (half maximal effective concentration (EC$_{50}$) 0.30 μM). Because the availability of carbon sources can potentially impact activity of chemical inhibitors against Mtb, V-59 was evaluated in different *in vitro* culture conditions. Similar to a previously characterized Rv1625c agonist (*37*), V-59 inhibits Mtb growth in cholesterol media (EC$_{50}$ 0.70 μM) (Fig. 4.2a and Table 4.1) but not in media containing the two-carbon fatty acid acetate, or in standard rich growth media (Fig. 4.2b and Table 4.1). V-59 also displayed a promising pharmacokinetic profile (Table 4.1) and was therefore selected for further investigation as a potential Rv1625c agonist.
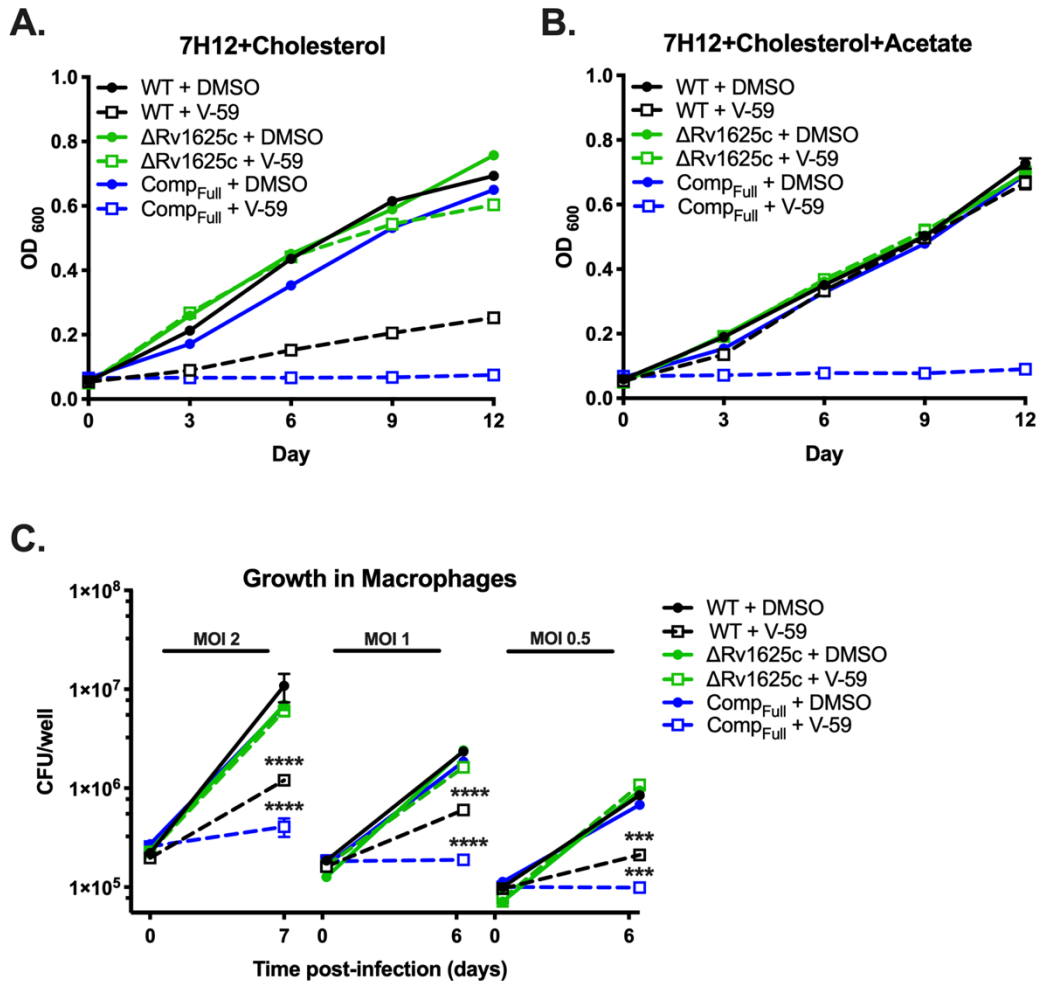
V-59 is structurally distinct from previous cholesterol utilization inhibitor candidates (Fig. 4.1). Similar to a subset of other cholesterol-dependent Mtb growth inhibitors we identified (*29*), a transposon insertion in the *rv1625c* gene (Tn::*rv1625c*) confers resistance to V-59 (Fig. 4.3a). Inversely, WT Mtb transformed with an *rv1625c* overexpression plasmid (2x*rv1625c*) was ~15-fold more susceptible to V-59 than WT (Fig 4.3a). This heightened susceptibility suggests a mechanism in which V-59 activates Rv1625c, and growth inhibition scales with Rv1625c enzyme levels. To test this further, we deleted the gene encoding Rv1625c (ΔRv1625c) and complemented this mutation with the entire *rv1625c* gene (Comp_{Full}). The ΔRv1625c mutant is refractory to V-59 inhibition in cholesterol media (Fig. 4.2a, Fig. 4.3b). Because macrophages contain various nutrients that can support Mtb growth (*38*) we determined that V-59 inhibits Mtb growth in murine macrophages *in vitro* and confirmed that Rv1625c is required for V-59 activity during macrophage infection (Fig. 4.2c). Importantly, the ΔRv1625c strain does not have a pan-drug resistance profile (Fig. 4.3c). Across all of these assays, the Comp_{Full} strain was more susceptible to V-59 treatment relative to WT, even in media containing acetate. This is likely because *rv1625c* is overexpressed in the Comp_{Full} strain relative to its native expression levels in WT (Fig. 4.3d). We conclude that a functional Rv1625c enzyme is required for V-59 activity, and that this compound inhibits Mtb growth in cholesterol media and macrophages.

Subseries	Screen hit		Advanced leads			Optimized lead
	V-59	mCIS635	mCLE299	mCLF177	mCLF178	mCLB073
	Furazan	Furazan	Triazole	Triazole	Triazole	Triazole
MW	371.36	371.36	404.82	398.84	416.83	421.28
In vitro potency assays						
Macrophages EC_{50} (µM)	0.3	0.27	--	0.13	>20	1.2
Cholesterol EC_{50} (nM)	700	150	115	83	83	27
7H9 OADC EC_{50} (µM)	>50	>50	--	>50	>50	>50
Cholesterol/acetate EC_{50} (µM)	>50	>50	--	--	--	>50
Toxicity						
HepG2/HEK293 CC_{50} (µM)	>20/>20	>20/>20	25/40	>20/>20	>20/>20	>20/>20
hERG IC_{50} (µM)	8.9	9.5	22.3	26.3	22.9	13.8
ADME						
PBB mouse/human (% bound)	82.7/--	94.4/--	86.3/90.3	91.7/91.4	88.4/88.9	96.3/97.6
Caseum binding (% unbound)	--	2.65	--	3.1	1.7	1.2
Cyp IC_{50} (µM)	>30	>50	>50	>50	>30	>50
ER mouse/human/rat/dog	0.3/0.3/--/--	0.4/0.3/--/--	0.3/0.3/0.2/0.3	0.3/0.3/0.2/0.3	0.3/0.3/0.2/0.3	0.3/0.3/0.2/0.3
Solubility (µM, pH 6.8)	4.63	34.4	196.8	197.7	185.9	160.1
Time over EC_{50} (20 mg/kg PO)	24 hr	>23 hr	>24 hr	>24 hr	>24 hr	>24 hr

**Table 4.1. Structures and activities of compounds.** MW, molecular weight; --, not determined; EC_{50}, half-maximal effective concentration; CC_{50}, 50% cytotoxic concentration; hERG, human ether-à-go-go-related gene; IC_{50}, half-maximal inhibitory concentration; ADME, absorption, distribution, metabolism, excretion; PPB, plasma protein binding; Cyp, cytochrome P450; ER, extraction ratio; PO, per oral.

	Rv1625c-Independent Cholesterol Breakdown Inhibitors		Analogs of Previously Published Rv1625c-Dependent Inhibitors	
	V-13-012725	V-13-011503	sCEB942	mCCY224
MW	244	276	426	468
Intramacrophage EC$_{50}$ (µM)	25	25	4.16	2.96
Cholesterol EC$_{50}$ (µM)	1.4	5	0.67	0.35
7H9 OADC EC$_{50}$ (µM)	>50	>50	>20	9.56
hERG (%)	--	--	--	89.09
HepG2 CC$_{50}$ (µM)	--	--	--	20
Cyp IC50 (µM, 2C19/2C9)	--	--	--	9.55/23.29
Mouse PPB (%)	--	--	89.61	99.96
Caseum binding (% unbound)	--	--	3.34	<<0.01
ER (mouse/human)	--	--	0.79/0.56	0.48/0.43
Solubility (mM, pH 6.8)	--	--	183.09	1
Time over EC$_{50}$	--	--	--	>12h
CLogP	--	--	3.42	4.04
PSA	--	--	109.7	59.3

Figure 4.1. V-59 is structurally distinct from other cholesterol utilization inhibitors. Chemical structure of previously published single-step cholesterol breakdown inhibitors, and resynthesized analogs of previously described Rv1625c-depedent inhibitors.

Figure 4.2. V-59 inhibits Mtb growth in an Rv1625c-dependent mechanism. (**A and B**) Impact of V-59 on Mtb growth in cholesterol media (A) and in media containing cholesterol and acetate (B). V-59 (10 μM) was added to the cultures every three days, and DMSO is the vehicle control. Data are representative of two experiments, with three technical replicates each. (**C**) Effect of V-59 on growth of Mtb in murine macrophages. Macrophages were treated with V-59 (25 μM) or DMSO. Data are from one experiment (MOI 1 and 0.5) with two or three technical replicates, or two experiments (MOI 2) with two technical replicates each (***$P < 0.001$, ****$P < 0.0001$, One-way ANOVA with Sidak's multiple comparisons test on calculated fold-change in CFU's). All data are means $\pm$ SEM.
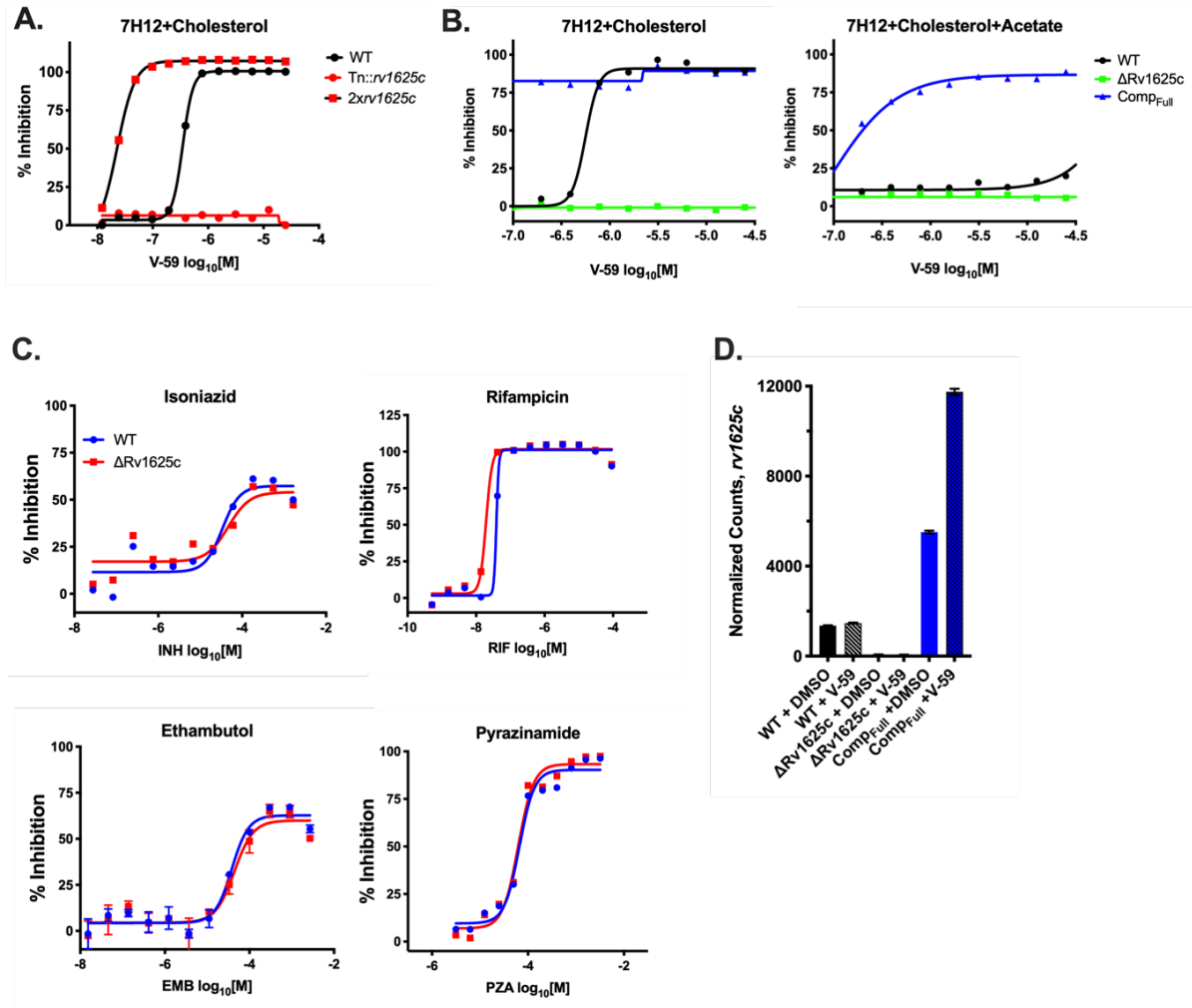
Figure 4.3. The inhibitory activity of V-59 in cholesterol media is dependent on Rv1625c. (**A**) Inhibitory activity of V-59 against WT, the Rv1625c transposon mutant (Tn::*rv1625c*), and WT transformed with an overexpression plasmid expressing the *rv1625c* gene (2x*rv1625c*) in 7H12+cholesterol media. (**B**) Inhibitory activity of V-59 against WT, ΔRv1625c, and Comp$_{full}$ in 7H12+cholesterol media (left) or 7H12+cholesterol+acetate media (right). Data shown are representative, from one experiment with two technical replicates. Symbols are mean data points, and curves display nonlinear fit of dose-response. (**C**) Effect of frontline antibiotics on WT and ΔRv1625 in 7H12+cholesterol (INH, RIF, EMB) or in MES-buffered 7H9OADC+glycerol, pH 5.9 (PZA). Data shown are representative, from one experiment with two technical replicates. Symbols are mean data points, and curves display nonlinear fit of dose-response. (**D**) RNA-seq derived normalized counts of *rv1625c* reads in WT, ΔRv1625c, and Comp$_{Full}$ strains in 7H12+cholesterol media.

4.3.2 Rv1625c is necessary and sufficient for V-59 to stimulate cAMP production

Rv1625c is a biochemically confirmed AC enzyme that catalyzes the intramolecular cyclization of ATP into cAMP (*30*). Therefore, we determined whether V-59 increases cAMP production in whole bacteria in an Rv1625c-dependent manner. V-59 induced cAMP by ~70-fold in WT and ~140-fold in Comp$_{Full}$, but did not affect the ΔRv1625c mutant (Fig. 4.4a). To determine whether Rv1625c is sufficient for V-59 to stimulate cAMP production, we heterologously expressed the *rv1625c* gene in an AC-deficient strain of *E. coli*. This strain is deficient in its own single AC (*cya⁻ E. coli*), ensuring that the cAMP produced in this experiment is due to Rv1625c activity (*37*). V-59 treatment significantly increased cAMP levels in *cya⁻ E. coli* transformed with the Rv1625c expression plasmid (Fig. 4.4b). In Mtb, we found that spontaneous mutations in *rv1625c* confer resistance to V-59 and an optimized analog of V-59 named mCLB073 (Fig. 4.4c, Fig. 4.5). Mutations predicted to truncate the Rv1625c protein and inactivate its cyclase domain resulted in resistance (Fig. 4.4c). We also identified missense mutations within the transmembrane and cyclase domains of Rv1625c that confer resistance; without further biochemical characterization, it is ambiguous whether these mutations generate resistance by preventing V-59 binding to Rv1625c, or by disabling Rv1625c enzyme activity. Together these results indicate that V-59 activates Rv1625c selectively in Mtb, and that Rv1625c expression is sufficient for V-59 to activate cAMP synthesis, which is necessary for V-59 to inhibit Mtb growth.

A. Total cAMP 24 hours

B. External cAMP *cya⁻ E. coli*

- ■ DMSO
- ▨ V-59 (10 μM)
- ▧ mCLB073 (10 μM)

C.

Mutant #	Location	Nature and Effect of Mutation
1	After G338	Insertion: IS3-like element IS987 family transposase
2	T017	Frameshift: Deletion of AC from (ACA)
3	L292	Missense: L (CTG) to R (CGG)
4	F400	Missense: F (TTC) to L (TTG)
5	W177	Nonsense: W (TGG) to Stop (TAG)
6	A244	Missense: A (GCC) to T (ACC)
7	L093	Missense: L (CTA) to R (CGA)
8	After G406	Insertion: IS3-like element IS987 family transposase
9	Stop 444	Missense: Stop (TGA) to R (AGA)
10	T104	Missense: T (ACG) to P (CCG)

Figure 4.4. V-59 binds Rv1625c and stimulates cAMP production. (**A**) Impact of V-59 on cAMP production in Mtb. Cultures were treated with V-59 or DMSO for 24 hours. Data are from two experiments with two technical replicates each (****$P < 0.0001$, Two-way ANOVA with Sidak's multiple comparisons test). (**B**) Impact of Rv1625c agonists on cAMP production in *cya⁻ E. coli* transformed with an empty vector control or an Rv1625c expression plasmid. Supernatants were collected 18 hours after addition of V-59, mCLB073, or DMSO. Data is from one experiment, with three independent expression clones, and two technical replicates each. (*$P < 0.05$, **$P < 0.01$, ****$P < 0.0001$, Two-way ANOVA with Tukey's multiple comparisons test). In (A) and (B) Data are normalized as total cAMP per 10^8 bacteria. DMSO is the vehicle control. Data are shown as means ± SEM. (**C**) Summary of mutations in the *rv1625c* gene that confer resistance to Rv1625c agonists. Mutations are grouped by their effect on the *rv1625c* sequence, with missense mutations (blue) and insertion or frameshift mutations (red) and mapped on the Rv1625c topology diagram to illustrate their approximate location relative to Rv1625c protein domains. Black circles represent amino acids that are essential for AC activity.

148
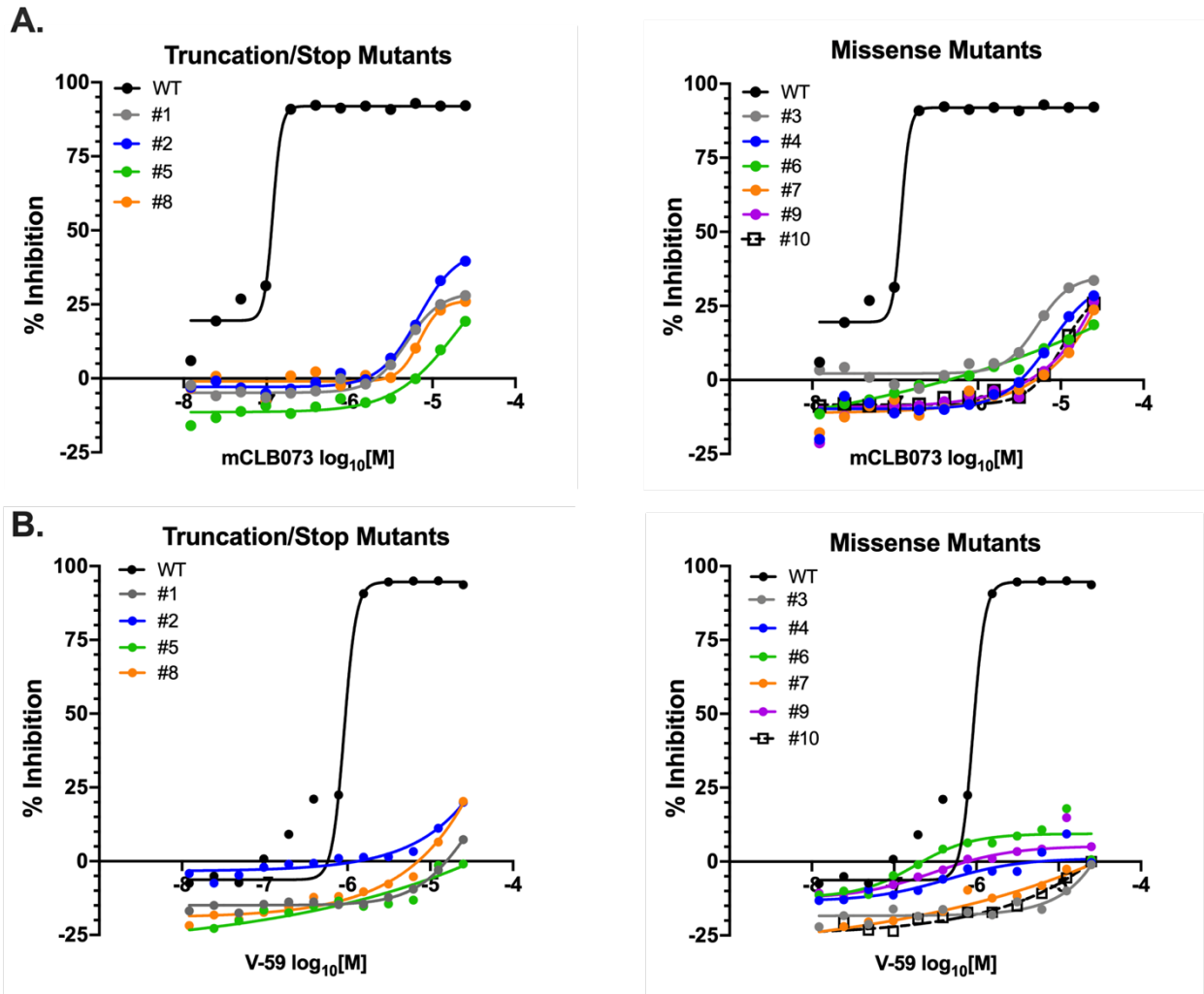
Figure 4.5. Growth inhibition by both V-59 and its analog mCLB073 is dependent on Rv1625c. (**A** and **B**) Inhibitory activity of mCLB073 (A) or V-59 (B) against spontaneous resistant mutants generated during culture with mCLB073. Data shown are representative, from one experiment with two technical replicates. Symbols are mean data points, and curves display nonlinear fit of dose-response. Data are from one experiment, with two technical replicates. Data are shown as means $\pm$ SEM.

4.3.3 Rv1625c is directly linked to cholesterol degradation in Mtb

Because V-59 impairs growth of Mtb in cholesterol media, we tested whether using V-59 to chemically activate Rv1625c inhibits the bacterium's ability to break down cholesterol. When Mtb degrades the A-ring of $[4\text{-}^{14}C]$-cholesterol, $[1\text{-}^{14}C]$-pyruvate is released; subsequently, pyruvate dehydrogenase activity mediates the conversion of $[1\text{-}^{14}C]$-pyruvate into acetyl-CoA and $^{14}CO_2$ (*6*). Therefore, to quantify cholesterol degradation in Mtb, we captured $^{14}CO_2$ released following $[4\text{-}^{14}C]$-cholesterol breakdown by the bacteria (*36*). We found that V-59 decreased $^{14}CO_2$ release in WT by ~89% (Fig. 4.6a). By contrast, V-59 had no measurable effect on $^{14}CO_2$ released from breakdown of the fatty acid $[U\text{-}^{14}C]$-palmitate (Fig. 4.7a). This suggests that chemically activating Rv1625c preferentially inhibits cholesterol utilization in WT Mtb, rather than equally inhibiting all lipid utilization by the bacterium.

Unexpectedly, we found that the ΔRv1625c mutant has an intrinsic defect in cholesterol degradation (Fig. 4.6a). In contrast to ΔRv1625c, the Rv1625c transposon mutant strain (Tn::*rv1625c*) had no defect in $^{14}CO_2$ release from $[4\text{-}^{14}C]$-cholesterol (Fig. 4.7b). The Tn::*rv1625c* strain has a transposon insertion within the coding sequence located after the last exit of Rv1625's six-helical transmembrane domain (amino acid Y302) (Fig. 4.7c). This likely truncates the protein, eliminating more than half of the C-terminal cyclase domain, while leaving the N-terminal cytoplasmic tail and six-helical transmembrane domain intact. Thus, we complemented the ΔRv1625c strain with a construct that expresses only the N-terminal cytoplasmic tail and six-helical transmembrane domain of Rv1625c (Comp$_{D204}$) (Fig. 4.7c). Cholesterol degradation was restored in the Comp$_{D204}$ strain (Fig. 4.6a), indicating that the transmembrane domain of Rv1625c is required for the complete degradation of cholesterol. Importantly, V-59 inhibited $^{14}CO_2$ release

in the $Comp_{Full}$ strain; however, V-59 did not prevent $^{14}CO_2$ release in the $Comp_{D204}$ strain which lacks the Rv1625c cyclase domain (Fig. 4.6a).

To further examine whether cholesterol degradation is blocked in ΔRv1625c Mtb, we used thin-layer chromatography (TLC) to track accumulation of $[4\text{-}^{14}C]$-cholesterol-derived metabolites. Compared to WT Mtb, the culture supernatant of ΔRv1625c was deficient in at least one cholesterol-derived degradation intermediate, and the production of this intermediate was restored in the $Comp_{Full}$ strain (Fig. 4.6b). Collectively, these results indicate that the cyclase domain of Rv1625c must be present for V-59 to inhibit cholesterol catabolism, and the transmembrane domain of Rv1625c is required for complete cholesterol breakdown, thereby establishing a direct link between the target of V-59 and the cholesterol pathway in Mtb. To our knowledge, this is the first time an individual AC has been linked to modulation of a downstream metabolic pathway in Mtb.
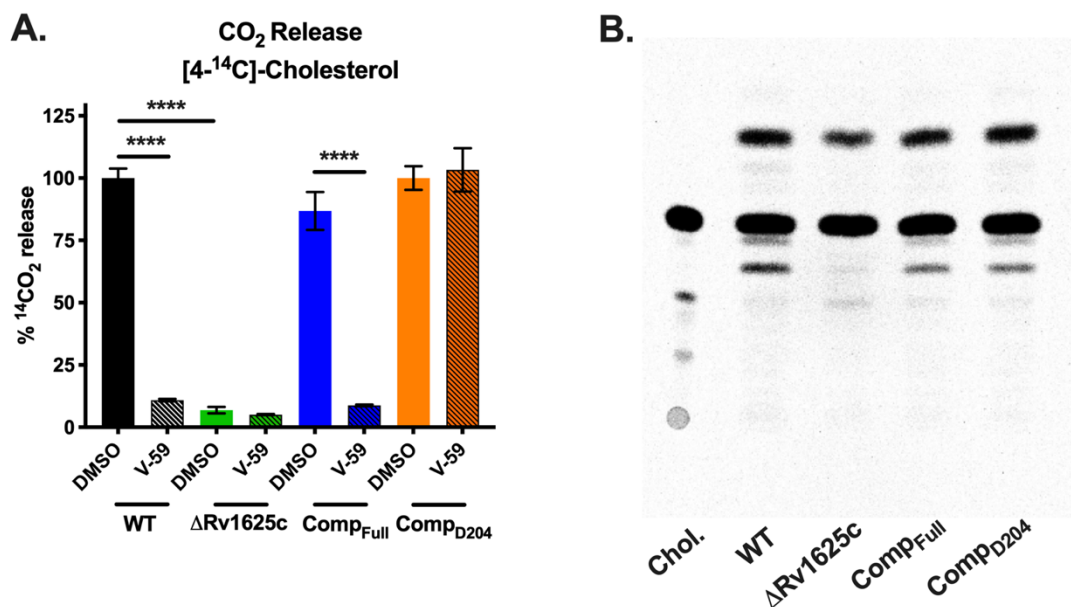
Figure 4.6. The transmembrane domain of Rv1625c is essential for complete degradation of cholesterol and the catalytic domain of Rv1625c is required for V-59 activity. (A) Catabolic release of $^{14}CO_2$ from [4-^{14}C]-cholesterol in WT, ΔRv1625c, Comp$_{Full}$, and Comp$_{D204}$ strains treated with V-59 (10 μM) or DMSO vehicle control. Data are from two experiments with three technical replicates, normalized to OD and quantified relative to WT treated with DMSO. Shown as means ± SEM (****$P < 0.0001$, Two-way ANOVA with Tukey's multiple comparisons test). **(B)** TLC comparing [4-^{14}C]-cholesterol-derived metabolites extracted from supernatants of Mtb. Image is representative of two experiments. Equivalent counts were spotted per lane. "Chol." = [4-^{14}C]-cholesterol.
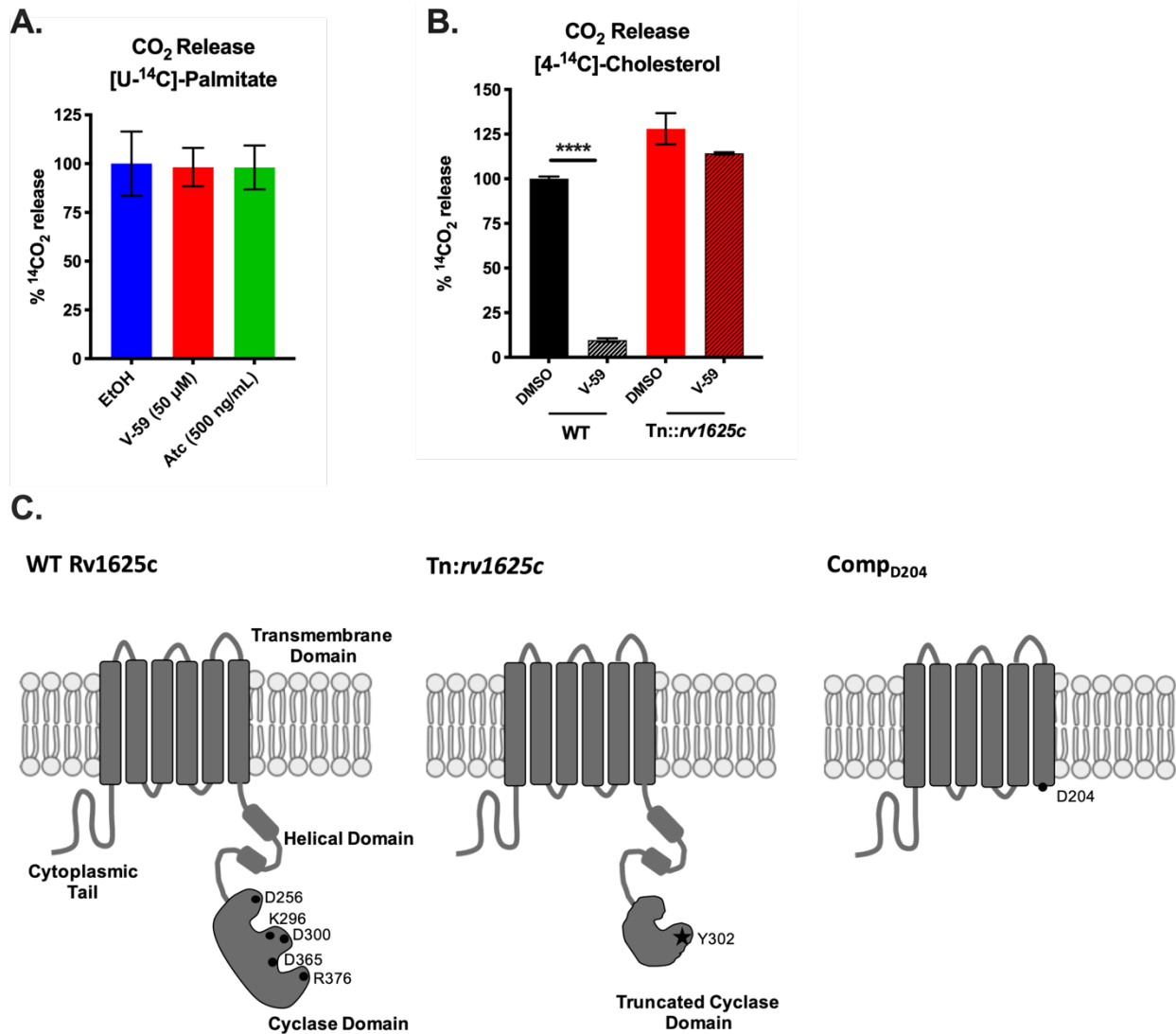
Figure 4.7. An intact cyclase domain of Rv1625c is required for V-59 to inhibit cholesterol degradation. (**A**) Catabolic release of $^{14}CO_2$ from [U-^{14}C]-palmitate in media containing fatty acid. EtOH (control), V-59, or Atc were added to the TetOn-cAMP Mtb cultures 24 hours prior to the start of the experiment. Data are from one experiment with three technical replicates, normalized to OD and quantified relative to EtOH control. Data are shown as means ± SEM (**B**) Catabolic release of $^{14}CO_2$ from [4-^{14}C]-cholesterol in media containing cholesterol and acetate. V-59 (10 μM) was added to the cultures once at the beginning of the experiments and DMSO was used as a vehicle control. Data are from one experiment with three technical replicates, normalized to OD and quantified relative to WT treated with DMSO. Data are shown as means ± SEM (****P < 0.001, One-way ANOVA with Sidak's multiple comparisons test). (**C**) Schematic illustrating the topology of the N-terminal transmembrane domain and essential residues of the C-terminal cyclase domain of Rv1625c (left). Schematics illustrating modified Rv1625c constructs used in these studies (center and right).
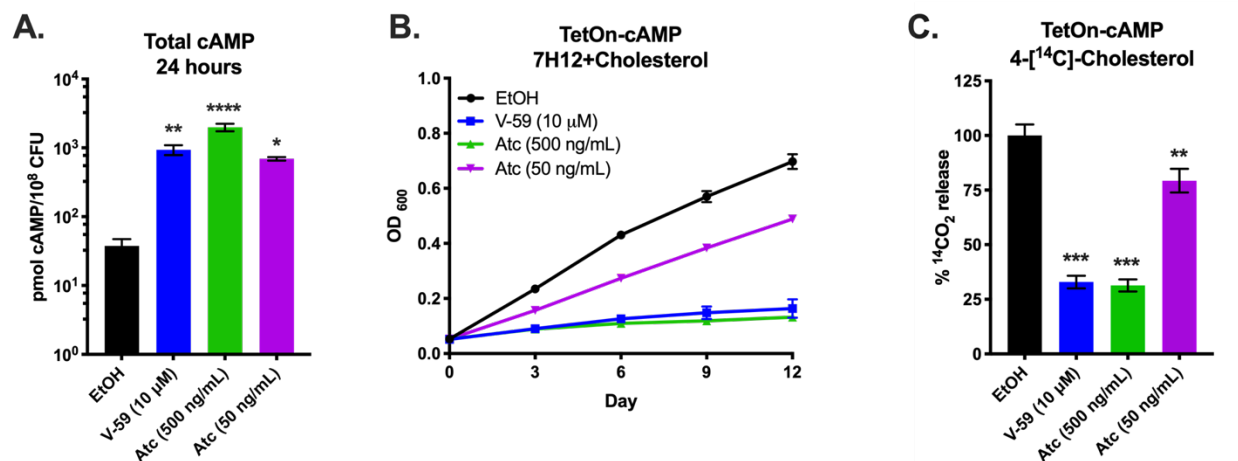
4.3.4   Inducing cAMP synthesis is sufficient to regulate cholesterol utilization

Next, we investigated whether cAMP signaling can modulate cholesterol metabolism in an Rv1625c-independent manner by using a novel inducible construct (TetOn-cAMP) to increase cAMP synthesis in Mtb. This TetOn-cAMP construct carries an anhydrotetracycline (Atc) inducible promoter that controls expression of the catalytic domain of the mycobacterial AC Rv1264 (*18*) (Fig. 4.8). Atc induced cAMP synthesis in WT Mtb carrying the TetOn-cAMP construct in a dose-dependent manner, reaching levels comparable with V-59 treatment (Fig. 4.9a). This tool is an advancement over previous approaches (*24, 39*) for several reasons: it does not rely on diffusion of an external cAMP analog into the bacteria, it requires the bacteria to synthesize cAMP from ATP which more closely models the dynamics of AC signaling, and it increases cAMP by 24 hours post-induction in a dose-dependent fashion. Atc treatment inhibited growth of WT bacteria carrying the TetOn-cAMP construct in cholesterol media (Fig 4.9b) and also decreased [4-^{14}C]-cholesterol degradation to $^{14}CO_2$ (Fig. 4.9c). Similar to V-59 treatment, activating cAMP synthesis with Atc did not inhibit degradation of the fatty acid [U-^{14}C]-palmitate to $^{14}CO_2$ (Fig. 4.7a).

As a control, we modified the TetOn-cAMP construct by mutating a catalytic residue of Rv1264 (TetOn-Rv1264$_{D265A}$) to render it catalytically inactive (*18*). Atc induced expression of the Rv1264$_{D265A}$ protein in WT Mtb carrying the TetOn-Rv1264$_{D265A}$ construct (Fig. 4.8b), but this strain did not produce increased cAMP in response to Atc (Fig. 4.10a). Inducing Rv1264$_{D265A}$ expression did not inhibit bacterial growth in cholesterol media (Fig. 4.10b) or cholesterol degradation (Fig. 4.10c, d). These results demonstrate that activating cAMP synthesis through a mechanism that is independent of Rv1625c is sufficient to regulate cholesterol utilization in Mtb in a dose-dependent manner.
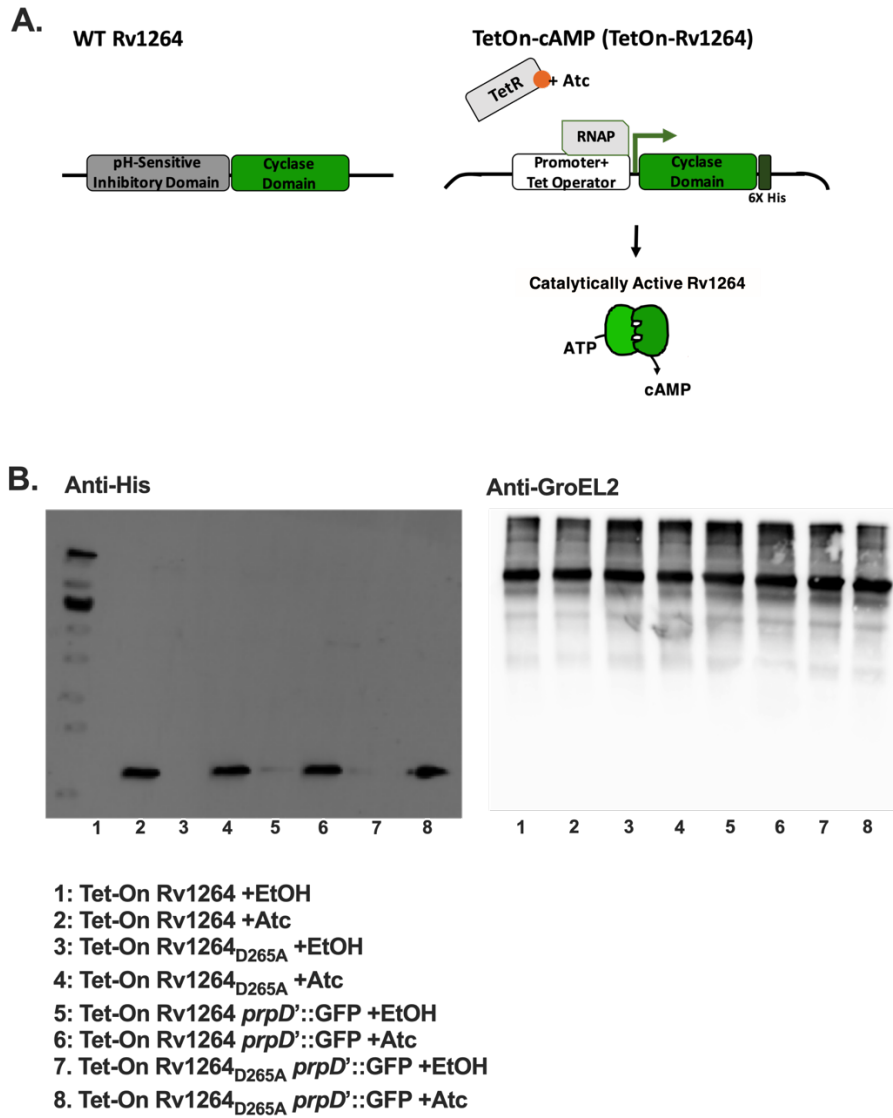
Figure 4.8. Construction and validation of TetOn-cAMP constructs. (**A**) Schematic illustrating the domains of the native Rv1264 adenylyl cyclase (left) and the design of the TetOn-cAMP construct (right). The TetOn-cAMP construct contains the minimum-necessary cyclase domain of Rv1264, and lacks the pH-sensitive inhibitory domain of the native Rv1264 protein. Expression of the cyclase domain is under control of a TetOn promoter. Upon treatment with Atc, release of the tetracycline repressor (TetR) causes initiation of transcription of the Rv1264 catalytic domain. The C-terminal end of the cyclase domain is His-tagged to allow immunoblotting. (**B**) Immunoblots of bacterial lysates confirm that the TetOn constructs are expressed in the presence of Atc and not the vehicle control EtOH. The anti-His blot detects the Rv1264 cyclase domain and the anti-GroEL2 blot is the loading control.

Figure 4.9. Inducing cAMP synthesis independent of V-59 and Rv1625c is sufficient to block cholesterol utilization. (**A**) Total cAMP induced in TetOn-cAMP Mtb. Cultures were treated with V-59 (10 μM), Atc (500 ng/mL or 50 ng/mL), or EtOH and samples were collected after 24 hours. Data are normalized as total cAMP per 10^8 Mtb and are from two experiments with two technical replicates each (*$P < 0.05$, **$P < 0.01$, ****$P < 0.0001$, One-way ANOVA with Dunnet's multiple comparisons test). (**B**) Impact of inducing TetOn-cAMP on the growth of Mtb in cholesterol media. Cultures were treated with V-59 (10 μM) or Atc for the duration of the experiment. Data are from two experiments with three technical replicates. (**C**) Catabolic release of $^{14}CO_2$ from [4-^{14}C]-cholesterol in the TetOn-cAMP strain treated with V-59, Atc, or EtOH. Data are from two experiments with three technical replicates, normalized to OD and quantified relative to EtOH (**$P < 0.01$, ***$P < 0.001$, One-way ANOVA with Dunnet's multiple comparisons test). EtOH is the vehicle control throughout. All data are means ± SEM.
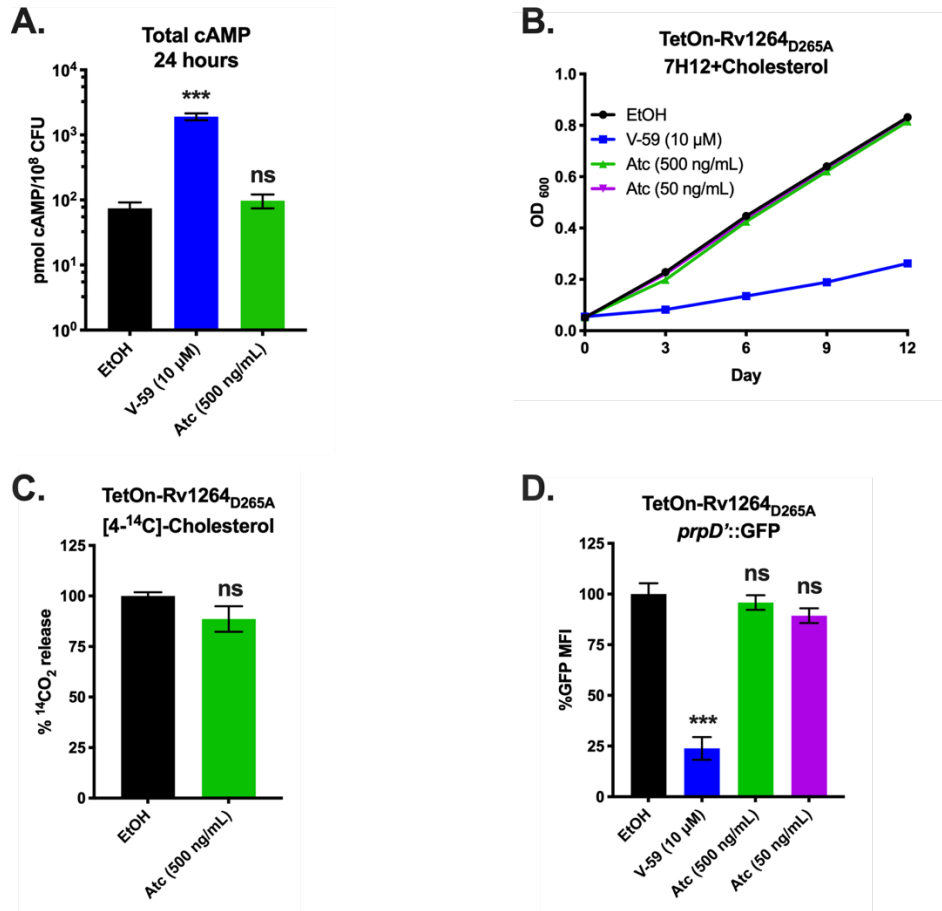
Figure 4.10. TetOn-Rv1264$_{D265A}$ is catalytically inactive and has no phenotype in cholesterol utilization assays. (**A**) Levels of cAMP in WT Mtb carrying the TetOn-Rv1264$_{D265A}$ construct cultured in cholesterol and acetate media and treated with EtOH, V-59 (10 μM), or Atc at the indicated concentrations. Samples were collected after 24 hours for ELISA. Data are displayed as total cAMP per 10^8 Mtb and are from two independent experiments with two technical replicates each, shown as means $\pm$ SEM (***$P < 0.001$, One-way ANOVA with Dunnett's multiple comparisons test). (**B**) Growth of TetOn-Rv1264$_{D265A}$ Mtb in 7H12+cholesterol media. EtOH, V-59 (10 μM), or Atc were added at the indicated concentrations initially and every three days for the duration of the experiment. Data are from one experiment with three technical replicates, shown as means $\pm$ SEM. (**C**) Catabolic release of $^{14}CO_2$ from [4-^{14}C]-cholesterol in media containing cholesterol and acetate. The TetOn-Rv1264$_{D265A}$ strain was treated with EtOH, V-59 (10 μM), or Atc at the indicated concentrations overnight and again one hour prior to the beginning of the experiments. Data are from two independent experiments with three technical replicates each, normalized to OD and quantified relative to EtOH vehicle control. Shown as means $\pm$ SEM (not significant, Student's t test). (**D**) Relative signal from the *prpD'*::GFP reporter in TetOn-Rv1264$_{D265A}$. Cultures were treated with EtOH, V-59 (10 μM), or Atc at the indicated concentrations in media with cholesterol and acetate. Data are normalized to EtOH vehicle control (***$P < 0.001$, One-way ANOVA with Dunnett's multiple comparisons test). GFP MFI was quantified from 10,000 mCherry$^+$ Mtb. Data are from two independent experiments with two technical replicates each, shown as means $\pm$ SEM.
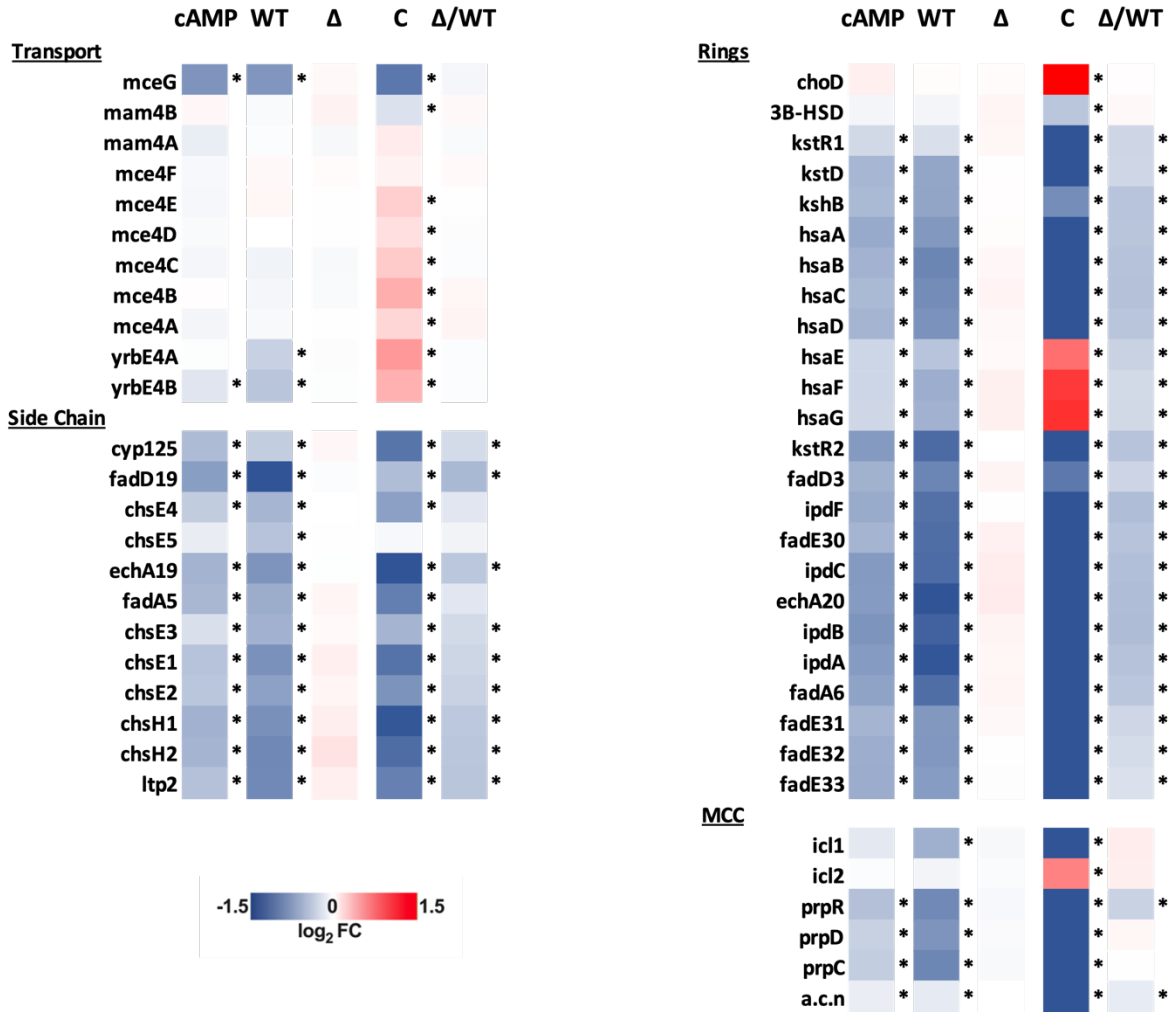
4.3.5 Shared transcriptional changes in cholesterol genes are associated with cAMP induction

Next, we characterized transcriptional responses of Mtb following V-59 treatment, or upon induction of the TetOn-cAMP construct, during growth in cholesterol media. The RNA-seq datasets revealed a shared pattern of differential gene expression that is consistent with an early blockade in the cholesterol degradation pathway. In Mtb, the side-chain and A-B rings of cholesterol are degraded by enzymes encoded in the Rv3574/KstR1 regulon (*6*). KstR1 is a TetR-like transcriptional repressor that binds the second cholesterol degradation intermediate, 3-hydroxy-cholest-5-ene-26-oyl-CoA, which de-represses the KstR1 regulon and permits cholesterol degradation to occur. Thus, increased expression of the KstR1 regulon is an indicator of cholesterol degradation in Mtb. Inducing cAMP synthesis, with V-59 or by activating TetOn-cAMP, prevented transcriptional induction of the KstR1 regulon in WT Mtb (Fig. 4.11). This included key genes required for cholesterol transport (*rv0655/mceG* and *rv3502/yrbE4B*) and cholesterol catabolism (*6*). Cholesterol degradation releases propionyl-CoA, and Mtb primarily assimilates this intermediate into central metabolism via the methylcitrate cycle (MCC) (*6*). As propionyl-CoA pools increase, Mtb upregulates expression of the genes encoding MCC enzymes (*rv0467/icl1*, *rv1130/prpD*, *rv1131/prpC*) (*40*). V-59 treatment and induction of the TetOn-cAMP construct in WT Mtb each prevented upregulation of MCC genes (Fig. 4.11). Paralleling previous experiments, V-59 induced more pronounced changes in the transcriptional signature in the Comp_Full strain. Notably, genes required for cholesterol transport and genes (*hsaEFG*) necessary for conversion of the cholesterol-derived catabolic intermediate 2-hydroxy-hexa-2,4-dienoic acid to pyruvate and propionyl-CoA were upregulated in the Comp_Full strain following V-59 treatment (*6*). It is plausible that these expression profiles reflect a compensatory response to inhibition of

cholesterol degradation by V-59, and a concomitant decrease in availability of MCC or tricarboxylic acid cycle intermediates. Consistent with our previous observations (Fig. 4.6), expression of cholesterol side-chain and ring degradation genes, but not transport or MCC genes, was intrinsically blocked in the ΔRv1625c strain relative to WT (Fig. 4.11). These observations further support the conclusion that Rv1625c is involved in downstream cholesterol metabolism in Mtb. Importantly, V-59 treatment did not alter the transcriptional signature of the ΔRv1625c strain.

To validate these findings, we used a reporter (*prpD'*::GFP) that expresses GFP under control of a MCC gene promoter (*prpD*), which indicates cellular levels of propionyl-CoA (*36*). V-59 decreased GFP signal in WT by ~50%, but did not impact the ΔRv1625c or Comp$_{D204}$ strains in cholesterol media or during macrophage infection (Fig. 4.12a). V-59 also dampened GFP signal by ~90% in the Comp$_{Full}$ strain (Fig. 4.12a). Similarly, inducing cAMP synthesis in WT Mtb carrying the TetOn-cAMP construct was sufficient to inhibit GFP signal during growth in cholesterol media and during macrophage infection (Fig. 4.12b). Inducing expression of the inactive Rv1264$_{D265A}$ protein (Fig. 4.8b) did not change the GFP signal (Fig. 4.10d). These data demonstrate that inducing cAMP synthesis in Mtb, via V-59 treatment or TetOn-cAMP activation, impairs cholesterol degradation and the release of key metabolic intermediates including propionyl-CoA in Mtb. Importantly, the effects of V-59 treatment require the catalytic domain of Rv1625c, and cAMP synthesis is a dominant signal in the mechanism by which V-59 inhibits Mtb growth.

Figure 4.11. V-59 treatment and induction of TetOn-cAMP are associated with shared transcriptional changes to cholesterol utilization genes. RNA-seq analysis quantifying differentially expressed genes from Mtb grown in cholesterol media, following V-59 treatment, or induction of TetOn-cAMP with Atc. Genes depicted are in the KstR regulons and involved in cholesterol utilization. MCC = methylcitrate cycle. Data are displayed as log_2 fold change in gene expression in response to cAMP-inducing vs. control treatment ("cAMP" = Tet-On cAMP Atc vs. EtOH, "WT" = WT V-59 vs. DMSO, "Δ" = ΔRv1625 V-59 vs. DMSO, "C" = Comp$_{Full}$ V-59 vs. DMSO). Also shown are differentially expressed genes intrinsic to ΔRv1625 ("Δ/WT" = ΔRv1625 DMSO vs. WT DMSO). Data are from two technical replicate samples from one experiment (*adjusted p-value $\leq$ 0.05).
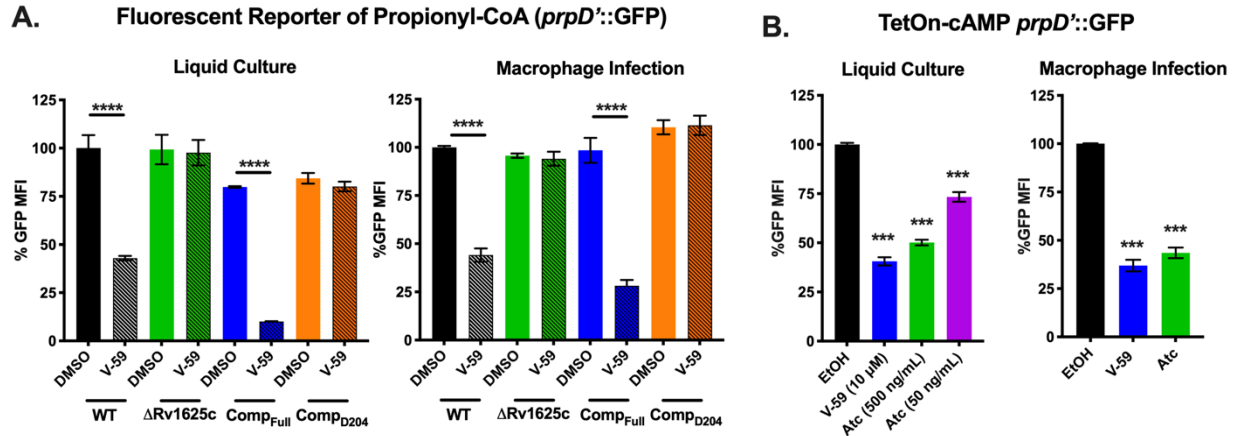
Figure 4.12. Activating cAMP synthesis decreases liberation of propionyl-CoA from cholesterol. (**A**) Relative GFP signal from the *prpD'*::GFP reporter in response to V-59 (10 μM) or DMSO treatment in murine macrophages or cholesterol media. Data are normalized to WT treated with DMSO (****$P < 0.0001$, Two-way ANOVA with Tukey's multiple comparisons test). (**B**) Relative GFP signal from the *prpD'*::GFP reporter in response to inducing TetOn-cAMP with Atc treatment in murine macrophages or cholesterol media. Data are normalized to EtOH vehicle control (***$P < 0.001$, One-way ANOVA with Dunnett's multiple comparisons test). GFP MFI was quantified from 10,000 mCherry[+] Mtb. Data are from two experiments with two technical replicates, shown as means ± SEM.

4.3.6 Investigating potential mediators of cAMP-dependent cholesterol inhibition in Mtb

Mt-Pat is not required to mediate inhibition of cholesterol utilization

Inducing cAMP synthesis blocks cholesterol utilization in Mtb, but the mechanism mediating this is unknown. Because fatty acid metabolism can be modulated by the cAMP-binding protein Rv0998/Mt-Pat (*27, 28*) we investigated whether Mt-Pat also mediates V-59-dependent inhibition of cholesterol utilization. However, inhibition of growth (Fig. 4.13a) and inhibition of MCC gene induction (Fig. 4.13b) by V-59 treatment were not altered in an Mt-Pat mutant.

Notably, across our experiments, the $Comp_{Full}$ strain was uniquely susceptible to cAMP induction in cholesterol media that was supplemented with the short chain fatty acid acetate (Fig. 4.2b). The TetOn-cAMP strain had a slightly greater defect in growth under this condition than bacteria treated with V-59, but this growth defect was much less severe than that exhibited by the $Comp_{Full}$ strain (Fig. 4.13c). Additionally, V-59 blocked MCC gene induction in the $Comp_{Full}$ strain when grown with odd-chain fatty acids (Fig. 4.13d). This suggests that additional metabolic defects, possibly in fatty acid utilization or central metabolism, are induced under these conditions. While these observations pertaining to fatty acid utilization correlate with a higher threshold of cAMP induction (Fig. 4.4a), we have not yet tested whether Mt-Pat mediates these additional effects. In the future, identifying the pathway by which inducing cAMP synthesis modulates cholesterol catabolism in Mtb may explain the differing effects of V-59 on carbon metabolism in these strains.

*Transcriptional changes in select CRP_{MT} regulon genes are associated with cAMP induction*

To define a set of commonly regulated cAMP-dependent genes using an unbiased analysis, we compared all of the statistically significant differentially expressed genes associated with V-59 treatment or TetOn-cAMP induction in WT Mtb. A shared set of 248 genes were identified (Fig.

4.14a). Because the selected growth condition was cholesterol media, 45 of these genes are associated with cholesterol utilization. As discussed above, those with biochemically confirmed roles in cholesterol utilization were noted (Fig. 4.11). Many of the remaining 203 genes do not have well defined functions in Mtb, and we chose to focus on a small subset that were previously predicted to be regulated by the cAMP-binding transcription factor Rv3676/CRP$_{MT}$.

Aside from Mt-Pat, CRP$_{Mt}$ is the best-studied cAMP-binding effector protein in Mtb. CRP$_{Mt}$ is designated as a cAMP-responsive transcription factor, with a predicted regulon of ~100 genes in Mtb (*25, 26, 41*). CRP$_{Mt}$ may also be required to maintain Mtb fitness in macrophages and during chronic infection in mice (*26*). We found that activating cAMP via V-59 treatment or TetOn-cAMP induction was associated with transcriptional changes to a shared set of 8 CRP$_{Mt}$ regulon genes during growth in cholesterol media (Fig. 4.14b). Among these, *rv0450c/mmpL4* and *rv0451c/mmpS4* are both downregulated following cAMP induction. Though *mmpL4* was not a predicted member of the CRP$_{MT}$ regulon, it is reasonable that these genes would be co-regulated given that MmpL4 and MmpS4 are encoded in the same putative operon and can form a protein complex that contributes to siderophore production in Mtb (*42*). This result is also notable because genetic screens have predicted that *mmpL4/mmpS4* are required for normal growth of Mtb in cholesterol media and in mouse models of TB (*12, 43*). We also noted that the predicted CRP$_{MT}$ regulon member *rv0805* is upregulated during V-59 treatment. Rv0805 is the only known phosphodiesterase in Mtb, and these enzymes contribute to cAMP signaling pathway homeostasis by hydrolyzing cAMP to AMP (*23*). Given that *rv0805* mutant Mtb also has a growth defect in cholesterol media (*43*), it is reasonable to speculate that *rv0805* is upregulated during V-59 treatment in the presence of cholesterol as a compensatory response to help decrease cAMP levels

and restore cholesterol utilization. Taken together, this is consistent with our other results indicating that a threshold of increased cAMP is inhibitory during cholesterol utilization in Mtb.

Surprisingly, an additional set of 13 predicted CRP_{Mt} regulon genes displayed intrinsic differential expression in the ΔRv1625c strain relative to WT (Fig. 4.14 b) but were not universally differentially expressed in response to cAMP induction. This suggests that Rv1625c might play a native role in regulating some CRP_{MT} operon genes during cholesterol utilization. Overall, these findings are significant because they demonstrate that a subset of predicted CRP_{Mt} genes are altered either in response to induction of cAMP synthesis, or through loss of Rv1625c, in the presence of cholesterol. While this study does not explain the native role of CRP_{MT} during infection, V-59 and TetOn-cAMP can be used as tools in future studies to examine regulation of this operon under different growth conditions or during infection which may provide insight into its function in Mtb pathogenesis.
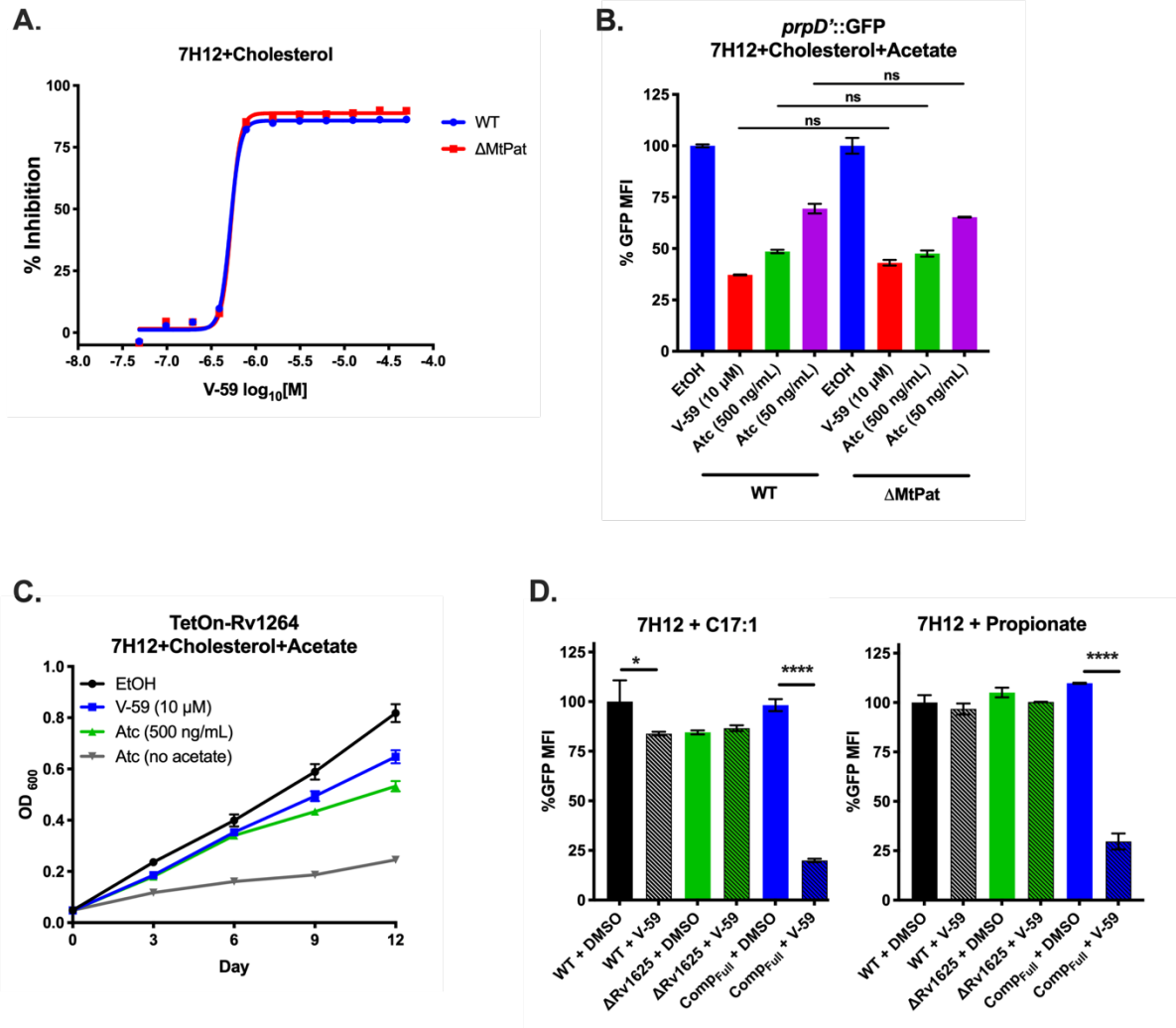
Figure 4.13. Activating cAMP synthesis inhibits lipid metabolism via an Mt-Pat independent mechanism, but can inhibit fatty acid utilization. (**A**) Activity of V-59 against WT or ΔMt-Pat in 7H12+cholesterol media. Symbols are mean data points, and curves display nonlinear fit of dose-response. (**B**) Relative GFP signal from the *prpD'*::GFP reporter in WT versus ΔMt-Pat strains carrying the TetOn-cAMP construct in media containing cholesterol and acetate. Cultures were treated in parallel with EtOH, V-59 (10 μM), or Atc. Each strain is normalized to EtOH vehicle control. Strain responses are not significantly different, Two-way ANOVA with Tukey's multiple comparisons test. Data are from one experiment with two technical replicates, shown as means ± SEM. (**C**) Effect of inducing TetOn-cAMP on the growth of Mtb in 7H12+cholesterol+acetate media. EtOH, V-59 (10 μM), or Atc were added at the indicated concentrations. Data are from one experiment with three technical replicates, shown as means ± SEM. (**D**) Relative GFP signal from the *prpD'*::GFP reporter in Mtb treated with V-59 or DMSO, in 7H12 media supplemented with C17:1 or propionate. Data are normalized to WT+DMSO. Data are from one experiment with two technical replicates, shown as means ± SEM (*P < 0.05, ****P < 0.0001, One-way ANOVA with Sidak's multiple comparisons test). Throughout, GFP MFIs were quantified from 10,000 mCherry positive Mtb.

165
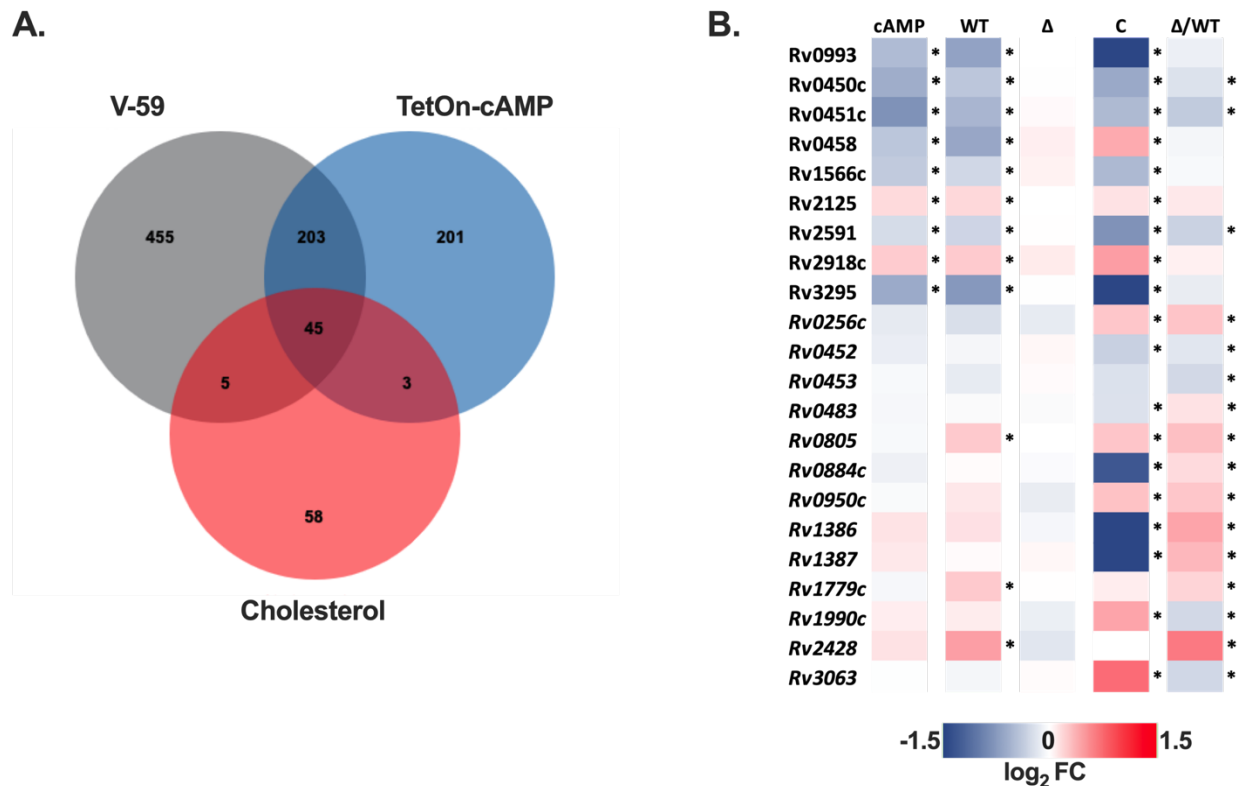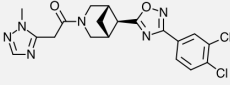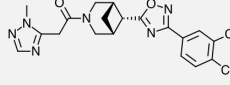
Figure 4.14. V-59 treatment and induction of TetOn-cAMP are associated with transcriptional changes in select CRP$_{Mt}$ regulon genes. (**A**) Venn diagram showing the number of significantly differentially expressed genes shared by WT Mtb treated with V-59 relative to DMSO and the TetOn-cAMP strain treated with Atc relative to EtOH, and how many of these belong to the KstR cholesterol-related regulon. (**B**) RNA-seq analysis quantifying differentially expressed genes from Mtb grown in cholesterol media, following V-59 treatment, or induction of TetOn-cAMP with Atc. Genes depicted are predicted members of the CRP$_{MT}$ regulon. Only genes with significant differential expression in both the V-59 and TetOn-cAMP conditions, or genes with intrinsic changes in the ΔRv1625 strain (in italics), are shown. "cAMP" = Tet-On cAMP Atc vs. EtOH, "WT" = WT V-59 vs. DMSO, "Δ" = ΔRv1625 V-59 vs. DMSO, "C" = Comp$_{Full}$ V-59 vs. DMSO, "Δ/WT" = ΔRv1625 DMSO vs. WT DMSO.

4.3.7   *mCLB073 is an optimized analog of the V-59 compound series*

Next, we sought to identify chemical features that are essential to a potent Rv1625c agonist, and to develop an optimized compound for use during future *in vivo* studies. The screening hit (V-59) was relatively potent against Mtb in macrophages and had several satisfactory pharmacological features including plasma exposure above the EC_{50} (as determined in cholesterol media) for approximately 24 hours following oral dosing in mice at 20 mg/kg (Table 4.1). We sought to improve the properties of the V-59 compound series with medicinal chemistry. Structure activity relationship studies determined that replacing the tetrazole ring in V-59 with an oxadiazole ring (mCIS635) improved potency and slightly improved solubility. Replacing the 4-methyl-1,2,5-oxadiazole ring in V-59 with a 1-methyl-1H-1,2,4-triazole ring addressed the liability of the oxadiazole ring and generated the lead compounds mCLE299, mCLF177, mCLF178, and mCLB073 that had improved properties including better potency and extended plasma exposure following oral administration in mice. We explored constraining the piperidine ring in order to increase compound solubility by lowering its lattice energy, through an azabicyclic ring and a chiral center in several molecules of this series (Table 4.1 and Table 4.2). Interestingly, the *cis* isomer (mCLF024) displayed potency similar to the advanced lead compounds in this series, while the *trans* isomer (mCLF025) was inactive (Table 4.2).

Among the optimized analogs, the lead compound (1-(4-(3-(3,4-dichlorophenyl)-1,2,4-oxadiazol-5-yl)-1-piperidinyl)-2-(2-methyl-2H-1,2,4-triazol-3-yl)-1-ethanone), named mCLB073, exhibited a ~17-fold potency improvement against Mtb in cholesterol media relative to V-59 while maintaining excellent pharmacokinetic properties and a good safety profile. We then verified that mCLB073 retained on-target activity. The ΔRv1625c strain was refractory to mCLB073 treatment (Fig. 4.15a), and mCLB073 activates cAMP synthesis (Fig. 4.4b and Fig.

4.15b). Additionally, we isolated spontaneous resistant mutants in Mtb cultured with mCLB073. All spontaneous resistant mutants we isolated contained mutations in *rv1625c* that conferred resistance to mCLB073 and cross-resistance to V-59 (Fig. 4.4c and Fig. 4.5a). These results indicate that mCLB073 is a genuine Rv1625c agonist. When dosed orally in mice, mCLB073 maintained plasma exposure over the EC_{50} identified in cholesterol media for at least 24 hours (Table 4.1). This demonstrated that mCLB073 is suitable for once-daily oral dosing in mouse models of infection and justified using this compound as a chemical probe during future *in vivo* studies.

	mCLF024	mCLF025
MW	433.29	422.29
	In vitro potency assays	
Macrophages EC_{50} (µM)	97	>30,000
Cholesterol EC_{50} (nM)	49	>30,000
	Toxicity	
hERG IC_{50} (µM)	11.8	--
	ADME	
PBB mouse (% bound)	97.8	--
Caseum binding (% unbound)	<0.01	--
ER mouse/human	<0.3/<0.3	--
Solubility (µM, pH 6.8)	94.0	--

Table 4.2. Structures and activities of isomer compounds. MW, molecular weight; --, not determined; EC_{50}, half-maximal effective concentration; IC_{50}, half-maximal inhibitory concentration; ADME, absorption, distribution, metabolism, excretion; PPB, plasma protein binding; ER, extraction ratio; PO, per os.
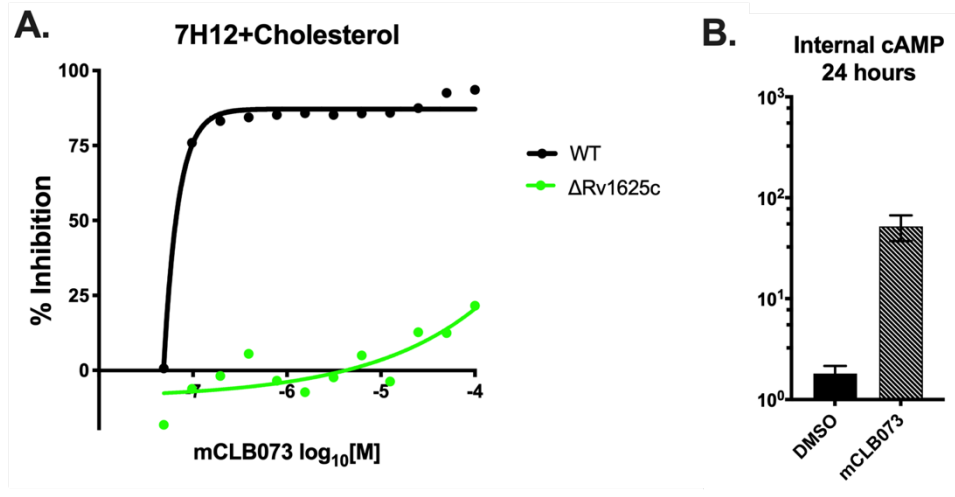
Figure 4.15. The V-59 analog mCLB073 is an Rv1625c agonist. (**A**) Inhibitory activity of mCLB073 against WT or ΔRv1625c in 7H12+cholesterol media. Data shown are representative, from one experiment with two technical replicates. Symbols are mean data points, and curves display nonlinear fit of dose-response. (**B**) Impact of mCLB073 on cAMP production in WT Mtb. ELISA was used to quantify cAMP from lysed cells 24 hours after addition of mCLB073, or vehicle control (DMSO). Data is from one experiment, with two technical replicates. Data are shown as means $\pm$ SEM.

4.4 Discussion

Mtb possesses an expanded repertoire of cAMP signaling pathway components compared to other bacteria, suggesting this is an important mechanism to coordinate physiological functions in response to environmental cues. However, how Mtb physiology can be regulated through cAMP signaling, particularly through activation of specific AC enzymes, is not well understood. It was also not previously established whether this signaling pathway could be manipulated pharmacologically to disrupt Mtb pathogenesis. This gap in knowledge is partly explained by the lack of chemical and genetic tools that are equivalent to the eukaryotic AC agonist forskolin in the Mtb system. In this study we identified a chemical AC agonist that is suitable for *in vitro* and *in vivo* studies. And in a complementary approach, we created and validated a TetOn-cAMP construct that permits dose-dependent induction of cAMP synthesis in Mtb. These tools allowed us to establish a link between induction of cAMP synthesis, downregulation of cholesterol utilization, and inhibition of Mtb growth during macrophage infection.

Here, we re-examined a collection of compounds that were identified in a high-throughput screen as inhibitors of Mtb growth in macrophages and cholesterol media. Based on a previous study (*29*) we knew that this collection contained at least three Rv1625c-dependent compounds, and sought to identify an additional Rv1625c agonist with improved potency and acceptable properties for use in future *in vivo* studies. From the screening hits, we identified a candidate small molecule named V-59 that displayed promising pharmacological properties (Table 4.1). We then determined that growth inhibition by V-59 in cholesterol media and in macrophages requires a functional Rv1625c enzyme (Fig. 4.2 and Fig. 4.4c), and V-59 induces cAMP synthesis in an Rv1625c-dependent manner (Fig. 4.4 a, b). By quantifying degradation of the A-ring of cholesterol, we found that V-59 indeed blocks cholesterol utilization, in a mechanism that requires

the cyclase domain of Rv1625c (Fig. 4.6). Our combined results support the conclusion that V-59 directly binds to the Rv1625c enzyme to activate AC activity, which artificially increases cAMP synthesis in Mtb to inhibit cholesterol utilization which impairs bacterial growth in cholesterol media and macrophages.

To study the impact of cAMP induction independent of V-59 and Rv1625c, we developed a TetOn-cAMP construct that increases cAMP synthesis in a dose-dependent manner (Fig. 4.8 and Fig. 4.9a). We found that inducing cAMP synthesis is sufficient to decrease growth of Mtb in cholesterol media (Fig. 4.9b) and to block cholesterol degradation (Fig. 4.9c). Transcriptional studies revealed hallmarks indicating that cholesterol degradation is inhibited early in the breakdown process following V-59 treatment, or induction of cAMP synthesis via the TetOn-cAMP construct (Fig. 4.11 and Fig. 4.12). Together, this demonstrates that inducing cAMP above a certain threshold through a different AC is sufficient to mimic the effects of an Rv1625c agonist, which suggests that AC activation is a general mechanism that can be leveraged to inhibit cholesterol utilization in Mtb. Collectively, our findings indicate that inducing cAMP synthesis in Mtb inhibits cholesterol degradation, blocks transcriptional activation of hallmark cholesterol utilization genes, and decreases propionyl-CoA pools in proportion to the amount of cAMP induced. Cholesterol breakdown is a many-stage process, and side chain and ring degradation can occur in tandem (*6*). Considering this, one interpretation consistent across these results is that robust activation of cAMP synthesis prevents cholesterol side chain and ring degradation simultaneously, and this decreases the breakdown of cholesterol to an early intermediate that is required to de-repress the KstR1 regulon.

While investigating the effect of V-59 on Rv1625c activity and cholesterol utilization, we unexpectedly discovered that the six-helical transmembrane domain of Rv1625c and the associated

N-terminal cytoplasmic tail is intrinsically required for complete cholesterol degradation in Mtb (Fig. 4.6). Given that Rv1625c had no previously predicted role in cholesterol utilization, this is a surprising connection between the AC that V-59 activates, and the metabolic pathway it inhibits. The native function of Rv1625c signaling during infection is not established, and Rv1625c is the first AC that has been linked to a specific downstream metabolic pathway in Mtb (*23*). Our finding that the Rv1625c transmembrane domain is required for cholesterol ring catabolism expands on work by others showing that the catalytic domain is not the only functionally relevant component of this AC (*32, 33, 44*), but the mechanism that mediates its involvement in cholesterol catabolism remains to be determined. It is not known if the transmembrane domain of Rv1625c mediates protein-protein interactions that are required to complete cholesterol catabolism and whether this, or an alternative mechanism, is involved in maximizing regulation of cholesterol utilization by Rv1625c agonists.

It is notable that the cholesterol utilization defect intrinsic to the ΔRv1625 strain was likely limited to ring catabolism (Fig. 4.6a), and was not sufficient to impact bacterial growth in cholesterol media or macrophages (Fig. 4.2a, c), or to inhibit transcriptional activation of methylcitrate cycle genes by liberation of propionyl-CoA (Fig. 4.11 and Fig. 4.12a). Because degradation of the cholesterol side chain and rings can proceed in tandem, it is conceivable that a blockage in ring catabolism could be present in ΔRv1625 Mtb, while growth on cholesterol via liberation of propionyl-CoA and acetyl-CoA from the side chain are maintained. This may supply enough two- and three-carbon intermediates to maintain growth. Two genes neighboring Rv1625c (*rv1626/pdtaR* and *rv1627c*) have been predicted to be required during cholesterol utilization (*43*). It will be helpful to determine whether Rv1625c interacts with these proteins, or others capable of regulating lipid metabolism in Mtb. Moreover, it would be interesting to examine whether the

binding of V-59 to Rv1625c not only activates cAMP synthesis but also alters an interaction between Rv1625c and a relevant protein. This would help explain the distinct but overlapping cholesterol utilization defects we observed in WT Mtb treated with V-59, the ΔRv1625 strain, and TetOn-cAMP Mtb treated with different doses of Atc. The amount of cAMP produced by the TetOn-cAMP strain was most similar to V-59 treatment at the lower dose of Atc (50 ng/mL) tested (Fig. 4.9a). This dose also correlated with less severe defects in growth in cholesterol media, $^{14}CO_2$ release from [4-^{14}C]-cholesterol, and propionyl-CoA liberation from cholesterol than the defects observed with V-59 treatment (Fig. 4.9 and Fig. 4.12b). Based on this and our observations in the ΔRv1625 strain, it is interesting to speculate that V-59 interacts with the Rv1625c protein, altering both a relevant protein interaction and increasing cAMP synthesis, both of which contribute to V-59's total effect on cholesterol utilization. However, the mechanism and kinetics of inducing cAMP synthesis with the TetOn-cAMP system are distinct from V-59 treatment, limiting our ability to conclude that a particular dose of Atc mimics V-59 treatment. Future experiments to identify cholesterol degradation intermediates that accumulate in WT Mtb treated with V-59 could help clarify this by allowing comparison of step(s) of the cholesterol degradation pathway that are blocked by V-59 treatment versus Tet-On cAMP induction or loss of the Rv1625c protein alone.

These findings expand our limited understanding of how cAMP signaling can alter metabolism in Mtb, and it remains to be determined whether a downstream cAMP-binding protein is required for V-59 or TetOn-cAMP induction to inhibit cholesterol utilization in Mtb. We investigated Rv0998/Mt-Pat because it is a cAMP-binding lysine acetyltransferase that was previously shown to acetylate and inactive the acetyl-CoA/propionyl-CoA ligase (Rv3667/Acs) and various FadD enzymes in Mtb, which can regulate incorporation of 2- and 3-carbon precursors into central metabolism (*27, 28*). Mt-Pat was not required for V-59 to inhibit Mtb growth (Fig. 4.13a) or

induction of MCC genes (Fig. 4.13b) in cholesterol media. This is consistent with data showing that acetate rescues growth during both V-59 treatment and TetOn-cAMP activation (Fig. 4.2b, Fig. 4.13c), suggesting the acetyl-CoA/propionyl-CoA ligase has not been inactivated by Mt-Pat in either condition. The FadD enzyme Rv3515c/FadD19 initiates cholesterol side chain degradation (6) but FadD19 is not a confirmed target of inactivation by Mt-Pat, and other FadD enzymes that are known to be acetylated by Mt-Pat are not established steps in cholesterol breakdown (28). Thus, it is reasonable to conclude that Mt-Pat is not a mediator of cAMP-dependent cholesterol inhibition under the conditions we tested.

Although Mt-Pat likely does not mediate inhibition of cholesterol utilization downstream of V-59 treatment or TetOn-cAMP induction, it is unclear whether any of the other eleven predicted cAMP-binding proteins in Mtb are involved in this mechanism (23). We examined the predicted operon of one other cAMP-binding protein, the transcription factor CRP_{MT}, and found that a handful of these genes were differentially expressed in a cAMP-dependent and/or Rv1625c-dependent manner during growth in cholesterol media (Fig. 4.14). Notably, three of these genes are required for optimal growth of Mtb in cholesterol media and/or in mouse models of TB, but are not directly involved in cholesterol side chain or ring breakdown. Most of the remaining genes do not have established functions, making it difficult to predict how changes in their expression could impact specific aspects of Mtb physiology. Further experiments are needed to determine whether these transcriptional changes are indeed mediated through CRP_{Mt} activity, and whether this contributes significantly to the cholesterol utilization defects observed in Mtb during V-59 treatment or in the ΔRv1625c strain. Alternatively, because cholesterol uptake by the bacterium and initiation of cholesterol side chain breakdown by FadD19 are both ATP-dependent processes,

it is possible that ATP depletion occurring during increased cAMP synthesis mediates inhibition of cholesterol utilization.

Compared to the previously-published Rv1625c agonist V-58 (*37*), V-59 represents a significant advance because it is the first Rv1625c agonist that is suitable for use in an *in vivo* model of TB. V-59 also provided a basis for understanding how to improve Rv1625c agonists through medicinal chemistry. We completed a medicinal chemistry effort focused on addressing the structural liabilities of V-59 and improving the potency of its activity against Mtb. This identified mCLB073, a stable molecule with improved potency and desirable chemical, pharmacological, pharmacokinetics and safety properties, which makes it a good drug candidate for clinical testing and a useful compound for further *in vivo* studies of this pathway in Mtb. While investigating the potency of compounds in this series with constrained piperidine rings, we also identified molecules whose potency differed widely based on the chirality of their azabicyclic rings. In the future, it would be interesting to identify the underlying explanation for the differential potency of these compounds on Rv1625c activity through structural biology.

Numerous studies have suggested that cholesterol utilization is a key metabolic adaptation that supports Mtb survival during chronic infection (*7-11*), but the efficacy of single-step inhibitors of cholesterol degradation may be limited, unless they are able to cause accumulation of toxic metabolites in the bacterium (*6, 8-10, 45*). Inhibitors that block this pathway early and/or shut down multiple steps present one desirable alternative. This study revealed that the Rv1625c agonists V-59/mCLB073 are an improvement over the single-step cholesterol degradation inhibitors we reported previously; these compounds inhibit cholesterol catabolism early and/or at both side chain and ring degradation steps and display excellent pharmacokinetic properties. In the

176

future, V-59/mCLB073 will facilitate single-agent and combination regimen studies to determine how these compounds affect bacterial fitness in mouse models of TB.

In summary, we have shown here that activating cAMP synthesis in Mtb, either by activating Rv1625c AC activity with a small molecule agonist or by inducing expression of the minimal catalytic subunit of Rv1264, blocks cholesterol degradation. Rv1625c is also the first AC in Mtb to be linked directly to a particular downstream pathway. Mtb has a cadre of structurally-diverse ACs and predicted cAMP-binding proteins with mostly uncharacterized functions, which may represent potential to alter pathways beyond cholesterol utilization in this bacterium. However, it is unknown whether agonists for ACs other than Rv1625c would have comparable downstream effects in Mtb. In other pathogenic bacteria, cAMP signaling is known not only for coordinating changes to carbon metabolism, but also for mediating diverse functions including biofilm formation, virulence gene expression, and secretion systems (*14*). In Mtb, AC activation is able to stall at least one metabolic pathway that supports *in vivo* survival, with the potential to yield a new antibiotic mechanism of action. It is interesting to speculate whether additional AC agonists could be developed as tools to study cAMP signaling during infection, or as antibiotics, in other bacteria. The mechanism(s) by which inducing cAMP synthesis modulates cholesterol utilization in Mtb is not yet fully explained, and will be an important area for future studies as our knowledge of the role cAMP signaling plays in Mtb physiology continues to expand.

4.5   References

1. W. H. Organization, Global Tuberculosis Report 2019. (World Health Organization, Geneva, 2019).

2. J. P. Sarathy, V. Dartois, Caseum: a Niche for Mycobacterium tuberculosis Drug-Tolerant Persisters. *Clinical microbiology reviews* **33**, (2020).

3. R. L. Hunter, C. Jagannath, J. K. Actor, Pathology of postprimary tuberculosis in humans and mice: contradiction of long-held beliefs. *Tuberculosis* **87**, 267-278 (2007).

4. P. Peyron, J. Vaubourgeix, Y. Poquet, F. Levillain, C. Botanch, F. Bardou, M. Daffe, J. F. Emile, B. Marchou, P. J. Cardona, C. de Chastellier, F. Altare, Foamy macrophages from tuberculous patients' granulomas constitute a nutrient-rich reservoir for M. tuberculosis persistence. *PLoS pathogens* **4**, e1000204 (2008).

5. M. J. Kim, H. C. Wainwright, M. Locketz, L. G. Bekker, G. B. Walther, C. Dittrich, A. Visser, W. Wang, F. F. Hsu, U. Wiehart, L. Tsenova, G. Kaplan, D. G. Russell, Caseation of human tuberculosis granulomas correlates with elevated host lipid metabolism. *EMBO Molecular Medicine* **2**, 258-274 (2010).

6. K. M. Wilburn, R. A. Fieweger, B. C. VanderVen, Cholesterol and fatty acids grease the wheels of Mycobacterium tuberculosis pathogenesis. *Pathogens and Disease* **76**, (2018).

7. A. K. Pandey, C. M. Sassetti, Mycobacterial persistence requires the utilization of host cholesterol. *Proceedings of the National Academy of Sciences of the United States of America* **105**, 4376-4380 (2008).

8. J. C. Chang, M. D. Miner, A. K. Pandey, W. P. Gill, N. S. Harik, C. M. Sassetti, D. R. Sherman, igr Genes and Mycobacterium tuberculosis Cholesterol Metabolism. *Journal of Bacteriology* **191**, 5232-5239 (2009).

9. N. M. Nesbitt, X. Yang, P. Fontan, I. Kolesnikova, I. Smith, N. S. Sampson, E. Dubnau, A thiolase of Mycobacterium tuberculosis is required for virulence and production of androstenedione and androstadienedione from cholesterol *Infection and Immunity* **78**, 275-282 (2010).

10. K. C. Yam, I. D'Angelo, R. Kalscheuer, H. Zhu, J.-X. Wang, V. Snieckus, L. H. Ly, P. J. Converse, W. R. Jacobs, Jr., N. Strynadka, L. D. Eltis, Studies of a Ring-Cleaving Dioxygenase Illuminate the Role of Cholesterol Metabolism in the Pathogenesis of Mycobacterium tuberculosis. *PLoS Pathogens* **5**, e1000344 (2009).

11. Y. Hu, R. van der Geize, G. S. Besra, S. S. Gurcha, A. Liu, M. Rohde, M. Singh, A. Coates, 3-Ketosteroid 9alpha-hydroxylase is an essential factor in the pathogenesis of Mycobacterium tuberculosis. *Molecular Microbiology* **75**, 107-121 (2010).

12. C. M. Smith, R. E. Baker, M. K. Proulx, B. B. Mishra, J. E. Long, S. Park, H. Lee, M. C. Kiritsy, M. M. Bellerose, A. J. Olive, K. C. Murphy, K. Papavinasasundaram, F. J. Boehm, C. J. Reames, R. K. Meade, B. K. Hampton, C. L. Linnertz, G. D. Shaw, P. Hock, T. A. Bell, S. Ehrt, D. Schnappinger, F. Pardo-Manuel de Villena, M. T. Ferris, T. R. Ioerger, C. M. Sassetti, Host-pathogen genetic interactions underlie tuberculosis susceptibility. *bioRxiv* **2020.12.01.405514**, (2021).

13. P. Aiewsakun, P. Prombutara, T. A. P. Siregar, T. Laopanupong, P. Kanjanasirirat, T. Khumpanied, S. Borwornpinyo, P. Tong-Ngam, A. Tubsuwan, P. Srilohasin, A. Chaiprasert, W. Ruangchai, P. Palittapongarnpim, T. Prammananan, B. C. VanderVen, M. Ponpuak, Transcriptional response to the host cell environment of a multidrug-resistant Mycobacterium tuberculosis clonal outbreak Beijing strain reveals its pathogenic features. *Scientific Reports* **11**, 3199 (2021).

14. K. A. McDonough, A. Rodriguez, The myriad roles of cyclic AMP in microbial pathogens: from signal to sword. *Nature Reviews Microbiology* **10**, 27-38 (2011).

15. V. Chubukov, L. Gerosa, K. Kochanowski, U. Sauer, Coordination of microbial metabolism. *Nat Rev Microbiol* **12**, 327-340 (2014).

16. R. C. Molina-Quiroz, C. Silva-Valenzuela, J. Brewster, E. Castro-Nallar, S. B. Levy, A. Camilli, Cyclic AMP Regulates Bacterial Persistence through Repression of the Oxidative Stress Response and SOS-Dependent DNA Repair in Uropathogenic Escherichia coli. *mBio* **9**, (2018).

17. A. R. Shenoy, S. S. Visweswariah, Mycobacterial adenylyl cyclases: biochemical diversity and structural plasticity. *FEBS Lett* **580**, 3344-3352 (2006).

18. I. Tews, F. Findeisen, I. Sinning, A. Schultz, J. E. Schultz, J. U. Linder, The structure of a pH-sensing mycobacterial adenylyl cyclase holoenzyme. *Science* **308**, 1020-1023 (2005).

19. P. D. Townsend, P. M. Holliday, S. Fenyk, K. C. Hess, M. A. Gray, D. R. Hodgson, M. J. Cann, Stimulation of mammalian G-protein-responsive adenylyl cyclases by carbon dioxide. *J Biol Chem* **284**, 784-791 (2009).

20. M. J. Cann, A. Hammer, J. Zhou, T. Kanacher, A defined subset of adenylyl cyclases is regulated by bicarbonate ion. *J Biol Chem* **278**, 35033-35038 (2003).

21. A. Abdel Motaal, I. Tews, J. E. Schultz, J. U. Linder, Fatty acid regulation of adenylyl cyclase Rv2212 from Mycobacterium tuberculosis H37Rv. *FEBS J* **273**, 4219-4228 (2006).

22. A. R. Shenoy, N. P. Sreenath, M. Mahalingam, S. S. Visweswariah, Characterization of phylogenetically distant members of the adenylate cyclase family from mycobacteria:

Rv1647 from Mycobacterium tuberculosis and its orthologue ML1399 from M. leprae. *The Biochemical journal* **387**, 541-551 (2005).

23. R. M. Johnson, K. A. McDonough, Cyclic nucleotide signaling in Mycobacterium tuberculosis: an expanding repertoire. *Pathogens and Disease* **76**, (2018).

24. M. A. Gazdik, G. Bai, Y. Wu, K. A. McDonough, Rv1675c (cmr) regulates intramacrophage and cyclic AMP-induced gene expression in Mycobacterium tuberculosis-complex mycobacteria. *Molecular microbiology* **71**, 434-448 (2009).

25. G. Bai, L. A. McCue, K. A. McDonough, Characterization of Mycobacterium tuberculosis Rv3676 (CRPMt), a cyclic AMP receptor protein-like DNA binding protein. *J Bacteriol* **187**, 7795-7804 (2005).

26. L. Rickman, C. Scott, D. M. Hunt, T. Hutchinson, M. C. Menendez, R. Whalan, J. Hinds, M. J. Colston, J. Green, R. S. Buxton, A member of the cAMP receptor protein family of transcription regulators in Mycobacterium tuberculosis is required for virulence in mice and controls transcription of the rpfA gene coding for a resuscitation promoting factor. *Molecular microbiology* **56**, 1274-1286 (2005).

27. E. S. C. Rittershaus, S. H. Baek, I. V. Krieger, S. J. Nelson, Y. S. Cheng, S. Nambi, R. E. Baker, J. D. Leszyk, S. A. Shaffer, J. C. Sacchettini, C. M. Sassetti, A Lysine Acetyltransferase Contributes to the Metabolic Adaptation to Hypoxia in Mycobacterium tuberculosis. *Cell Chemical Biology* **25**, 1495-1505 e1493 (2018).

28. S. Nambi, K. Gupta, M. Bhattacharyya, P. Ramakrishnan, V. Ravikumar, N. Siddiqui, A. T. Thomas, S. S. Visweswariah, Cyclic AMP-dependent protein lysine acylation in mycobacteria regulates fatty acid and propionate metabolism. *Journal of Biological Chemistry* **288**, 14114-14124 (2013).

29. B. C. VanderVen, R. J. Fahey, W. Lee, Y. Liu, R. B. Abramovitch, C. Memmott, A. M. Crowe, L. D. Eltis, E. Perola, D. D. Deininger, T. Wang, C. P. Locher, D. G. Russell, Novel inhibitors of cholesterol degradation in Mycobacterium tuberculosis reveal how the bacterium's metabolism is constrained by the intracellular environment. *PLoS Pathogens* **11**, e1004679 (2015).

30. Y. L. Guo, T. Seebacher, U. Kurz, J. U. Linder, J. E. Schultz, Adenylyl cyclase Rv1625c of Mycobacterium tuberculosis: a progenitor of mammalian adenylyl cyclases. *EMBO Journal* **20**, 3667-3675 (2001).

31. Y. L. Guo, U. Kurz, A. Schultz, J. U. Linder, D. Dittrich, C. Keller, S. Ehlers, P. Sander, J. E. Schultz, Interaction of Rv1625c, a mycobacterial class IIIa adenylyl cyclase, with a mammalian congener. *Molecular microbiology* **57**, 667-677 (2005).

32. S. K. Reddy, M. Kamireddi, K. Dhanireddy, L. Young, A. Davis, P. T. Reddy, Eukaryotic-like adenylyl cyclases in Mycobacterium tuberculosis H37Rv: cloning and characterization. *Journal of Biological Chemistry* **276**, 35141-35149 (2001).

33. I. Vercellino, L. Rezabkova, V. Olieric, Y. Polyhach, T. Weinert, R. A. Kammerer, G. Jeschke, V. M. Korkhov, Role of the nucleotidyl cyclase helical domain in catalytically active dimer formation. *Proceedings of the National Academy of Sciences of the United States of America* **114**, E9821-E9828 (2017).

34. S. Beltz, J. Bassler, J. E. Schultz, Regulation by the quorum sensor from Vibrio indicates a receptor function for the membrane anchors of adenylate cyclases. *eLife* **5**, (2016).

35. M. Ziegler, J. Bassler, S. Beltz, A. Schultz, A. N. Lupas, J. E. Schultz, Characterization of a novel signal transducer element intrinsic to class IIIa/b adenylate cyclases and guanylate cyclases. *FEBS Journal* **284**, 1204-1217 (2017).

36. E. V. Nazarova, C. R. Montague, T. La, K. M. Wilburn, N. Sukumar, W. Lee, S. Caldwell, D. G. Russell, B. C. VanderVen, Rv3723/LucA coordinates fatty acid and cholesterol uptake in Mycobacterium tuberculosis. *eLife* **6**, (2017).

37. R. M. Johnson, G. Bai, C. M. DeMott, N. K. Banavali, C. R. Montague, C. Moon, A. Shekhtman, B. VanderVen, K. A. McDonough, Chemical activation of adenylyl cyclase Rv1625c inhibits growth of Mycobacterium tuberculosis on cholesterol and modulates intramacrophage signaling. *Molecular Microbiology* (2017).

38. D. G. Russell, L. Huang, B. C. VanderVen, Immunometabolism at the interface between macrophages and pathogens. *Nature Reviews Immunology* **19**, 291-304 (2019).

39. M. A. Gazdik, K. A. McDonough, Identification of cyclic AMP-regulated genes in Mycobacterium tuberculosis complex bacteria under low-oxygen conditions. *J Bacteriol* **187**, 2681-2692 (2005).

40. J. E. Griffin, A. K. Pandey, S. A. Gilmore, V. Mizrahi, J. D. McKinney, C. R. Bertozzi, C. M. Sassetti, Cholesterol catabolism by Mycobacterium tuberculosis requires transcriptional and metabolic adaptations. *Chemistry & Biology* **19**, 218-227 (2012).

41. Y. Akhter, S. Yellaboina, A. Farhana, A. Ranjan, N. Ahmed, S. E. Hasnain, Genome scale portrait of cAMP-receptor protein (CRP) regulons in mycobacteria points to their role in pathogenesis. *Gene* **407**, 148-158 (2008).

42. R. M. Wells, C. M. Jones, Z. Xi, A. Speer, O. Danilchanka, K. S. Doornbos, P. Sun, F. Wu, C. Tian, M. Niederweis, Discovery of a siderophore export system essential for virulence of Mycobacterium tuberculosis. *PLoS Pathog* **9**, e1003120 (2013).

43.   J. E. Griffin, J. D. Gawronski, M. A. DeJesus, T. R. Ioerger, B. J. Akerley, C. M. Sassetti, High-Resolution Phenotypic Profiling Defines Genes Essential for Mycobacterial Growth and Cholesterol Catabolism. *PLoS Pathog* **7**, (2011).

44.   J. Bassler, J. E. Schultz, A. N. Lupas, Adenylate cyclases: Receivers, transducers, and generators of signals. *Cellular Signaling* **46**, 135-144 (2018).

45.   A. M. Crowe, I. Casabon, K. L. Brown, J. Liu, J. Lian, J. C. Rogalski, T. E. Hurst, V. Snieckus, L. J. Foster, L. D. Eltis, Catabolism of the Last Two Steroid Rings in Mycobacterium tuberculosis and Other Bacteria. *mBio* **8**, (2017).

CHAPTER FIVE

Chemically activating cAMP synthesis in *M. tuberculosis* during infection decreases

bacterial fitness and alters host inflammatory signatures

5.1 Introduction

We previously identified a series of compounds that act as agonists of the *Mycobacterium tuberculosis* (Mtb) adenylyl cyclase Rv1625c. These compounds increase synthesis of the second-messenger cAMP in Mtb, which inhibits cholesterol utilization by the bacterium and impairs growth of Mtb during macrophage infection. Early iterations of Rv1625c agonist compounds were unsuitable for use during *in vivo* studies in mice due to poor pharmacokinetic properties and sub-optimal potency. However, in our previous work, we identified an Rv1625c agonist named V-59 with promising pharmacokinetic properties, and a medicinal chemistry effort based on serial structure-activity relationship optimization produced an improved Rv1625c agonist named mCLB073 (Chapter 4). These compounds are suitable for once-daily dosing by oral gavage in mice, as they maintain plasma exposure over the EC_{50} for at least 24 hours. Thus, V-59 and mCLB073 provided a novel opportunity to study how activating cAMP synthesis in Mtb impacts bacterial fitness and host pathology during infection *in vivo* and *in vitro*.

Because cholesterol utilization has repeatedly been identified as an important contributor to Mtb growth or persistence during chronic infection, a compound that effectively targets cholesterol utilization by the bacterium is predicted to impair Mtb survival during infection (*1*). As described above, V-59 and mCLB073 represent improved cholesterol inhibitors in Mtb compared to conventional, single-step inhibitors of the cholesterol breakdown pathway (Chapter 4). Thus, we first sought to evaluate how these Rv1625c agonists impact Mtb survival during infection. We addressed this by performing single-agent studies with V-59 and mCLB073 in two tractable mouse models of chronic infection.

Two main mechanisms are used by Mtb to maintain cAMP homeostasis. First, Mtb expresses a single known phosphodiesterase (Rv0805) that is capable of degrading cAMP to AMP within

the cytoplasm (*2*). Introducing an additional copy of *rv0805* under its native promoter in WT Mtb leads to increased expression of the Rv0805 protein associated with a ~30% decrease in cAMP levels in Mtb (*3*). Second, Mtb is unique in that it secretes a significant amount of the cAMP it synthesizes into its extracellular environment (*4*). Our previous work with Rv1625c agonists is consistent with this, as we found an ~85-fold increase in cAMP/10^8 CFUs secreted into the surrounding media during the first 24 hours of treatment of with V-59 in WT Mtb, relative to the vehicle control (Chapter 4). This number was further increased to ~110-fold in a complement strain (Comp$_{Full}$) that overexpresses *rv1625c* relative to WT. Typically pathogenic bacteria secrete adenylyl cyclase toxins capable of cAMP synthesis or modulation of host cell AC signaling, rather than directly secreting cAMP that was synthesized within the bacterial cell (*5*). Thus, the mechanism by which cAMP is secreted from of Mtb is not established, and a homologous system in other bacteria has not been proposed. However, it is reasonable to predict secretion of cAMP from Mtb may involve efflux through one of the bacterium's ATP-binding cassette transporters, which would be analogous to proposed mechanisms of cAMP extrusion from some eukaryotic cells (*6, 7*).

Mtb is primarily an intracellular pathogen, and resides in an arrested early endosome-like compartment within macrophages, or occasionally within the cytosol, for much of its life cycle (*8*). Studies examining activation of the cytosolic stimulator of interferon genes (STING) signaling pathway have suggested that Mtb-derived DNA and/or cyclic-di-AMP can reach the host cell cytosol during infection, where they regulate type I IFN expression (*9*). Transmission of small molecules like cAMP from the Mtb phagosome to the cytosol may be mediated through one of Mtb's type VII secretion systems, but this remains controversial. As such, we anticipate that the excess cAMP secreted from Mtb during V-59/mCLB073 treatment might access the host cell

endosomal network and/or cytosol and affect cAMP-dependent effector proteins. In eukaryotic cells, cAMP activates mediators like protein kinase A (PKA) or the guanine nucleotide exchange factor proteins directly activated by cAMP (Epac). When activated, PKA and Epac proteins are able to modulate macrophage functions including the production of inflammatory mediators, microbicidal activities, and phagocytosis (*10-12*). Recent work examining the localization of cAMP signaling in eukaryotic cells has introduced a new model in which sustained cAMP production can occur at endosomal membranes after ligand-GPCR complexes are internalized along with their Gαs and AC partners (*13, 14*). This does not invalidate the traditional model, in which plasma membrane localized GPCR/AC signaling is important for shorter bursts of cAMP induction. However, it suggests that if cAMP levels surrounding endosomal compartments are increased during Mtb infection, this might plausibly position cAMP near its PKA target (*14*).

PKA-mediated effects on cytokine production can include decreased Leukotriene B$_4$, TNFα, CCL3, and/or IL-12, and increased G-CSF and/or IL-10 (*10, 15, 16*). These effects are at least partly mediated by crosstalk of PKA with the transcription factor NFκB (*11*). Decreased FcγR-, complement receptor-, and scavenger receptor-mediated phagocytosis and dampened bactericidal activity of alvelolar macrophages against *Klebsiella pneumoniae* have been linked to Epac-1 mediated effects, or shared PKA/Epac signaling (*10*). Similarly, cAMP produced inside myeloid phagocytes by the CyaA AC toxin of *Bordetella pertussis* has been associated with inhibition of the superoxide burst and phagocytosis, dampened maturation of dendritic cells, and decreased production of CCL3, IL-12, and TNFα and/or increased production of IL-6 and IL-10 (*17-19*). However, cAMP-dependent changes to macrophage function are cell type- and context-specific, and compartmentalization of cAMP pools has a significant role in influencing the outcome of cAMP signaling in eukaryotic cells (*10, 11, 16*). Here we have begun to investigate the possibility

188

that the excess cAMP secreted from Mtb during V-59/mCLB073 treatment signals within the host macrophage to modulate its inflammatory response. We generated preliminary data that suggests chemically activating cAMP synthesis by Mtb through V-59/mCLB073 can modulate the inflammatory response of infected macrophages *in vitro* and change the balance of inflammatory mediators in the lungs of infected mice.

5.2 Materials and Methods

Compound formulations for in vivo experiments

V-59 and isoniazid (Sigma Aldrich) were solubilized in 10% DMSO, 70% PEG 300, and 20% D5W (Dextrose 5% in ddH_2O) with heating and sonication for intranasal BALB/c and C3HeB/FeJ experiments. For mCLB073 studies, compounds were solubilized at the indicated concentrations in 0.5% methyl cellulose, 0.5% Tween-80 (intranasal infection experiment) or 10% 2-hydroxypropyl-β-cyclodextrin + 10% lecithin (aerosol infection experiment) to obtain a fine suspension. Doses of 0.1mL were delivered by oral gavage.

Mouse infections

Animal work was approved by Cornell University IACUC (protocol number 2013-0030). All protocols conform to the USDA Animal Welfare Act, institutional policies on the care and humane treatment of animals, and other applicable laws and regulations. Isoflurane was delivered via nebulizer for anesthesia during oral delivery of compounds. Euthanasia was performed via delivery of carbon dioxide. Six to eight-week-old BALB/cJ mice (Jackson Laboratories) were infected with 1,000 CFU of Erdman Mtb intranasally where indicated. C3HeB/FeJ (Kramnik) mice (Jackson Laboratories) were infected with 500 CFU of Erdman Mtb intranasally. At weeks 4 through 8 post-infection, compounds or vehicle controls were administered once-daily by oral gavage. For aerosol infections, BALB/cJ mice (Jackson Laboratories) were infected via an aerosol inhalation exposure system (Glass-Col) with a calibrated dose of 200 CFU of Erdman Mtb. Experimental compounds or vehicle control were administered once-daily at weeks 4 through 8 post-infection by oral gavage. After treatment, lung tissues were collected and processed for histology and CFU enumeration. For CFUs, lungs were homogenized in PBS, 0.05% Tween-80 and plated on 7H10

OADC. Inflammatory area was scored by measuring the percent of tissue inflamed (granulomatous tissue with peripheral and peribronchial lymphocytes and plasma cells) per low power microscopic field. In a blinded fashion, 4-15 fields were analyzed per lung sample.

cAMP production by cultured human cells

cAMP production was evaluated in HepG2 cells (ATCC HB-8065, human liver), HEK293 cells (ATCC CRL-3216, human kidney) and human monocyte derived macrophages (HMDM). HepG2 and HEK293 cells were cultured in DMEM supplemented with 10% FBS and maintained in a humidified incubator (37°C in 5% CO2). HMDM cells derived from human peripheral blood mononuclear cells (PBMCs) that were obtained from Elutriation Core Facility, University of Nebraska Medical Center. HMDM cells were cultured in DMEM supplemented with 10% human serum, L-glutamine (2 mmol), sodium pyruvate (1 mmol), penicillin (100 U/mL), and streptomycin (100 µg/mL) (Corning) and maintained in a humidified incubator (37°C in 5% CO_2). Cells were cultured at a density of 1e6 per T-25 flask and were treated with V-59 (10 µM) for 24 hours before harvesting the cells with trypsin treatment (HepG2 and HEK293) or scraping into cold PBS (HMDM). Cells were harvested by centrifugation and cAMP levels were quantified from the cell pellet following, resuspension in lysis buffer (0.1M HCl, 1% Triton X-100 in ddH_2O). The cell-free lysates were used to measure internal cAMP by ELISA (Enzo Life Sciences).

Cell viability assays

BMDMs were isolated from female BALB/c mice, and seeded at $1x10^5$ cells per well in a 96-well plate. Macrophages were infected with WT CDC1551 Mtb at an MOI of 1 and treated with vehicle control, cycloheximide, V-59, or mCLB073 for at a range of doses. The CellTiter-Glo luminescent

assay (Promega) was used to quantify cell viability via ATP levels after 24 hours of compound exposure. For flow cytometric quantification of cell viability, BMDMs were infected with WT, ΔRv1625c, or Comp$_{Full}$ CDC1551 Mtb at an MOI of 2 and treated with DMSO control or V-59 (25μM). Cells were infected for one week and media including compounds was replenished daily. Cells were collected and stained with eFluor 506 fixable viability dye (eBioscience/ThermoFisher), fixed in 4% PFA, and the relative number of dead cells was quantified by flow cytometry.

Measurement of cAMP in infected BMDMs

BMDMs were isolated from female BALB/c mice, and seeded at $5X10^6$ cells/flask in T25 flasks. Macrophages were infected with WT, ΔRv1625c, or Comp$_{Full}$ CDC1551 Mtb at an MOI of 7. Infected cells were treated with DMSO or mCLB073 (25 μM) for 24 hours. Media was removed and cells were isolated in PBS and centrifuged at 1,000 rpm. Cells were lysed in 0.1 M HCl, 1% Triton X-100 in screw top tubes via vigorous vortexing. Debris was centrifuged at 15,000 rpm, and the supernatant was analyzed in a cAMP ELISA (Enzo) to determine the amount of cAMP per flask of infected cells.

Host Cell RNA-seq

Cells were isolated, infected, and treated with compounds for 24 hours as described above. Cells were lysed in Trizol-LS, Mtb and cell debris was removed by centrifugation, and samples were stored at -80 °C prior to RNA extraction. Total RNA was isolated by chloroform extraction and precipitated in isopropanol with GlycoBlue reagent (Thermo Fisher), RNA was resuspended in

nuclease-free water, and genomic DNA contamination was removed using the Turbo-DNA free kit (Invitrogen) as described in (*20*). RNA enrichment was performed by Poly(A) selection, Sample quality was determined via Fragment Analyzer (Advanced Analytical) and TruSeq-barcoded RNAseq libraries were generated with the NEBNext Ultra II Directional RNA Library Prep Kit (New England Biolabs). Sequencing was performed at the Cornell University Transcriptional Regulation and Expression Facility on a NextSeq500 instrument (Illumina) at a depth of 20 M single-end 75 bp reads. Reads were trimmed for low quality and adaptor sequences with TrimGalore, and aligned to the *Mus musculus* reference genome with STAR. DESeq2 was used with default parameters and alpha = 0.05 to generate the differential gene expression results. Multiple test correction was performed using the Benjamini Hochberg method.

Cytokine analyses in lung homogenates

Six to eight-week-old BALB/cJ mice (Jackson Laboratories) were infected with 2,000 CFUs of WT Erdman Mtb. The infection proceeded for two weeks, and then mice were treated with a vehicle control (0.5% methylcellulose, 0.5% Tween 80), mCLB073 (10 mg/kg), or INH (1 mg/kg, 5 mg/kg, or 10 mg/kg) once-daily by oral gavage for an additional seven days. Lungs were collected and homogenized, plated for CFUs, and the remainder was filtered through a 0.1 μM syringe filter for ELISAs. Cytokines were quantified by ELISA as follows: TNFα at dilution factor 1.3 (TNF alpha Mouse Uncoated ELISA Kit, Invitrogen), CXCL1 at dilution factor 3 (Mouse CXCL1/KC DuoSet ELISA, R&D Systems), IL-1β at dilution factor 8 (Mouse IL-1 beta/IL-1F2 DuoSet ELISA, R&D Systems).

5.3 Results

5.3.1 Activation of cAMP synthesis by Rv1625c agonists inhibits Mtb pathogenesis *in vivo*

First we examined whether treatment with Rv1625c agonists would alter Mtb survival in a mouse model of infection that is relatively resistant to Mtb. We infected BALB/c mice with WT Mtb, and administered a vehicle control, V-59, or isoniazid by oral gavage once-daily during weeks 4 through 8 post-infection. V-59 (50 mg/kg) caused a ~0.4-$\log_{10}$ reduction in lung CFU's and reduced the extent of lung inflammation by ~50% (Fig. 5.1a, b). Similar results were obtained in CFU counts (~0.5-$\log_{10}$ reduction) in the lungs of C3HeB/FeJ mice infected and treated in the same manner (Fig. 5.1c, d). The C3HeB/FeJ Mtb infection model was used because these mice produce type I IFN- and neutrophil-driven pathology that results in well-organized necrotic granulomas containing high numbers of extracellular bacterial (*21-24*). Thus, the finding that an Rv1625c agonist inhibits bacterial growth and limits lung pathology in both a relatively resistant and a susceptible model of TB suggests that this compound series could be effective against Mtb persistence despite the heterogeneous host response mounted in Mtb infections (*25*). To verify the improved potency of mCLB073 that was observed *in vitro* against Mtb *in vivo*, we infected BALB/c mice with WT Mtb via the intranasal route, and administered a vehicle control, mCLB073 at escalating doses, or isoniazid by oral gavage once-daily during weeks 4 through 8 post-infection. Treatment with a lower dose of mCLB073 (30mg/kg) reduced Mtb CFUs in the lungs of mice significantly (~0.4-$\log_{10}$ reduction), similar to the effect 50mg/kg V-59 had (Fig. 5.1e, Fig. 5.1a). Treatment with mCLB073 also decreased the extent of lung pathology by ~45% and significantly reduced the pathology score even at a dose of 10mg/kg (Fig. 5.1f). In a separate study of BALB/c mice that were aerosol infected and treated in the same manner, we observed a similar reduction

in lung CFUs (~0.4-log$_{10}$ reduction) even at a lower dose of mCLB073 (5mg/kg) which further confirms the improved pharmacological properties of mCLB073 (Fig. 5.1g).

Because the mechanism of action of mCLB073 is novel, we tested whether mCLB073 treatment would lead to an undesired increased tolerance to a frontline TB drug (rifampicin) during infection. We found that the addition of mCLB073 (30 mg/kg) to a sub-optimal dose of rifampicin did not increase the bacterial burden in the lungs of BALB/c mice, suggesting this mechanism of action does not promote tolerance to other TB antibiotics (Fig. 5.2a). Finally, we addressed the potential concern that this chemotype would activate off-target, mammalian AC enzymes. We found no evidence that V-59 increases cAMP synthesis in mammalian cells uninfected with Mtb (Fig. 5.2b), and the low toxicity profile of the Rv1625c-activating compounds (Chapter 4) suggests limited off-target activation of mammalian ACs. Treatment with V-59 or mCLB073 during *in vitro* culture of Mtb infected macrophages also did not decrease relative levels of ATP in host cells at 24 hours of compound treatment (Fig. 5.2c). V-59 was not associated with increased cell death during one week of treatment in infected BMDMs, and was instead associated with an increased proportion of live cells at the one week endpoint (Fig. 5.2d). These results demonstrate the increased potency of mCLB073 relative to V-59 *in vivo*, and suggest that chemically activating cAMP synthesis in Mtb during chronic infection confers a fitness cost to the bacterium while decreasing pulmonary pathology.
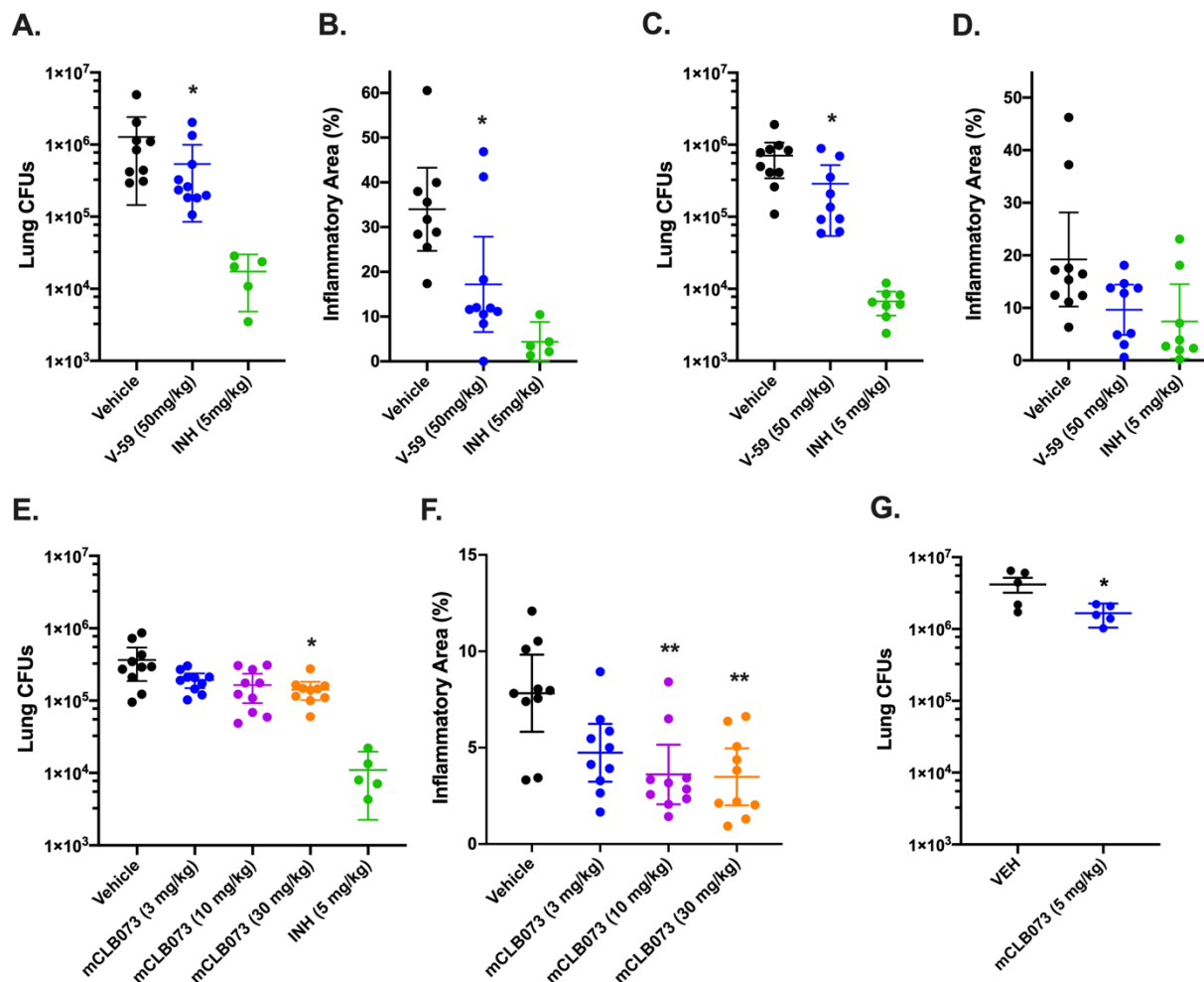
Figure 5.1. Chemically activating Rv1625c reduces Mtb pathogenesis *in vivo*. Effect of V-59 treatment on bacterial burden and pathology in the lungs of BALB/c (**A and B**) or C3HeB/FeJ mice (**C and D**). In (A-D) mice were infected and treated with V-59, INH, or vehicle control. Data are from two independent experiments with 5 mice (A and B), or one experiment with 10 mice (C and D) per group. Outliers with CFUs below the infectious dose were excluded from the analyses (*$P < 0.05$, Mann-Whitney test). All data are shown as means $\pm$ SEM. (**E and F**) Impact of mCLB073 treatment on bacterial burden (E) and pathology (F) in BALB/c mice infected and treated with the indicated doses of mCLB073, INH, or vehicle control (*$P < 0.05$, **$P < 0.01$, Kruskal-Wallis test and Dunn's multiple comparisons test). Infections in (A-F) were by the intranasal route. Data are from one experiment with 10 mice per group. (**G**) Impact of mCLB073 treatment on bacterial burden in BALB/c mice infected by aerosol and treated with 5mg/kg mCLB073 or vehicle control. Data are from one experiment with 5 mice per group (*$P < 0.05$, Kruskal-Wallis test and Dunn's multiple comparisons test). All data are shown as means $\pm$ SEM.
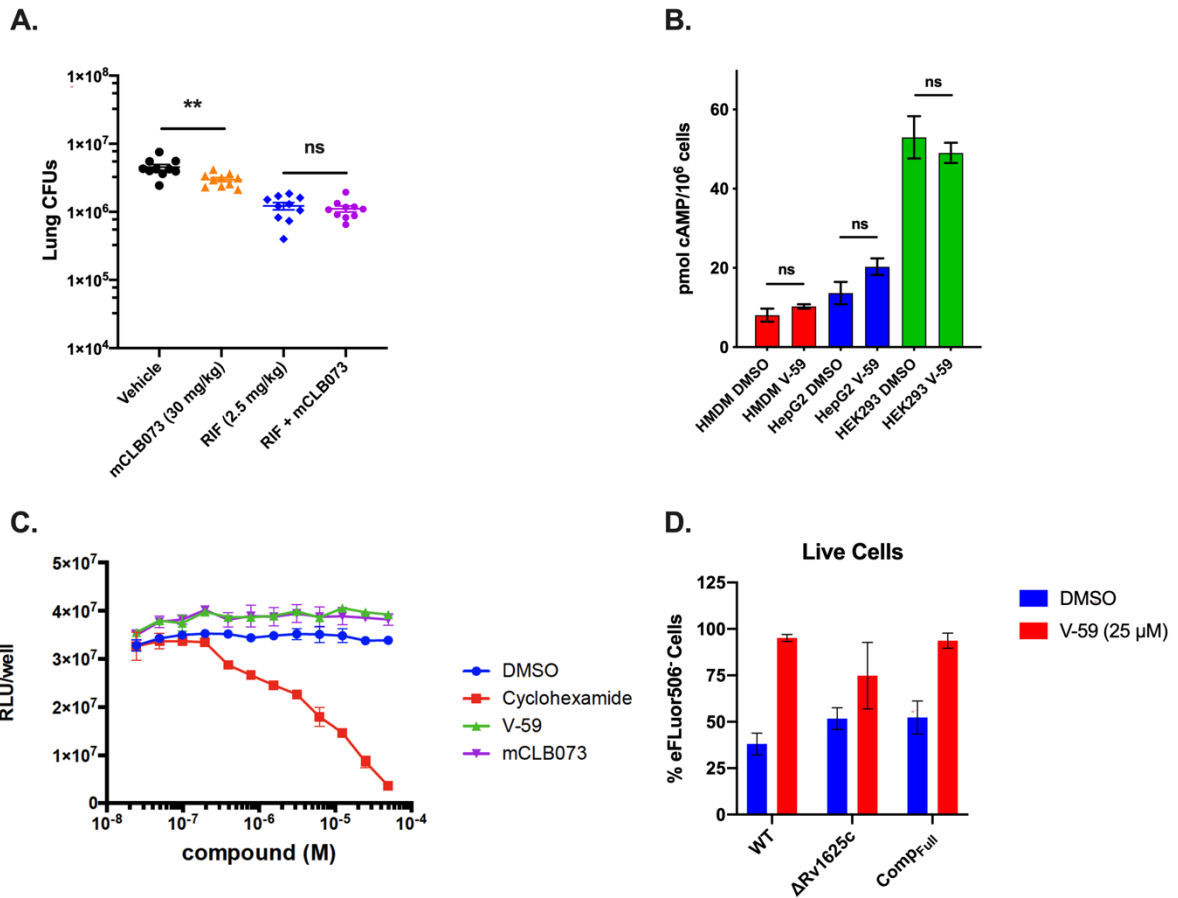
Figure 5.2 Treatment with Rv1625c agonist compounds does not promote tolerance to rifampicin and does not increase cAMP synthesis or cell death in mammalian cells. (A) Effect of mCLB073 treatment combined with a sub-optimal dose of rifampicin (RIF) in infected BALB/c mice. Data are from one experiment with 10 mice per group (**$P < 0.01$, Mann-Whitney test). **(B)** Quantification of cAMP in uninfected human cell lines treated with V-59 (10 μM) or DMSO control. Data are from one experiment with two technical replicates, and are shown as means $\pm$ SEM. V-59 did not significantly increase cAMP (not significant, One-way ANOVA with Sidak's multiple comparisons test).**(C)** Relative ATP levels in macrophages during treatment with Rv1625c agonists. ATP in Mtb-infected BMDMs was quantified by the CellTiter-Glo ATP assay after 24 hours of compound treatment. Cycloheximide is the positive control. Data is representative, from one experiment with three technical replicates. **(D)** Relative proportion of live cells in population of BMDMs infected *in vitro* after one week of compound treatment. Live cells were quantified using viability dye staining and flow cytometry quantification of 500-1,500 cells. Data is from one experiment with three replicates of each sample.
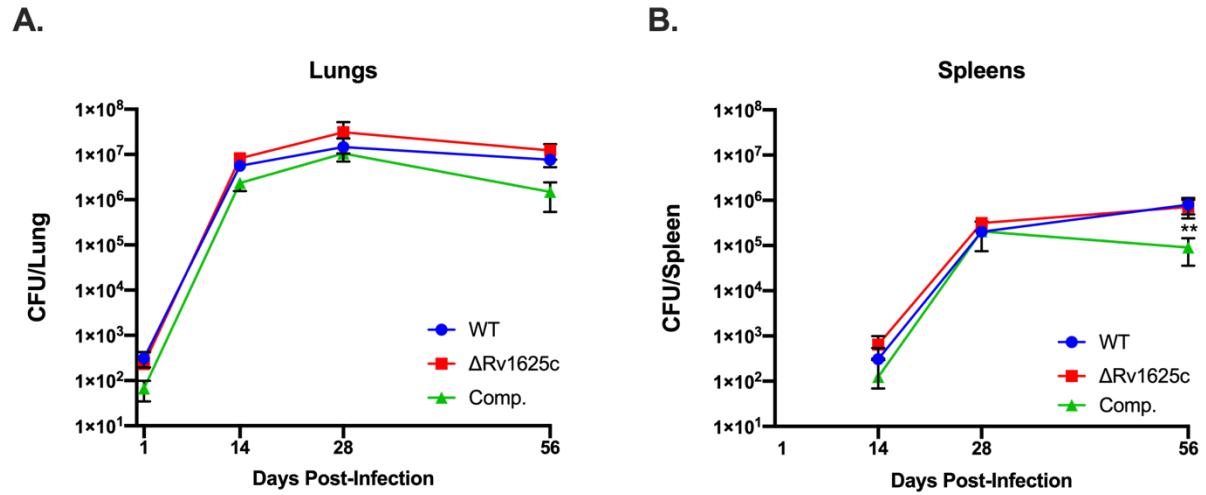
5.3.2 Overexpressing *rv1625c* generates a fitness defect in Mtb during infection and minimally enhances mCLB073 treatment

The most tractable mechanism by which Mtb could develop resistance to V-59/mCLB073 is by carrying mutations in the *rv1625c* gene at residues that inactivate its ability to synthesize cAMP, which would preclude the downstream activity of the compounds on the cholesterol utilization pathway. However, if inactivation of Rv1625c enzyme activity also confers an intrinsic fitness cost to the bacterium, this could reduce the likelihood of Mtb carrying these resistance mutations. We previously observed that an Rv1625c deletion strain (ΔRv1625c) had an intrinsic limited, ring-associated defect in cholesterol utilization but no growth defect during macrophage infection. Therefore we wanted to determine whether the loss of Rv1625c confers a fitness cost to Mtb during infection *in vivo*. We infected BALB/c mice by the aerosol route with WT, ΔRv1625c, and a complement strain that overexpresses *rv1625c* (Comp$_{Full}$) Mtb and quantified the bacterial load in the lungs and spleens at 2, 4, and 8 weeks post-infection. Although loss of Rv1625c did not confer a fitness cost to Mtb during infection, surprisingly the Comp$_{Full}$ strain exhibited a non-significant trend toward lower CFUs in the lungs (~0.75-log$_{10}$ reduction) and a significant decrease in bacterial burden in the spleens (~1-log$_{10}$ reduction) of mice selectively during the chronic stage of infection (Fig. 5.3a,b). This was unexpected because we did not observe any intrinsic defect in growth of the Comp$_{Full}$ strain during macrophage infection *in vitro* (Chapter 4). Because this strain has no defect in growth in liquid media and the observed growth defect is limited to the chronic stage of infection in mice, this result suggests that the activation of cAMP synthesis by Rv1625c may be linked to a signal or stress that is specific to growth or persistence in the *in vivo* environment. Compared to WT bacteria, activation of Rv1625c by this unknown signal in the Comp$_{Full}$ strain that overexpresses *rv1625c* may generate a growth defect by causing excess cAMP

synthesis in the bacteria and disrupting cholesterol utilization, similar to our observations with the Rv1625c agonist compounds (Fig. 5.1).

When we examined the effect of V-59 treatment on Mtb growth during macrophage infection *in vitro*, we found that the Comp$_{Full}$ strain also exhibited enhanced susceptibility during V-59 compound treatment (Chapter 4). Our data also suggests that the Comp$_{Full}$ strain may have additional metabolic defects, potentially in fatty acid utilization or central metabolism, during treatment with V-59, likely associated with the enhanced levels of cAMP the bacteria produces in response to compound treatment relative to WT (Chapter 4). To test whether our findings in macrophages translate to infection *in vivo*, we tested whether the efficacy of mCLB073 was enhanced in the Comp$_{Full}$ strain relative to WT in mice. We infected BALB/c mice by the aerosol route with WT, ΔRv1625c, or Comp$_{Full}$ Mtb and quantified the bacterial load in the lungs and spleens after treatment with a vehicle control or mCLB073 (30 mg/kg) during weeks 4-8 post-infection (Fig. 5.4). This is the first *in vivo* experiment in which we did not observe a difference in the average bacterial load in mice infected with WT Mtb and treated with 30 mg/kg mCLB073 (Fig. 5.4a). However, the magnitude of the effect of this compound on bacterial burden in this mouse strain has consistently been small (~0.5 log$_{10}$ reduction) (Fig. 5.1). Combined with the heterogeneity in CFUs that is an intrinsic challenge during infection of animals with Mtb, it is not entirely surprising that no mean difference would be observed occasionally within a single experiment including only 5 mice per group. However, the Comp$_{Full}$ strain did have an intrinsic growth defect in the lungs of these mice (~0.6 log$_{10}$ reduction) consistent with our earlier observations, and treatment with mCLB073 was associated with a further ~0.5 log$_{10}$ reduction in bacterial burden. In the spleens, mCLB073 treatment significantly reduced the bacterial burden of WT Mtb by ~0.7 log$_{10}$ CFUs (Fig. 5.4b). Treatment with mCLB073 did not alter the bacterial

burden in mice infected with ΔRv1625c Mtb, and the Comp$_{Full}$ strain had an intrinsic defect in bacterial burden that was not decreased further by mCLB073 treatment (Fig. 5.4b). Altogether, these preliminary results suggest that artificially enhancing cAMP synthesis in Mtb, either through overexpression of *rv1625c* and/or through treatment with Rv1625c agonists, confers a fitness defect during chronic infection in BALB/c mice and that Rv1625c may have a native activating signal during the chronic stage of infection. Activating cAMP synthesis seems to affect bacterial dissemination or persistence in the spleens of mice to a greater degree than in the lungs. However, these results are from preliminary studies, and should be replicated to compensate for the intrinsic variability in aerosol infection with Mtb before firm conclusions are drawn on these points.

Figure 5.3 Overexpressing *rv1625c* in Mtb is sufficient to generate a growth defect during infection in mice. Bacterial burden in the lungs (**A**) and spleens (**B**) of BALB/c mice infected with ~200 CFUs of WT, ΔRv1625c, or Comp$_{Full}$ Mtb by the aerosol route. Data are from one experiment with 5 mice per group and are shown as means $\pm$ SD (**$P < 0.01$, Kruskal-Wallis test and Dunn's multiple comparisons test).
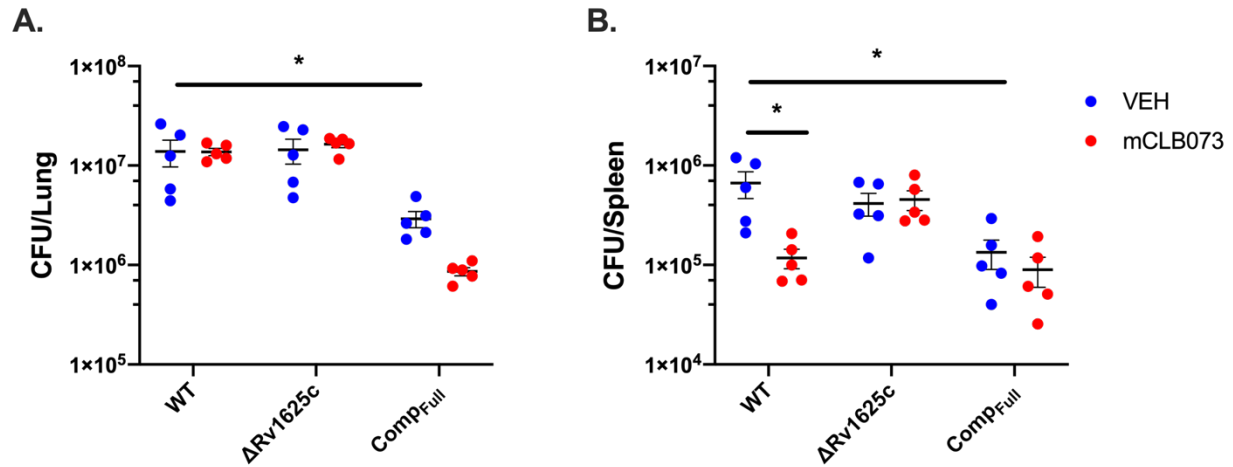
Fig. 5.4 Overexpressing *rv1625c* marginally enhances the efficacy of mCLB073 *in vivo*. Bacterial burden in the lungs (**A**) and spleens (**B**) of BALB/c mice infected with ~200 CFUs of WT, ΔRv1625c, or Comp$_{Full}$ Mtb by the aerosol route. Mice were treated with vehicle control or mCLB073 (30 mg/kg) by oral gavage, once-daily during weeks 4-8 post-infection. Data are from one experiment with 5 mice per group and are shown as means ± SD (*$P < 0.05$, Two-way ANOVA with Tukey's multiple comparisons test).

5.3.3 Rv1625c agonists increase cAMP in infected macrophages in an Rv1625c-dependent manner.

Next, we followed up on previously published results that indicated treatment with another Rv1625c agonist compound (V-58) alters cytokine production in infected macrophages *in vitro* *(26)*. Before performing transcriptional profiling on infected macrophages during compound treatment, we first verified that treatment with Rv1625c agonists (mCLB073) enhances cAMP levels in infected macrophages, in an Rv1625c-dependent manner. Murine BMDMs infected with WT Mtb had a ~10-fold increase in cAMP after 24 hours relative to the vehicle control, which was absent in macrophages infected with ΔRv1625c Mtb (Fig. 5.5). Importantly, macrophages infected with Comp$_{Full}$ Mtb had further enhanced levels of cAMP compared to WT during V-59 treatment, which is consistent with our previous results showing the enhanced effects of V-59/mCLB073 in this strain. The method we used to lyse these macrophages is unlikely to lyse Mtb as well, because efficient lysis of Mtb requires a bead beating step even in the presence of detergents. Therefore, it is reasonable to predict that the cAMP quantified here is derived from the host cell and cAMP secreted into the host environment from Mtb, rather than the cAMP within Mtb cells at the time of cell lysis. However, we have not directly ruled out partial lysis of Mtb contributing to the total cAMP levels in this assay.
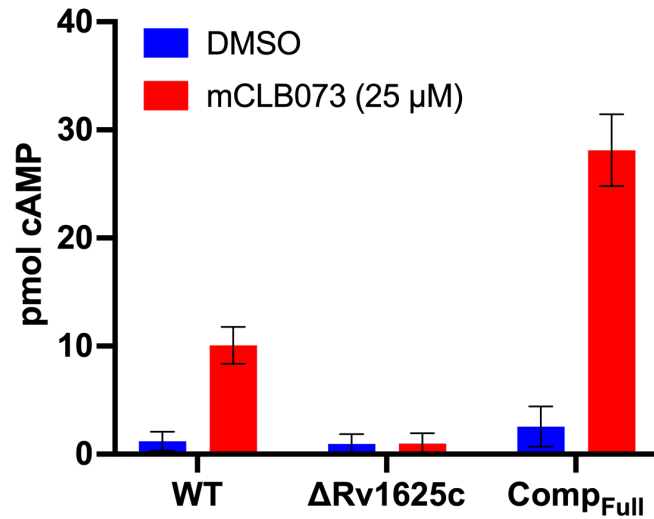
Figure 5.5 Treatment with mCLB073 increases cAMP levels in infected macrophages. Quantification of cAMP in whole murine BMDMs infected with the indicated strains of Mtb at an MOI of 7. Cells were lysed and cAMP levels were quantified by ELISA. Magnitude of cAMP indicates total cAMP per flask of infected cells. Data shown are representative of two experiments with two or three technical replicates per group and are shown as means ± SEM. Data courtesy of C. Montague.

5.3.4 Activating cAMP synthesis in Mtb changes the transcriptional profile of infected macrophages *in vitro*.

Because cAMP signaling can have various cell type-dependent effects in mammalian cells, we next characterized the transcriptional signature of host macrophages during treatment with V-59 by RNA-seq. Murine BMDMs derived from BALB/c mice were infected with WT Mtb and then treated with a vehicle control or V-59 for 24 hours. Given the extremely slow doubling time of Mtb (approximately 18-54 hours in liquid culture) we expect no significant change in CFUs between the treatment groups at this short timepoint, which might otherwise generate trivial differences in inflammatory signatures (*27*). Overall, 150 genes were significantly differentially expressed in macrophages treated with V-59 relative to DMSO during Mtb infection. We categorized these genes based on STRING network analysis, and identified two groups that were the most relevant to our interests in inflammation and lipid utilization. Sterol biosynthesis and LDL receptor genes (e.g. *Ldlr, Hmgcr, Sqle, Insig1, Msmo1*) were relatively downregulated. This could reflect a decreased need to replenish cholesterol pools in the host cell, driven by decreased cholesterol utilization by the bacterium during V-59 treatment (*28*). In inflammatory pathway genes, we sought to focus on genes that were differentially expressed in response to V-59 treatment in macrophages and are also known to play important roles in host susceptibility or protection during Mtb infection *in vivo*. Notably, genes related to IL-1 signaling (*Il1a, Il1b, Nlrp3*) and neutrophil recruitment (*Cxcl1, Cxcl2, Ccl3*) were downregulated during V-59 treatment. Because both of these pathways play complex roles in influencing host protection versus susceptibility during Mtb infection, we chose to focus on these going forward (Chapter 1).

Our previous work demonstrated that another Rv1625c agonist (V-58) decreased TNFα secretion by the murine J774 macrophage cell line during infection with Mtb (*26*). However, J774

cells and primary BMDMs are known to respond differently to Mtb infection, and the expression of the *Tnfa* gene was not significantly downregulated in this RNA-seq data set (*29*). However, when we performed GSEA on all of the genes from this data set, we found that the TNFα Signaling Via NFκB Hallmark gene set was enriched in the control relative to V-59 treatment, resulting in a negative enrichment score. This indicates that a subset of the genes in this pathway are downregulated during V-59 treatment, and is consistent with a small but significant decrease in paracrine TNFα signaling (Fig. 5.6b). TNFα ELISAs confirmed a trend toward lower TNFα secretion in each biological replicate during V-59 treatment, but with variability in the magnitude (Fig. 5.6c). Like IL-1 and neutrophil recruitment pathways, TNFα is known to play a complex role in balancing host susceptibility versus protection during Mtb infection (Chapter 1), so we chose to follow up on the potential for V-59/mCLB073 to alter TNFα signaling also.
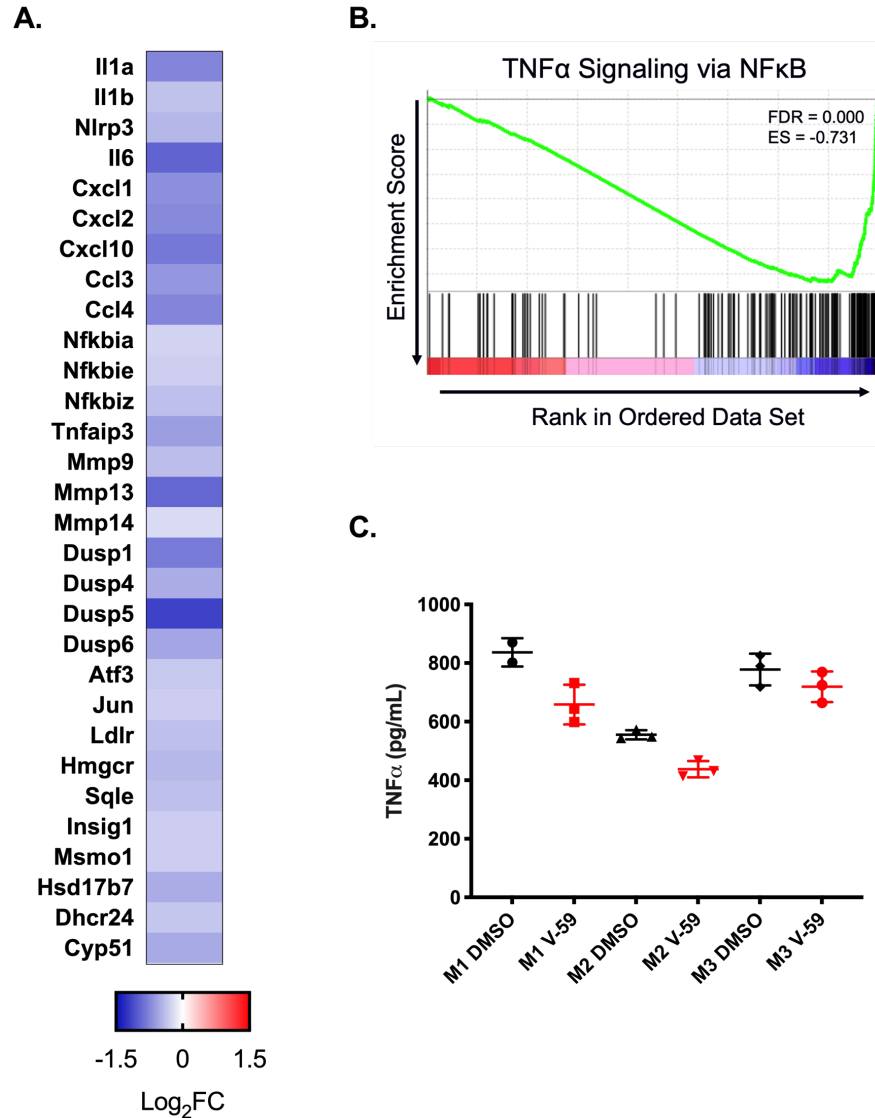
Figure 5.6 V-59 dampens the transcriptional expression of inflammatory genes in Mtb infected macrophages. (A) RNA-seq analysis quantifying differentially expressed genes from murine BMDMs infected with WT Mtb at an MOI of 7, and treated with DMSO as a vehicle control or V-59 (25μM) for 24 hours. Data are displayed as $\log_2$ fold change in gene expression in response to V-59 vs. control treatment. Data are from n=3 mice. Genes shown are a subset of the significantly differentially expressed genes selected based on function by STRING network analysis (adjusted p-value ≤ 0.05). **(B)** GSEA enrichment plot of DMSO and V-59 treated cells. Shown is the Hallmark TNFα Signaling via NFκB gene set. **(C)** TNFα quantification by ELISA in the supernatants of each set of macrophages used for RNA-seq (M1, M2, and M3 are macrophages from 3 mice, treated with DMSO or V-59).

5.3.4 Rv1625c agonists alter pulmonary cytokine levels *in vivo*.

To verify whether the changes in gene expression observed in our RNA-seq study translated to changes in protein production, we began to follow up on these findings using ELISAs. However, in our hands the level of cytokine produced by primary BMDMs isolated from different mice during Mtb infection can vary substantially, and we have found it difficult to verify these phenotypes using *in vitro* BMDM infection experiments for this reason (Fig. 5.6c and data not shown). As an alternative, we infected BALB/c mice for two weeks by the intranasal route, and then treated them with a vehicle control, various concentrations of the frontline TB antibiotic isoniazid (INH), or mCLB073 (10mg/kg) for one week. We isolated whole lung homogenates from these mice and quantified the bacterial burden and cytokine levels in these samples. Because production of cytokines can be affected in proportion to changes in Mtb CFUs, we included a series of INH concentrations in this study to determine whether mCLB073 changes cytokine production in the lungs in a manner that is separable from its effect on bacterial burden. Plotting the level of cytokines in the lung homogenates relative to CFUs for each of these treatment conditions revealed that mCLB073 is associated with a decrease in TNFα that is proportional to that observed with INH treatment (Fig. 5.7a). However, CXCL1 and IL-1β are disproportionately decreased by mCLB073 treatment compared to INH treatment (Fig. 5.7b,c). This indicates that, at least in an acute model of murine infection, the increased cAMP synthesis induced by mCLB073 in Mtb may lead to changes in host cell CXCL1 and IL-1β production, which could indicate a secondary effect of Rv1625c agonist compounds in infected hosts and change lung pathology.
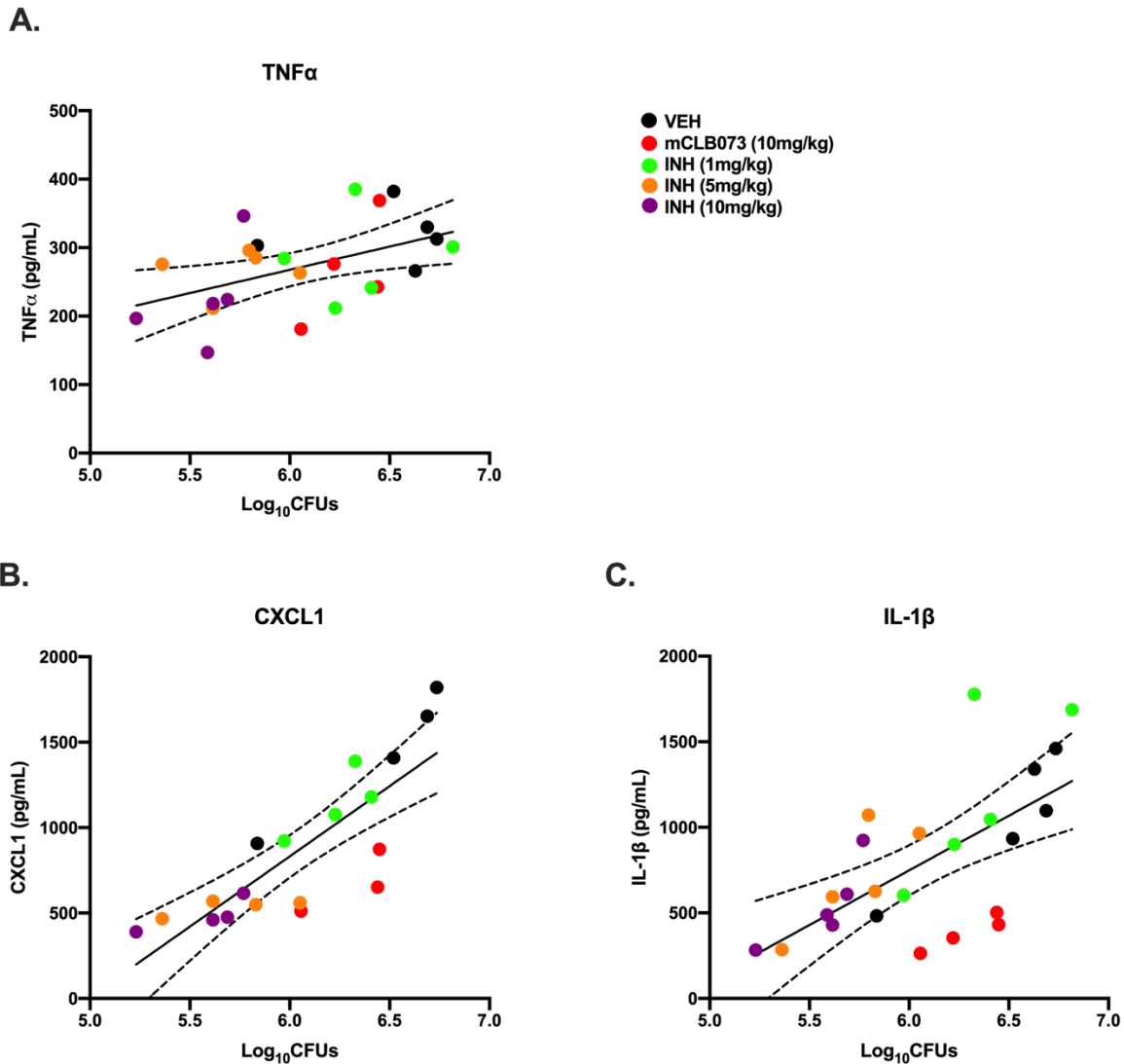
Figure 5.7 Treatment with mCLB073 is associated with decreased CXCL1 and IL-1β in lung homogenates that is separable from changes in bacterial burden. Mice were infected with WT Mtb by the intranasal route and dosed with vehicle control, mCLB073, or INH at the indicated doses once-daily by oral gavage during week 3 post infection. Whole lung homogenates were generated and bacterial burden and cytokine levels were quantified. (**A**) TNFα concentration versus bacterial burden. (**B**) CXCL1 concentration versus bacterial burden. (**C**) IL-1β versus bacterial burden. Simple linear regression was used including all of the data points to plot the line of best fit (dotted lines indicate 95% confidence interval), which identifies mCLB073 treated samples as outliers in CXCL1 and IL-1β production. Data are from one experiment with 4 or 5 mice per group. Each dot represents one mouse.

5.4 Discussion

This work utilized AC agonists for *in vivo* studies of cAMP signaling in Mtb, which revealed that chemically activating cAMP synthesis may be an untapped mechanism for manipulating bacterial fitness during infection, redefining the traditional mechanism for an anti-virulence compound. Chemical tools like V-59/mCLB073 that can be used to modulate distinct pathways in Mtb in infection models are valuable because it is difficult to predict the *in vivo* metabolic state and vulnerabilities Mtb experiences during infection (*30-34*). We developed V-59/mCLB073 as the first compounds that can effectively modulate cAMP synthesis and block cholesterol utilization in Mtb, while being suitable for *in vivo* studies.

Single-agent studies using V-59/mCLB073 established that cAMP induction modestly impairs bacterial growth and lung pathology in mouse models of TB (Fig. 5.1). A recent study also found that the "MKR superspreader" strain of Mtb, an emergent multidrug-resistant strain of the modern Beijing lineage, displayed enhanced upregulation of cholesterol utilization genes during macrophage infection relative to the H37Rv reference strain (*35*). V-59 was used to show that activating Rv1625c to inhibit cholesterol utilization in the MKR strain selectively reduced intracellular survival of the bacteria in infected macrophages (*35*). This suggests that efficacy of Rv1625c agonists *in vivo* may be potentiated by cholesterol-related metabolic adaptations that are especially crucial to the intracellular survival of at least one multi-drug resistant strain of Mtb. Identifying this link between cAMP signaling, cholesterol utilization, and Mtb fitness during infection is important because it is challenging to target metabolic pathways in Mtb that are not redundant and are sufficiently distinct from human pathways to limit side-effects (*30, 36, 37*). Much is not yet known about the restrictions Mtb encounters *in vivo* where the bacterium co-catabolizes multiple complex substrates, and future infection studies that combine V-59/mCLB073

treatment with chemical modulators of other pathways in Mtb may provide interesting insights on this topic.

Consistent with our *in vitro* studies of these compounds in Mtb (Chapter 4), we found that overexpressing *rv1625c* in Mtb (Comp$_{Full}$ Mtb) during murine infection was sufficient to induce a fitness defect during the chronic stage infection in both the lungs and spleens of these animals (Fig. 5.3 and Fig. 5.4). Rv1625c is a membrane protein, and overexpression of membrane proteins can cause growth defects in bacteria. However, given that the growth defect we observed here is specific to particular stage of infection and was not noted in liquid media or during macrophage infection *in vitro*, we predict that this reflects a genuine induction of cAMP synthesis by Rv1625c during infection, which could be activated in response to an as-yet unidentified environmental signal. In this case, Rv1625c would be activated in both the WT and Comp$_{Full}$ strains by this environmental signal, but the increased level of Rv1625c in the Comp$_{Full}$ bacteria could be associated with higher levels of cAMP in the cells. As we established previously, above a certain threshold, increased levels of cAMP synthesis are sufficient to disrupt cholesterol utilization in Mtb (Chapter 4). Cholesterol utilization defects in Mtb have often been associated with decreased growth during the chronic, but not the acute, stage of infection in animal models of TB (*38-41*). Therefore, the defect observed *in vivo* in the Comp$_{Full}$ strain seems consistent with a defect in cholesterol utilization, and/or an associated decrease in ATP levels in the bacterium. Lipophilic molecules or CO_2 have been speculated as potential ligands of Rv1625c, and other signals such as pH, fatty acids, and secreted proteins have been identified as ligands that can activate other Mtb adenylyl cyclase enzymes (*42-45*). Given the variety of potential ligands, it is difficult to speculate which, if any of these, could be the native agonist of Rv1625c during infection.

In preliminary experiments, we also identified that Rv1625c agonist treatment is associated with increased cAMP levels in host cells, in an Rv1625c dependent mechanism. Because cAMP is a universal second messenger, Mtb is a persistent intracellular pathogen, and cAMP is known to modulate host cell inflammatory signaling in macrophages, we chose to investigate whether treatment with these compounds during Mtb infection has a secondary effect on the host cell inflammatory phenotype. RNA-seq analysis on macrophages infected with Mtb and treated with an Rv1625c agonist *in vitro* revealed that treatment with these compounds is associated with downregulation of a group of cytokine genes as well as several cholesterol homeostasis genes (Fig. 5.6). We were particularly interested in genes involved in neutrophil recruitment, IL-1 signaling, and TNFα signaling because these are known to be important to the balance of host protection and susceptibility during the chronic stage of infection (Chapter 1). In a translational setting, V-59/mCLB073 compounds would be used during the chronic stage of infection, when mature granulomas with heterogeneous features are already established. Investigating whether these compounds have the capacity to skew the balance of these inflammatory mediators in a host-beneficial direction is important because this represents either an advantageous secondary effect of these compounds, an insignificant innocuous effect, or a potential safety concern. During these preliminary studies, we tested this using an acute model of infection in BALB/c mice to expedite secondary screening of our RNA-seq hits. Results from this model suggest that mCLB073 disproportionately decreases CXCL1 and IL-1β but not TNFα in the lungs of infected mice, compared to the frontline TB drug INH (Fig. 5.7). Overall, Rv1625c agonist treatment is associated with decreased bacterial burden and/or lower lung pathology scores, even in chronic models of infection (Fig. 5.1 and Fig. 5.7). This suggests that the overall effects of these compounds are beneficial. Given the strong association of excess neutrophil recruitment and bacterial lipid

utilization with host susceptibility during active TB, the potential of these compounds to reduce excessive neutrophil recruitment while inhibiting Mtb nutrient utilization is especially interesting for future studies (Chapter 1). Past studies investigated the utility of modulating cAMP signaling during Mtb infection by an alternative mechanism, chemically inhibiting host phosphodiesterase activity. They found that enhancing cAMP via this pathway was associated with decreased TNFα gene expression in the lungs, reduced tolerance-associated responses of Mtb to INH, and improved bacterial clearance during INH treatment (*46*). This is consistent with evidence that elevated host immune stresses enhance drug tolerance in Mtb (*47*). This suggests that, though counterintuitive, ameliorating certain pathways of the host immune response after Mtb infection is established can be beneficial when paired with antibiotic treatment.

Further work will be needed to verify whether CXCL1 and IL-1β are also uniquely reduced by mCLB073 during chronic infection. Additional studies quantifying other cytokines, measuring neutrophil accumulation in the lungs, differentiating pro-IL-1 from active IL-1, and distinguishing effects of mCLB073 treatment in different subsets of infected versus bystander phagocytes are also planned (Chapter 6). Taken together, Rv1625c agonist compounds represent a novel mechanism of action, which may be capable of inhibiting both a key pathway of Mtb nutrient utilization and altering the inflammatory balance in the granuloma during TB.

5.5 References

1.   K. M. Wilburn, R. A. Fieweger, B. C. VanderVen, Cholesterol and fatty acids grease the wheels of Mycobacterium tuberculosis pathogenesis. *Pathogens and Disease* **76**, (2018).

2.   A. R. Shenoy, N. Sreenath, M. Podobnik, M. Kovacevic, S. S. Visweswariah, The Rv0805 gene from Mycobacterium tuberculosis encodes a 3',5'-cyclic nucleotide phosphodiesterase: biochemical and mutational analysis. *Biochemistry* **44**, 15695-15704 (2005).

3.   N. Matange, D. M. Hunt, R. S. Buxton, S. S. Visweswariah, Overexpression of the Rv0805 phosphodiesterase elicits a cAMP-independent transcriptional response. *Tuberculosis (Edinb)* **93**, 492-500 (2013).

4.   G. S. Knapp, K. A. McDonough, Cyclic AMP Signaling in Mycobacteria. *Microbiol Spectr* **2**, (2014).

5.   K. A. McDonough, A. Rodriguez, The myriad roles of cyclic AMP in microbial pathogens: from signal to sword. *Nature Reviews Microbiology* **10**, 27-38 (2011).

6.   M. Cassio Barreto de Oliveira, A. Balan, The ATP-Binding Cassette (ABC) Transport Systems in Mycobacterium tuberculosis: Structure, Function, and Possible Targets for Therapeutics. *Biology (Basel)* **9**, (2020).

7.   C. Osycka-Salut, F. Diez, J. Burdet, M. G. Gervasi, A. Franchi, L. G. Bianciotti, C. Davio, S. Perez-Martinez, Cyclic AMP efflux, via MRPs and A1 adenosine receptors, is critical for bovine sperm capacitation. *Mol Hum Reprod* **20**, 89-99 (2014).

8.   C. J. Queval, R. Brosch, R. Simeone, The Macrophage: A Disputed Fortress in the Battle against Mycobacterium tuberculosis. *Frontiers in microbiology* **8**, 2284 (2017).

9.   L. Moreira-Teixeira, K. Mayer-Barber, A. Sher, A. O'Garra, Type I interferons in tuberculosis: Foe and occasionally friend. *J Exp Med* **215**, 1273-1285 (2018).

10.   C. H. Serezani, M. N. Ballinger, D. M. Aronoff, M. Peters-Golden, Cyclic AMP: master regulator of innate immune cell function. *Am J Respir Cell Mol Biol* **39**, 127-132 (2008).

11.   S. Gerlo, R. Kooijman, I. M. Beck, K. Kolmus, A. Spooren, G. Haegeman, Cyclic AMP: a selective modulator of NF-kappaB action. *Cell Mol Life Sci* **68**, 3823-3841 (2011).

12.   D. M. Aronoff, J. K. Carstens, G. H. Chen, G. B. Toews, M. Peters-Golden, Short communication: differences between macrophages and dendritic cells in the cyclic AMP-dependent regulation of lipopolysaccharide-induced cytokine and chemokine synthesis. *J Interferon Cytokine Res* **26**, 827-833 (2006).

13.   J. P. Vilardaga, F. G. Jean-Alphonse, T. J. Gardella, Endosomal generation of cAMP in GPCR signaling. *Nat Chem Biol* **10**, 700-706 (2014).

14.   G. E. Peng, V. Pessino, B. Huang, M. von Zastrow, Spatial decoding of endosomal cAMP signals by a metastable cytoplasmic PKA network. *Nat Chem Biol* **17**, 558-566 (2021).

15.   D. M. Aronoff, C. Canetti, C. H. Serezani, M. Luo, M. Peters-Golden, Cutting edge: macrophage inhibition by cyclic AMP (cAMP): differential roles of protein kinase A and exchange protein directly activated by cAMP-1. *J Immunol* **174**, 595-599 (2005).

16.   E. A. Wall, J. R. Zavzavadjian, M. S. Chang, B. Randhawa, X. Zhu, R. C. Hsueh, J. Liu, A. Driver, X. R. Bao, P. C. Sternweis, M. I. Simon, I. D. Fraser, Suppression of LPS-induced TNF-alpha production in macrophages by cAMP is mediated by PKA-AKAP95-p105. *Sci Signal* **2**, ra28 (2009).

17.   J. N. Ahmad, P. Sebo, Adenylate Cyclase Toxin Tinkering With Monocyte-Macrophage Differentiation. *Frontiers in immunology* **11**, 2181 (2020).

18. J. Vojtova, J. Kamanova, P. Sebo, Bordetella adenylate cyclase toxin: a swift saboteur of host defense. *Current opinion in microbiology* **9**, 69-75 (2006).

19. D. L. Confer, J. W. Eaton, Phagocyte impotence caused by an invasive bacterial adenylate cyclase. *Science* **217**, 948-950 (1982).

20. D. Pisu, L. Huang, J. K. Grenier, D. G. Russell, Dual RNA-Seq of Mtb-Infected Macrophages In Vivo Reveals Ontologically Distinct Host-Pathogen Interactions. *Cell Rep* **30**, 335-350 e334 (2020).

21. E. R. Driver, G. J. Ryan, D. R. Hoff, S. M. Irwin, R. J. Basaraba, I. Kramnik, A. J. Lenaerts, Evaluation of a mouse model of necrotic granuloma formation using C3HeB/FeJ mice for testing of drugs against Mycobacterium tuberculosis. *Antimicrobial agents and chemotherapy* **56**, 3181-3195 (2012).

22. D. X. Ji, L. H. Yamashiro, K. J. Chen, N. Mukaida, I. Kramnik, K. H. Darwin, R. E. Vance, Type I interferon-driven susceptibility to Mycobacterium tuberculosis is mediated by IL-1Ra. *Nature microbiology* **4**, 2128-2135 (2019).

23. L. Moreira-Teixeira, O. Tabone, C. M. Graham, A. Singhania, E. Stavropoulos, P. S. Redford, P. Chakravarty, S. L. Priestnall, A. Suarez-Bonnet, E. Herbert, K. D. Mayer-Barber, A. Sher, K. L. Fonseca, J. Sousa, B. Ca, R. Verma, P. Haldar, M. Saraiva, A. O'Garra, Mouse transcriptome reveals potential signatures of protection and pathogenesis in human tuberculosis. *Nature immunology* **21**, 464-476 (2020).

24. L. Moreira-Teixeira, P. J. Stimpson, E. Stavropoulos, S. Hadebe, P. Chakravarty, M. Ioannou, I. V. Aramburu, E. Herbert, S. L. Priestnall, A. Suarez-Bonnet, J. Sousa, K. L. Fonseca, Q. Wang, S. Vashakidze, P. Rodriguez-Martinez, C. Vilaplana, M. Saraiva, V. Papayannopoulos, A. O'Garra, Type I IFN exacerbates disease in tuberculosis-susceptible

mice by inducing neutrophil-mediated lung inflammation and NETosis. *Nat Commun* **11**, 5566 (2020).

25. A. Lenaerts, C. E. Barry, 3rd, V. Dartois, Heterogeneity in tuberculosis pathology, microenvironments and therapeutic responses. *Immunological Reviews* **264**, 288-307 (2015).

26. R. M. Johnson, G. Bai, C. M. DeMott, N. K. Banavali, C. R. Montague, C. Moon, A. Shekhtman, B. VanderVen, K. A. McDonough, Chemical activation of adenylyl cyclase Rv1625c inhibits growth of Mycobacterium tuberculosis on cholesterol and modulates intramacrophage signaling. *Molecular Microbiology* (2017).

27. W. P. Gill, N. S. Harik, M. R. Whiddon, R. P. Liao, J. E. Mittler, D. R. Sherman, A replication clock for Mycobacterium tuberculosis. *Nat Med* **15**, 211-214 (2009).

28. M. Zimmermann, M. Kogadeeva, M. Gengenbacher, G. McEwen, H. J. Mollenkopf, N. Zamboni, S. H. E. Kaufmann, U. Sauer, Integration of Metabolomics and Transcriptomics Reveals a Complex Diet of Mycobacterium tuberculosis during Early Macrophage Infection. *mSystems* **2**, (2017).

29. N. Andreu, J. Phelan, P. F. de Sessions, J. M. Cliff, T. G. Clark, M. L. Hibberd, Primary macrophages and J774 cells respond differently to infection with Mycobacterium tuberculosis. *Scientific reports* **7**, 42225 (2017).

30. T. Beites, K. O'Brien, D. Tiwari, C. A. Engelhart, S. Walters, J. Andrews, H. J. Yang, M. L. Sutphen, D. M. Weiner, E. K. Dayao, M. Zimmerman, B. Prideaux, P. V. Desai, T. Masquelin, L. E. Via, V. Dartois, H. I. Boshoff, C. E. Barry, 3rd, S. Ehrt, D. Schnappinger, Plasticity of the Mycobacterium tuberculosis respiratory chain and its impact on tuberculosis drug development. *Nature Communications* **10**, 4970 (2019).

31.   D. F. Warner, V. Mizrahi, Shortening treatment for tuberculosis—back to basics. *New England Journal of Medicine* **371**, 1642-1643 (2014).

32.   Y. Zhang, D. Mitchison, The curious characteristics of pyrazinamide: a review. *International Journal of Tuberculosis and Lung Disease* **7**, 6-21 (2003).

33.   N. C. Howard, S. A. Khader, Immunometabolism during Mycobacterium tuberculosis Infection. *Trends Microbiol* **28**, 832-850 (2020).

34.   K. Pethe, P. C. Sequeira, S. Agarwalla, K. Rhee, K. Kuhen, W. Y. Phong, V. Patel, D. Beer, J. R. Walker, J. Duraiswamy, J. Jiricek, T. H. Keller, A. Chatterjee, M. P. Tan, M. Ujjini, S. P. S. Rao, L. Camacho, P. Bifani, P. A. Mak, I. Ma, S. W. Barnes, Z. Chen, D. Plouffe, P. Thayalan, S. H. Ng, M. Au, B. H. Lee, B. H. Tan, S. Ravindran, M. Nanjundappa, X. Lin, A. Goh, S. B. Lakshminarayana, C. Shoen, M. Cynamon, B. Kreiswirth, V. Dartois, E. C. Peters, R. Glynne, S. Brenner, T. Dick, A chemical genetic screen in Mycobacterium tuberculosis identifies carbon-source-dependent growth inhibitors devoid of in vivo efficacy. *Nature Communications* **1**, 57 (2010).

35.   P. Aiewsakun, P. Prombutara, T. A. P. Siregar, T. Laopanupong, P. Kanjanasirirat, T. Khumpanied, S. Borwornpinyo, P. Tong-Ngam, A. Tubsuwan, P. Srilohasin, A. Chaiprasert, W. Ruangchai, P. Palittapongarnpim, T. Prammananan, B. C. VanderVen, M. Ponpuak, Transcriptional response to the host cell environment of a multidrug-resistant Mycobacterium tuberculosis clonal outbreak Beijing strain reveals its pathogenic features. *Scientific Reports* **11**, 3199 (2021).

36.   U. Ganapathy, J. Marrero, S. Calhoun, H. Eoh, L. P. S. de Carvalho, K. Rhee, S. Ehrt, Two enzymes with redundant fructose bisphosphatase activity sustain gluconeogenesis and virulence in Mycobacterium tuberculosis. *Nature Communications* **6**, 7912 (2015).

37.   E. S. C. Rittershaus, S. H. Baek, I. V. Krieger, S. J. Nelson, Y. S. Cheng, S. Nambi, R. E. Baker, J. D. Leszyk, S. A. Shaffer, J. C. Sacchettini, C. M. Sassetti, A Lysine Acetyltransferase Contributes to the Metabolic Adaptation to Hypoxia in Mycobacterium tuberculosis. *Cell Chemical Biology* **25**, 1495-1505 e1493 (2018).

38.   A. K. Pandey, C. M. Sassetti, Mycobacterial persistence requires the utilization of host cholesterol. *Proceedings of the National Academy of Sciences of the United States of America* **105**, 4376-4380 (2008).

39.   N. M. Nesbitt, X. Yang, P. Fontan, I. Kolesnikova, I. Smith, N. S. Sampson, E. Dubnau, A thiolase of Mycobacterium tuberculosis is required for virulence and production of androstenedione and androstadienedione from cholesterol *Infection and Immunity* **78**, 275-282 (2010).

40.   Y. Hu, R. van der Geize, G. S. Besra, S. S. Gurcha, A. Liu, M. Rohde, M. Singh, A. Coates, 3-Ketosteroid 9alpha-hydroxylase is an essential factor in the pathogenesis of Mycobacterium tuberculosis. *Molecular Microbiology* **75**, 107-121 (2010).

41.   K. C. Yam, I. D'Angelo, R. Kalscheuer, H. Zhu, J.-X. Wang, V. Snieckus, L. H. Ly, P. J. Converse, W. R. Jacobs, Jr., N. Strynadka, L. D. Eltis, Studies of a Ring-Cleaving Dioxygenase Illuminate the Role of Cholesterol Metabolism in the Pathogenesis of Mycobacterium tuberculosis. *PLoS Pathogens* **5**, e1000344 (2009).

42.   P. D. Townsend, P. M. Holliday, S. Fenyk, K. C. Hess, M. A. Gray, D. R. Hodgson, M. J. Cann, Stimulation of mammalian G-protein-responsive adenylyl cyclases by carbon dioxide. *J Biol Chem* **284**, 784-791 (2009).

43.   S. Beltz, J. Bassler, J. E. Schultz, Regulation by the quorum sensor from Vibrio indicates a receptor function for the membrane anchors of adenylate cyclases. *eLife* **5**, (2016).

44.   M. Ziegler, J. Bassler, S. Beltz, A. Schultz, A. N. Lupas, J. E. Schultz, Characterization of a novel signal transducer element intrinsic to class IIIa/b adenylate cyclases and guanylate cyclases. *FEBS Journal* **284**, 1204-1217 (2017).

45.   R. M. Johnson, K. A. McDonough, Cyclic nucleotide signaling in Mycobacterium tuberculosis: an expanding repertoire. *Pathogens and Disease* **76**, (2018).

46.   S. Subbian, L. Tsenova, P. O'Brien, G. Yang, M. S. Koo, B. Peixoto, D. Fallows, V. Dartois, G. Muller, G. Kaplan, Phosphodiesterase-4 inhibition alters gene expression and improves isoniazid-mediated clearance of Mycobacterium tuberculosis in rabbit lungs. *PLoS Pathog* **7**, e1002262 (2011).

47.   Y. Liu, S. Tan, L. Huang, R. B. Abramovitch, K. H. Rohde, M. D. Zimmerman, C. Chen, V. Dartois, B. C. VanderVen, D. G. Russell, Immune activation of the host cell induces drug tolerance in Mycobacterium tuberculosis both in vitro and in vivo. *J Exp Med* **213**, 809-825 (2016).

CHAPTER SIX

## Final discussion and future directions

6.1 Overview

In this work, we have described how both the hydrolysis of ATP to power lipid uptake and the cyclization of ATP to form cAMP contribute to regulation of cholesterol utilization in Mtb. As presented above (Chapter 3), the ATPase activity of MceG is required for both cholesterol and fatty acid metabolism in Mtb, likely by powering the translocation of these lipids into the bacterial cell through their respective Mce complexes (Fig. 6.1).

Based on preliminary findings from a high-throughput chemical screen, we investigated the link between activating cAMP synthesis in Mtb and inhibiting cholesterol utilization by the bacterium (Chapter 4). Specifically, we found that the small molecule V-59 and the optimized analog mCLB073 increase cAMP synthesis in Mtb in an Rv1625c-dependent manner and this is associated with inhibition of cholesterol utilization. We studied how the two apparent components of this mechanism of action interact with the cholesterol utilization pathway in Mtb (Fig. 6.1). We developed a genetic method (TetOn-cAMP) for inducing cAMP synthesis in Mtb independent of V-59/mCLB073 and Rv1625c, which allowed us to establish that increasing cAMP synthesis is sufficient to inhibit cholesterol utilization. Our results from both the TetOn-cAMP and a strain that overexpresses *rv1625c* are broadly consistent with the conclusion that inducing cAMP synthesis inhibits cholesterol utilization in a dose-dependent manner in Mtb. We also identified that Rv1625c itself has an intrinsic role in cholesterol utilization that appears to be limited to ring degradation and related to its six-helical transmembrane domain.

One key advance presented in this study compared to our previous work is the identification of Rv1625c agonists that are suitable for use during infection in mice. This allowed us to examine whether activating cAMP synthesis during infection impairs Mtb pathogenesis or reduces lung pathology (Chapter 5). We presented evidence that chemically activating cAMP synthesis modestly decreases CFUs in murine models of chronic infection while reducing lung pathology, and preliminary data indicates that compound treatment has a more pronounced effect on Mtb CFUs in the spleens which are a site of bacterial dissemination during infection. Notably, we observed a similar enhanced phenotype in the spleens compared to the lungs of mice infected with ΔMceG bacteria (Chapter 3). We also presented preliminary evidence that chemically enhancing the amount of cAMP secreted from Mtb can alter the balance of cytokines produced by infected macrophages *in vitro*, and these changes were predictive of an altered balance in inflammatory mediators in whole lung samples from infected mice (Fig. 6.1).

Some of the major outstanding questions related to this work and potential ways to address these in the future are discussed below.
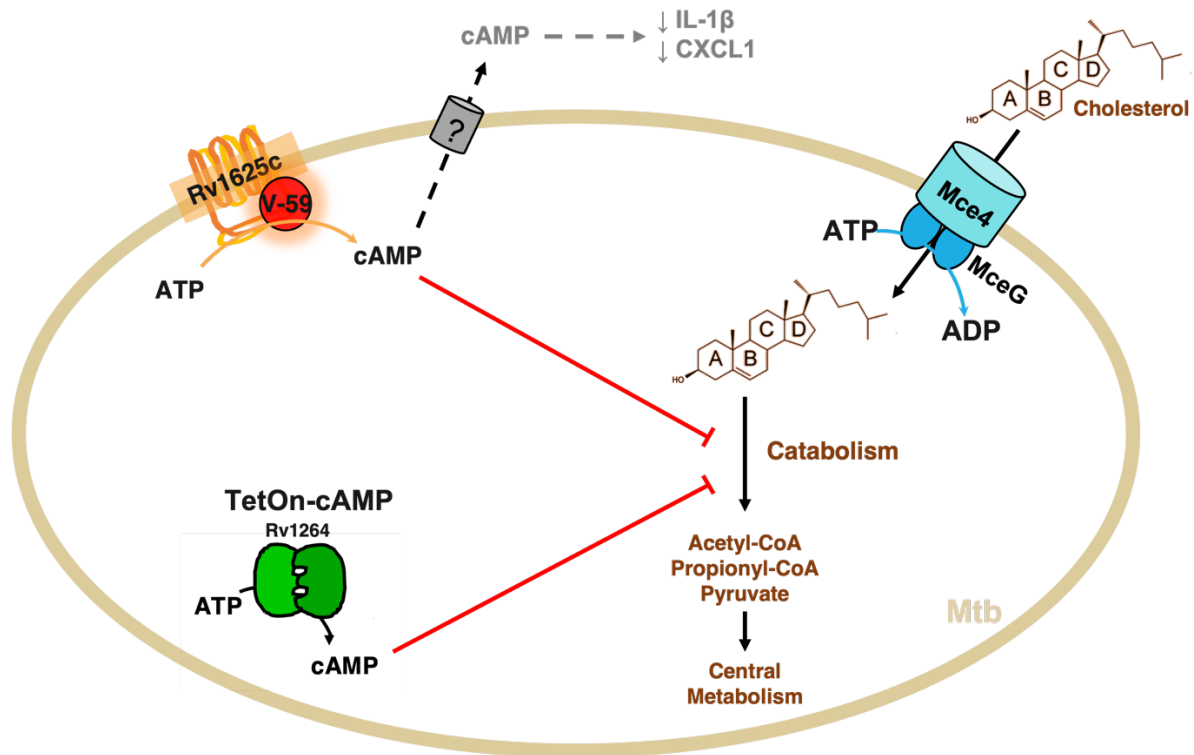
Figure 6.1 Overview of findings presented in this work. Summary of the relationship identified between ATP, cAMP, and cholesterol utilization in Mtb. Proposed relationship between excess cAMP secreted from Mtb and host cell cytokines identified in preliminary data.

6.2 Addressing the missing links between Rv1625c, cAMP synthesis, and lipid utilization in

M. tuberculosis

Two major questions remain regarding the mechanisms that connect Rv1625c, cAMP synthesis, and lipid utilization in Mtb. First, in the future it will be important to address the mechanism through which Rv1625c itself, particularly its transmembrane domain, is connected to cholesterol utilization in Mtb. Second, the mechanism by which cAMP synthesis inhibits cholesterol degradation should be studied further, particularly in comparison to cAMP-dependent regulation of fatty acid utilization in Mtb.

The physiological roles of the six-helical transmembrane domains found in Rv1625c and other class III ACs remain elusive, but they have been speculated to possess additional functions beyond their role in membrane anchoring (*1*). Multiple studies using chimeric protein constructs have begun to provide evidence that the six-helical transmembrane anchors of these ACs may be able to bind environmental ligands directly and transduce this signal to the cytoplasmic cyclase domains to regulate cAMP synthesis (*1*). Construction of chimeric proteins has been used to circumvent the problem that there are currently no established ligands for the six-helical transmembrane domain of any AC enzyme. When only the six-helical transmembrane domain of Rv1625c is replaced with similar six-helical transmembrane domains from quorum-sensing receptors (either CqsS from *Vibrio harveyi* or LqsS from *Legionella pneumophila*), treatment with their autoinducer ligands (*Cholera* autoinducer-1 or *Legionella* autoinducer-1, respectively) induces cAMP synthesis by the Rv1625c cyclase domain (*2, 3*). This transduction response is ligand-specific, and requires a conserved "cyclase-transducing element" which corresponds to the cytoplasmic helical domain that was found to promote homodimerization of the Rv1625c homolog from *Mycobacterium intracellulare* (Chapter 2) (*2, 4*). While this evidence does not establish that

the transmembrane domain of Rv1625c itself can receive a particular signal, it suggests that these domains are modular and the idea that they can play functional roles in signal transduction merits further investigation. The autoinducer ligands that bind to the six-helical transmembrane domains of quorum-sensing receptors in bacteria are small, highly lipophilic molecules that resemble fatty acids, which makes it interesting to speculate that a lipid species could be a potential ligand for Rv1625c (*3*). However, at least six clusters of six-helical transmembrane domains exist across eukaryotic and bacterial proteomes; the anchors from bacterial class IIIa ACs cluster separately from the quorum sensors and share more pairwise matches with eukaryotic transmembrane domains (*3*). Eukaryotic membrane-anchored ACs are regulated by interactions with G_α proteins via their cyclase domain. The closest parallel to this identified in Mtb thus far is the direct interaction of a soluble AC (Rv2212) with the protein Rv3810/Erp, which was found to increase cAMP synthesis by Rv2212 (*5*). This opens up the possibility that protein-protein interactions can regulate AC activity in Mtb. However, without more information, it is difficult to speculate what the native signal of the Rv1625c transmembrane domain could be and how this is integrated into the cholesterol utilization pathway in Mtb.

Several approaches are readily available to us to begin establishing how Rv1625c and its transmembrane domain are integrated into Mtb physiology. We have hypothesized that the ΔRv1625c strain has a defect in cholesterol ring metabolism while maintaining cholesterol uptake and side chain metabolism because this strain grows normally in media where cholesterol is the primary carbon source, suggesting portions of cholesterol catabolism remain functional. Identifying the missing cholesterol metabolite(s) we first observed by radio-TLC (Fig. 4.6) may allow us to identify which step(s) in the cholesterol breakdown pathway are defective in the absence of Rv1625c and restored by re-introducing the transmembrane domain versus the full-

length Rv1625c protein. We and others have analyzed cholesterol metabolite accumulation in the past to identify regulatory targets in this complex pathway (*6, 7*). If we identify a candidate step in cholesterol breakdown that is Rv1625c-dependent, this would assist in designing follow up experiments to identify the mechanism through which the two are linked.

Additionally, it is reasonable to predict that Rv1625c may participate in a multi-protein signaling complex or that protein-protein interactions may regulate Rv1625c activity. Identifying protein partners of Rv1625c may give us insight into its function. We are particularly interested in whether Rv1625c is associated with any other cholesterol- or lipid metabolism-coordinating proteins. In collaboration with the lab of Dr. Volodymyr Korkhov we have recently confirmed one protein interaction partner of Rv1625c. A pull-down using full-length Rv1625c against an *M. smegmatis* lysate identified two strong candidates for Rv1625c protein partners: Rv1421 and Rv0513 (Korkhov Lab, unpublished data). Using the yeast two-hybrid-like mycobacterial protein fragment complementation assay (M-PFC) (*8, 9*), we confirmed that Rv1625c and Rv1421 interact when co-expressed in *M. smegmatis* (Fig. 6.2). Surprisingly, this interaction is lost when V-59 is present, which may indicate that V-59 displaces Rv1421 from its binding interface with Rv1625c.

Rv1421 belongs to the RapZ-like family of nucleotide binding proteins, which includes RapZ in *E. coli* and YvcJ in *Bacillus subtilis (10, 11)*. Rv1421 is more similar to YvcJ than RapZ based on protein sequence alignment (63% similar to YvcJ versus 56% similar to RapZ), and both Rv1421 and YvcJ are missing a consensus sequence that is present in RapZ and confers RNA binding to this protein (*12*). In both *E. coli* and *B. subtilis*, these proteins are integrated into a complex feedback loop that optimizes peptidoglycan precursor synthesis in proportion to the amount of glycolytic precursors available to the bacterium (*10, 12*). In *B. subtilis*, two proteins YvcJ and YvcK/GlmR work together to regulate the enzyme glucosamine-6-phosphate synthase

(GlmS). GlmS is the entry point that diverts sugars from glycolytic carbon metabolism into the peptidoglycan synthesis pathway, generating a key feedback product uridine diphosphate N-acetylglucosamine (UDP-GlcNAc). Stimulation of GlmS activity is not necessary for normal peptidoglycan synthesis when bacteria are grown on glycolytic carbon sources, where ample precursors for this pathway and high UDP-GlcNAc levels are available. In this case, an interaction between UDP-GlcNAc-bound YvcJ and UDP-GlcNAc-bound GlmR occurs and this prevents GlmR from stimulating GlmS activity in *B. subtilis (12)*. But when growing on non-glycolytic carbon sources (low GlcNAc levels), this interaction does not occur; GlmR is free to stimulate GlmS activity, which is necessary for accurate peptidoglycan synthesis and correct cell morphology (*12, 13*). Unfortunately, it is unknown what function YvcJ plays when stabilized by its interaction with GlmR under glycolytic conditions, or when free from this interaction under non-glycolytic conditions. Mtb does conserve a YvcK/GlmR-like protein (Rv1422) encoded adjacent to its YvcJ orthologue (Rv1421). Rv1422 was predicted to function in both Mce1- and Mce4-mediated lipid utilization pathways by genetic interaction screening, and an Rv1422 mutant strain of Mtb has morphological defects when grown in minimal media supplemented with cholesterol (*14, 15*). Our preliminary data indicates ΔRv1421 and ΔRv1422 Mtb strains may have minimal or no defect in growth in media supplemented with cholesterol, but diminished $^{14}CO_2$ release from ring-labeled cholesterol, similar to ΔRv1625c (Fig. 6.3). Surprisingly, a preliminary RNA-seq study also suggests that inducing overexpression of *rv1421* in Mtb is sufficient to increase MCC gene expression even in the absence of a source of propionyl-CoA, while decreasing DosR regulon expression (Fig. 6.3). The DosR regulon can interact with lipid utilization via the triacylglycerol synthase gene (*tgs1*), and this lipid anabolism pathway may be used as a sink for fatty acid storage in triacylglycerols while supporting maintenance of $NAD^+/NADH$ balance

especially under hypoxia (*16*). Importantly, Rv1625c is also the only AC in Mtb that is required during bacterial adaptation to hypoxic conditions in the presence of fatty acids, a condition in which DosR regulon genes are also essential for optimal growth (*17*). The prediction that genes adjacent to *rv1625c* (*rv1626/pdtaR, rv1627c, rv1628c*) are essential for normal growth on cholesterol and have protein partners in the KstR pathway should also be investigated further (*17, 18*). Rv1626/PdtaR and its signaling partner Rv3220c/PdtaS are involved in regulating a nitric oxide stress resistance system, but were also independently identified in a genetic screen that pinpointed pathways that help detoxify propionyl-CoA by shunting it toward cell wall lipid synthesis in the presence of fatty acids (*19, 20*).

Taken together, the literature and preliminary data is not yet sufficient to propose a coherent model explaining the significance of the Rv1625c and Rv1421 interaction, or the role of Rv1625c and its adjacent genes in cholesterol utilization. However, it suggests they could be involved in coordinating peptidoglycan synthesis with the channeling of cholesterol/fatty acid products toward cell wall lipid synthesis versus toward the TCA cycle or storage as triacylglycerol (Chapter 2). In the future, this may be clarified by identifying additional Rv1625c and Rv1421/Rv1422 protein partners via pull downs using Strep-tagged proteins (Rv1625c, Rv1421, Rv1422) against Mtb lysates grown under different conditions, or by generating M-PFC constructs suitable for screening for interactions against a library of random Mtb protein fragments (*9*). Comparing the growth phenotypes, metabolite profiles, and transcriptional responses of Rv1625c-associated mutants under additional combinations of carbon sources and/or stresses (e.g. cholesterol, fatty acids, cholesterol and fatty acids together, MCC inactivation, hypoxia) could also help reveal how they contribute to lipid metabolism in Mtb. Biochemical assays can also be used to establish whether Rv1421/Rv1422 do indeed have similar functions to YvcJ/GlmR.
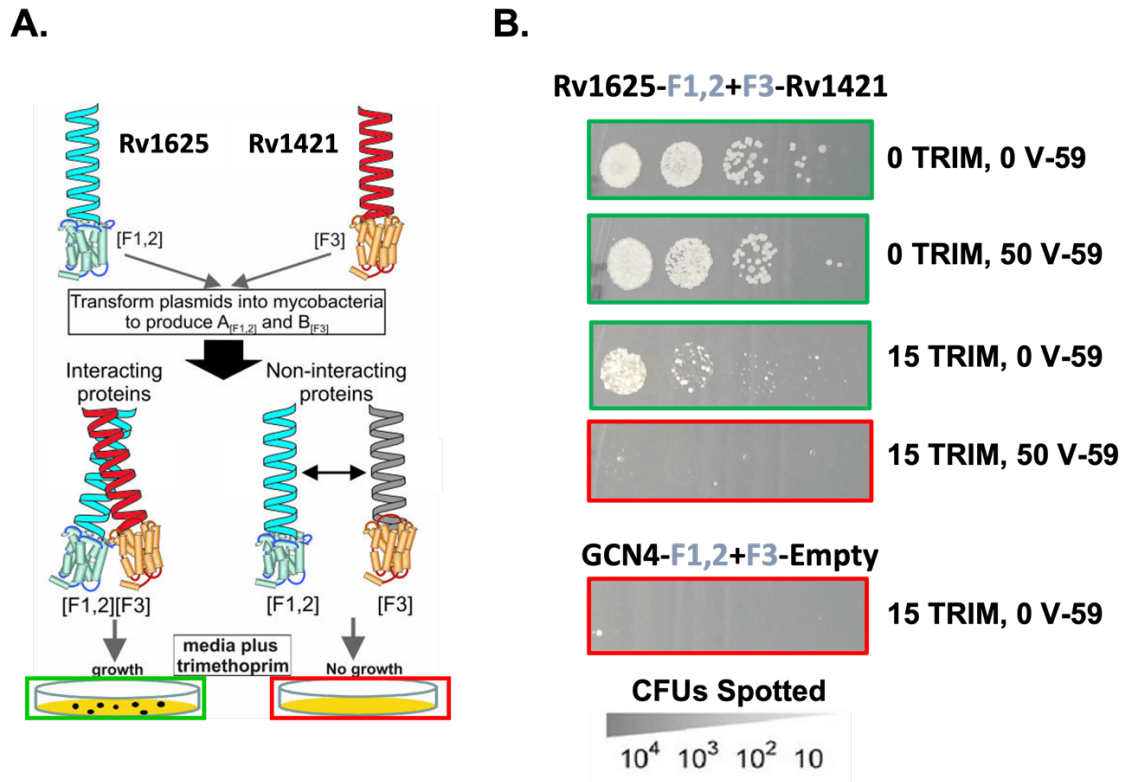
Figure 6.2 Rv1625c interacts with at least one protein partner, Rv1421. (A) Diagram of the yeast two-hybrid-like system used in *M. smegmatis* (Mycobacterial Protein Fragment Complementation, M-PFC) to test protein interactions. Rv1625c was fused via its C-terminus to the F1,2 fragment of the dihydrofolate reductase gene. Rv1421 was fused via its N-terminus to the F3 fragment. Figure adapted from (*8*), Copyright (2006) National Academy of Sciences. **(B)** Dilutions of *M. smegmatis* (10^4-10^1) carrying both the Rv1625c-F1,2 and F3-Rv1421 constructs were plated on agar containing no antibiotics, trimethoprim alone, V-59 alone, or trimethoprim and V-59 together. Results are representative of three experiments. Positive interactions are framed in green, and negative interactions are framed in red. Bacteria carrying a GCN4-F1,2 construct paired with an empty F3 construct serves as a negative control (no protein-protein interaction in the presence of trimethoprim). TRIM = trimethoprim. Data courtesy of C. Montague and K. Garcia-Martinez.
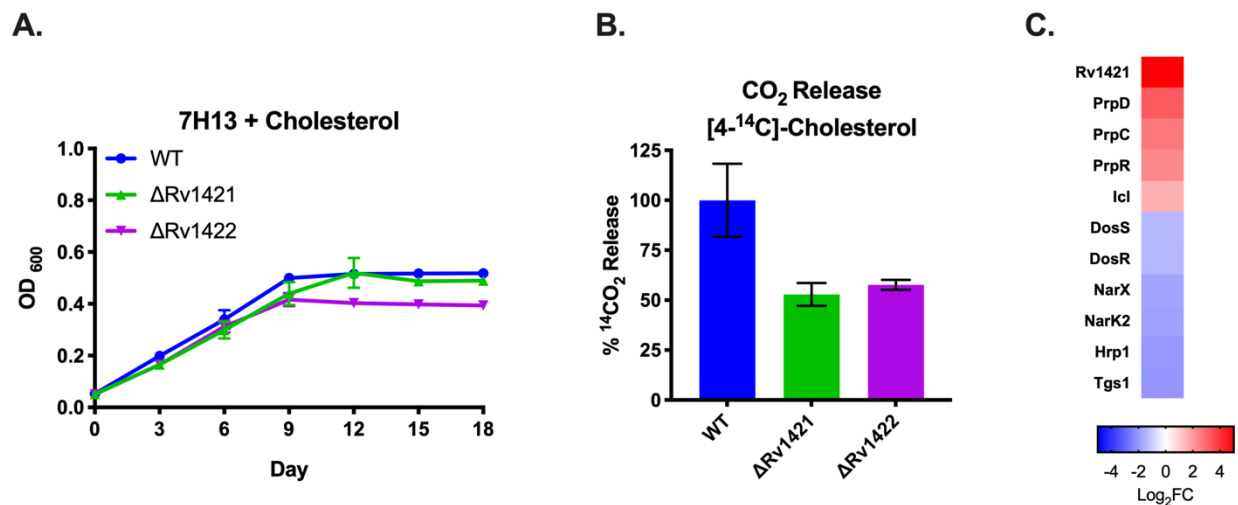
Figure 6.3 Preliminary evidence links Rv1421/Rv1422 to lipid metabolism in Mtb. (A) Growth by OD600 measurement of ΔRv1421 and ΔRv1422 Mtb in minimal media supplemented with cholesterol. **(B)** Catabolic release of $^{14}CO_2$ from [4-^{14}C]-cholesterol in WT, ΔRv1421 or ΔRv1422 Mtb pre-grown in cholesterol media. **(C)** RNA-seq profile of MCC and select DosR regulon genes in a TetOn-Rv1421 strain of Mtb. Gene expression is in Rv1421 induction versus control conditions. Bacteria were grown in standard culture conditions, without a source of propionyl-CoA. All experiments are preliminary, from one experiment with three technical replicates. RNA-seq data courtesy of B. VanderVen.

The second critical question this work leaves unanswered is the mechanism through which cAMP synthesis is linked to cholesterol utilization in Mtb. Given that the precursor for cAMP synthesis is ATP, and we have shown in this work that ATP has an important role in both fatty acid and cholesterol utilization, it is reasonable to hypothesize that the depletion of ATP rather than the increased presence of cAMP could be responsible for the ability of V-59/TetOn-cAMP to inhibit cholesterol utilization. Alternatively, given the large network of potential cAMP-responsive effector proteins in Mtb, the increased cAMP may signal through a cAMP-dependent effector protein to alter cholesterol utilization.

If ATP depletion is a primary mechanism driving the inhibition of cholesterol utilization in our propionyl-CoA reporter (*prpD'*::GFP) and CO_2 release assays, then we would expect ATP levels to be depleted in Mtb treated with V-59 under the same time points and conditions used in these assays. Preliminary experiments indicate that under conditions paralleling the CO_2 release assay (5 hours of compound treatment), V-59 treatment marginally decreases ATP levels in WT Mtb (Fig. 6.4a) Under conditions paralleling the *prpD'*::GFP assays (24 hours of compound treatment), ATP levels are unchanged by V-59 in WT Mtb. This suggests that ATP is not the dominant signal modulating cholesterol utilization in WT Mtb during V-59 treatment, but additional timepoints matching previous growth curve assay conditions would help confirm this. Moreover, as we noted earlier, inducing cAMP was associated with an increase in the expression of *rv0805*, Mtb's only known phosphodiesterase (Chapter 4). This may be interpreted as a compensatory mechanism to hydrolyze the excess cAMP to AMP. The fact that *rv0805* mutations disrupt growth of Mtb in cholesterol media also suggests that cAMP plays a role in signaling related to the cholesterol pathway (*18*). Altogether, this suggests that ATP depletion is not the dominant signal contributing to cholesterol inhibition in WT Mtb treated with V-59. However, we

have not yet tested this using the TetOn-cAMP system to separate this from Rv1625c. We have also not yet constructed a targeted ΔRv0805 Mtb strain to confirm that this protein is required for normal growth on cholesterol and cholesterol metabolism. Additionally, we have not tried overexpressing Rv0805 in WT Mtb to determine if this helps restore cholesterol utilization during V-59 treatment, which would add further support to this model.

By contrast, throughout our experiments, the Comp$_{Full}$ strain consistently displayed enhanced lipid utilization defects during V-59 treatment compared to WT Mtb. This phenotype was associated with higher levels of cAMP synthesis and is potentially associated with severe depletion of ATP (Chapter 4, Fig. 6.4a). We also noted that during V-59 treatment the Comp$_{Full}$ strain i) was not rescued for growth by supplementation with the two-carbon fatty acid acetate, ii) had substantial defects in *prpD'*::GFP signal in the presence of both long (C17:1) and short (propionate) chain fatty acids, and iii) is not rescued for growth by supplementation with the even-chain fatty acid oleate (Chapter 4, Fig. 6.4 b, c). Therefore, in light of the ATP assay results, it seems possible that a combination of cAMP signaling and ATP depletion explain the enhanced phenotypes of the Comp$_{Full}$ strain. We have not yet used radiolabeled assays to confirm whether fatty acid uptake and breakdown are also defective under this condition, but this would be predicted based on our work with MceG (Chapter 3).

When comparing the two rescue curves with fatty acid supplementation (7H12+cholesterol+acetate versus 7H12+cholesterol+oleate), we noted that WT Mtb did have a delayed growth defect during V-59 treatment in media supplemented with oleate but not acetate. If fatty acid uptake and β-oxidation were operating fully under these conditions, one would expect oleate to be able to fill the same pathways as acetate and confer growth rescue. This defect would not have been captured in our previous CO_2 release assay using radiolabeled palmitate because the

compound treatment period for this assay was only 24 hours (Chapter 4). This suggest that, outside of the early time points we tested, V-59 treatment may induce a delayed long-chain fatty acid utilization defect in WT Mtb. Fatty acid uptake and metabolism assays at later time points after compound addition would help resolve this question, and this can also be examined during BMDM infection via Bodipy-C16 (*9, 21*). We also have not yet determined if this is specific to Rv1625c-dependent cAMP synthesis or can be generalized to the TetOn-cAMP system, if this effect is associated with ATP depletion at later timepoints, and whether Mt-Pat or another cAMP-dependent effector protein contributes to this.

We have attempted to identify whether a cAMP-dependent effector protein mediates downstream changes to cholesterol utilization during V-59 treatment by using several unbiased genetic screening approaches. All of these screening approaches were designed to identify mutations that confer resistance to signature effects of V-59 (decreased growth on cholesterol media or decreased *prpD'*::GFP signal). However, even when we expressed a second copy of *rv1625c* in a WT background, we repeatedly identified only *rv1625c* mutations from these screens and did not identify another candidate for downstream cAMP-mediated signaling (C. Montague, data not shown). We also found that the prime candidate based on the literature, Mt-Pat, is not required to downregulate cholesterol utilization during cAMP induction based on early exploratory experiments (Chapter 4). However, we have yet to test targeted mutations in any of the other 10 predicted cAMP-binding effector proteins of Mtb. A CRISPR interference platform was recently developed in Mtb that can be used to transcriptionally silence libraries of target genes (*22*). In the future, we will generate a library of CRISPRi strains that silence each of the cAMP-binding proteins in Mtb, and test whether silencing any of these effector proteins rescues or partially improves Mtb growth during V-59 treatment.

Finally, given the potentially complex yet poorly-understood connections between Rv1625c, cAMP signaling, lipid metabolism, and hypoxia suggested above, it may be interesting to explore how inducing cAMP via V-59 or TetOn-cAMP under combinations of fatty acids and cholesterol (or cholesteryl esters) influences lipid breakdown, lipid anabolism, and NAD^+/NADH balance during normoxia versus hypoxia. Both Rv1625c and Mt-Pat were proposed to be necessary for optimal growth of Mtb during the transition to hypoxia based on genetic screening in liquid media supplemented with fatty acids (*17*). However, the authors of this study did not confirm whether Mt-Pat is activated under this condition by cAMP derived from Rv1625c, nor did they directly identify acetylation targets for Mt-Pat under this condition. We also do not understand how the addition of cholesterol utilization would interact with their proposed model of Mt-Pat-mediated adaptations to hypoxia, when an abundant supply of propionyl-CoA derived from cholesterol breakdown may confer additional metabolic constraints (Chapter 2). Altogether, the V-59 and TetOn-cAMP tools present opportunities to dissect how inducing cAMP signaling can modulate Mtb metabolism in a variety of conditions that we and others have not yet explored.
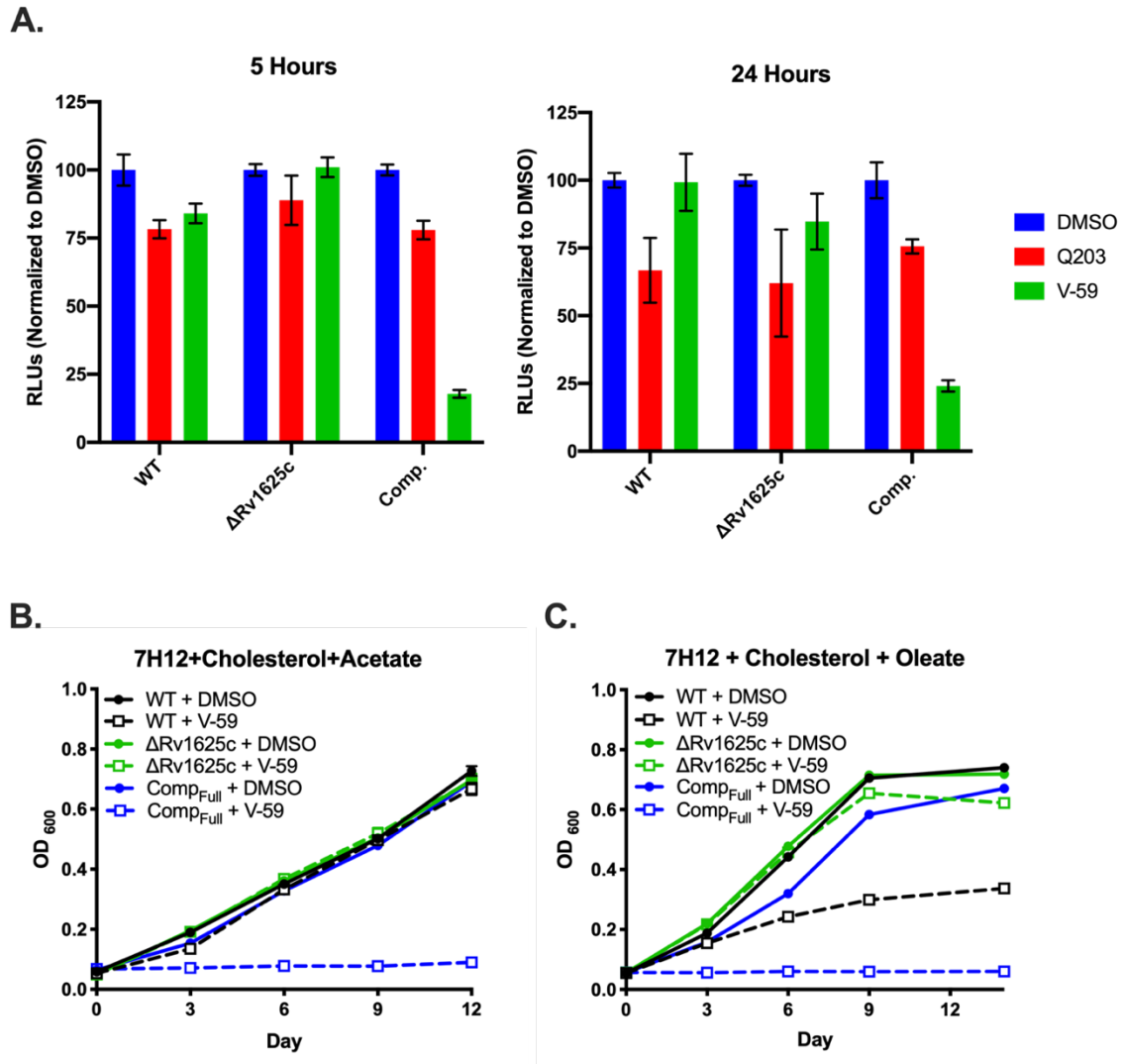
Figure 6.4 V-59 does not drive ATP depletion and cholesterol utilization defects simultaneously in WT Mtb, but ATP depletion is a dominant feature in Comp_Full Mtb during V-59 treatment. (A) Relative ATP levels in WT, ΔRv1625c, and CompFull (*rv1625c* overexpressing) Mtb treated with DMSO (vehicle), Q203 (positive control, or V-59 for 5 hours or 24 hours. Cells were cultured in 7H12+cholesterol+acetate media to match CO2 release and prpD'::GFP assay conditions. An equivalent number of bacteria were collected and processed via the BacTiter-Glo assay to quantify ATP levels. (B)

6.3 The potential of Rv1625c agonists to modulate host inflammation

The results presented in Chapter 5 demonstrate that V-59/mCLB073 reduces Mtb burden and lung pathology in murine models of TB infection when given in a single-agent regimen. However, we have not yet addressed how V-59/mCLB073 may be integrated into a TB drug regimen, which necessitates pairing multiple antibiotics. Additionally, our preliminary results suggest that chemically inducing cAMP synthesis by Mtb during infection not only modulates lipid utilization by the bacterium, but also may skew cytokine production by infected macrophages via the excess cAMP secreted from Mtb into its environment. Many of these results are preliminary, and require repetition to strengthen our conclusions. Regardless, here we outline potential future directions for exploring this unusual drug-dependent host-pathogen interaction.

Addressing the first point, in the future we will investigate whether integrating V-59/mCLB073 into existing TB antibiotic regimens confers improved disease outcomes. For example, V-59/mCLB073 would be useful if adding it to a regimen reduces the time to sterilization during treatment. It will also be important to test whether the addition of V-59/mCLB073 can reduce disease relapse after drug treatment is completed. Either of these positive outcomes would suggest that V-59/mCLB073 promotes clearance of a population of Mtb that normally contributes to drug persistence and/or reactivation of disease during standard treatment. New antibiotics that enhance the rate of sterilization may eventually contribute to shorter treatment, curtail the development of side effects, and promote durable cure. These positive findings with V-59/mCLB073 would help confirm the long-held hypothesis that utilization of lipids by Mtb supports a persistent, slow-growing phenotype that promotes bacterial survival during antibiotic treatment and/or re-emergence of a population of bacteria after treatment (*23*). To this point, genetic screening has been used in a high-dose model of mouse infection to identify mutations in

Mtb that confer increased or decreased bacterial clearance during treatment with a front-line drug combination regimen (INH, RIF, PZA, EMB) (*24*). Transposon mutations in the Mce4 operon but not the Mce1 operon showed a trend toward enhancing clearance during drug treatment, but out of these only *mce4E* and *mam4b* mutations were predicted to significantly change the rate of clearance (*24*). Disease relapse was not addressed in this study. Inducible methods for interfering with lipid utilization in Mtb (e.g. genetic methods like Tet-controllable gene inhibition, or chemical means like V-59/mCLB073) offer a more precise approach for testing this hypothesis in the future, as these approaches are not confounded by the necessity for high-dose intravenous infection or difficulties accounting for colonization defects in bacterial fitness prior to the start of drug treatment. Additionally, we do not yet know which other TB antibiotics pair synergistically with V-59/mCLB073. *In vitro* assays in liquid media are the most tractable method for empirically testing drug synergy, and recent work by Larkins-Ford et al. proposed that performing multiple drug combination assays representing different individual environmental conditions, especially high lipid content, may improve how predictive these assays are of effective combinations in mouse studies (*25*). However, it remains to be seen whether prioritizing new combinations based on their recommended suite of the most predictive, lipid dominant *in vitro* assays will be sufficient to account for the complex combinations of stresses that determines true drug efficacy *in vivo* (*26*). As discussed in Chapter 1, testing in mouse models alone is also not considered sufficient to draw conclusions about the potential of a new drug. Ultimately, modeling drug combinations in animals like non-human primates that more closely recapitulate human disease would be necessary to judge whether V-59/mCLB073 has realistic potential to add value to the existing frontline regimen or to the newly developed Nix-TB regimen (Chapter 1).

Addressing the second point, our preliminary results suggest that there is a correlation between chemically activating Rv1625c, increasing cAMP synthesis and secretion from Mtb, and decreasing the production of at least two cytokines from infected phagocytes. However, further repetition of these experiments will be necessary to strengthen these results, and there are a variety of future experiments that could be performed to expand our understanding. As discussed in Chapter 1, the host protectiveness of individual granulomas is likely dictated significantly by the phenotype of local immune cells present in the lesion. Because our preliminary data suggests that V-59/mCLB073 primarily alters Mtb metabolism but may also have secondary immunomodulatory effects during infection, our first goal has been to define the scope and magnitude of the changes these compounds may exert on the innate immune cells Mtb resides in. As a starting point, we performed RNA-seq using BMDMs, and then confirmed that two of the cytokines predicted to be affected by mCLB073 treatment *in vitro* (IL-1β and CXCL1) were also disproportionately decreased by mCLB073 treatment *in vivo*. Thus far we have confirmed that the effect of mCLB073 treatment on IL-1β seems Rv1625c-dependent in BMDMs *in vitro*, but have yet to confirm that these changes are Rv1625c-dependent *in vivo* (Fig. 6.5). To our knowledge, little is known about how various TB antibiotics might differentially affect the host immune response as they trigger bacterial death via different mechanisms. We have attempted to distinguish trivial CFU-dependent changes in cytokines from unique cAMP-dependent changes in our *in vivo* experiments by comparing mCLB073 treatment with INH treatment. However, to strengthen our claim that effects we observe with mCLB073 are specific to the mechanism of this compound, we could compare mCLB073 with additional TB antibiotics besides INH that have different bacterial targets throughout our experiments. We could also attempt experiments with lower doses of mCLB073 or shorter dosing times to try to assay changes in cytokines before a

decrease in CFUs occurs. Importantly, our work so far in mice has been performed using acute infection models to expedite the verification of candidate cytokines, but ultimately these findings should be verified in a chronic model of infection after an adaptive immune response has developed.

Our experiments using whole lung lysates in mice do not distinguish phenotypic changes in different populations of cells, for example infected versus bystander cells or different subsets of macrophages and neutrophils. To address this, we have begun developing a flow cytometry protocol for murine lung-derived cells that is compatible with intracellular cytokine staining. This will allow us to distinguish Mtb infected versus uninfected cells, and to quantify cytokine changes in neutrophils and two major macrophage populations (alveolar and interstitial macrophages) that were associated with differential control of Mtb burden in the past (27). We are also testing a strain of Mtb that stably expresses a red fluorescent protein for longer than 2-3 weeks *in vivo*, because antibiotic selection is not present during mouse infection to promote retention of the episomal plasmids on which our fluorescent Mtb strains currently rely (28). This would allow us to perform these experiments during the chronic stage of infection when adaptive T cell responses are present and significantly influence macrophage responses and the host pressures Mtb encounters. We also have tools in place for sorting live cell subsets from infected mice, which facilitates quantifying cell-type dependent changes in culturable bacterial burden, host and bacterial dual transcriptional signatures, and cellular metabolism *ex vivo* where appropriate.

We have not yet examined the downstream functional implications of our preliminary findings in mice. For example, if mCLB073 significantly decreases CXCL1 production in the lung during Mtb infection via activating cAMP synthesis, then we would predict that neutrophil accumulation in the lungs and the proportion of infected neutrophils might be decreased during

mCLB073 treatment in an Rv1625c-dependent manner. Preliminary flow cytometry experiments suggest fewer neutrophils are present in the lungs of BALB/c mice acutely infected with Mtb and treated with mCLB073 for one week (Fig. 6.6). However, we have not yet controlled for the decrease in Mtb CFUs we observed in these early experiments, and we did not define whether specific cell populations are producing less CXCL1. In the future we could also investigate whether other important neutrophil chemokines (e.g. CXCL2, CXCL5, CXCL8) are decreased by mCLB073, and whether any changes are limited to the lung environment or are detectable systemically in plasma. Examining this in additional relatively resistant (C57BL/6J) and relatively susceptible mouse backgrounds could be useful to determine whether this observation is restricted to the Th2-skewed immune response of BALB/c mice. As discussed in Chapter 1, multiple single-gene knockout mice on a C57BL/6J background ($Irg1^{-/-}$, $Atg5^{-/-}$, $Nos2^{-/-}$) have increased susceptibility to Mtb that is characterized by enhanced neutrophil recruitment. If substantially decreasing neutrophil recruitment is a general immunomodulatory effect of mCLB073, then mCLB073 treatment may be able to improve measures of disease outcome in these mice (e.g. decrease necrosis, decrease granuloma size, prolong survival, decrease Mtb burden) while being correlated with less neutrophil accumulation in an Rv1625c-dependent manner.

Similarly, more work would be needed to determine whether IL-1 signaling is indeed decreased by mCLB073 *in vivo*, and whether this is beneficial during chronic infection. As discussed in Chapter 1, IL-1 signaling is thought to interact with a complex counter-regulatory loop during TB infection. IFNγ is consistently proposed to influence IL-1 production after the adaptive T cell response has developed, suggesting analysis of this pathway in the context of chronic infection will be especially important. While sufficient IL-1 signaling is thought to be required to promote disease control early after Mtb infection, excessive IL-1 signaling during

chronic infection is associated with disease severity and neutrophil accumulation. Indeed, in animal models, administering an IL-1 receptor antagonist (Anakinra) in combination with the TB antibiotic linezolid reduced total lung inflammation, limited neutrophil recruitment, and partially reversed harmful side effects associated with linezolid, without impairing bacterial clearance or the host response (*29*). If mCLB073 significantly reduces IL-1 production during chronic infection, then administration of mCLB073 may promote similar outcomes as those reported during αIL-1R1 administration alone in WT C57BL/6J, *Nos2*$^{-/-}$, and/or C3HeB/FeJ mice (less neutrophil accumulation, less lung inflammation, smaller lesion size, ameliorated weight loss) in an Rv1625c-dependent manner (*29*). This could work in concert with changes in neutrophil chemoattractants discussed above. We have not yet investigated whether other cytokines that may interact with the IL-1 regulatory loop are also altered during mCLB073 treatment, in a manner that is independent of changes in CFUs and dependent on Rv1625c. Based on the literature, secondary effects of IL-1 suppression by mCLB073 could include a concomitant decrease in PGE2 and increases in 12-hydroxyeicosatetraenoic acid, Type I IFNs, IL-10 and/or IL-1Ra (*30, 31*). IL-1Ra is particularly important to quantify, because the balance of both IL-1 (receptor agonist) and IL-1Ra (receptor antagonist) influences the IL-1 signaling output. It will also be important to establish whether ELISA results reflect differences in the levels of pro-IL-1α/β versus their active, cleaved forms. As discussed above, flow cytometry analyses on lung cells isolated *ex vivo* and stained for cytokine production could help distinguish whether mCLB073 induces changes in IL-1 production in particular phagocyte populations, and in infected versus uninfected cells.

Although this discussion is focused on *in vivo* follow up experiments, complementary *in vitro* experiments using BMDMs or J774 cells would be helpful to examine mechanisms underlying any links we identify between mCLB073/V-59, increased cAMP secretion by Mtb, and

modulation of macrophage phenotypes. As discussed earlier, past studies that examined cAMP-dependent changes to phagocyte phenotypes relied on methods known to increase cAMP in the cytosol. Currently we do not know where excess cAMP secreted by Mtb during macrophage infection is localized and how this intersects with localization of cAMP-dependent effector proteins (PKA or Epac) in the cell. To strengthen the claim that changes we see in particular cytokines during mCLB073/V-59 treatment are dependent on excess cAMP secreted from Mtb, we would need to demonstrate that Rv1625c-dependent changes during compound treatment are mediated in a manner dependent on PKA. Numerous tools (e.g. knockdown of PKA, inhibitors of kinase anchoring protein (AKAP) interactions with PKA, phosphospecific antibodies for targets of PKA) are available to track activation of this pathway and its effect on NF-κB-dependent gene induction (*32, 33*). Alternatively, it is possible that the changes we observe in the macrophage phenotype are not due to a direct interaction of cAMP with host cell signaling. Some or all of the changes could be mediated by an unidentified Mtb protein or cell wall component that is modulated in a cAMP-dependent manner and has immunogenic properties. Thus, Rv1625c agonist compounds present a novel opportunity to explore mechanisms by which these and other macrophage functions identified in our RNA-seq data (modulation of dual-specificity phosphatase genes or cholesterol homeostasis) may be influenced by upregulating cAMP synthesis in Mtb.
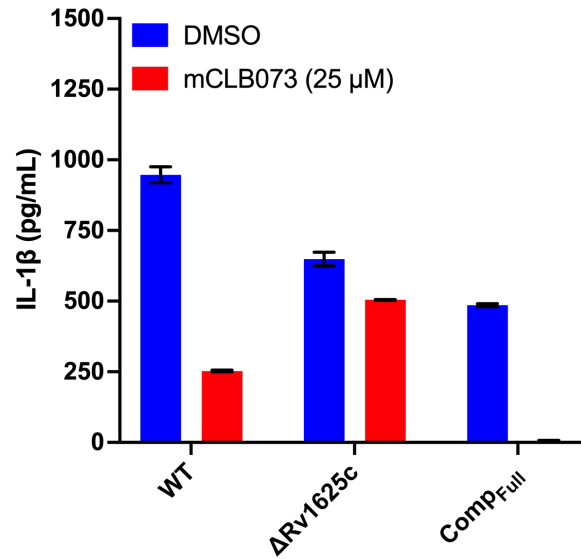
Figure 6.5 Preliminary quantification of IL-1β secreted by Mtb-infected BMDMs. Murine BMDMs from BALB/c mice were infected at an MOI of 7 with CDC1551 strains of Mtb as indicated. After 24 hours of treatment with vehicle control (DMSO) or mCLB073 (25μM), supernatants were collected and processed via ELISA to quantify IL-1β. Data are from one experiment with two technical replicates in each group. Data courtesy of C. Montague.
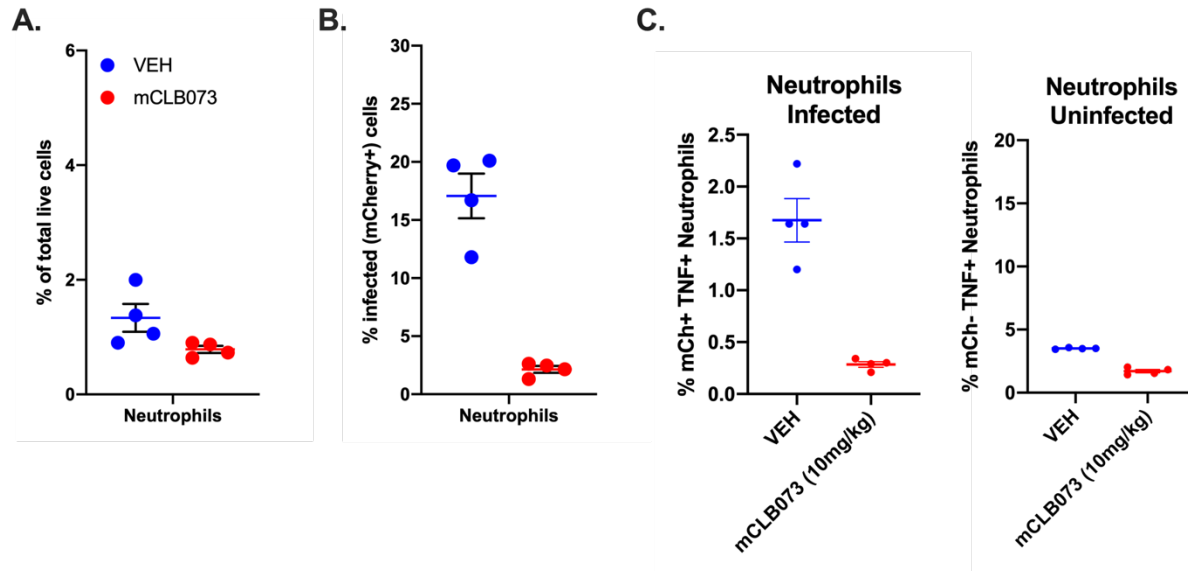
Figure 6.6 Preliminary quantification of neutrophils following mCLB073 treatment in lungs of Mtb infected mice. BALB/c mice were infected with 2,000 CFUs of mCherry-expressing Mtb Erdman for two weeks. Mice were given vehicle control or mCLB073 (10mg/kg) by oral gavage during days 7-13 post-infection. On day 14 post-infection, lungs were collected and processed for flow cytometry and intracellular cytokine staining. **(A)** Percentage of neutrophils quantified within the total live cell population. **(B)** Percentage of neutrophils infected with Mtb based on positive mCherry signal. **(C)** Percentage of infected (left) or uninfected (right) neutrophils that are positive for TNFα staining. Data are representative of two experiments. Data shown is from one experiment with 4 mice per group.

6.4 Final thoughts

As discussed in Chapter 1, identifying novel mechanisms that can be chemically targeted to accelerate Mtb clearance, provide durable cure, and promote granuloma resolution in the face of host granuloma heterogeneity and bacterial tolerance is the telos of TB therapeutic research. Here we have presented data detailing how the transformation of ATP, by hydrolysis or cyclization, lies at the center of lipid utilization pathways in Mtb, which suggests potential future mechanisms for antibiotic development. Specifically, we have investigated compounds that chemically activate cAMP synthesis from ATP in Mtb, while displaying promising safety and pharmacokinetic profiles. This is an unusual mechanism of action that may be able to exert dual beneficial effects by limiting Mtb lipid utilization while downregulating host inflammatory signaling associated with neutrophil infiltration. This mechanism may prove to be the most effective in poorly-controlling granulomas, characterized by enhanced neutrophil influx where fatty acid uptake, cholesterol utilization, and gluconeogenesis are predicted to be especially important for Mtb survival (*31*). Populations of Mtb associated with host stress, slow net growth, and drug tolerance are closely linked with metabolic realignments centered around lipid utilization. In at least one case, multi-drug resistance is also associated with a shift toward cholesterol metabolism (*34*). Much is left to be learned about the intersection of ATP, cAMP and mixed nutrient metabolism in Mtb and in the host. This work suggests future opportunities to examine whether counterbalancing at the local level the typical lipid and/or inflammatory niche Mtb constructs for itself will be a powerful tool to reduce antibiotic tolerance, expedite bacterial clearance, and promote durable cure in combination with other TB antibiotics. .

6.5 References

1. M. Finkbeiner, J. Grischin, A. Seth, J. E. Schultz, In search of a function for the membrane anchors of class IIIa adenylate cyclases. *Int J Med Microbiol* **309**, 245-251 (2019).

2. M. Ziegler, J. Bassler, S. Beltz, A. Schultz, A. N. Lupas, J. E. Schultz, Characterization of a novel signal transducer element intrinsic to class IIIa/b adenylate cyclases and guanylate cyclases. *FEBS J* **284**, 1204-1217 (2017).

3. S. Beltz, J. Bassler, J. E. Schultz, Regulation by the quorum sensor from Vibrio indicates a receptor function for the membrane anchors of adenylate cyclases. *eLife* **5**, (2016).

4. I. Vercellino, L. Rezabkova, V. Olieric, Y. Polyhach, T. Weinert, R. A. Kammerer, G. Jeschke, V. M. Korkhov, Role of the nucleotidyl cyclase helical domain in catalytically active dimer formation. *Proceedings of the National Academy of Sciences of the United States of America* **114**, E9821-E9828 (2017).

5. A. A. Ganaie, G. Trivedi, A. Kaur, S. S. Jha, S. Anand, V. Rana, A. Singh, S. Kumar, C. Sharma, Interaction of Erp Protein of Mycobacterium tuberculosis with Rv2212 Enhances Intracellular Survival of Mycobacterium smegmatis. *J Bacteriol* **198**, 2841-2852 (2016).

6. B. C. VanderVen, R. J. Fahey, W. Lee, Y. Liu, R. B. Abramovitch, C. Memmott, A. M. Crowe, L. D. Eltis, E. Perola, D. D. Deininger, T. Wang, C. P. Locher, D. G. Russell, Novel inhibitors of cholesterol degradation in Mycobacterium tuberculosis reveal how the bacterium's metabolism is constrained by the intracellular environment. *PLoS Pathogens* **11**, e1004679 (2015).

7. S. T. Thomas, B. C. VanderVen, D. R. Sherman, D. G. Russell, N. S. Sampson, Pathway Profiling in Mycobacterium tuberculosis: elucidation of a cholesterol-derived catabolite

and the enzymes that catalyze its metabolism. *Journal of Biological Chemistry* **286**, 43668-43678 (2011).

8. A. Singh, D. Mai, A. Kumar, A. J. Steyn, Dissecting virulence pathways of Mycobacterium tuberculosis through protein-protein association. *Proceedings of the National Academy of Sciences of the United States of America* **103**, 11346-11351 (2006).

9. E. V. Nazarova, C. R. Montague, T. La, K. M. Wilburn, N. Sukumar, W. Lee, S. Caldwell, D. G. Russell, B. C. VanderVen, Rv3723/LucA coordinates fatty acid and cholesterol uptake in Mycobacterium tuberculosis. *eLife* **6**, (2017).

10. Y. Gopel, M. A. Khan, B. Gorke, Menage a trois: post-transcriptional control of the key enzyme for cell envelope synthesis by a base-pairing small RNA, an RNase adaptor protein, and a small RNA mimic. *RNA Biol* **11**, 433-442 (2014).

11. J. Luciano, E. Foulquier, J. R. Fantino, A. Galinier, F. Pompeo, Characterization of YvcJ, a conserved P-loop-containing protein, and its implication in competence in Bacillus subtilis. *J Bacteriol* **191**, 1556-1564 (2009).

12. E. Foulquier, F. Pompeo, D. Byrne, H. P. Fierobe, A. Galinier, Uridine diphosphate N-acetylglucosamine orchestrates the interaction of GlmR with either YvcJ or GlmS in Bacillus subtilis. *Scientific reports* **10**, 15938 (2020).

13. E. Foulquier, F. Pompeo, A. Bernadac, L. Espinosa, A. Galinier, The YvcK protein is required for morphogenesis via localization of PBP1 under gluconeogenic growth conditions in Bacillus subtilis. *Molecular microbiology* **80**, 309-318 (2011).

14. S. M. Joshi, A. K. Pandey, N. Capite, S. M. Fortune, E. J. Rubin, C. M. Sassetti, Characterization of mycobacterial virulence genes through genetic interaction mapping.

Proceedings of the National Academy of Sciences of the United States of America **103**, 11760-11765 (2006).

15. M. Mir, S. Prisic, C. M. Kang, S. Lun, H. Guo, J. P. Murry, E. J. Rubin, R. N. Husson, Mycobacterial gene cuvA is required for optimal nutrient utilization and virulence. *Infect Immun* **82**, 4104-4117 (2014).

16. A. Singh, D. K. Crossman, D. Mai, L. Guidry, M. I. Voskuil, M. B. Renfrow, A. J. Steyn, Mycobacterium tuberculosis WhiB3 maintains redox homeostasis by regulating virulence lipid anabolism to modulate macrophage response. *PLoS Pathog* **5**, e1000545 (2009).

17. E. S. C. Rittershaus, S. H. Baek, I. V. Krieger, S. J. Nelson, Y. S. Cheng, S. Nambi, R. E. Baker, J. D. Leszyk, S. A. Shaffer, J. C. Sacchettini, C. M. Sassetti, A Lysine Acetyltransferase Contributes to the Metabolic Adaptation to Hypoxia in Mycobacterium tuberculosis. *Cell Chemical Biology* **25**, 1495-1505 e1493 (2018).

18. J. E. Griffin, J. D. Gawronski, M. A. DeJesus, T. R. Ioerger, B. J. Akerley, C. M. Sassetti, High-Resolution Phenotypic Profiling Defines Genes Essential for Mycobacterial Growth and Cholesterol Catabolism. *PLoS Pathog* **7**, (2011).

19. W. Lee, B. C. VanderVen, R. J. Fahey, D. G. Russell, Intracellular Mycobacterium tuberculosis exploits host-derived fatty acids to limit metabolic stress. *Journal of Biological Chemistry* **288**, 6788-6800 (2013).

20. J. A. Buglino, G. D. Sankhe, N. Lazar, J. M. Bean, M. S. Glickman, Integrated sensing of host stresses by inhibition of a cytoplasmic two-component system controls M. tuberculosis acute lung infection. *eLife* **10**, (2021).

21. E. V. Nazarova, C. R. Montague, L. Huang, T. La, D. Russell, B. C. VanderVen, The genetic requirements of fatty acid import by Mycobacterium tuberculosis within macrophages. *eLife* **8**, (2019).

22. A. I. Wong, J. M. Rock, CRISPR Interference (CRISPRi) for Targeted Gene Silencing in Mycobacteria. *Methods Mol Biol* **2314**, 343-364 (2021).

23. J. P. Sarathy, V. Dartois, Caseum: a Niche for Mycobacterium tuberculosis Drug-Tolerant Persisters. *Clinical microbiology reviews* **33**, (2020).

24. M. M. Bellerose, S. H. Baek, C. C. Huang, C. E. Moss, E. I. Koh, M. K. Proulx, C. M. Smith, R. E. Baker, J. S. Lee, S. Eum, S. J. Shin, S. N. Cho, M. Murray, C. M. Sassetti, Common Variants in the Glycerol Kinase Gene Reduce Tuberculosis Drug Efficacy. *mBio* **10**, (2019).

25. J. Larkins-Ford, T. Greenstein, N. Van, Y. N. Degefu, M. C. Olson, A. Sokolov, B. B. Aldridge, Systematic measurement of combination-drug landscapes to predict in vivo treatment outcomes for tuberculosis. *Cell Syst*, (2021).

26. M. M. Bellerose, M. K. Proulx, C. M. Smith, R. E. Baker, T. R. Ioerger, C. M. Sassetti, Distinct Bacterial Pathways Influence the Efficacy of Antibiotics against Mycobacterium tuberculosis. *mSystems* **5**, (2020).

27. L. Huang, E. V. Nazarova, S. Tan, Y. Liu, D. G. Russell, Growth of Mycobacterium tuberculosis in vivo segregates with host macrophage metabolism and ontogeny. *J Exp Med* **215**, 1135-1152 (2018).

28. K. Kolbe, A. C. Bell, G. A. Prosser, M. Assmann, H. J. Yang, H. E. Forbes, S. Gallucci, K. D. Mayer-Barber, H. I. Boshoff, C. E. Barry Iii, Development and Optimization of

Chromosomally-Integrated Fluorescent Mycobacterium tuberculosis Reporter Constructs. *Frontiers in microbiology* **11**, 591866 (2020).

29.   C. G. Winchell, B. B. Mishra, J. Y. Phuah, M. Saqib, S. J. Nelson, P. Maiello, C. M. Causgrove, C. L. Ameel, B. Stein, H. J. Borish, A. G. White, E. C. Klein, M. D. Zimmerman, V. Dartois, P. L. Lin, C. M. Sassetti, J. L. Flynn, Evaluation of IL-1 Blockade as an Adjunct to Linezolid Therapy for Tuberculosis in Mice and Macaques. *Frontiers in immunology* **11**, 891 (2020).

30.   K. D. Mayer-Barber, A. Sher, Cytokine and lipid mediator networks in tuberculosis. *Immunol Rev* **264**, 264-275 (2015).

31.   B. B. Mishra, R. R. Lovewell, A. J. Olive, G. Zhang, W. Wang, E. Eugenin, C. M. Smith, J. Y. Phuah, J. E. Long, M. L. Dubuke, S. G. Palace, J. D. Goguen, R. E. Baker, S. Nambi, R. Mishra, M. G. Booty, C. E. Baer, S. A. Shaffer, V. Dartois, B. A. McCormick, X. Chen, C. M. Sassetti, Nitric oxide prevents a pathogen-permissive granulocytic inflammation during tuberculosis. *Nature microbiology* **2**, 17072 (2017).

32.   E. A. Wall, J. R. Zavzavadjian, M. S. Chang, B. Randhawa, X. Zhu, R. C. Hsueh, J. Liu, A. Driver, X. R. Bao, P. C. Sternweis, M. I. Simon, I. D. Fraser, Suppression of LPS-induced TNF-alpha production in macrophages by cAMP is mediated by PKA-AKAP95-p105. *Sci Signal* **2**, ra28 (2009).

33.   S. Gerlo, R. Kooijman, I. M. Beck, K. Kolmus, A. Spooren, G. Haegeman, Cyclic AMP: a selective modulator of NF-kappaB action. *Cell Mol Life Sci* **68**, 3823-3841 (2011).

34.   P. Aiewsakun, P. Prombutara, T. A. P. Siregar, T. Laopanupong, P. Kanjanasirirat, T. Khumpanied, S. Borwornpinyo, P. Tong-Ngam, A. Tubsuwan, P. Srilohasin, A. Chaiprasert, W. Ruangchai, P. Palittapongarnpim, T. Prammananan, B. C. VanderVen, M.

Ponpuak, Transcriptional response to the host cell environment of a multidrug-resistant Mycobacterium tuberculosis clonal outbreak Beijing strain reveals its pathogenic features. *Scientific Reports* **11**, 3199 (2021).